UNIVERSITAT DE BARCELONA

Anticancer Effect and Molecular Target Identification of Novel Anionophores in Lung Cancer

Ananda Marina Rodilla Martín

ANTICANCER EFFECT AND MOLECULAR TARGET IDENTIFICATION OF NOVEL ANIONOPHORES IN LUNG CANCER

Ananda Marina Rodilla Martín

Doctoral Thesis 2018

Faculty of Medicine
Pathology and Experimental Therapeutics Department
PhD in "Medicine and Translational Research" Program 2014-2018

ANTICANCER EFFECT AND MOLECULAR TARGET IDENTIFICATION OF NOVEL ANIONOPHORES IN LUNG CANCER

Siguiendo la línea de investigación en Cáncer y Genética Humana, esta tesis ha sido realizada bajo la dirección del Dr. Ricardo Pérez Tomás y la Dr. Vanessa Soto Cerrato en el grupo de investigación de Biología Celular del Cáncer del Departamento de Patología y Terapéutica Experimental de la Universidad de Barcelona

Ananda Marina Rodilla Martín

Dr. Ricardo Pérez Tomás

Dr. Vanessa Soto Cerrato

Memoria presentada por Ananda Marina Rodilla Martín para optar al grado de Doctora por la Universidad de Barcelona.

A mi familia,

ACKNOWLEDGMENTS

El trabajo cinco años de laboratorio puede quedar más o menos resumido en una tesis de unas ciento y pico páginas como esta, en cambio, creo que es muy difícil recoger en sólo unas páginas todo lo que han significado estos años para mí. Con la escritura de esta tesis finaliza una de las etapas más importantes de mi vida. Una etapa que me ha permitido adentrarme en el mundo de la investigación, enriquecerme con nuevos conocimientos y además, ha sido un periodo de crecimiento tanto a nivel personal como profesional. Así bien, llegado el final de esta etapa, me gustaría agradecer a todos los que habéis formado parte de este trabajo y que me habéis acompañado en este camino.

En primer lugar, tengo que darle las gracias al Dr. Ricardo Pérez, director de esta tesis, porque cinco años atrás me abrió las puertas del laboratorio dejándome formar parte de esta gran aventura. Tengo que agradecerle toda la confianza que ha depositado en mí durante estos años, y el estar ahí como buen orientador y fuente de apoyo de este trabajo.

En segundo lugar me gustaría agradecer a la Dra. Vanessa Soto no sólo la dirección de esta tesis sino también la confianza, el apoyo recibido. Agradecerte el hecho de que siempre hayas estado cerca como una guía, para transmitir conocimientos, y las ganas por un trabajo bien hecho. Eres todo un ejemplo de superación, ha sido un placer aprender de ti.

Por otra parte, también quiero darle las gracias al Dr. Luis Korrodi. Por su tiempo, disponibilidad y paciencia. Gracias por todas tus aportaciones, por enseñarme a trabajar con rigor, y por esas discusiones científicas de las que he aprendido tanto.

También tengo que agradecerle a la Dra. Cèlia García su presencia en el laboratorio, gracias por ser como eres, porque allá donde vas, siempre nos transmites alegría y tranquilidad.

Todo este trabajo no hubiera sido posible sin Pili, David, Lesly, y Rosa… los tiki-tikis! Cualquier cosa que escriba queda corta… Me considero muy afortunada porque no podría haber tenido mejores compañeros de laboratorio! Gracias por todo el trabajo en equipo, pero sobre todo gracias por llenar las horas de experimentos con risas. Gracias por los vichys, las cenas, los bailes, los viajes, y todas las aventuras que hemos vivido juntos en estos años. Porque no somos sólo compañeros, nos hemos convertido en amigos y en una pequeña familia. Sé que podré contar con vosotros siempre.

Durante estos años también he compartido el laboratorio con Rafa, Aina y Pep, del grupo de Desarrollo Neural. Gracias por todas las grandes conversaciones entre poyatas, en el despacho, y a la hora de comer, que han hecho que las horas se pasen volando. También les tengo que dar las gracias a los laboratorios vecinos. Al laboratorio de Microbiología, en especial a Rocío, gracias por ser siempre tan atenta! Y a Dencho y Salima, del grupo del IBEC.

A Xavi, Marc y Marta, del grupo de Farmacología, gracias por todas las experiencias que hemos vivido juntos, y en concreto gracias por enseñarme que la ciencia es divertida. Entre todos habéis hecho que esta etapa de mi vida sea inolvidable! A Marta en especial, le doy las gracias por compartir innumerables aventuras desde hace más de diez años, y por esos cafés en la tercera planta que ponen solución a todos los problemas.

Y como no todo es ciencia, también tengo que dar las gracias a todos aquellos que me habéis acompañado fuera de las paredes del laboratorio. A “los del máster”, todos ya grandes doctores, Molinos, Albert, Xavi, Manu,… gracias por esos vermuts y esas noches de raval. A mis amigas de aquí y de allí, a Mery, Cris, Sara, Leo, María, Noa, Belén… ¿qué puedo decir? Gracias por escucharme una y otra vez, confiar en mí y darme ánimo en todo momento.

A ti, que sabes mejor que nadie que no ha sido un camino fácil, gracias por todo. Por poner luz y color a mis oscuridades. Por estar a mi lado y confiar siempre en mí. Por ayudar a superarme y a conseguir mis metas. Gracias por enseñarme lo que de verdad importa, y a ver la vida de otra manera.

A los más importantes, mi familia. Nunca podré agradecerles todo el amor que he recibido. Porque a pesar de la distancia, siempre los he sentido cerca. Porque saben todo lo que esto ha supuesto para mí, gracias de todo corazón por toda vuestra paciencia, vuestras palabras, y por no dejarme caer nunca. Sin duda son los responsables de que haya podido llegar hasta aquí, sin ellos no hubiera sido posible.

Porque cada una de estas páginas tiene un poco de cada uno de vosotros, **GRACIAS**.

INDEX

TABLE OF CONTENTS

ABBREVIATIONS

A

AIF Apoptosis-inducing factor mitochondrion-associated 1
AKT Protein kinase B
ALK Anaplastic lymphoma receptor tyrosine kinase
AMPK AMP-activated protein kinase
AO Acridine orange
APAF1 Apoptotic proteaseactivating factor 1
Asp Aspartate
ATG Autophagy related proteins
ATP Adenosine-5'-triphosphate

B

BAK BCL-2 homologous antagonist/killer
BAX BCL-2-associated X
BH BCL-2 homologous antagonist/killer
BID BH3 interacting domain death agonist
BIR Baculovirus IAP repeat domain
BLC-2 B-cell lymphoma 2
BMK Big MAP kinases

C

CDDP cis-Dichlorodiammineplatinum(II)
cMYC Myelocytomatosis virus oncogene cellular homolog
COX8A Cytochrome c oxidase subunit 8A
CSC Cancer stem cells
CT Computed Tomography
CYPD Cyclophilin D
CytC Cytochrome C

D

DAMPs Danger-associated molecular patterns
DIABLO Direct IAP binding protein with low pI
DISC Death-inducing signaling complex
DMSO Dimethyl sulfoxide

E

EEA1 Early Endosomal Antigen 1
EGFR Epidermal growth factor receptor
EML4 Echinoderm microtubule-associated protein-like 4
EMT Epithelial-mesenchymal transition
ERKs Extracellular-signal-regulated kinases
ERKs Extracellular-signal-regulated kinases

F

FADD FAS-associated death domain
FAS-L FAS ligand
FIP200 Focal adhesion kinase family interacting protein of 200 kD
FLIPs FLICE-like inhibitory proteins
FOXO Forkhead family of transcription factors

G

G418 Neomycin
Glu Glutamate
GPCR G protein–coupled receptor
GSK-3 Glycogen synthase kinase 3

H

HIF1 hypoxia-inducible factor

I

IAPs Inhibitors of apoptosis proteins
IC Inhibitory concentration
ICAD inhibitor of the caspase-activated DNase
IGF1R Insulin-like growth factor receptor
IRS1 insulin receptor substrate-1
ITGA5 Integrin integrin subunit alpha 5
ITGB8 Integrin subunit beta 8

J

JNKs Jun amino-terminal kinases

K

KRAS Kirsten rat sarcoma viral oncogene homolog

L

LAMP1 Lysosome-associated membrane protein
LC3 Light chain 3
LDH Lactate dehydrogenase
LKB1 liver kinase B1
LMP Lysosomal membrane permeabilization

M

MAPKs Mitogen-activated protein kinases
MCL-1 Myeloid leukemia cell differentiation 1
MET N-methyl-N'-nitroso-guanidine human osteosarcoma transforming gene
miRNAs microRNAs
MLKL mixed lineage kinase domain-like
MMP Mitochondrial membrane permeabilization
MOMP Mitochondrial outer membrane permeabilization
MPT Mitochondrial permeability transition
MRI Magnetic Resonance Imaging
mTORC1 Mammalian target of rapamycin complex 1
mTORC2 Mammalian target of rapamycin complex 2

N

NHEs Na^+/H^+ exchangers
NSCLC Non-small cell lung cancer
NT Negative transporter compound

O

OXPHOS Oxidative phosphorylation

P

PARP Poly (ADP-ribose) polymerase
PD-1 Programmed cell death protein 1
PDK1 Pyruvate dehydrogenase kinase, isozyme 1
PET Positron Emission Tomography
PFK1 Phosphofructokinase 1
pHi Intracellular pH
PHLPP2 PH domain and leucine rich repeat protein phosphatase 2
PI Propidium Iodide
PI3K Phosphatidylinositol 3-kinase
PI3P Phosphatidylinositol3-phosphate
PIP2 3-phosphorylated phosphatidylinositol
PKA Protein kinase A
PTEN Phosphatase and tensin homolog
PTPC Permeation transition pore complex

R

Rab7 Ras-related protein
RAS Rat sarcoma oncogene
RIP Receptor-interacting protein kinase
RN Regulated Necrosis
ROCK1 Rho-associated coiledcoil forming kinase 1
ROS Reactive oxygen species
RT Room temperature
RTK Receptor tyrosine kinase

S

SAL Salinomycin
SAPKs Stress-activated protein kinases
SCLC Small cell lung cancer
SMAC Second mitochondria-derived activator of caspase
SNARE soluble N-ethylmaleimide-sensitive factor attachment protein receptor
SPR Surface plasmon resonance
SQSTM1 Sequestosome-1

T

TCA Tricarboxylic acid cycle
TEM Transmission Electron Microscopy
TK Tyrosine kinase
TKIs Tyrosine kinase inhibitors
TNF Tumor necrosis factor
TNFR1 Tumor necrosis factor receptor type 1
TOMM20 Translocase of outer mitochondrial membrane 20
TP53 Tumor protein 53 gene
TRADD TNF receptor-associated death domain
TRAIL Tumor necrosis factor-related apoptosis-inducing ligand
TSC2 Tuberous sclerosis 2

U

ULK1 UNC-51-Like Kinase

V

V-ATPase Vacuolar-type H^+-ATPase
VEGF Vascular endothelial growth factor

W

WHO World Health Organization

X

XIAP X chromosome-linked IAP

#

$\Delta\Psi_m$ Mitochondrial membrane potential

ABSTRACT

El cáncer de cavidad oral y de pulmón se engloban dentro de las enfermedades de vías respiratorias más comunes, siendo este último una de las principales causas de mortalidad en el mundo. A pesar de los nuevos avances en el diagnóstico y la atención clínica, el éxito de los tratamientos convencionales es todavía limitado, ya que los pacientes acaban desarrollando resistencias y presentando recidivas. Debido a las limitaciones terapéuticas para abordar estas patologías, es necesario identificar nuevos compuestos con diferentes mecanismos de acción y mayor eficacia para combatir este tipo de neoplasias.

Las células cancerosas adquieren una serie de características durante la carcinogénesis, como un gradiente de pH invertido en comparación con las células normales, lo cual favorece la progresión del cáncer mediante el aumento de la proliferación y la evasión de la apoptosis. Recientemente se ha propuesto una nueva estrategia terapéutica contra el cáncer la cual implica la modulación del pH intracelular. Es por esto que nuestro grupo de investigación estudia el potencial de compuestos transportadores de aniones como nuevos agentes quimioterapéuticos, ya que poseen la capacidad de disminuir el pH intracelular selectivamente.

En concreto, este trabajo de tesis se ha centrado en caracterizar el efecto anticanceroso de anionóforos, compuestos transportadores de aniones, derivados de moléculas naturales llamadas tambjaminas, tanto a nivel celular como molecular. En primer lugar, se ha determinado el efecto de los análogos sintéticos de tambjamina sobre la viabilidad celular en líneas de cáncer oral y pulmonar, así como en células madre cancerosas derivadas de tumores de pacientes, demostrando ser potentes agentes citotóxicos. A su vez, se ha estudiado qué implicación tiene la pérdida de la homeostasis iónica impulsada por estos compuestos a nivel celular. En este sentido, se ha caracterizado cómo los compuestos inducen la alcalinización de los lisosomas, y provocan una vacuolización masiva en el citoplasma que se corresponde con el hinchamiento de la mitocondrias. Estos dos fenómenos conllevan la pérdida de función de ambos orgánulos. Al mismo tiempo, se han estudiado en detalle los mecanismos de acción ligados al desequilibrio osmótico provocado por los compuestos. Por una parte, se ha observado cómo estos anionóforos estimulan un aumento en la actividad de proteínas relacionadas con respuesta a estrés celular, y cómo provocan la activación de la vía apoptótica, sin que ésta sea la responsable directa de la muerte de toda la población celular. Conjuntamente, se ha detectado una acumulación de autofagosomas, relacionado con el bloqueo de la autofagia, consecuencia del fallo lisosomal tras el tratamiento con estos compuestos. A su vez, se ha podido observar cómo las células tratadas con estos anionóforos pierden la integridad de la membrana plasmática, indicando que el proceso citotóxico culmina en necrosis en una gran mayoría de la población celular.

Por otro lado, en esta tesis doctoral, mediante experimentos computacionales *in silico,* se ha identificado la proteína AKT como una posible diana molecular de uno de nuestros compuestos. A su vez, se ha corroborado por espectroscopia mediante resonancia de plasmones superficiales, que la afinidad de unión entre el análogo de tambjamina y AKT es elevada, situada en un rango micromolar. Asimismo, se ha detectado una disminución tanto de la fosforilación, como de la proteína total AKT

tras el tratamiento con tambjamina. Igualmente, gracias al estudio de la modificación de los patrones de expresión de miRNA tras el tratamiento con el compuesto, se han dilucidado las principales rutas de señalización involucradas en el proceso citotóxico, siendo las más afectadas PI3K/AKT, apoptosis y autofagia.

Por último, para completar los estudios preclínicos, se ha evaluado la toxicidad y eficacia de estos compuestos *in vivo* en modelos murinos de cáncer de pulmón en estudios preliminares, mostrando una potente capacidad antitumoral tanto en el modelo ectópico como ortotópico.

Por todo esto, los análogos sintéticos de tambjamina pueden ser considerados una buena herramienta para inducir muerte en células cancerosas mediante una nueva estrategia terapéutica que modifica el pH intracelular y podrían llegar a ser buenos fármacos para abordar el tratamiento de tumores resistentes a la apoptosis.

Oral and lung cancer are included in the most prevalent respiratory diseases, being the latter one of the main causes of mortality worldwide. Despite new advances in diagnosis and clinical care, success of conventional treatments is still limited since patients end up developing resistances and presenting recurrences. Due to the therapeutic limitations to address these pathologies, it is necessary to identify new compounds, with different mechanisms of action and greater efficiency to overcome these neoplasms.

Cancer cells acquire a series of characteristics during carcinogenesis, as a reversed pH gradient compared to normal cells, which favors cancer progression promoting proliferation and evasion of apoptosis. Recently, a new therapeutic strategy against cancer, which involves the modulation of intracellular pH has been proposed. Accordingly, our research group is focused on analyzing the potential of anion transporter compounds as new chemotherapeutic agents, since they possess the ability to selectively lower the intracellular pH.

In particular, this doctoral thesis is focused on the anticancer effect characterization, at the cellular and molecular level, of novel anionophores, derived from natural compounds known as tambjamines. Firstly, the effect of the synthetic analogues on cell viability in oral and pulmonary cancer cell lines, as well as in cancer stem cells derived from patients' tumors, has been determined, proving to be potent cytotoxic agents.

Likewise, the implication of ion homeostasis disruption driven by these compounds has been studied at the cellular level. In this regard, it has been characterized how the compounds induce lysosomal alkalization and cause a massive vacuolization in the cytoplasm, which is consistent with mitochondrial swelling. These two phenomena led to the loss of function of both organelles.

At the same time, the mechanisms of action linked to the osmotic imbalance caused by the compounds have been studied in detail. On one hand, it has been observed how these anionophores increase the activity of proteins related to cellular stress response, and how the apoptotic pathway is triggered, although this is not directly responsible for the death of the entire cell population. Likewise, an accumulation of autophagosomes, has been detected after treatment with these compounds,

which might be related to the blockade of autophagy, consequence of the lysosomal failure after treatment with these compounds. Moreover, it has also been observed how the cells treated with these anionophores lose the integrity of the plasma membrane, indicating that the cytotoxic process culminates in necrosis in the vast majority of the cell population.

Besides this, in this doctoral thesis, AKT protein has been identified as a potential molecular target of one of our compounds, using *in silico* docking experiments. In turn, it has been corroborated by surface plasmon resonance that the binding affinity between the selected tambjamine analogue and AKT is high, in the micromolar range. Likewise, a decrease in protein activity and in the total amount of AKT protein has been detected after treatment. Furthermore, the main signaling pathways involved in the cytotoxic process have been elucidated studying the modifications of miRNA expression patterns after the treatment with tambjamine, being the most affected PI3K/AKT, apoptosis and autophagy.

Finally, to complete the preclinical studies, the toxicity and efficacy of these compounds in murine models of lung cancer have been evaluated in *in vivo* preliminary studies, showing a potent antitumor capacity in both ectopic and orthotopic models.

Overall, these synthetic analogues of tambjamine may be considered a good tool to induce death in cancer cells through a new therapeutic strategy that modifies the intracellular pH and these compounds may become a good therapeutic option for apoptosis-resistant tumors.

INTRODUCTION

1. A DEFINITION OF CANCER

Cancer accompanies the human being since ancient times. The origin of the word cancer is credited to the Greek physician Hippocrates (460-370 BC), using the terms *carcinos* and *carcinoma* to describe non-ulcer forming and ulcer-forming tumors. In Greek, these words refer to a crab, most likely applied to the disease because the finger-like spreading projections of a cancer resemble the shape this crustacean (The American Cancer Society, 2014).

After centuries of study and research it is known that our body is constituted by organs, and these in turn by cells, which are divided in a controlled manner in order to maintain their integrity and correct functioning. When control mechanisms cease to function properly, cells divide without control and can invade nearby tissues. This is called a malignant tumor, commonly known as a cancer. That is a term given to a collection of related diseases since it can start almost anywhere in the human body. Cancer cells can also spread to other parts of the body through the blood and lymph systems in a process called metastasis.

1.1. LUNG CANCER

The term lung cancer encompasses multiple epithelial, mesenchymal or lymphoproliferative neoplasms, among others. Of the total number of variants described, 95% correspond to malignant epithelial tumors or carcinomas, which mean that in clinical practice the term lung carcinoma or bronchogenic carcinoma becomes synonymous with lung cancer. Therefore, lung cancer is used to refer to any malignant tumor originated in the lining or glandular epithelium of the bronchial tree (Travis, 2011).

1.1.1. Epidemiology

For many years, lung cancer has been the most commonly diagnosed tumor in developed countries and also the one with the highest mortality. It is a public health problem because its high incidence figures are combined with modest long-term survival rates, despite notable advances in diagnostic and treatment techniques (Torre *et al.*, 2015).

According to statistics, an estimated 1.8 million new lung cancer cases occurred in 2012, accounting for about 13% of total cancer diagnoses worldwide. In terms of incidence, in both men and women is the second most diagnosed type of cancer after prostate and breast cancer, respectively. Lung cancer maintains the highest mortality rates, estimated to be responsible for nearly 1.6 million deaths in 2012, more than the other three leading cancers combined (breast, prostate and colorectal cancer), accounting for approximately 20% of total cancer deaths (figure 1) (Ferlay *et al.*, 2015).

In Spain lung cancer values follow the same trend, being among the most common diagnosed in 2012 with 26,715 new cases and with 21,118 estimated deaths; an increase in incidence is expected to occurs in the following years and more than 40,000 people will suffer this disease in 2035 (SEOM, 2016).

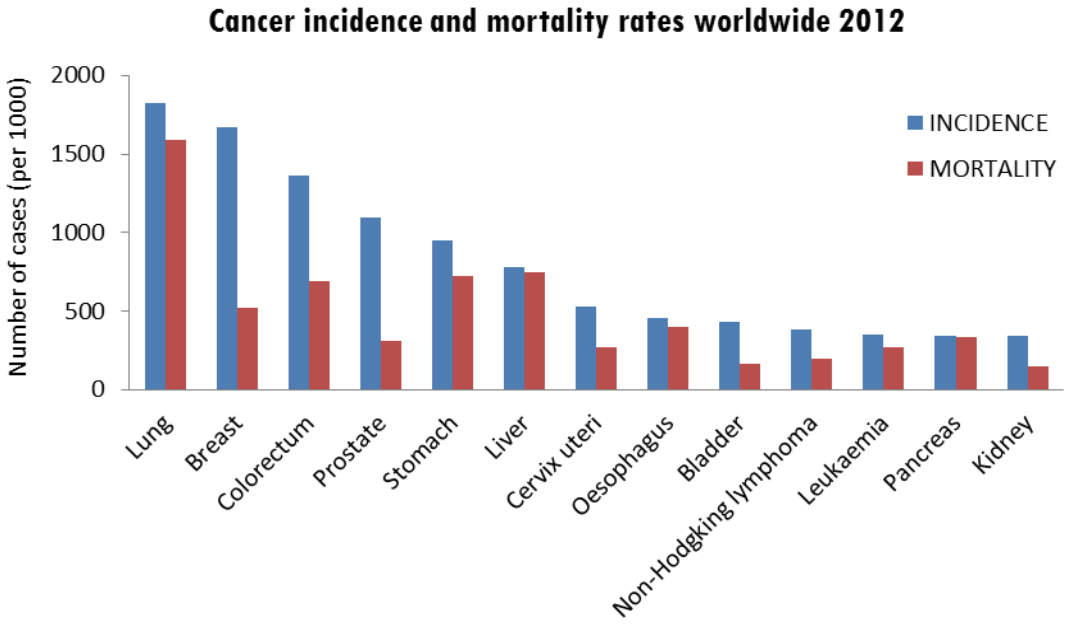

Figure 1. Bar chart showing incidence and mortality of the most commonly diagnosed cancers in 2012. Data acquired from (Ferlay *et al.*, 2015).

1.1.2. Lung cancer risk factors

There are many factors that may contribute to the development of cancer. Cancers are caused by mutations that may be inherited or induced by environmental factors. Moreover, a recent study suggests that mutations due to DNA replication errors are responsible for two-thirds of the total driver gene mutations in human cancer (Tomasetti, Li and Vogelstein, 2017). Determination of the contribution of each factor depends on the type of cancer. According to epidemiological studies, nearly 90% of all lung cancer cases are preventable and linked to direct tobacco smoking. Cigarette smoke contains a complex mixture of chemicals including over 60 identified as carcinogens. The polycyclic aromatic hydrocarbons, such as benzo[a]pyrene and the tobacco-specific nitrosamine known as nicotine-derived nitrosoaminoketone, are the most potent carcinogens. Their catalysis generates electrophilic and reactive intermediates. The covalent binding of these metabolites to DNA leads to mutations and genomic instability (U.S. National Library of Medicine, 2010; Hecht, 2012).

An estimated 10-25% of lung cancers worldwide are not attributable to smoking. To date, epidemiological studies have identified several factors associated with lung cancer in never smokers. They are summarized in figure 2.

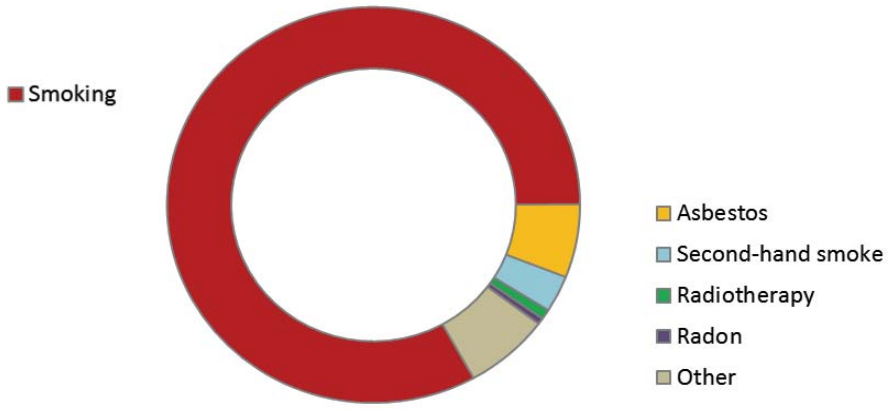

Figure 2. **Estimated causes of lung cancer.** Image adapted from (Bender, 2014).

The exposure to environmental tobacco smoke, due to the same toxic substances diluted in air, is considered a human carcinogen. Among other environmental agents, we can find exposure to radon, an inert gas naturally produced from radium in the decay series of uranium (found in rocks and soil) that is an ubiquitous contaminant of indoor air. Decay of radon results in the emission of α radiation that directly damages DNA in respiratory epithelium (Subramanian and Govindan, 2007).

Another well-established occupational risk factor for lung cancer is asbestos. Asbestos refers to naturally occurring silicate mineral fibers, which have been widely used in industry. The risk for lung cancer from asbestos exposure is dependent on both fiber type and on their biological persistence in the lungs (Sun, Schiller and Gazdar, 2007).

Host factors including family history of lung cancer, history of chronic obstructive pulmonary disease or infections have also been associated with lung cancer risk. It is the case of germline transmission of *EGFR* (epidermal growth factor receptor) gene mutations found in high percentage in both non-smokers and smokers (Couraud *et al.*, 2012).

Indeed, variations in genetic profiles contribute to differential susceptibility to environmental factors. For instance, polymorphisms of cytochrome P450 1A1 genes involved in carcinogens metabolism, or differences in DNA repair capacity also play an important role in lung carcinogenesis (Subramanian and Govindan, 2007).

1.1.3. Diagnosis

The vast majority of lung cancer patients are asymptomatic and symptoms do not appear until the disease is already at an advanced stage. This may delay the diagnosis. For all patients with suspected lung cancer the overall goal is appropriate diagnosis and accurate staging to provide the best possible treatment, but the process is often complex.

To perform an initial screening of the thorax and upper abdomen there are a series of non-invasive imaging tests that can be used such as Computed Tomography (CT), Magnetic Resonance Imaging (MRI) or Positron Emission Tomography (PET).

The most widely used is CT along with PET-CT to assess whether a primary lesion is likely to be malignant, to check possible involvement of regional lymph node and to detect distant metastases (National Collaborating Centre for Cancer, 2011).

To identify the type and stage of lung tumor samples they must be examined through further histopathological test. Biopsies can be obtained through different minimally invasive procedures like bronchoscopy, autofluorescence bronchoscopy, endobronchial ultrasound, thoracentesis or needle aspiration among others.

The pathology report may include immunohistochemical and molecular tests. Classifying the tumor and observing changes in certain genes, such as *EGFR*, *ALK* (anaplastic lymphoma receptor tyrosine kinase) or *KRAS* (Kirsten rat sarcoma viral oncogene homolog), to determine the most accurate type of treatment that can be provided to the patient (American Cancer Society, 2016a).

1.1.4. Histological classification

From the first histological classification of lung tumors carried out by the World Health Organization (WHO) in 1981, considerable progress has been made in the knowledge of pathogenesis, histology and molecular biology of lung cancer, which has resulted in new and successive classifications. Lung carcinomas are classified into two large groups according to the morphology of the tumor cells from which they are derived, non-small cell lung cancer and small cell lung cancer (figure 3). This morphological distinction is related to their molecular biology characteristics and it defines patients with completely different clinical tumor behavior and management (Travis *et al.*, 2010, 2011).

Small cell lung cancer (SCLC)

This group constitutes about 15% of all lung cancers. Although the cell of origin of SCLC has not been formally identified, some papers describe that SCLC displays neuroendocrine markers and is believed to derive from neuroendocrine cells or neuroendocrine progenitors in the lung. It is preferentially located in the central area of the lungs and infiltrates the submucosa leading to narrowing of bronchial airways. It is described as a malignant epithelial tumor consisting of small cells with scant cytoplasm, undefined cell borders, finely granular nuclear chromatin, and absent or inconspicuous nucleoli. They are characterized by their high aggressiveness and rapid growth due to their high mitotic index (Bunn *et al.*, 2016).

Non-small cell lung cancer (NSCLC)

NSCLC accounts for 85% of lung cancers. It arises from the epithelial cells of the central bronchi to terminal alveoli of the lung. NSCLC is a heterogeneous aggregate of histologies. The most common include the following:

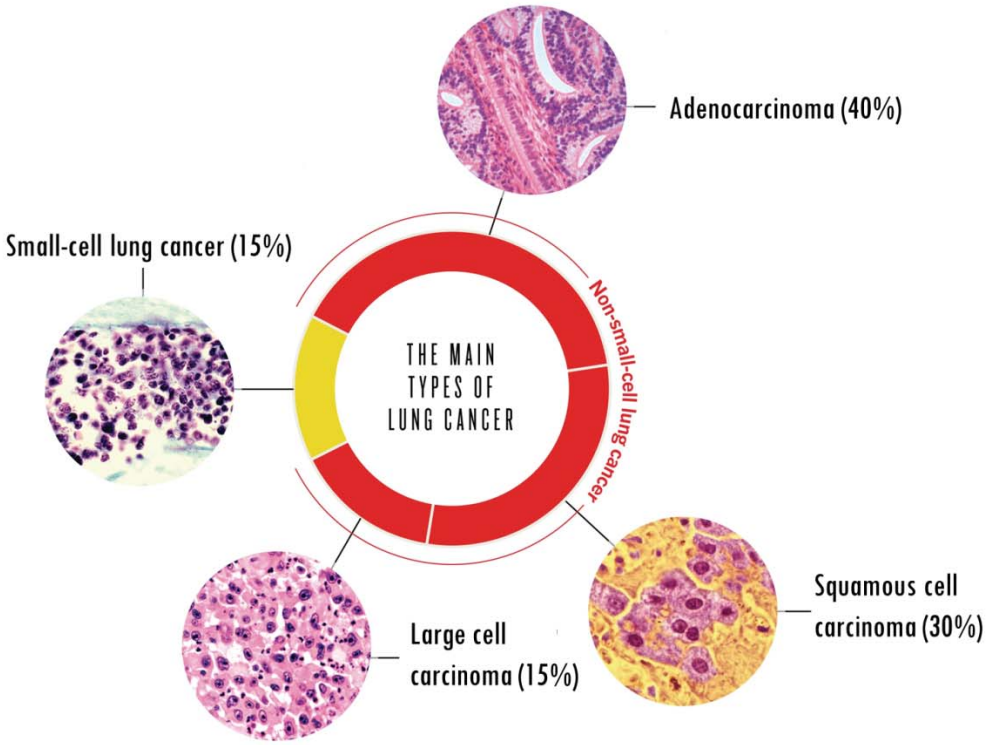

Figure 3. **Main types of lung cancer.** Image adapted from (Bender, 2014).

- **Adenocarcinoma:** originated in peripheral lung tissue, it is the most common subtype, representing 40% of lung carcinomas, and it has a great histologic heterogeneity. According to the WHO definition, adenocarcinoma are all those malignant epithelial tumors with glandular differentiation or mucin production, showing acinar, papillary, bronchioloalveolar or solid with mucin growth patterns or a mixture of these patterns.
- **Squamous or epidermoid carcinoma:** representing 30% of lung cancers, it is a malignant epithelial tumor that presents keratinization and/or intercellular bridges that arises from bronchial epithelium. Squamous carcinoma is usually located in the central part of the lungs, in the main stem, lobar or segmental bronchi. It has a slow growth.
- **Large cell carcinoma:** is the least frequent type of bronchopulmonary carcinomas, representing 15% of them. It is a heterogeneous group of undifferentiated malignant neoplasms with absence of the cytological and architectural features of small cell carcinoma and glandular or squamous differentiation.

1.1.5. Staging

Once lung cancer has been diagnosed, based on the results of physical exams, biopsies and imaging tests, clinical and pathological stages can be determined. Staging is an evaluation of the degree of spread of the cancer from its original source and it affects the prognosis and potential treatment of lung cancer.

The TNM Classification of Malignant Tumors (TNM), a cancer staging notation system, is used to classify NSCLC based on size of the primary tumor (T), lymph node involvement (N), and distant metastasis (M).

Once the T, N, and M categories have been assigned, this information is combined to assign an overall stage of 0, I, II, III, or IV for lung cancer.

- Stage I: tumor mass is smaller than 3 or 5 centimeters and it has not spread to the lymph nodes.
- Stage II: the tumor involves nearby structures and may also have spread to the nearby lymph nodes. The tumor at this stage may be larger than 5 centimeters but less than 7 centimeters.
- Stage III: this stage may indicate large tumors that have grown into nearby structures in the lung, or a smaller tumor and appearance of cancer cells in lymph nodes located in the center of the chest, which is outside the lung.
- Stage IV: cancer has spread over the border of the affected lung to the other lung (within the chest) or to distant areas of the body (Goldstraw *et al.*, 2016).

The TNM classification is also useful in estimating prognosis in SCLC. However, SCLC is traditionally classified as being limited or extensive. Limited indicates cancer is limited to one lung. Extensive indicates cancer has spread beyond the one lung.

1.1.6. Clinical management

The first line treatments are surgery, chemotherapy and radiotherapy. Each of them can be used alone or together. The treatment provided depends on the type and stage of lung cancer, the location of the tumor and general health of the patient.

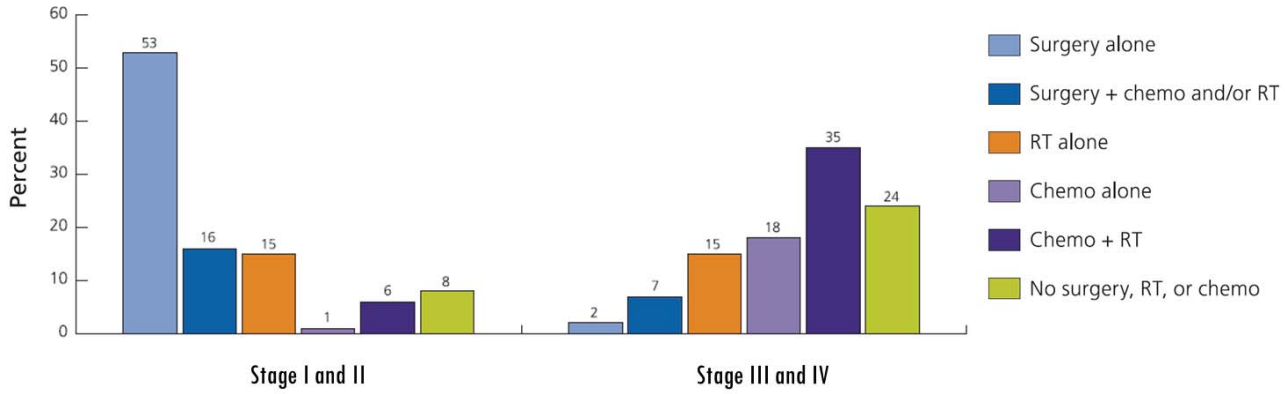

Figure 4. **Non-small cell lung cancer treatment patterns (%) by stage**. Chemo indicates chemotherapy (includes immunotherapy and targeted therapy); RT, radiation therapy (Miller *et al.*, 2016).

Surgery

Most stage I, II and stage III non-small cell lung cancers are treated with surgery to remove the tumor. Depending on its position a wedge resection, lobectomy or pneumonectomy is performed in order to remove a section, a lobe or the whole lung respectively.

The tumor must be removed with a surrounding border or margin of healthy lung tissue and the nearby lymph nodes in the chest to look for possible spread of the cancer (American Cancer Society, 2016b).

Radiation

Radiation therapy is the use of high energy x-rays or other particles to destroy cancer cells. There are two main types of radiation therapy: external beam radiation therapy that center radiation from outside the body on the cancer, and brachytherapy, internal radiation therapy to minimize size tumors in the airway.

Radiation could function as the main treatment, before surgery to shrink the tumor, or after surgery (alone or along with chemotherapy) in order to eliminate small remaining areas of cancer (American Cancer Society, 2016b).

Chemotherapy

Chemotherapy is the use of cytotoxic drugs to destroy cancer cells by disrupting their growth. This strategy is used as a treatment in both SCLC and NSCLC. In the same manner, chemotherapy can be administrated as the main treatment in the case of advanced stages, before or after surgery as adjuvant therapy, or along with radiation therapy.

Chemotherapy drugs tend to be administered in combination of two or more compounds, better than single drugs. In NSCLC, depending on the stage, cisplatin or carboplatin are combined with vinorelbine gemcitabine, paclitaxel, docetaxel, doxorubicin, etoposide or pemetrexed. In the case of SCLC, the chemotherapeutic regimen includes either cisplatin or carboplatin along with etoposide or gemcitabine.

Depending on the individual and the dose used, most of these therapies are associated with side effects since chemotherapy kills uncontrolled dividing cells but also damages healthy tissues that need a replacement of cells. Examples of theses side effects are hair loss, loss of appetite, fatigue, nausea and vomiting, increased chance of infections and easy bruising or bleeding, among others (Cancer Research UK, 2017).

Targeted therapies

As a result of the discovery of certain differentially expressed proteins in tumors compared to healthy tissues involved in growth, progression and spread of cancer in NSCLC patients, the use of targeted therapies has been possible. This approach uses drugs that interfere with these molecular targets blocking cancer development while limiting side effects. The most commonly tested mutations for lung cancer patients are the *EGFR* and *ALK* genes.

EGFR is a transmembrane growth factor receptor with tyrosine kinase (TK) activity. This protein is expressed on the cell surface. The binding of EGFR ligands induces its dimerization and allows the phosphorylation of the receptor. As a result, downstream EGFR signaling pathway is activated leading to increased proliferation, angiogenesis, metastasis, and decreased apoptosis (da Cunha Santos, Shepherd and Tsao, 2011).

For NSCLC patients with reported mutations in *EGFR* gene that result in constitutive TK activity, tyrosine kinase inhibitors (erlotinib, afatiniband gefitinib) are used. These block EGFR activation, which can help stop or slow tumor growth.

A subset of NSCLC patients may express an *ALK* gene mutation as a result of *ALK* and *EML4* (echinoderm microtubule-associated protein-like 4) gene rearrangement, which in turn encodes for an abnormal fusion kinase protein. Activation of its downstream signaling pathway results in uncontrolled cellular proliferation and survival (Shaw and Engelman, 2013). These patients are sensitive to small-molecule ALK kinase inhibitors, such ascrizotinib, ceritinib and alectinib, which induce tumor regression.

Another therapeutic strategy is called anti-angiogenic therapy and is focused on blocking blood vessels growth that keeps the tumor nourished. Monoclonal antibodies as bevacizumab or ramicirumab are used to block VEGF (vascular endothelial growth factor) a protein needed for vessels development, or VEGF receptor respectively (American Cancer Society, 2017b).

Immunotherapy

Recently emerged as a new treatment option, it is designed to boost the immune system in order to recognize and destroy cancer cells more effectively.

It offers new weapons against cancer, for example through modulating immune checkpoints as PD-1 (Programmed cell death protein 1) pathway. PD-1 is a receptor expressed on the surface of activated T cells. Its ligand PD-L1 is present on the surface of the antigen presenting cells. Their interaction functions as a checkpoint, limiting T cell effector response within tissues in order to ensure that the immune system is active only at the right time, avoiding the possibility of chronic autoimmune inflammation. Tumor cells take advantage of this feature and overexpress PD-L1 to evade detection and inhibit the immune response.

For this reason in squamous carcinoma was approved the use of nivolumab, a monoclonal antibody that blocks the PD-1 and induces sustained tumor regression (Pardoll, 2012).

It must be considered that immunotherapy is not suitable for everyone, since it is a very effective treatment for some cancer patients but not for others. Moreover, the rest of therapies may lose effectiveness if cancer cells develop mechanisms of resistance to chemotherapy or activate compensatory signaling loops, in the case of targeted therapies. Therefore, new drugs and therapeutic approaches need to be designed for lung cancer treatment.

1.2. ORAL CANCER

Encompassed within the category of head and neck cancer, the term oral cancer includes any cancerous tissue growth located in the oral cavity. Tumors that are located at the end of the oral cavity, in the oropharynx, are known as oropharyngeal cancer.

1.2.1. Epidemiology

Globally, lip, oral cavity, and pharyngeal cancers have been estimated to be responsible for 529,500 incident cases and 292,300 deaths in 2012, representing approximately 3.8% of all cancer cases and 3.6% of cancer deaths (Ferlay *et al.*, 2015). In particular, an estimated 300,400 new cases and 145,400 deaths occurred that year from oral cavity cancer worldwide. It is a major public health problem since it carries a considerable mortality rate, being strongly associated to the stage of the disease (Torre *et al.*, 2015). Moreover, oral cancer is one of widely prevalent cancers types worldwide with highest prevalence rate reported in developing countries (Gupta *et al.*, 2017).

1.2.2. Oral cancer risk factors

As in all types of cancer, the likelihood of a person developing oral cancer depends on many variables including age, genetics and exposure to risk factors. Among them, lifestyle factors such as tobacco and alcohol consumption appears to be the major determinants. On one hand, tobacco in its different forms, including smoking, chewing and in betel quid have carcinogenic impact in oral cavity. On the other hand, alcohol increases the risk of suffering oral cancer since it may facilitate the entry of carcinogens into the exposed cells (Ram *et al*., 2011).

Biological factors like human papillomavirus (HPV), syphilis and dietary deficiencies can raise the risk of developing oral cancer (Walker, Boey and McDonald, 2003). HPV infection, more common in recent years, has been connected to a subset of oral cancers, especially the one that is caused by the strain HPV-16 (Martín-Hernán *et al.*, 2013).

1.2.3. Diagnosis

Oropharyngeal cancers may be found early during regular dental examinations. Nevertheless, these cancers have a tendency to be detected at an advanced stage as a consequence of symptoms absence in previous stages.

Evaluation of the oral cavity and oropharynx is mostly done by clinical examination and endoscopy (pharyngoscopy, laryngoscopy or panendoscopy techniques). Once tumor has been spotted, tissue samples are taken by exfoliative cytology, incisional biopsy or fine needle aspiration (FNA) biopsy. The histopathological study provides information about the alterations and the malignancy degree of the tissue, which allows tumor classification. Furthermore imaging test, such as CT, PET or MRI, are used for staging and allow to determine size, thickness and depth of the pathology beneath the mucosa, and detects invasion of nearby structures (American Cancer Society, 2017a).

1.2.4. Classification

More than 90% of cancers of the oral cavity and oropharynx are squamous cell carcinomas because oropharynx origin tissue is lined with stratified squamous epithelium. The presence of minor salivary glands, fibromuscular structures, and lymphoid tissue opens the possibility to a variety of less frequent tumors like salivary gland tumors, intra-oral sarcomas (Kaposi's sarcoma), mucosal malignant melanoma and lymphomas among others (IARC, 2005).

1.2.5. Staging

The severity of oropharyngeal cancers is based on TNM staging criteria and they are classified in five main stages:

- Stage 0 refers to cancer that has not spread and has stayed exactly where it began, also known as carcinoma *in situ*.
- Stage I refers to a 2 centimeters or less tumor mass which has not spread to the lymph nodes or to surrounding areas.
- Stage II corresponds to those tumors of size between 2 and 4 centimeters, which have not spread.
- Stage III includes tumors larger than 4 centimeters which has not spread to the lymph nodes or any size primary tumor that may have extended to the lymph nodes.
- Stage IV is further divided into 3 sub-stages (IVA, IVB and IVC). This stage encompasses any size tumor with lymph node and distant metastases.

Determining the stage of the tumor is the key to provide a suitable treatment option for patients and predicting their prognosis (Chi, Day and Neville, 2015).

1.2.6. Clinical management

Treatment for oral cancer heavily depends on the stage of the disease and its location. The main treatment options for these types of cancers are surgery, radiation therapy and chemotherapy.

For early stage cancers, either radiation alone, to shrink the tumor, or surgery alone are indicated. Advanced cancers require combinations of surgery followed by radiation and/or chemotherapy.

Depending on the tumor location and its dissemination the surgical process required may be different, including: Mohs micrographic surgery for lip cancers, glossectomy (removal of the tongue), mandibulectomy (removal of the jaw bone), maxillectomy or even neck dissection to remove lymph nodes.

Chemotherapy may be prescribed before radiation therapy or surgery to reduce the size of a tumor or may also be dispensed in conjunction with radiation treatments. Combination of cisplatin, carboplatin, 5-fluorouracil, paclitaxel or docetaxel, are the drugs most commonly used for these cancers.

Targeted therapies are also applied with chemotherapy, for instance, cetuximab is used to block the EGFR receptor present in oral cancer tumor cells, reducing tumor growth (American Cancer Society, 2017c).

1.3. CARCINOGENESIS

Carcinogenesis is a multistage process whereby normal cells are transformed into cancer cells undergoing metabolic and behavioral changes, leading them to proliferate uncontrollably. These changes arise through genetic or epigenetic alterations, modifying DNA sequence or chromatin conformation, in proto-oncogenes, tumor suppressor genes, and DNA repair genes. Together, these mutations may cause the cells to become cancerous because these genes are involved in controlling cell division, differentiation, and survival, processes that have to be strictly regulated to ensure the integrity of tissues and organs (Weinberg, 1996).

Therefore, cancer develops from normal tissues through the accumulation of genetic alterations that confer a malignant phenotype. There are different theories about which cell population undergoes these changes and causes cancer.

The classical theory of multistage carcinogenesis can be divided into four stages: tumor initiation, tumor promotion, malignant conversion, and tumor progression. These stages may progress over many years. The carcinogenic process can be initiated by the presence of a mutation in a cell, generally an epithelial cell, which confers to the cell some advantage over its proliferation or survival ability. The mutated cell undergoes a clonal expansion that will allow generating a cellular population where other mutations can accumulate, a condition termed hyperplasia. Besides excessive proliferation, descendant cells appear abnormal in form and orientation. This anomalous development is known as dysplasia. The process evolves through multiple cycles of clonal mutation and expansion, and the contribution of increased genome instability becoming an *in situ* cancer. This tumor may remain contained indefinitely, or maybe some cells may undergo genetic changes that facilitate the invasion of the surrounding tissue and the entry of tumor cells into the blood or lymph. In that moment, the mass has become malignant. Invasive cells are likely to establish new tumors (metastases) throughout the body and these can become lethal by disrupting a vital organ (figure 5) (Sherman, 2005; Talmadge and Fidler, 2010).

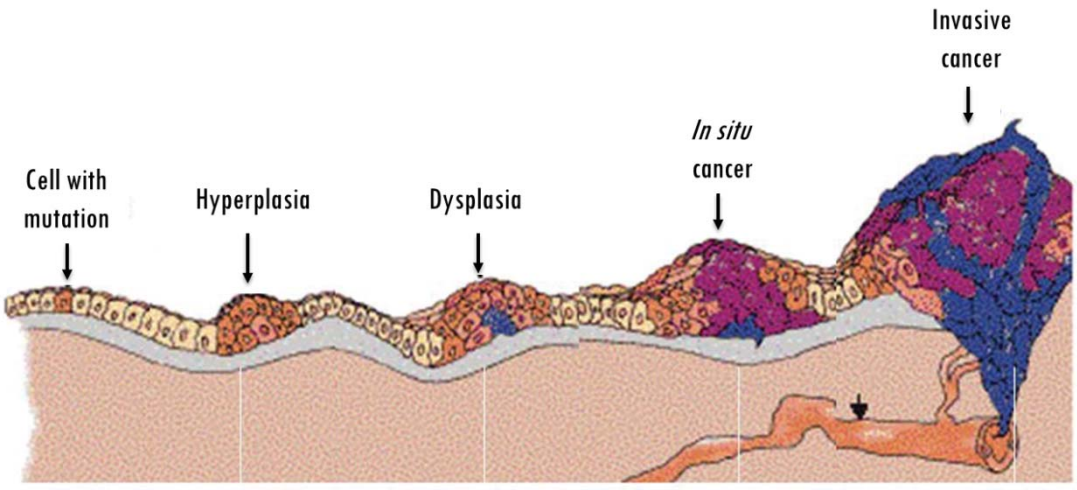

Figure 5. Stages in the tumor development. Adapted from How Cancer Arises (Weinberg, 1996).

More recently, the cancer stem cell hypothesis proposes that cancer arises from organ-specific stem cells transformation. These cells have inherent properties such as self-renewal and the ability to migrate to distant parts of the body. As a result of this, tumors are composed of multiple cell types and maintained by pluripotent stem cells. Understanding the biology of carcinogenesis is crucial to develop effective therapeutic strategies (Polyak and Hahn, 2006; Wicha, Liu and Dontu, 2006).

1.3.1. Hallmarks of cancer

Douglas Hanahan in collaboration with Robert A. Weinberg made a compilation of all those factors that differentiate a normal cell from a cancerous one, those that allow them to grow out of control and become invasive (figure 6) (Hanahan and Weinberg, 2011). The essential alterations in cell physiology that collectively dictate malignant growth are:

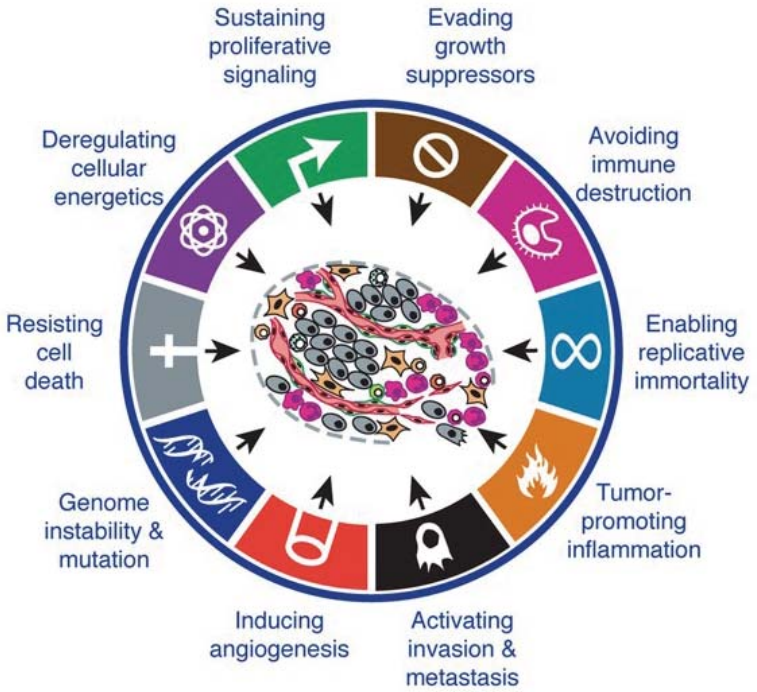

Figure 6. Hallmarks of cancer. Adapted from Hanahan & Weinberg, 2011.

- **Self-sufficiency in growth signals.** Normal tissues carefully control the production and release of growth-promoting signals in order to ensure tissue homeostasis. The presence of these signals allows the growth and division of the cells; its absence determines that the cell cycle stops. However, cancer cells do not require stimulation from external signals to propagate. Actually, cancer cells can either produce their own growth factors (resulting in autocrine proliferative stimulation), or they constitutively activate components of proliferative signaling pathways, without the need to stimulate these pathways by ligand-mediated receptor activation (Hanahan and Weinberg, 2011).

- **Insensitivity to growth-inhibitory signals.** In normal tissue, proliferation is blocked by growth inhibitory signals that control cell division. However, cancer cells become insensitive to these signals that might otherwise stop and regulate their growth. This is usually the result of mutations

in tumor suppressor genes. Some of the most relevant are the RB (retinoblastoma-associated) and TP53 (tumor protein p53) proteins, which govern the decisions of cells to proliferate or, alternatively, activate senescence and apoptotic programs, respectively. Moreover, as the tumor expands, it exerts pressure on tissue adjacent tissue, which emits chemical messages that would normally block cell division. Cancer cells proliferate evading these contact inhibition mechanisms issued by neighboring cells (Hanahan and Weinberg, 2011).

- **Evasion of programmed cell death (apoptosis).** Apoptosis is a form of programmed cell death, the mechanism by which cells are programmed to die in the event they become old or damaged. In this manner, growth is limited and cells with damaged DNA are discarded, preventing propagation of errors in the body. Cancer cells progress avoiding apoptosis. Apoptosis signals can be disrupted when there is a defect in tumor suppressor genes such as p53 (gene that elicits apoptosis in response to DNA damage), or apoptosis machinery proteins suffer mutations (Hanahan and Weinberg, 2011). In response to diverse intracellular damage signals, whether a cell undergoes apoptosis or not relies on the interactions between members of BCL-2 (B-cell lymphoma 2) family (pro and antiapoptotic proteins). Overexpression of a pro-survival family member or loss of a proapoptotic relative leads to an impaired apoptosis, critical in cancer development (Adams and Cory, 2007).

- **Limitless replicative potential.** Healthy cells have a determined lifespan, they are able to undergo only a limited number of successive cell growth-and-division cycles (approximately 100 times according to the Hayflick limit (Hayflick, 1965) until cell enters into a phase of senescence (non-proliferative but viable state) or cell dies (phase of crisis, which involves cell death). The machinery for controlling how many times a cell divide depends on the telomeric DNAs at the ends of chromosomes. The telomeres are specialized sequences that operate to prevent end-to-end fusion of chromosomes. Every time the cell divides, the telomeres are shortened. Eventually, the loss of telomeres reaches a critical point in which the DNA is unprotected, and the cell dies. In non-immortalized cells, the telomerase, a specialized DNA polymerase, that is able to extend the telomeres, is absent. Nevertheless, malignant cells are able to overcome the proliferative limit, since they express telomerase at functionally significant levels. This enzyme protects the ends of chromosomes from this erosion, maintaining telomeric DNA length sufficient to avoid triggering senescence or apoptosis (Hanahan and Weinberg, 2011).

- **Sustained angiogenesis.** Angiogenesis is the process by which new blood vessels are formed. Like normal tissues, tumors need a system to bring in nutrients and take out wastes. In an organism under normal conditions, angiogenesis is turned on transiently, new blood vessels are formed during the development of embryos, during wound repair and during the female reproductive cycle. The balance between pro and anti-angiogenic factors modulates endothelial cell proliferation and motility. This is known as angiogenic capability. During tumor progression, an ‘‘angiogenic switch’’ is almost always activated. An unbalanced mix of pro-angiogenic signals stimulate formation of new blood vessels into the tumor mass to supply it with adequate nutrients just like any organ in the body (Hanahan and Weinberg, 2011).

- **Tissue invasion and metastasis.** Cancer cells, unlike normal cells, can metastasize, that is, destroy tissue barriers to invade surrounding tissue and spread to distant body organs. This is strongly linked to the level of malignancy of a tumor. Malignant cells have to undergo a series

of rapid changes in cellular phenotype also known as epithelial-mesenchymal transition (EMT). During EMT, epithelial cells down-modulate cell-cell adhesion structures, alter their polarity and reorganize their cytoskeleton, acquiring mesenchymal features in order to invade, resist apoptosis, and disseminate (Klymkowsky and Savagner, 2009; Polyak and Weinberg, 2009).

- **Reprogramming of energy metabolism.** The chronic uncontrolled cell proliferation that represents the essence of tumor progression involves adjustments of energy metabolism in order to boost growth and cell division. Under physiological conditions, the cell gets energy through cellular respiration, a set of metabolic reactions which encompasses three main stages: glycolysis, tricarboxylic acid cycle (TCA) and oxidative phosphorylation (OXPHOS). First, during glycolysis glucose, a six carbon sugar, is split into two molecules of a three carbon sugar (pyruvate). This process can occur with or without oxygen in the cytoplasm. In presence of oxygen, these molecules are metabolized through TCA and OXPHOS in the mitochondria, obtaining a large amount of ATP (adenosine-5'-triphosphate). Cancer cells suffers a "metabolic switch", known as Warburg effect, characterized by fermentation (aerobic glycolysis) of glucose to acid lactic (Warburg, 1956) even in the presence of normal levels of oxygen and completely functioning mitochondria (Liberti and Locasale, 2016). Converting glucose to acid lactic is far less efficient as less ATP is generated per unit of glucose metabolized. Therefore, cancer cells upregulate glucose transporters, notably GLUT1, which substantially increases glucose import into the cytoplasm to support rapid tumor progression (Liberti and Locasale, 2016).

- **Evasion of immune destruction.** According to the concept of cancer immunosurveillance proposed in 1909 by Ehrlich (Ehrlich, 1909), the host immune system behaves like a significant barrier to tumor formation and progression because emerging cancer cells and nascent tumors are constantly identified and eradicated. However, successful cancers manage to avoid detection long enough to develop in patients with a fully functional immune system. The concept of immunosurveillance has been updated and refined into a theory termed 'immunoediting' (Mittal *et al*., 2014), in which host immune system shapes tumor fate in three phases:

    - **Elimination**, where innate and adaptive responses detect and destroy early tumors before they become clinically visible.
    - In the **equilibrium** phase, the immune system holds the tumor in a quiescent state thanks to a balance between anti-tumor (IL-12, IFN-γ) and tumor promoting cytokines (IL-10, IL-23). Due constant immune pressure some cancer cells may develop new adaptations to evade immune recognition and induce immunosuppression, which finally lead to cancer progression (causing clinically apparent disease).
    - **Escape phase** can be mediated through various mechanisms, such as reduced immune recognition (antigen loss or defects in antigen-presentation), increased resistance to immune cells attack or the development of an immunosuppressive tumor microenvironment (PD-1) (Mittal *et al.*, 2014; Muenst *et al.*, 2016).

Moreover, the authors described two enabling characteristics of neoplastic cells that facilitate acquisition of hallmark capabilities: genome instability and tumor-promoting inflammation.

- **Genome instability.** The genetic information of a cell (DNA) is encoded in genes, and in turn these are packaged in chromosomes within the cell nucleus. DNA can suffer damage and mutations including deletion of whole genes, or addition of extra copies of genes. This is called genomic instability. These changes may happen through the deregulation of any of these mechanisms: DNA replication in S-phase, chromosome segregation in mitosis, and DNA repair (Shen, 2011). An increased tendency of these alterations in the genome (especially in oncogenes, tumor suppressor genes or DNA repairing genes) during cell cycle promotes the acquisition of cancer hallmarks. This affects to the probability and rate of cancer development (Hanahan and Weinberg, 2011).
- **Tumor-promoting inflammation.** In response to tissue injury, a multifactorial network of chemical signals initiates in order to heal the afflicted tissue. The acute inflammatory response is normally localized and is protective. This involves activation and directed migration of immune leukocytes (neutrophils, monocytes and eosinophils) from the venous system to damaged sites. These cells in turn are capable of producing cytokines and cytotoxic mediators that dictates the natural evolution of the inflammatory response. Tumor cells produce various cytokines and chemokines that also attract eukocytes into the tumor mass leading to a chronic tumor-associated inflammatory response (Coussens and Werb, 2002). Tumor-associated macrophages (TAMs), derived from circulating monocytes, contribute to hallmarks capabilities by supplying bioactive molecules to the tumor microenvironment, including growth factors to promote tumor development, survival factors that limit cell death, pro-angiogenic factors, extracellular matrix-modifying enzymes that facilitate angiogenesis, invasion, and metastasis, and inductive signals that lead to activation of EMT. Moreover, inflammation is a source of reactive oxygen species (ROS) that are capable of inducing DNA damage and genomic instability (Grivennikov, Greten and Karin, 2010; Hanahan and Weinberg, 2011).

1.3.2. Tumor microenvironment and cancer stem cells

Tumors are not just masses of cancer cells, they can be considered as a complex organ, to which many other cells are recruited and can be corrupted by the transformed cells. It includes cells of hematopoietic and mesenchymal origin, and non-cellular components (Balkwill, Capasso and Hagemann, 2012; Mittal *et al.*, 2016).

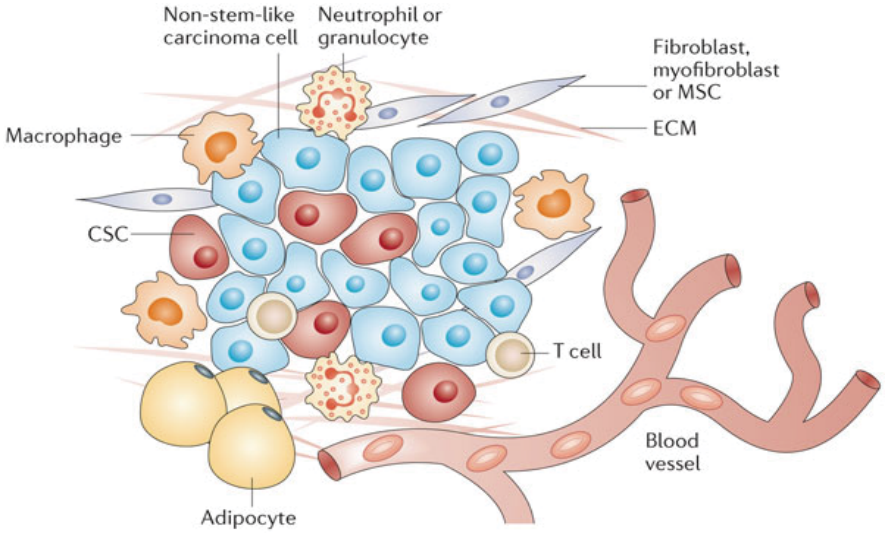

Figure 7. Scheme of tumor microenvironment cells types (Pattabiraman and Weinberg, 2014).

- Cells of hematopoietic origin arise from the bone marrow and are subdivided into cells of the lymphoid lineage (T cells, B cells and natural killer cells) and those of the myeloid lineage (macrophages, neutrophils and myeloid-derived suppressor cells).
- Cells of mesenchymal origin encompass fibroblasts, myofibroblasts, mesenchymal stem cells, adipocytes and endothelial cells. Interactions between malignant and non-transformed cells create the tumor microenvironment.
- Non-cellular components include proteins (type IV collagen, laminin and fibronectin), glycoproteins and proteoglycans that form the extracellular matrix.

Among the cancer cells of a tumor, cancer stem cells (CSC) are a class of pluripotent cells that possesses a capacity for sustained self-renewal, able to divide into another CSC and/or to differentiate into some of the spectrum of cell types observed in tumors through stemness pathways, such as Wnt, TGF-β, STAT, and Hippo-YAP/TAZ, among others. Usually, in normal stem cells, these pathways are strictly regulated; in contrast, stemness pathways in CSCs are significantly dysregulated (Ajani *et al.,* 2015).

The origin of CSCs within a solid tumor may be diverse. In some tumors, normal tissue stem cells may undergo oncogenic transformation into CSCs. In others, the EMT process, in which epithelial cells are transformed into a mesenchymal phenotype, may involve acquisition of stemness (Chang, 2016).

CSCs have been involved in tumor development, cell proliferation, and metastatic dissemination in numerous cancer models. This kind of cells also exhibits resistance to chemotherapy and radiotherapy, being responsible for tumor recurrences. The mechanisms underlying acquired resistance are an active area of investigation, since tumors become insensitive to conventional treatments, leading to tumor progression and relapse (Vidal *et al.*, 2014). Therefore, the identification and characterization of CSCs has revealed the need for developing specific therapies that target the key signaling pathways supporting proliferation of these cells.

1.3.3. Metabolic adaptations of cancer cells

Metabolism is the term that is used to describe the integrated network of chemical reactions involved in sustaining growth, proliferation and survival of cells. These reactions are carried out by enzymes and are regulated by signaling pathways that respond to specific cellular needs. In particular, tumor cells have to alter their metabolism in order to satisfy the energetic and biosynthetic demands associated to a higher rate of growth and division (Cairns, Harris and Mak, 2011).

In this regard, the different hallmarks of cancer metabolism have recently been compiled by Pavlova and Thompson. In summary, they describe that cancer metabolic alterations affect, on one hand, the metabolite influx, conferring an increased ability to acquire the necessary nutrients from a frequently nutrient-poor environment. On the other hand, metabolic remodeling involves changes in the way nutrients are used in specific metabolic pathways to sustain cancer cell demands. In turn, long-term effects on cell fate take place, including alterations in gene regulation driven by diverse metabolites, and alterations in tumor microenvironment, which reciprocally affects the cancer cell metabolism and signaling to support tumor growth and dissemination (Pavlova and Thompson, 2016).

To maintain cellular process and rapid cell division, proliferating tumor cells need to generate energy from glucose. Predominantly, these cells shift ATP generation from OXPHOS to aerobic glycolysis (Warburg effect). As a result, cancer cells produce energy from incoming glucose by glycolysis followed by lactic acid fermentation in the cytosol, rather than by glycolysis followed by oxidation of pyruvate in the mitochondria, as most normal cells do. Aerobic glycolysis generate less ATP per unit of glucose consumed than OXPHOS, therefore cancer cells must increase the import of glucose to sustain their increased energetic, biosynthetic and redox needs (Cairns, Harris and Mak, 2011). Although this process has a lower energetic yield, it produces ATP faster than OXPHOS and provides selective advantages to cancer cells such as maintenance of the appropriate balance of ROS, high production of metabolic intermediates for macromolecular biosynthesis and acidification of extracellular microenvironment due to lactate excretion (Liberti and Locasale, 2016).

This metabolic reprogramming of tumor cells derives from alterations in multiple signaling pathways: the activation of PI3K (phosphatidylinositol 3-kinase), C-MYC (myelocytomatosis virus oncogene cellular homolog) and hypoxia-inducible factor HIF1, or the loss-of-function mutations in tumor suppressor TP53 and liver kinase B1 (LKB1) contribute to the glycolytic phenotype (Cairns, Harris and Mak, 2011).

1.3.4. Dysregulated pH in cancer cells

High proliferative and glycolytic rates generate large amounts of H^+ (including lactic and carbonic acids, which are end products of metabolic pathways). This creates the problem of intracellular acidification and lactate accumulation. To avoid acidification of intracellular pH, tumor cells have changed the expression and/or activity of plasma membrane ion pumps and transporters that facilitate acidic catabolites efflux and preserve a slightly alkaline intracellular pH (pH_i) (Neri and Supuran, 2011; Schulze and Harris, 2012; Parks *et al*., 2013).

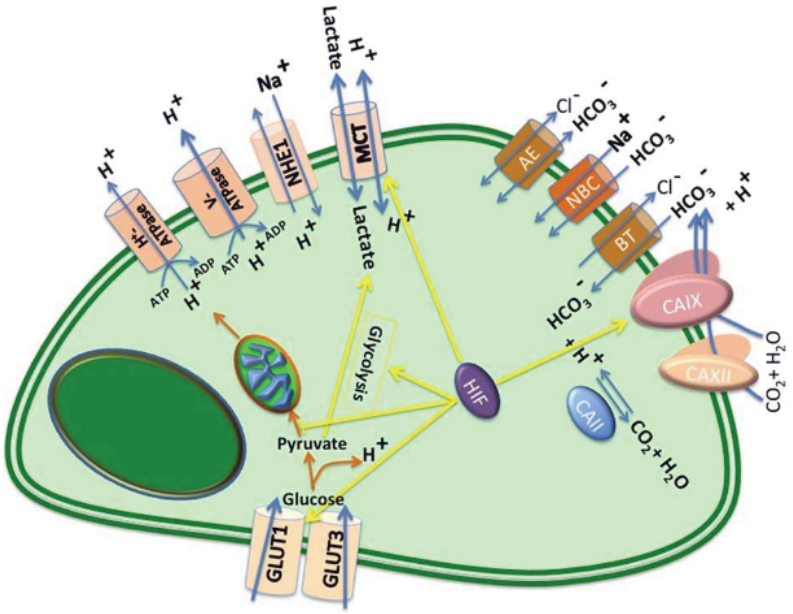

Figure 8. Major pH regulators in a cancer cell (Damaghi, Wojtkowiak and Gillies, 2013

The main acid-regulatory systems implicated in the pH regulation of cancer cells involve Na^+/H^+ exchangers (NHEs), carbonic anhydrases (CAIX and CAXII), HCO^{3-} transporters, monocarboxylate transporter 1 (MCT1) and MCT4, also known as lactate/H^+ symporters and intracellular H^+ pumps (Damaghi, Wojtkowiak and Gillies, 2013; Parks et al., 2013). Among them, the most important and most studied proton transporter is Na^+/H^+ exchanger isoform 1, NHE1. Its elevated activity in cancer is considered to be the major factor in promoting tumor extracellular acidity, and contributing to malignant cellular transformation and tumor development (Alfarouk *et al.*, 2014).

As a result of overexpression and increased activity of these transporters, a reversion of the normal pH gradients occurs, so that cancer cells cause a significant acidification of the extracellular microenvironment, decreasing pH values from 7.4 to 6.7-7.1, while they maintain an alkaline pH_i of 7.4 in comparison with normal values of 7.2 (Webb *et al.*, 2011).

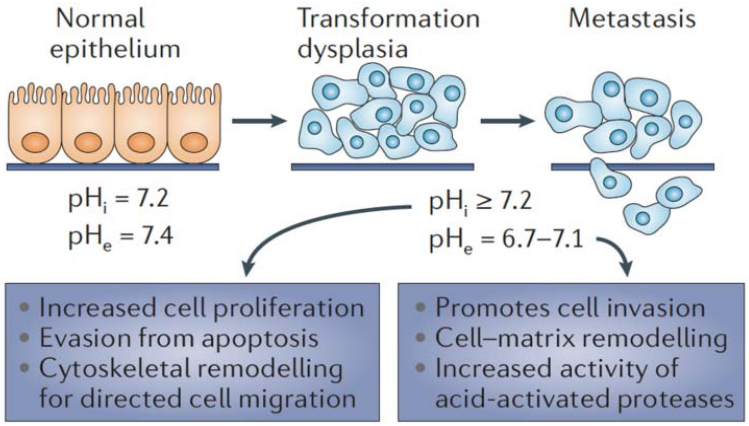

Figure 9. Reversed pH gradient supports cancer progression (Webb *et al.*, 2011).

Maintaining an alkaline intracellular milieu is a permissive signal for cell proliferation because it increases the rate at which cells enter in S-phase and progress through the G2/M phases, and also confers the adaptive advantage of bypassing cell cycle checkpoints (Webb *et al.*, 2011). Moreover,

the sustained higher pH_i is essential for cancer-cell survival since intracellular acidification is related to apoptosis (Lagadic-Gossmann, Huc and Lecureur, 2004). This pH_i change facilitates a metabolic adaptation promoting glycolysis because the activity of the enzymes lactate dehydrogenase (LDH) and phosphofructokinase 1 (PFK1), which regulate this process, increases at alkaline pH (White, Grillo-Hill and Barber, 2017). Finally, increased pH_i promotes actin remodeling and focal adhesion turnover necessary for efficient cell migration. On the other hand, acidification of the extracellular microenvironment provides the optimal conditions for matrix metalloproteinases and acidic proteases (urokinase-type plasminogen activator, cathepsin D, B and L) to degrade extracellular matrix, supporting cancer-cell invasion and metastasis (Stock and Schwab, 2009; White, Grillo-Hill and Barber, 2017).

1.3.5. Dysregulated pathways in cancer

The carcinogenesis process at the molecular level is mainly the result of alterations in different proteins of cell signaling pathways that control processes such as survival, proliferation or differentiation. Among all signaling pathways, some of them seem to be altered in the vast majority of cancers, such as PI3K/AKT/mTOR (mechanistic target of rapamycin) and MAPK. On the other hand, alterations in microRNAs also lead to the deregulation of cellular homeostasis, being able to induce the process of carcinogenesis.

1.3.5.1. PI3K/AKT pathway

Since its identification as a proto-oncogene, the serine-threonine kinase AKT, also known as protein kinase B (PKB), has taken a key role in the PI3K pathway, regulating a wide range of physiological functions including metabolism, proliferation, survival, growth, angiogenesis, migration and invasion (Toker and Marmiroli, 2014). AKT belongs to the AGC family of protein kinases and exists as three isoforms in mammals: AKT1 (PKBα) and AKT2 (PKBβ), expressed in most tissue types, and AKT3 (PKBy), expressed in testes and brain. The isoforms share three conserved functional domains: an amino-terminal pleckstrin homology (PH) domain that regulates intracellular trafficking of the protein, a central catalytic domain, and a carboxy-terminal regulatory domain (Davies, 2011).

Activation of AKT isoforms is dependent on PI3K stimulation with the binding of growth factors, hormones, and cytokines to the receptor tyrosine kinase (RTK), cytokine receptor, or GPCR (G protein–coupled receptor) at the plasma membrane. This binding results in a subsequent increase of PIP3 (3-phosphorylated phosphatidylinositol) that recruits AKT through its PH domain to the cell membrane. Once there, AKT is activated through a dual phosphorylation mechanism. PDK1 (Pyruvate dehydrogenase kinase, isozyme 1), which also possesses a PH domain that facilitates its binding to the plasma membrane, phosphorylates AKT within its activation loop at threonine 308. To stabilize the activated conformation of AKT, a second phosphorylation at serine 473 within the carboxy terminus is also required and is carried out by the mammalian target of rapamycin complex, mTORC2 (Davies, 2011).

Another way to activate the AKT pathway implies the disruption of its negative feedback mechanisms. The lipid phosphatase PTEN (phosphatase and tensin homolog) is a tumor suppressor that catalyzes the dephosphorylation of PIP3 acting as a negative regulator of AKT. The loss of PTEN function is correlated with many human cancers (Zhang and Yu, 2010). AKT activity is also negatively regulated by phosphatases (PP2A, PHLPP1, PHLPP2) that dephosphorylate AKT itself (Davies, 2011).

Activated AKT regulates a variety of cellular processes through the phosphorylation of its downstream substrates, some of which are illustrated in figure 10.

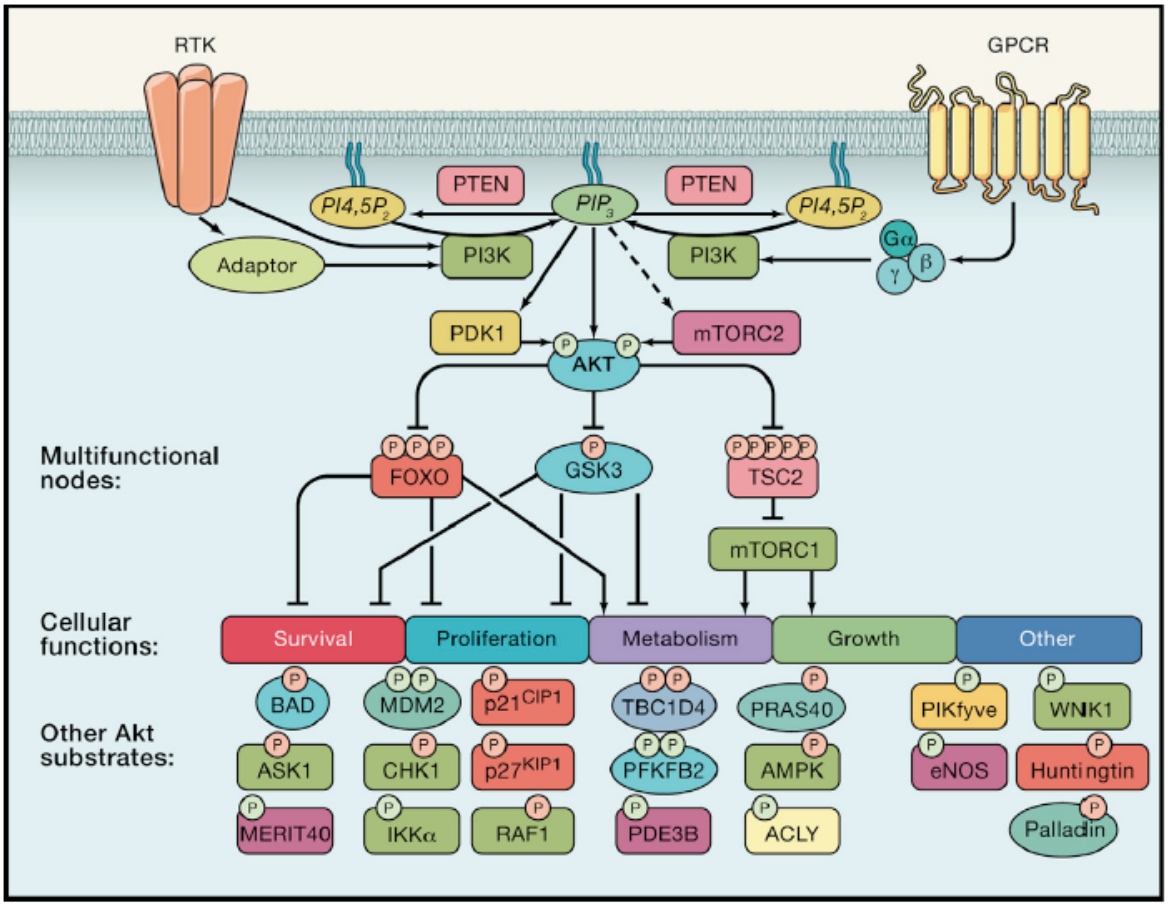

Figure 10. **AKT signaling pathway** (Manning and Toker, 2017).

AKT promotes cell growth and protein synthesis through activation of the mTOR signaling pathway, directly or indirectly blocking its inhibitor protein TSC2 (tuberous sclerosis 2). Through inhibitory phosphorylation of GSK-3 (glycogen synthase kinase 3), AKT exerts a role on cell metabolism, increasing the glycogen storage and also stimulating cell cycle progression. AKT controls cell survival via the negative regulation of some proapoptotic BCL-2 family members such as BAD, BIM and BAX and members of the FOXO factors (Forkhead family of transcription factors) (Hers, Vincent and Tavaré, 2011).

As a result of the central role of Akt in several biological processes, aberrant signaling of this protein is found in different pathologies other than cancer, such as diabetes or cardiovascular diseases (Hers, Vincent and Tavaré, 2011).

1.3.5.2. MAPK pathways

Mitogen-activated protein kinases (MAPKs) are a highly conserved family of protein kinases that mediate intracellular signaling and control a large number of elemental cellular processes. A broad range of extracellular stimuli such as mitogens, cytokines, growth factors, and environmental stressors initiate a cascade of three core kinases. This starts with the activation of MAPKK kinases (MAPKKKs) through interactions with GTPases or phosphorylation by protein kinases downstream

from cell surface receptors. Then the MAPKKK directly phosphorylates and activates the MAPK kinase (MAPKK), which in turn, activates the MAPK by phosphorylation. Activated MAPKs phosphorylate various substrate proteins including transcription factors, resulting in regulation of a variety of cellular activities including growth, proliferation, differentiation, migration, stress response, and survival and apoptosis (Morrison, 2012).

The MAP kinases can be classified into four main groups: ERKs (extracellular-signal-regulated kinases), JNKs (Jun amino-terminal kinases), BMK (Big MAP kinases) and p38/SAPKs (stress-activated protein kinases). The p38 MAP kinases, one of the main families, are strongly activated in response to stress signals, growth factors, and inflammatory cytokines (Koul, Pal and Koul, 2013). These stimuli entail that MAPKKK, typically a MEKK or a mixed kinase (MLK), phosphorylates and activates MKK3/6 and these in turn activate p38 MAPK. Phosphorylated p38 MAPK is involved in activation of a wide range of substrates that include transcription factors, protein kinases, cytosolic and nuclear proteins. Therefore the downstream activities attributed to these phosphorylation events are diverse. In cancer, p38 MAPK function is considered as tumor-suppressive since its activation is associated with suppression of malignant phenotype development. According to several publications, p38 MAPK decreases cell proliferation through cell cycle arrest and regulates cell survival promoting apoptosis or cellular senescence (Coulthard *et al.*, 2009).

1.3.5.3. MicroRNA regulation

In recent years, there has been a growing interest to investigate the role of microRNAs in cancer since its dysregulation has been shown to favor the hallmarks of cancer. MicroRNAs (miRNAs) are a family of small (21-24 nucleotide) non-coding RNAs that regulate a wide array of biological processes through regulation of gene expression (Peng and Croce, 2016).

The miRNA are encoded in the genome. The biogenesis begins with its gene transcription by RNA polymerase II into primary miRNA transcript (pri-miRNA). The pri-miRNAs are then cleaved in the nucleus by a complex involving Drosha (type III RNase) and DGCR8 microprocessor complex, forming the precursor miRNA hairpin (pre-miRNA). This is subsequently exported to the cytoplasm by Ran/GTP/Exportin 5 complex, where it is cleaved by another multiprotein complex. This complex includes the RNase III Dicerand TRBP (trans-activation-responsive RNA-binding protein). Pre-miRNAis transformed into duplex sequences miRNA/miRNA*. Where* indicates the passenger strand and the complementary one is the mature or guide strand. The miRNA duplex is loaded onto an Argonaute protein (AGO). This protein unwinds the miRNA duplex and the passenger strand is released. The mature strand is retained to form an effector complex, called RNA-induced silencing complex (miRISC), which mediates gene silencing. The miRNA guides the miRISC to target mRNAs with partial sequence complementarity in their 3'-UTRs and induces mRNA decay or translational repression (Ha and Kim, 2014; Daugaard and Hansen, 2017).

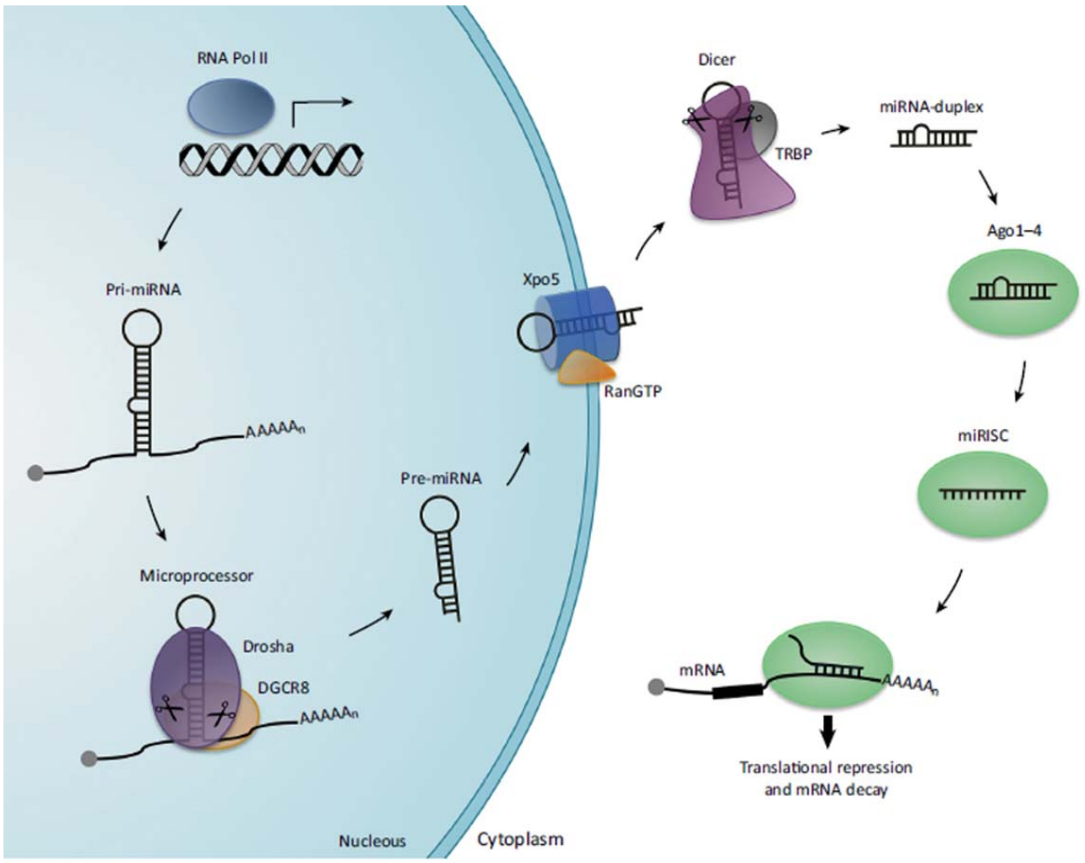

Figure 11. **miRNA biogenesis** (Daugaard and Hansen, 2017).

On one hand, miRNAs are responsible of the regulation of gene expression according to cellular requirements. On the other hand, miRNA help to confer robustness in cellular responses by reinforcing transcriptional programs and attenuating aberrant transcripts (Hayes, Peruzzi and Lawler, 2014). The biogenesis of miRNAs is under tight control at multiple levels. During the past decade it has been seen that miRNA expression is dysregulated in human malignancies like cancer. The underling mechanisms include chromosomal abnormalities, transcriptional control changes, epigenetic changes and defects in the miRNA biogenesis machinery. In this regard, dysregulated miRNAs could affect cancer hallmarks, depending on their target genes, miRNA could function as either oncogene or tumor suppressor under certain circumstances (Peng and Croce, 2016).

Nowadays, miRNAs offer many potential applications as biomarkers for cancer detection, diagnosis and prognosis assessment in both tumor tissue and circulation (Peng and Croce, 2016).

2. CELL DEATH MECHANISMS

Cell death is a crucial process in multicellular organisms since it helps to maintain tissue homeostasis and eliminate potentially harmful cells. According to the Nomenclature Committee on Cell Death, it is possible to distinguish among three major subtypes of cell death: accidental, regulated and programmed (L Galluzzi *et al.*, 2015). Among all the mechanisms of death described, this thesis focuses on explaining the most relevant types of cell death according to their morphological and biochemical characteristics.

2.1. APOPTOSIS

Apoptosis is a genetically programmed mechanism of cell death that occurs in multicellular organisms. It plays important physiological roles during embryonic development and adult tissue homeostasis. Moreover, apoptosis also occurs as a defense mechanism with the aim to eliminate damaged or infected cells that may interfere with normal tissue function.

This process is characterized by specific morphological and biochemical changes of the dying cells. The defining morphological characteristics of apoptosis include rounding of the cell, retraction of pseudopods, cell shrinkage, nuclear fragmentation, chromatin condensation, few or no ultrastructural modifications of cytoplasmic organelles, and plasma membrane blebbing with the development of apoptotic bodies, which preserve the plasma membrane integrity. Biochemical changes involve chromosomal DNA cleavage into internucleosomal fragments, phosphatidylserine externalization, loss of mitochondrial membrane potential ($\Delta\Psi_m$) and a number of intracellular substrate cleavages by specific proteolysis (Ouyang *et al*., 2012).

2.1.1. Caspases

The apoptotic process is orchestrated by the aspartic acid proteases known as caspases. Initially, caspases are synthetized as inactive procaspases that require dimerization and often cleavage for activation, to avoid unwanted cell lethality. Besides the apoptotic roles, these proteases participate in other processessuch as cytokine maturation, inflammation and differentiation.

- **Initiator caspases.** This group includes caspases 8 and 9, among others. These caspases contain a protease and a protein interaction domain, and are activated by dimerization induced by upstream signaling events. Dimerization promotes autocatalytic cleavage of protease domain into a large and small subunit, which stabilizes the dimmer (McIlwain, Berger and Mak, 2013).
- **Executioner caspases.** Caspases 3, 6 and 7 are produced as inactive procaspase dimers that must be cleaved by initiator caspases for their activation. Once initiator caspases cleave them between the large and small subunits, the executioner caspases undergo an activation conformational change that confers them the ability to cleave a variety of proteins leading to the execution of the programmed cell death (McIlwain, Berger and Mak, 2013).

2.1.2. Apoptosis activation pathways

Apoptosis can be triggered by two different initiation pathways depending on the nature of the death stimuli, being the intrinsic or mitochondrial pathway and the extrinsic or death receptor pathway.

2.1.2.1. The extrinsic pathway

Extrinsic apoptosis involves the interaction between extracellular signals, or death receptor ligands, with its death receptors. On one hand, these ligands include tumor necrosis factor-α (TNFα), CD95-ligand (CD95-L; also known as Fas-L), APO2 ligand (APO2L; also known as TRAIL) and TNF-like ligand 1A (TL1A), among others. On the other hand, their corresponding death receptors are members of the tumor necrosis factor (TNF) superfamily and encompass TNF receptor-1 (TNFR1), CD95 (also called Fas and APO-1), death receptor 3(DR3), TNF-related apoptosis-inducing ligand receptor-1 (TRAIL-R1; also called DR4), and TRAIL-R2 (also known as DR5). The binding ligand-receptor prompts the assembly of the death-inducing signaling complex (DISC) through the adaptor protein FAS-associated death domain (FADD) or TNFR-associated death domain (TRADD). They recruit the apoptosis-initiating proteases caspase 8, which dimerize and become active. Subsequently, apoptosis is initiated directly by cleaving, and thereby activating, executioner caspases 3 and 7 (figure 12) (Jin and El-Deiry, 2005).

2.1.2.2. The intrinsic pathway

This pathway is activated by a vast array of cellular stresses including DNA damage, growth factor withdrawal, hypoxia, hormones, cytokines and accumulation of unfolded proteins, among others. These stimuli produce intracellular signals that act directly on the mitochondrial membrane integrity. The apoptotic mitochondrial events are highly regulated by a balance between the anti and pro-apoptotic members of the BCL-2 protein family (Elmore, 2007). This family is characterized by sharing the BCL-2 homology (BH) domains. The anti-apoptotic group includes BCL-2 (BCL-2), BCL-XL (BCL-extralarge) and MCL-1 (myeloid leukemia cell differentiation 1). The pro-apoptotic proteins can be divided into two groups: the BH1-3 proteins, such as BAX (BCL-2-associated X), BAK (BCL-2 homologous antagonist/killer), and the BH3-only proteins (BIM, BAD, BID, PUMA and NOXA) (Lomonosova and Chinnadurai, 2008; Youle and Strasser, 2008). In resting state, pro-survival proteins counteract the function of the BH3-only proteins as well as directly act to inhibit BAX and BAK. Cytotoxic stress signals induce BH3 only proteins activation and they execute their pro apoptotic activity though neutralization of the pro-survival BCL-2 family proteins and direct activation of the pro apoptotic effectors BAX and BAK (Czabotar et al., 2014). Then, these two effectors trigger mitochondrial outer membrane permeabilization (MOMP) and allow Cytochrome C (CytC) and SMAC/DIABLO (second mitochondrial activator of caspases/direct IAP binding protein with low pI) molecules to be released to the cytoplasm. These events promote, on one hand, the assembly of the apoptosome, consisting of several copies of the scaffold protein APAF1 (apoptotic protease activating factor 1), plus the CytC and Caspase 9. This complex serves as the activation platform for Caspase-9, which in turn activates Caspase 3 (figure 12) (Jin and El-Deiry, 2005). On the other hand, SMAC/DIABLO protein release will block the IAPs (inhibitors of apoptosis proteins), the most important negative regulators of caspases, permitting their activation.

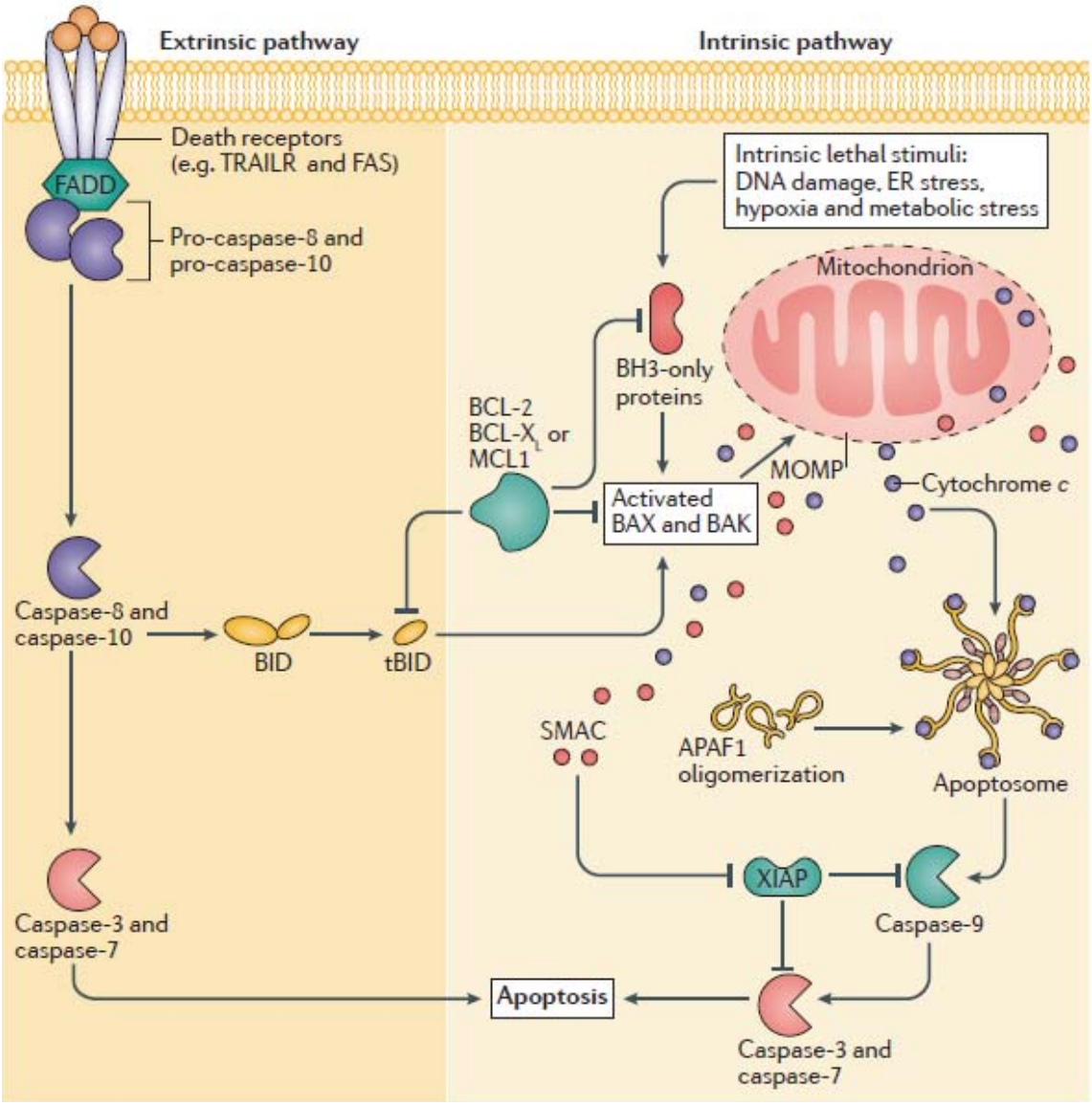

Figure 12. **Extrinsic and intrinsic apoptotic signaling pathways** (Ichim and Tait, 2016).

The extrinsic and intrinsic pathways also cross-talk through the caspase-8 induced cleavage of the BH3-only protein BID (BH3 interacting domain death agonist). This generates tBID, the active and truncated form of BID that triggers MOMP, through the activation of the pro-apoptotic BCL-2 family members (Kantari and Walczak, 2011).

2.1.3. Execution pathway

At the moment in which the executioner caspases are activated, the final apoptosis pathway begins. The executioner caspases cleave a series of substrates (ICAD (inhibitor of the caspase-activated deoxyribonuclease), ROCK1 (Rho-associated coiledcoil forming kinase 1), poly (ADP-ribose) polymerase (PARP, a DNA repair enzyme), actin, fodrin and lamin) which produce the characteristic phenotypic changes of this cellular demolition (Lawen, 2003). Through the cleavage of the Rho effector, ROCK1, the actin cytoskeleton contracts leading to plasma membrane blebbing, as well as nuclear fragmentation. Moreover, the nuclear fragmentation is facilitated by the proteolysis of nuclear lamins. Proteolysis of

proteins at focal adhesion sites and cell-cell adhesion sites contributes to the rounding, detachment and retraction seen in the early stages of apoptosis. This cytoskeletal reorganization prompts the disintegration of the cell into apoptotic bodies, without plasma membrane breakage (Elmore, 2007). Beside this, there is a shutdown of essential cellular functions, such as transcription and translation, since proteins involved in these processes are also targets of caspases. Additionally, caspase 3 specifically activates the endonuclease CAD (caspase-activated DNase) through the cleavage of its inhibitor ICAD. Then CAD degrades internucleosomal DNA within the nuclei and provokes chromatin condensation. Other events that are characteristic of apoptosis and are orchestrated by these proteases are the fragmentation of cellular organelles, such as the Golgi apparatus and the endoplasmic reticulum (figure 13). During apoptosis, executioner caspases are also required for the exposure of phosphatidylserine (PS) and other phagocytic signals on the cell surface. These events contribute to the consumption of the dead cell by phagocytes and prevent the release of cellular constituents into the surrounding mileu (Slee, Adrain and Martin, 2001; Taylor, Cullen and Martin, 2008).

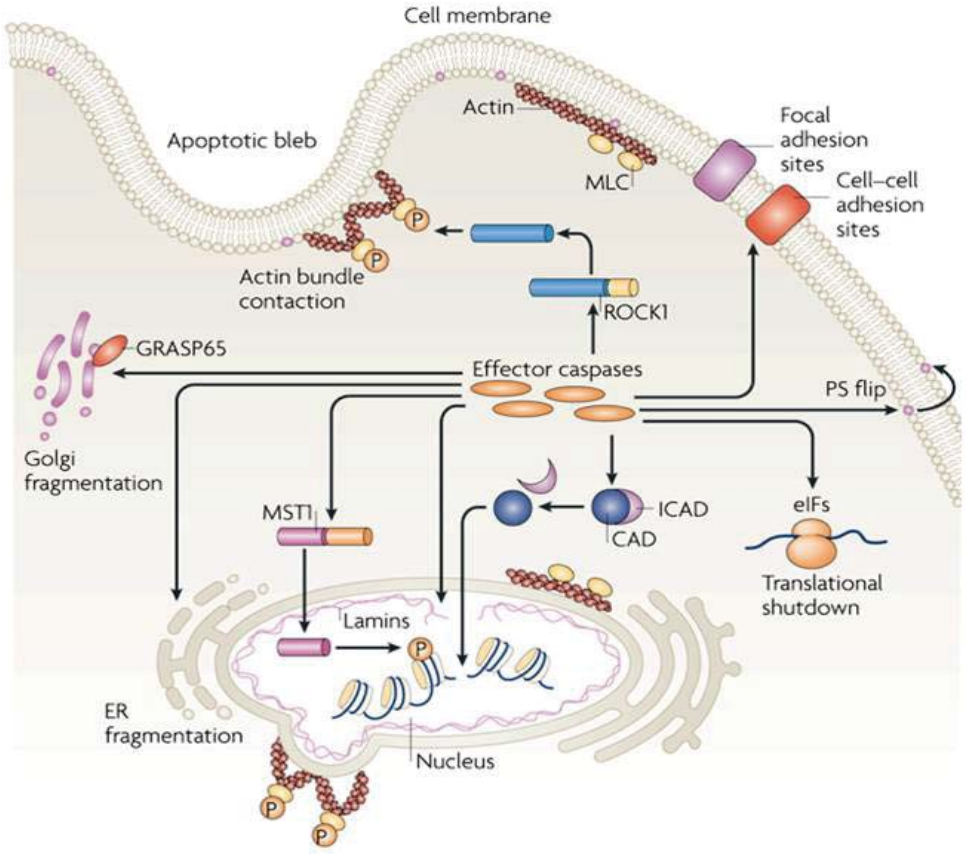

Figure 13. Demolition of key cellular structures and organelles by executioner caspases (Taylor, Cullen and Martin, 2008).

2.1.4. Apoptosis regulation

In normal cells, the balance between pro- and anti-apoptotic proteins is tightly regulated. In human cancers, this balance has been altered. The anti-apoptotic members of the aforementioned BCL-2 protein family are overexpressed in some types of cancer (Delbridge *et al.*, 2016). This fact has been linked to tumor progression, treatment resistance, and poor prognosis (Bai and Wang, 2014).

Another group of anti-apoptotic molecules are the eight IAPs proteins in humans: neuronal apoptosis inhibitory protein (also known as BIRC1), cellular IAP1 (c-IAP1; also known as BIRC2), cellular IAP2 (c-IAP2; also known as BIRC3), X chromosome-linked IAP (XIAP; also known as BIRC4), survivin (also known as BIRC5), ubiquitin-conjugating BIR domain enzyme apollon (also known as BIRC6), melanoma IAP (ML-IAP; also known as BIRC7), and IAP-like protein 2 (ILP2; also known as BIRC8). This family of proteins shares the BIR (baculovirus IAP repeat) domain for protein-protein binding and some of them also have a carboxy-terminal RING domain that acts as E3 ubiquitin ligase. In resting state, its function is to inhibit caspases that have been spontaneously activated, preventing apoptosis. In the presence of apoptotic stimuli, a signal is transmitted to the mitochondria, leading to the MOMP and the release of SMAC/DIABLO, and therefore the inhibition of IAPs, and caspase activation (Fulda and Vucic, 2012).

In this regard, the deep knowledge of the apoptotic regulation has led to the development of new strategies for the treatment of cancer, which aim to target these anti-apoptotic proteins with small-molecules, specially BH3 or SMAC mimetics (Bai and Wang, 2014; Panayotopoulou *et al.*, 2017).

2.2. AUTOPHAGY

Macroautophagy, referred to hereafter simply as autophagy, is a catabolic process whereby cells degrade their own components by enveloping them in double-membrane vesicles called autophagosomes and targeting them for lysosomal degradation (Hale *et al.*, 2013). At basal levels, it plays a housekeeping role maintaining the integrity of intracellular organelles and proteins and prevents the toxic accumulation of cellular waste products. As a self-degrading process, it is also important for balancing sources of energy to sustain metabolism during starvation (Parzych and Klionsky, 2014). Although autophagy has these cytoprotective functions, excessive autophagy is deleterious and its deregulation has been linked to several pathologies (Wirawan *et al.*, 2012).

The concept of autophagic cell death, also known as type 2 cell death, describes a kind of cell death that occurs in the absence of chromatin condensation and accompanied by massive autophagic vacuolization of the cytoplasm. However there is some controversy about this type of cell death, since it represents a cell death with autophagy and not a cell death executed by the autophagic mechanism (Kroemer and Levine, 2008; Kroemer *et al.*, 2009; Denton, Nicolson and Kumar, 2012).

2.2.1. The molecular mechanism of the autophagy pathway

There are three major kinases that regulate autophagy: the cAMP-dependent protein kinase A (PKA), mTOR and AMPK (AMP-activated protein kinase). These kinases respond to a wide range of cellular stresses, including nutrient starvation, the availability of insulin and other growth factors, hypoxia, energy deficiency and endoplasmic reticulum stress (figure 14) (Parzych and Klionsky, 2014). One of the most studied protein is mTOR, which inhibits autophagy and promotes cell growth in a situation of abundance of nutrients. When nutrients are scarce, mTOR activity is repressed and autophagy is induced as a compensatory mechanism (Glick, Barth and Macleod, 2010).

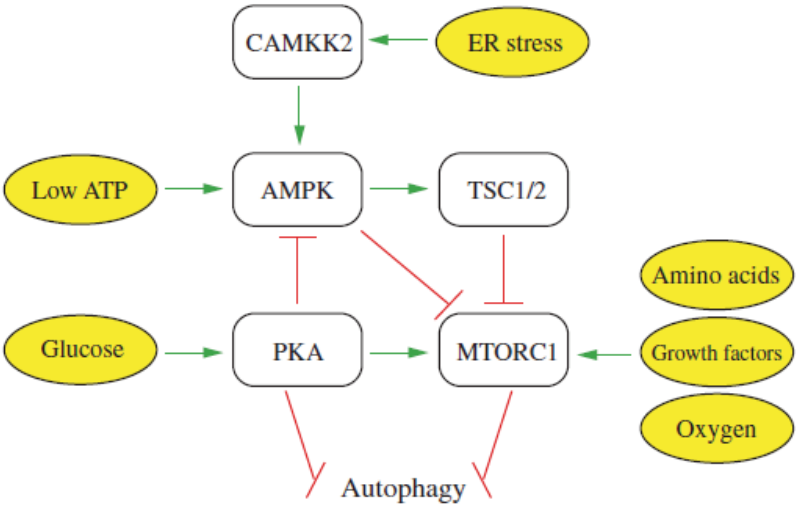

Figure 14. **Regulation of autophagy** (Parzych and Klionsky, 2014).

The process of autophagy begins with the surrounding and sequestering of cytoplasmic organelles and proteins within an isolated membrane called phagophore. Autophagy inducers cause activation of the ULK complex (ULK1 (UNC-51-Like Kinase), ATG13, ATG101 (autophagy related proteins 13 and 101, respectively) and FIP200 (focal adhesion kinase family interacting protein of 200 kDa), which dissociates from the mTORC1 complex and in turn activates the Class III PI3K complex (PI3KC3 complex). Activation of this complex also requires the release of Beclin 1 from the interaction with the protein BCL2, process regulated by the upstream kinases sensitive to starvation. The interaction of Beclin 1 with other components of the PI3KC3 complex (ATG14, VPS34 and VPS15 (phosphatidylinositol 3-kinases)) promotes the generation of phosphatidylinositol3-phosphate (PI3P). This is essential for vesicle nucleation since it serves as a platform for recruitment of other autophagy-related proteins involved in the next step, the elongation reaction. In this step, the expansion of the phagophore membrane takes place, resulting in the formation of the autophagosome, a closed double-membrane structure, around the cargo. The vesicle elongation is mediated by two conjugation systems. First, E1- and E2-ligases, named ATG7 and ATG10 respectively, modify ATG12. Modified ATG12 binds to ATG5 followed by ATG16L binding to form the ATG5-ATG12-ATG16L complex. This complex promotes the recruitment and conversion of cytosolic-associated protein light chain 3 (LC3 I) to the membrane-bound LC3 II form, with a phosphatidylethanolamine group attached. LC3 II also binds to the adaptor protein p62/ sequestosome1 (SQSTM1) that is involved in trafficking proteins to the proteasome and serves to facilitate degradation of ubiquitinated protein aggregates by autophagy (Green and Levine, 2014; Kim and Lee, 2014). The late events in autophagy involve the fusion of mature autophagosomes with lysosomes to form an autolysosome, structure where the cargo is digested by hydrolytic enzymes. This is tightly regulated by several groups of proteins, including: lysosomal membrane proteins such as the V-ATPase (vacuolar-type H^+-ATPase) complex and LAMP1 (lysosome-associated membrane protein); small GTPases such as Rab7 (Ras-related protein); and SNARE (soluble N-ethylmaleimide-sensitive factor attachment protein receptor) proteins, among others (Shen and Mizushima, 2014).

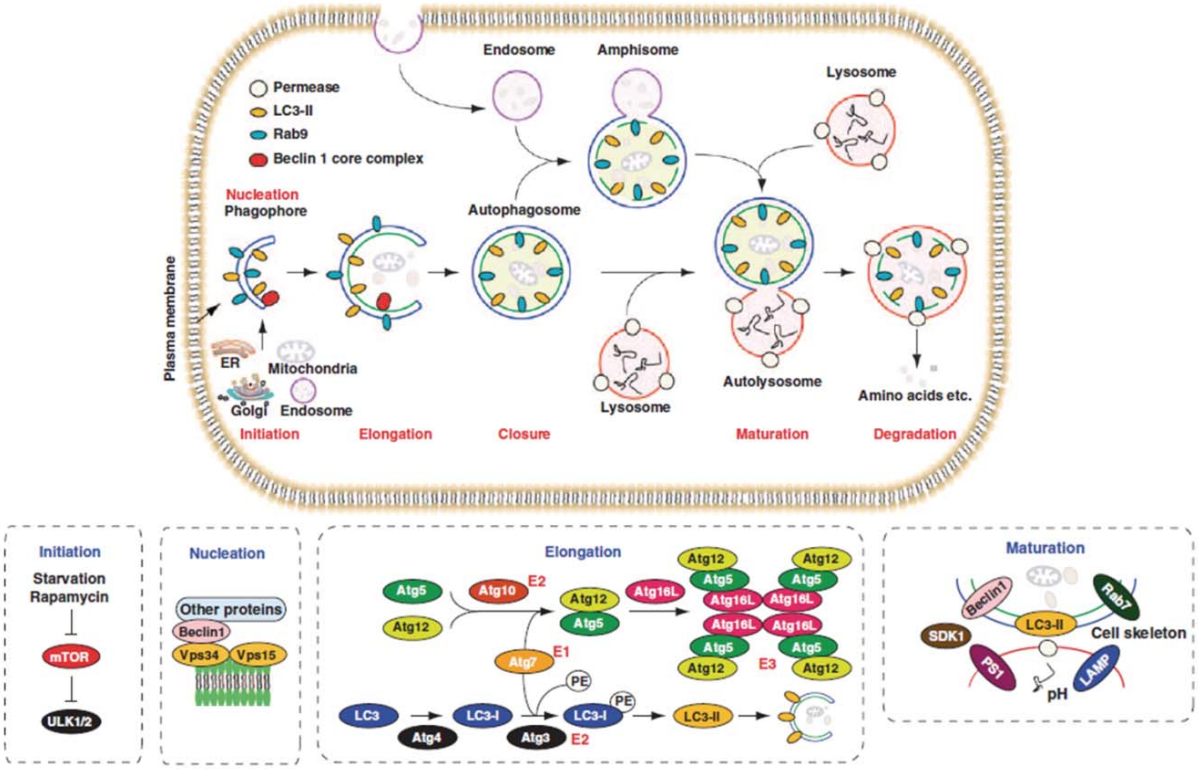

Figure 15. **Stages of autophagy.** Modified from (Kang *et al.*, 2011).

2.3. METHUOSIS

Methuosis, a novel form of nonapoptotic cell death, which is mainly characterized by the displacement of the cytoplasm by large fluid-filled vacuoles derived from a dysfunctional macropinocytosis process. Macropinocytosis is a clathrin-independent endocytic process by which cells internalize extracellular fluid and nutrients through vesicles known as macropinosomes. Nascent macropinosomes are generated from lamellipodial membrane projections or ruffles. After that, these vesicles mature to acquire characteristics of late endosomes and fuse with lysosomes. During methuosis, instead of merging with lysosomes and being recycled, macropinosomes coalesce to form progressively larger vacuoles and fill the cytoplasm. This dysfunctional trafficking of macropinosomes compromises cell viability and ultimately results in cell rupture (Maltese and Overmeyer, 2014; Mbah, Overmeyer and Maltese, 2017).

This cell death phenotype has been established mainly in cells that have been genetically or pharmacologically manipulated *in vitro*. Initially, this phenomenon was observed in glioblastoma cells with overexpression of *RAS* (rat sarcoma oncogene) by Maltese research group (Overmeyer *et al.*, 2008). Subsequent work from the same group has developed a synthetic indole-based chalcone compound known as MOMIPP. This chemical is capable of inducing methuosis in several cancer cell types, finally provoking cell death (Overmeyer *et al.*, 2011; Robinson *et al.*, 2012; Maltese and Overmeyer, 2014).

2.4. REGULATED NECROSIS

Necrosis had traditionally been considered an accidental cell death that occurs without intracellular control. Necrotic cell death is morphologically characterized by an uncontrolled degeneration that involves increase in cell volume, swelling of organelles, plasma membrane rupture, and leakage of intracellular contents. Necrosis can occur simply as a consequence of extensive physicochemical insults that disrupt the cell integrity (Green and Llambi, 2015). After damage-induced lesions, a sequence of intracellular events specific to necrotic cell death occurs. These include: mitochondrial dysfunction, enhanced production of ROS, swelling of mitochondria, ATP depletion, failure of Ca^{2+} homeostasis, activation of calpains and cathepsins proteases, lysosomal rupture, and ultimately plasma membrane rupture (Golstein and Kroemer, 2007).

However, necrotic cell death is not always an accidental or passive process and can also be triggered in a regulated manner (Green and Llambi, 2015). In the last years, the existence of multiple pathways of regulated necrosis (RN) has been revealed. Thus, multiple modes of cell death that share necrotic morphological hallmarks are now classified as RN cell death (figure 16) (Berghe *et al*., 2014). In this regard, some of the best known molecular mechanisms of RN are mitochondrial permeability transition or MPT-dependent regulated necrosis, parthanatos or necroptosis.

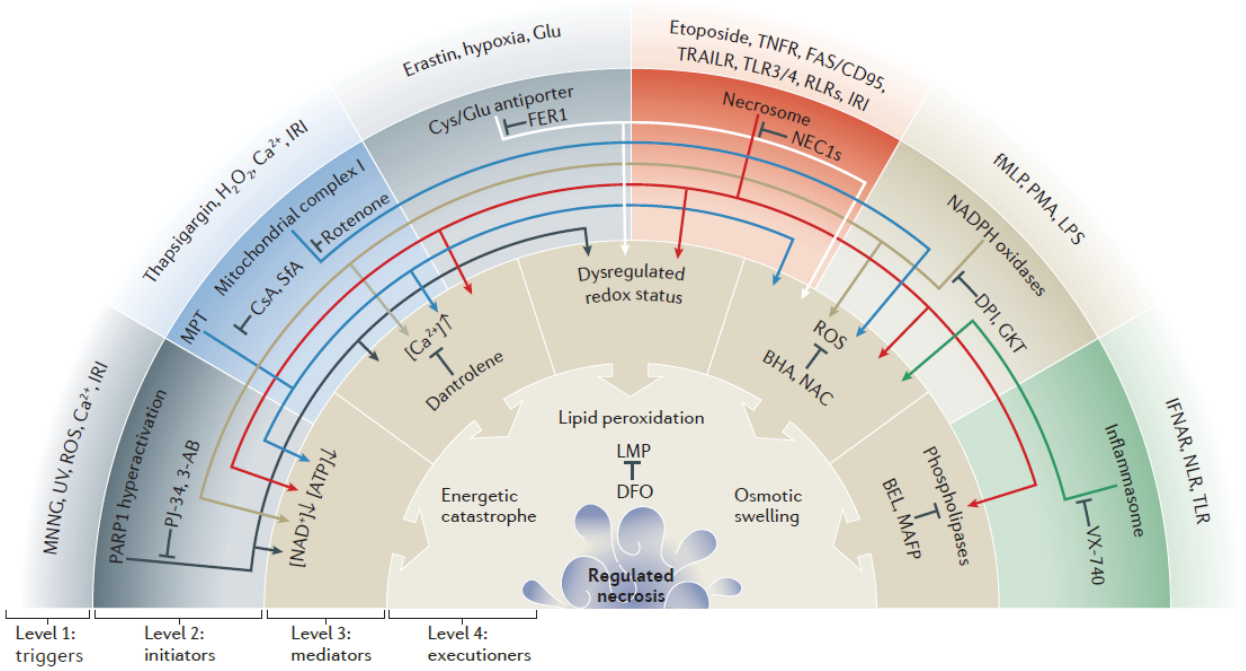

Figure 16. **The emerging modes of regulated necrosis** (Berghe *et al*., 2014).

Mitochondria are essential organelles for the execution of some RN cell death types, especially MPT-driven necrosis and parthanatos. On one hand, there are several perturbations of intracellular homeostasis that can cause MPT. This implies the permeation transition pore complex (PTPC) assembly, where Cyclophilin D (CYPD) is the crucial regulator. MPT involves an abrupt increase in the permeability of the inner mitochondrial membrane. This implies a massive entry of water into the mitochondrial matrix, the cessation of all functions linked to the mitochondrial transmembrane potential, and the release of solutes that initiate cell death pathways (Galluzzi, Bravo-San Pedro and Kroemer, 2014; Galluzzi, Kepp and Kroemer, 2016). On the other hand, the transduction cascade leading to parthanatos

cell death relies on the hyperactivation of PARP1. This triggers a bioenergetic crisis and the release of apoptosis-inducing factor mitochondrion-associated 1 (AIF) from the mitochondria, which induces cell death (Berghe *et al.*, 2014; Galluzzi, Kepp and Kroemer, 2016).

All forms of RN culminate with loss of cellular integrity and cellular leakage. Likewise, note that morphologic features of necrosis can also be observed at late stages of an apoptotic cell death program. When there is a defect in the clearance of the cell, cell disintegrates and releases its components (Berghe *et al.*, 2010). Due to the release of danger-associated molecular patterns (DAMPs) and pro-inflammatory cytokines that alert the innate immune system, necrosis cell death can stimulate inflammatory responses (Linkermann *et al.*, 2014).

2.4.1. Necroptosis

the best-characterized form of regulated necrosis is receptor-interacting protein kinase (RIP)-dependent necrosis, also known as necroptosis (Berghe *et al.*, 2014). This cell death includes the following morphological features: loss of plasma membrane integrity, leakage of intracellular contents, organelle swelling, accumulation of autophagosomes, and permeability of mitochondrial and lysosomal membrane.

2.4.1.1. Execution of necroptosis

Necroptosis can be induced by the binding of ligands to death receptors, including CD95, TNFR1, TNFR2, TRAILR1 and TRAILR2. This cell death mechanism can also be initiated by members of the pathogen recognition receptor family, induced by pathogenassociated molecular patterns, such as viral or bacterial elements. Moreover, interferon receptors were also shown to induce necroptosis (Berghe *et al.*, 2014). However, necroptosis is not the default pathway activated downstream of the above-mentioned receptors. For instance, the binding of TNF to its receptor (TNFR1), one of the best studied intracellular signaling pathways of necroptosis induction, can result also in cell survival or apoptosis depending on the cellular conditions (figure 17) (Vandenabeele *et al.*, 2010). Necroptotic response can only occur under conditions where there is a down-regulation or inhibition of IAPs or caspase 8. Thus, in response to TNF stimulation, TNFR recruits proteins to the plasma membrane to form the complex I. This complex includes: TRADD (TNFR1−associated death domain), RIPK1, TRAF2 (TNF receptor-associated factor 2), cIAP1, cIAP2 and LUBAC (linear ubiquitin chain assembly complex). cIAPs catalyze the polyubiquitination of RIP1. Formation of complex I entails the activation of the NF-kB (nuclear factor kappa B) and MAPK pathways, resulting in proinflammatory signaling and cell survival (Pasparakis and Vandenabeele, 2015). When the enzyme cylindromatosis (CYLD) removes polyubiquitins from RIPK1, the complex I becomes unstable, allowing RIPK1 to dissociate from the plasma membrane and interact with RIPK3, TRADD, FADD, pro-caspase 8 and FLICE-like inhibitory proteins (FLIPs). These proteins form the complex IIa, where caspase 8 inactivates RIP1 and RIP3 by proteolytic cleavage and initiates the pro-apoptotic caspase activation cascade resulting in apoptosis. By contrast, when caspase 8 is not present, RIPK1 and RIPK3 associate, autophosphorylate and aggregate in microfilament-like complexes that are referred to as necrosomes or complex IIc. The phosphorylation of RIPK1 and RIPK3 recruit MLKL (mixed lineage kinase domain-like), which is subsequently phosphorylated (Moreno-Gonzalez,

Vandenabeele and Krysko, 2016). MLKL oligomerizes and execute necroptosis cell death through disruption of the cell membrane (Petrie, Hildebrand and Murphy, 2017). Moreover, when cells are depleted of cIAPs, the RIPK1-dependent complex IIb or the 'ripoptosome' is formed including RIPK1, RIPK3, FADD, FLIP and caspase-8. This complex can cause both necroptosis and apoptosis, depending on the absence or presence of caspase 8, similar to the complex IIa (Berghe *et al.*, 2014).

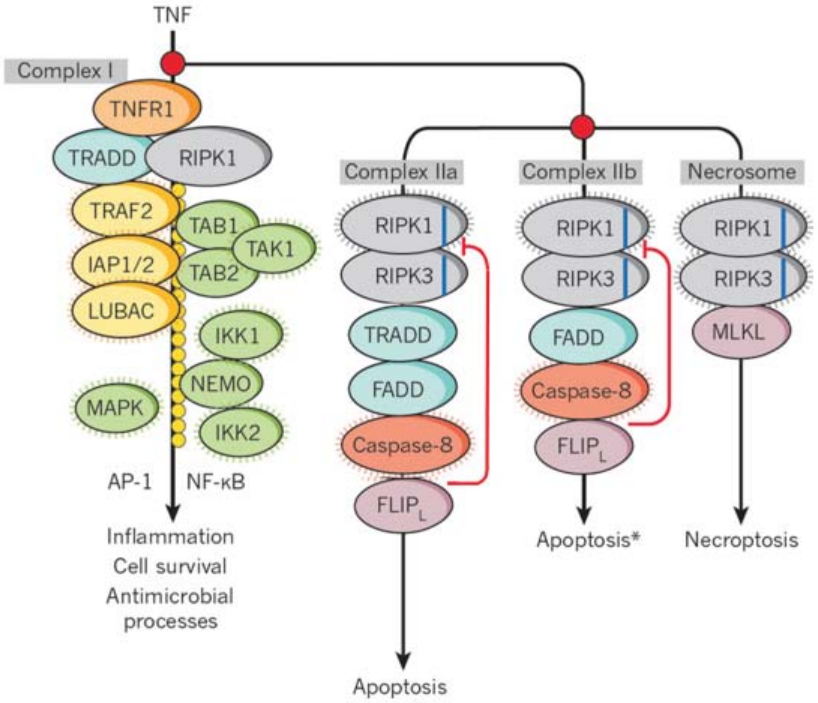

Figure 17. **Pathway leading to necroptosis.** Modified from (Pasparakis and Vandenabeele, 2015).

3. ION TRANSPORTERS

Maintenance of the ion homeostasis of cells is crucial to maintain and control a great variety of physiological processes, such as defining cell membrane potential and volume, regulating intracellular signaling events, and activating specific cellular responses including proliferation, differentiation and apoptosis (Pedersen and Stock, 2013). The ions cannot diffuse freely through the membranes; therefore their transport must be facilitated by ion channels, integral membrane proteins that allow the passage of certain ions into and out of the cell (Davis, Okunola and Quesada, 2010). Alterations in the transport of these ions contribute to dysregulation of ion concentrations and fluxes are responsible for many diseases known as channelophaties, such as cystic fibrosis (Hübner and Jentsch, 2002).

There is growing evidence that ion channels contribute to the malignant phenotype of cancer cells. The aberrant expression and function of several types of ion channels involve the failure in different processes such as proliferation, differentiation, cell adhesion and even cell death, among others. These alterations are considered as a boost for cancer hallmarks (Prevarskaya, Skryma and Shuba, 2010; Litan and Langhans, 2015).

Therefore, in the last decade ion carriers compounds have been studied with a therapeutic purpose in order to supply the function of defective channels, or because of their potential to disturb cellular ion gradients in case of cancer (Busschaert and Gale, 2013). These compounds may be divided into cationophores or anionophores, depending on whether they are cation or anion selective, respectively. Some relevant ionophores with biological activities are explained below.

3.1. SALINOMYCIN

Salinomycin (SAL, figure 18), isolated from *Streptomyces albus,* is a natural ionophore with diverse biological activities. SAL is currently used as an antibiotic in veterinary medicine. From 2009, it has become particularly important since it was reported that this compound was almost 100-fold more effective against cancer stem cells than paclitaxel, a commonly used cytostatic drug for breast cancer treatment (Gupta *et al.*, 2009).

SAL is a carboxylic polyether ionophore that exists in a pseudo-cyclic structure because of the binding between the carboxylic group on the one side of the molecule and two hydroxyl groups on the opposite side. Thanks to this structure, polar inner core with oxygen atoms and one carboxylic group is able to form complexes with monovalent cations, especially K^+. Moreover, because of its lipophilic surface, SAL has the capability of transporting these monovalent cations across lipid cytoplasmic and mitochondrial membranes. The steady state of normal cells relies on the intracellular and extracellular levels of Na^+ and K^+. Intracellular concentration of K^+ is higher than that of Na^+, and extracellular concentrations are respectively reversed. At the time when SAL disrupts the ion balance, it ends up triggering cell death (Huczynski, 2012).

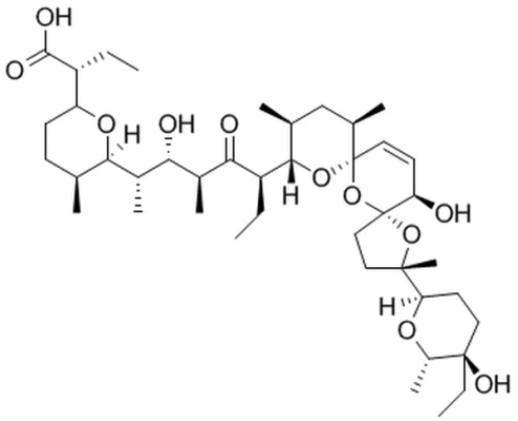

Figure 18. Salinomycin chemical structure

3.1.1. Properties and mechanism of action

SAL was shown to possess antimicrobial activity against Gram-positive bacteria and some parasitic protozoa responsible for poultry diseases. Owing to several reports and published studies in which SAL was considered to be toxic for mammals, it has not been used for human diseases. This has recently changed, since SAL has demonstrated to eliminate human breast CSCs selectively in mice and following publications have shown that SAL causes massive apoptosis in cancerous cells of different origins. The underlying mechanism by which SAL removes CSCs is not exactly understood, but it has been reported that in CSCs from different origin, SAL induces diverse pathways that converge in apoptosis. Moreover, SAL inhibits Wnt signaling involved in stem cell self-renewal, and is able to promote differentiation in CSCs. Finally, SAL interferes with the ion balance, promoting K^+ efflux from mitochondria and cytoplasm, which is also linked to cytotoxicity and induction of apoptosis (Naujokat and Steinhart, 2012).

3.2. PRODIGIOSIN

The anionophore prodigiosin, one of the most studied compounds within the red-pigmented prodiginines family, is an alkaloid, a secondary metabolite produced by several microorganisms, including *Serratia marcecens.*

The structure of prodigiosin (figure 19) or 2-methyl-3-pentyl-6-methoxyprodiginine ($C_{20}H_{25}N_3O$) was clarified in the early 1960s by partial and total chemical synthesis revealing a pyrrolyl-dipyrromethene core skeleton. Prodigiosinexists in solution in two interconverting conformations, cis (or β) and trans (or α). The equilibrium between these forms is dependent on the solution pH since it has the ability to protonate itself (Darshan and Manonmani, 2015).

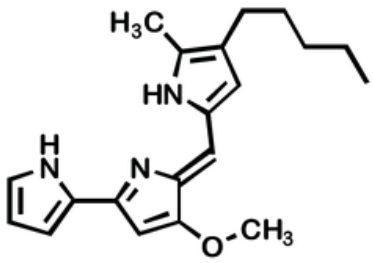

Figure 19. Prodigiosin chemical structure

3.2.1. Properties and mechanism of action

This tripyrrole natural product has received attention due to its wide range of pharmacological activities. Prodigiosin has been described as a potent antimalarial agent showing high toxicity against *Plasmodium falciparum*, the protozoan that causes the disease (Castro, 1967; Lazaro *et al.*, 2002). Likewise, it has been characterized with antibacterial properties, inhibiting Gram positive and negative bacterial growth (Ibrahim *et al.*, 2014); and with antifungal properties (Kalbe, Marten and Berg, 1996; Berg, 2000). Moreover, prodigiosin blocks lymphocytes T activation by inhibiting primarily IL-2Rα (interleukin-2 receptor α-chain) expression, showing that this compound possesses immunosuppressive capacity (Han *et al.*, 2001). On the other hand, this compound has gained relevance due to its capacity to trigger apoptosis in malignant cancer cells (Montaner and Perez-Tomas, 2003; Soto-Cerrato *et al.*, 2004). In this regard, this small molecule has been referred as an anticancer compound both *in vitro* and *in vivo* in many occasions (Manderville, 2001; Perez-Tomas *et al.*, 2003; Perez-Tomas and Vinas, 2010).

The mechanism of action by which it exerts cytotoxicity in cancer cells is not entirely elucidated, but could involve multiple processes since it is a small molecule and it has shown to have multiple cellular targets. Prodigiosin has shown to induce cellular stresses, one of the mechanism by which prodigiosin may show anticancer activity is related to its ability to uncouple vacuolar-type ATPase through promotion of H^+/Cl^- symport in lysosomal compartment, leading to the consequent disruption of pH gradient (Sato *et al.*, 1998; Jonathan L Sessler *et al.*, 2005). This can lead to a cell cycle arrest or cell death by apoptosis (Montaner and Perez-Tomas, 2003; Castillo-Avila *et al.*, 2005). Another mode of action involves the copper mediated cleavage of double stranded DNA. Prodigiosin intercalates into the DNA and inhibits topoisomerases I and II activity, resulting in DNA rupture that leads also to apoptosis cell death (Montaner and Perez-Tomas, 2001; Perez-Tomas and Vinas, 2010).

3.3. OBATOCLAX

Obatoclax mesylate or GX15-070MS (figure 20), is an synthetic analogue derived from the prodiginine family, that has been in phase II of clinical trials in combination with first line drugs for the treatment of hematological malignancies and solid tumors (Chiappori *et al.*, 2014; Langer *et al.*, 2014; Schimmer *et al.*, 2014).

This small molecule shares the three pyrrolic rings skeleton with prodigiosin and its chemical structure is 2-[2-[(3,5-dimethyl-1H-pyrrol-2-yl)methylidene]-3-methoxy-2H-pyrrol-5-yl]-1H-indole monomethanesulfonate.

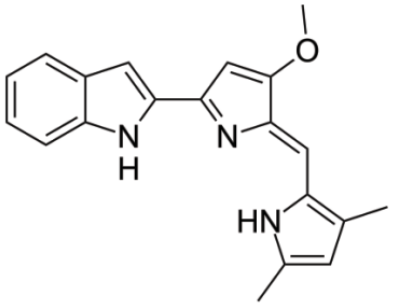

Figure 20. Obatoclax mesylate (GX15-070MS) chemical structure.

3.3.1. Properties and mechanism of action

In first place, this small molecule has been described as an inhibitor of all relevant antiapoptotic members of the BLC2 family of proteins (Nguyen *et al.*, 2007). Thus, GX15-070MS prevents their binding to pro-apoptotic proteins BAX and BAK, triggering the activation of the apoptotic pathway in BCL2-overexpressing cancer cells (Goard and Schimmer, 2013). Apart from apoptosis, Obatoclax has been reported to promote different forms of programmed cell death, such as autophagic cell death (Heidari, Hicks and Harada, 2010; McCoy *et al.*, 2010; Espona-Fiedler *et al.*, 2012), and necroptosis (Basit, Cristofanon and Fulda, 2013).

3.4. TAMBJAMINES

Tambjamines are a group of natural products that are structurally related to prodiginines. These alkaloids, shown in figure 21, are derived from bacteria of the genus *Pseudoalteromonas* and from a large group of marine invertebrates which includes bryozoans, nudibranchs and ascidians (Soliev, Hosokawa and Enomoto, 2011).

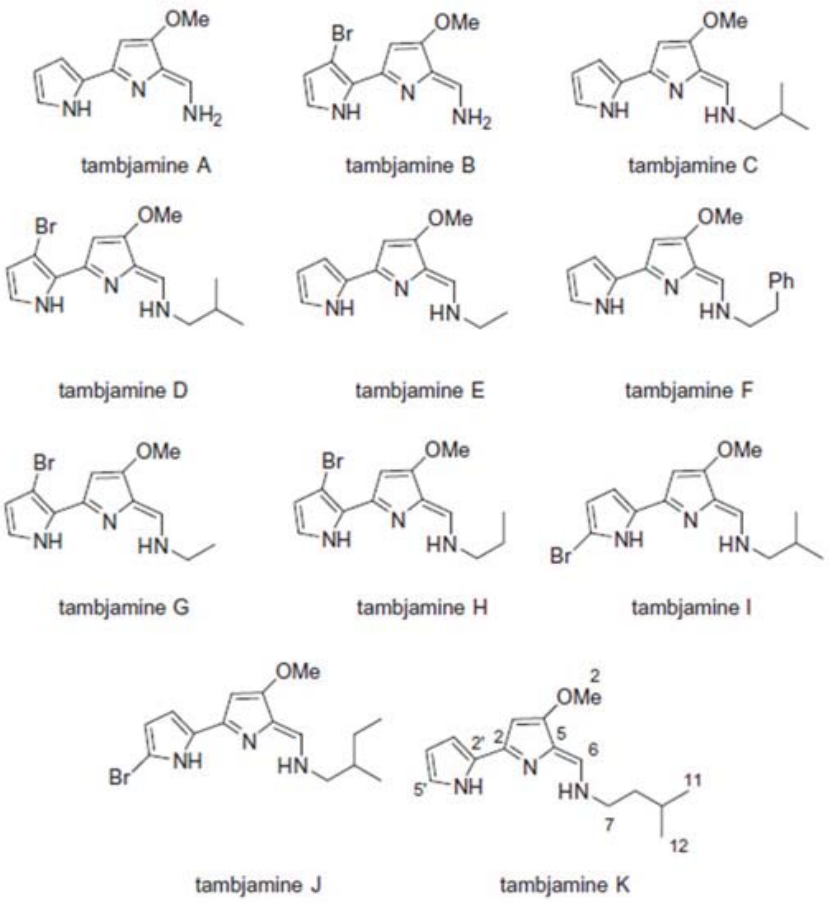

Figure 21. **Chemical structures of the tambjamines.** Modified from (Aldrich, 2010).

They are composed of two pyrrole rings with a methoxy group at C-4 and an enamine moiety at C-5 and many of them have short alkyl chains in the place of the enamine nitrogen (Carbone *et al.*, 2010).

Tambjamines serve as chemical defenses against predators in marine organisms, and have shown diverse biological activities such as antimicrobial, cytotoxic or antitumor agents. The first studies to check the biological activities of these compounds were related to tambjamines A-D, demonstrating their antimicrobial effect (Granato *et al.*, 2005; Pinkerton *et al.*, 2010). Later other studies proved their cytotoxic and antitumor activity on several tumor cell lines (Aldrich *et al.*, 2010; Carbone *et al.*, 2010). These reports describe their capacity of DNA binding and cleavage as their mechanism of cell death induction (Cavalcanti *et al.*, 2008).

Due to the fact that these compounds display intriguing pharmacological activities, our group in collaboration with Dr. Quesada's research group are interested on the design and synthesis of novel synthetic tambjamine analogues with better anion transport abilities and potential better pharmacological properties.

HYPOTHESIS

Cellular homeostasis involves continuous adaptations and changes at many levels in response to internal or environmental factors that disturb the system from its equilibrium. It is through homeostatic mechanisms, like correct ion exchange across cell membranes, that cells kept osmotic balance and intracellular pH. These parameters control many key biological processes. For example, variation in the concentration of certain ions regulates the proliferative capacity of cells, their differentiation and can even control programmed cell death. Consequently, when pH is not preserved at a favorable level, different pathologies may occur, as it is the case of cancer. In this regard, cancer cells during the process of carcinogenesis acquire a "reversed pH" that consists in acidification of the extracellular pH and alkalinization of the internal pH. This metabolic adaptation is crucial for the growth, survival and metastatic dissemination of tumor cells. In this sense, modulation of intracellular pH may be considered a new therapeutic strategy against cancer. Therefore, the identification of new compounds able to disrupt the ionic homeostasis of cancer cells may be a successful strategy to find novel potential chemotherapeutic agents. Based on these premises, our hypothesis is that synthetic tambjamine analogue compounds, which are potent anion transporters, will be able to generate an ionic unbalance in cancer cells generating disturbances at different cellular levels leading to cytotoxicity.

Therefore, the aim of the present work is to identify new tambjamine analogues as potent anticancer agents and to elucidate their mechanism of action and molecular targets, as well as evaluate their potential therapeutic effects *in vivo*.

OBJECTIVES

Main objective:

Identification, study of the mechanism of action and evaluation of the therapeutic potential *in vivo* of novel anionophore compounds for lung cancer treatment.

Specific objectives:

1. Evaluation of the anticancer effects of novel synthetic tambjamine analogues anionophores.

    1.1. Identification of the most cytotoxic compounds in oral and lung cancer cell lines.

    1.2. Effect of the compounds on cancer stem cells obtained from cell lines and tumor samples from lung cancer patients.

2. Characterization of the anticancer effects induced by the most potent compounds.

    2.1. Study of the cytostatic effect triggered by the selected compounds.

    2.2. Characterization of the type of cell death induced by the selected compounds.

3. Study of anion transport induced by selected compounds in cells and its effects on intracellular pH.
4. Identification of possible molecular targets of the synthetic tambjamine analogues
5. Analysis of changes in miRNA expression after treatment with the selected compound.
6. Evaluation of the therapeutic effects of selected compounds through efficacy studies in *in vivo* lung cancer models.

MATERIAL AND METHODS

1. Cell lines and culture conditions

Cell line	Origin
A549	Human lung cancer adenocarcinoma
DMS53	Human lung small cell carcinoma
H460	Human lung large cell carcinoma
SW900	Human lung squamous cell carcinoma
CAL27	Human oral squamous cell carcinoma
HN4	Human oral squamous cell carcinoma

Table 1. Cell lines used in this project.

Human lung cancer and oral cancer cell lines were used (table 1). Lung cancer cell lines were obtained from the American Type Culture Collection (ATCC, Manassas, VA, USA), and human oral cancer cell lines (table 1) were kindly provided by Dr. Silvio Gutkind (Oral and Pharyngeal Cancer Branch, National Institute of dental and Craniofacial Research, NIH, Bethesda, USA).

Cells referenced in table 1 were cultured in pyruvate-free high glucose (25 mM) DMEM or RPMI (DMS53, H460, and SW900) medium (Biological Industries, Beit Haemek, Israel). All media were supplemented with 10% fetal bovine serum (FBS; GIBCO, Paisley, UK) and 100 U/mL penicillin, 100mg/mL streptomycin, and 2 mM L-glutamine, all from Biological Industries. Cells at passage 10–25 were grown in a humidified atmosphere of air containing 5% CO_2 at 37 ºC. Cells were cultured in 10 cm plates and splitted 2-3 times per week using 0.05% trypsin EDTA-solution (Invitrogen).

2. Cancer stem cells isolation and characterization

Cancer stem cells were obtained from resected patient tumor samples or isolated from cancer cell lines in collaboration with the laboratories of Dr. Farràs and Dr. Jantus-Lewintre from Research Foundation at General University Hospital of Valencia and Principe Felipe Research Centre, respectively.

2.1. Tumor cell preparation

On one hand, resected tumor samples were sent to laboratory in phosphate buffer saline (PBS) with antibiotics within the first hour after being extracted from patients. Samples were washed with PBS with antibiotics three times, chopped with a sterile blade, and incubated in 0.001% DNase (Sigma-Aldrich, St Louis, MO, USA), 1 mg/mL collagenase/dispase (Roche, Indianapolis, IN, USA), 200 U/mL penicillin, 200 µg/mL streptomycin, 0.5 µg/mL amphotericin B (GIBCO) in DMEM/F12 medium (GIBCO) at 37°C in a water bath for 2 h with intermittent shaking. After incubation, the samples were washed with medium and centrifuged at 3000 x g for 5 min. Then, the suspensions were repeatedly triturated

with a Pasteur pipette, passed through 70 µm and 40 µm cell strainers (BD Biosciences, San Jose, CA, USA), and centrifuged at 2000 x g for 5 min at 4°C. Cells were resuspended in 500 µL DMEM/F12 and 10 mL red blood cell lysis buffer (BD Biosciences) for 15 min at room temperature (RT) with intermittent shaking, then centrifuged at 2000 x g for 5 min before resuspension in 2 mL serum-free medium. After lysis, cell viability was evaluated by trypan blue dye exclusion. Patient samples acquisition protocol and informed consent were approved by the local ethics committee.

CSC were cultured as a cell suspension in RPMI medium supplemented with 50 µg/mL Epidermal Growth Factor, 20 µg/mL basic Fibroblast Growth Factor, 1 x Insulin-Transferrin-Selenium, 0.4% BSA and 2% B27™ (GIBCO).

On the other hand, A549 human lung cancer cell line was gently dissociated into single cells and cultured in suspension on non-adherent plates to test their ability to grow as tumor spheres, showing cancer stem cell (CSC) properties. Cells were seeded in DMEM:F12 (2:1) medium without serum, supplemented with EGF (20 ng/mL), bFGF (20 ng/mL), at a cellular density of 1 x 10^3 cells/mL. At this cellular density the sphere assay gave rise to clonal spheres as described by Eramo and colleagues in their publication (Eramo *et al.*, 2008). Serial passages were performed every 7 days. All of them needed to be enzymatically and mechanically disaggregated in order to obtain single cell suspension before subculturing.

2.2. Characterization of cancer stem cells (tumor spheres) from NSCLC cell lines and primary NSCLC tumors

Obtained CSCs were characterized through evaluation of stem cell surface markers (table 2) by flow cytometry. 1x10^6 cells were incubated with 100 µl of PBS containing 1 µg of the indicated conjugated antibodies for 1 h in the dark on ice. Labeled cells were washed with PBS, resuspended in 500 µl of DMEM and analyzed by flow cytometer (BD Biotechnology). Isotypic IgG and unstained cells served as negative controls.

Antibody	Catalog number	Supplier
CD44	560533	BD Pharmingen™
Isotype IgG2b,k PE-Cy7	560542	BD Pharmingen™
CD90	562385	BD Pharmingen™
Isotype IgG1, κ PE-CF594	562292	BD Pharmingen™
CD133	130-098-129	MiltenyiBiotec
Isotype IgG2b, APC	130-098-890	MiltenyiBiotec
CD166	46-1668-41	eBioscience
Isotype IgG1, k PerCP-eFluor 710	46-4714-80	eBioscience
E-cadherin	FAB18381P	R&D
Isotype IgG2B, PE	IC0041P	R&D
Epcam	130-080-301	MiltenyiBiotec
Isotype IgG1, FITC	130-092-213	MiltenyiBiotec

Table 2. List of antibodies used for flow cytometry analysis

Moreover, tumorigenic properties of tumor spheres were assessed through subcutaneous transplantation in 6 week old NOD.CB17-Prkdc^{scid}/NcrCrl mice (Jackson Laboratories, Bar Harbor, ME, USA). Primary lung tumor spheres of patients FIS302 and FIS303 were dissociated into single cells. 2.000, 20.000 or 100.000 cells from FIS303 or FIS302 were resuspended in 50 ul serum-free medium and Matrigel (BD) (1:1) and injected. Tumor growth curves were monitored once a week during 3 months.

3. Evaluated compounds: synthetic tambjamine analogues

Tambjamine analogues were synthesized by Dr. Roberto Quesada and colleagues, from Chemistry Department of Burgos University (Burgos, Spain) as previously reported (Hernando *et al.*, 2014). As a result of the search for compounds with efficient transport activity, molecules derived from the already known natural alkaloids tambjamines were synthesized. Naturally occurring tambjamines are characterized by a 2,2´bipyrrole-enamine structure with a 4-methoxy substituent and different alkyl chains as amine substituents. On the other hand, these synthetic compounds are characterized by the presence of aromatic amine groups bearing both electron donating and electron withdrawing substituents (figure 22). In addition to these compounds, the replacement of the methoxy group characteristic of the natural compounds by a benzyloxy group was also explored (figure 22, right column), generating pairs of parent compounds.

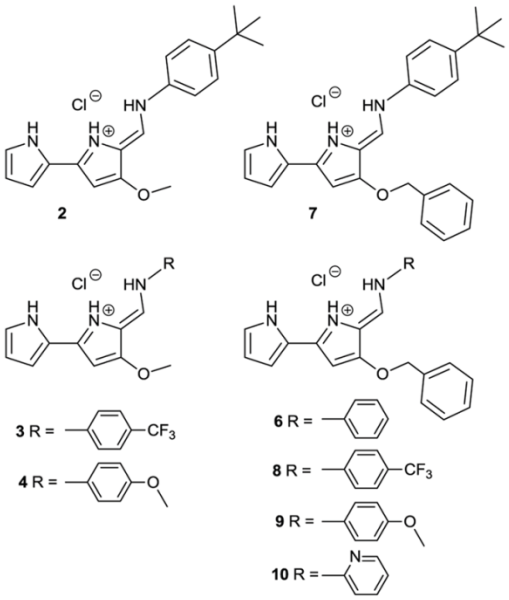

Figure 22. Structures of synthetic tambjamine analogues. Modified from (Hernando *et al.*, 2014).

Drugs were dissolved at 10 mM in dimethyl sulfoxide (DMSO) and stored at -20 °C. Subsequent dilutions for biological assays were made in culture medium and a maximum concentration of 1% DMSO was used for the cellular assays.

4. Ion-selective electrode transport assays

Once the compounds are synthesized, their anion transport capacity in liposomes was evaluated in liposomal model.

A chloroform solution (20 mg/mL) of 1-palmitoyl-2-oleoyl-snglycero-3-phosphocholine (POPC) (Sigma-Aldrich) was evaporated in vacuo using a rotary evaporator and the resulting lipid film was dried under vacuum for at least 2 h. After that, it was rehydrated by addition of a sodium chloride solution (489 mM NaCl and 5 mM phosphate buffer, pH 7.2 or 451 mM NaCl and 20 mM phosphate buffer, pH 7.2) followed by careful vortexing. The obtained lipid suspension was subjected to nine freeze-thaw cycles and twenty-nine extrusions through a 200 nm polycarbonate Nucleopore membrane using a LiposoFastBasic extruder (Avestin Inc., Ottawa, Canada). In order to remove the unencapsulated chloride, the obtained vesicles were dialyzed against a NaNO3 solution (489 mM NaNO3 and 5 mM phosphate buffer, pH 7.2) or a Na_2SO_4 solution (150 mM Na_2SO_4 and 20 mM phosphate buffer, pH 7.2), respectively. For the NO_3^-/Cl^- assays, vesicles prepared as described above (rehydrated with 489 mM NaCl), were suspended in a solution 489 mM $NaNO_3$ and 5 mM phosphate buffer, pH 7.2 to a final lipid concentration of 0.5 mM in a total volume of 5 mL. Using a chloride selective electrode (CRISON 96 52 C I.S.E. electrode) the chloride efflux was monitored over time. After 60 s, an aliquot of the transmembrane anion carrier in DMSO was added (the amount of DMSO was always less than 20 µL in order to avoid influence of the solvent molecules in the assay). After five minutes (t = 360 s), a pulse of detergent was added (Triton™ X-100 10% dispersion in water, 20 µL), thus vesicles were lysed. The obtained final reading was considered as the 100% of the chloride encapsulated and used as such. For (HCO_3^-/Cl^-) assays, the vesicles were rehydrated with 451 mM NaCl and suspended in the Na_2SO_4 solution. Again, the final lipid concentration in each experiment was 0.5 mM and the total volume in each experiment 5 mL. A volume of the carrier molecule was added at the beginning of the experiment (t = 0 s). A minute later (t = 60 s), an aliquot of $NaHCO_3$ (in 150 mM Na_2SO_4 buffered to pH 7.2 with 20 mM sodium phosphate salts) was added for a final concentration of 40 mM. The chloride efflux was measured during 5 min and then the detergent was added (t = 360 s). The data were used as described previously.

5. Cell viability assay

Cell viability was determined by the MTT (3-(4,5-dimethylthiazol-2-yl)-2,5-diphenyltetrazolium bromide) assay. This method consists of a colorimetric assay that involves the cleavage and conversion of the water soluble MTT, which in solution has a yellowish color, to the insoluble purple formazan salts through the reduction carried out by active mitochondrial dehydrogenases of living cells.

Cancer cell lines listed in table 1 were seeded at a concentration of 1 x 10^5 cells/mL in 96-well microtiter plates in 100 µL per well of the respective culture medium, and incubated for 24 h to allow cells to attach. Afterwards, they were treated for 24 h with the corresponding treatment. In the case of single point experiments cells were treated with 10 µM of each compound. To calculate the inhibitory concentrations (IC) of 25%, 50% and 75% of cell population, dose-response curves were performed ranging from 0.8 to 100 µM. The drug concentrations corresponding to IC_{25}, IC_{50},

and IC_{75} values were used in subsequent experiments. Cisplatin (Sigma-Aldrich), used as positive control, was tested at concentrations ranging from 2.34 to 300 µM, DMSO or H_2O were used as negative control at a concentration of 1% (v/v). Moreover, in the case of A549 we tested another cis-Dichlorodiammineplatinum(II) (CDDP) from Accord Healthcare (North Harrow, United Kingdom) in a range of concentrations from 1.56 to 200 µM.

Cell viability assays along with cell death inhibitors were performed with A549, the most representative lung cancer cell line. Cells were seeded following the procedure previously described. The day after seeding, cells were incubated for 1 h, prior to compound **2** addition, with the apoptotic inhibitor Z-VAD-FMK (BD Biosciences) at 10 µM or the autophagic inhibitor 3-Methyladenine (3-MA) from Sigma-Aldrich at a concentration of 5 mM. After the incubation time with the inhibitor, the treatment with 3 or 5 µM of compound **2** was added.

After 24 h with the respective treatment, 10 µM of MTT (Sigma-Aldrich) diluted in 1 x PBS was added to each well for an additional 4 h. The medium was removed and the MTT formazan precipitate was dissolved in 100 µL of DMSO.

Absorbance was read on a Multiskan multiwell plate reader (Thermo Fisher Scientific Inc., Waltham, MA, USA) at 570 nm. For each condition, at least three independent experiments were performed in triplicate. Cell viability was expressed as a percentage of control cells, and data are shown as the mean value ± S.D. The IC_{25}, IC_{50} and IC_{75} values were calculated with GraphPadPrism™5 software (Graph Pad Software, San Diego, CA, USA).

For single-point cell viability assays in cancer stem cells, monolayer cells (passage 10-20) and sphere-forming cells (passage 10-20) were seeded in 96-well plates at 1-2 x 10^3 or 3.5 x 10^3 cells/mL, respectively, in 200 µL per well. One day after seeding, compound 2 and 7 were added in three replicates at 10 µM for each cell line or cultures derived from patients.

Cell viability was measured after 24 h, using the CellTiter 96™ AQueous One Solution Cell Proliferation Assay (Promega, Madison, WI, USA) and following the instructions of the manufacturer. Absorbance at 490 nm was detected using a VICTOR3™ Multilabel Plate Reader (Perkin Elmer-Cetus, Norwalk, CT, USA). Cell viability was normalized to the respective control cells and presented as a percentage of them. For each condition, three independent experiments were performed and mean ± SD is shown.

6. Cell cycle analysis

Measurement of DNA content by flow cytometry is the most frequently used method to analyze and distinguish cells in different phases of cell cycle. Cells are stained with a fluorescent DNA intercalating agent. Consequently, the fluorescence intensity observed by flow cytometry correlates with the amount of DNA from each phase.

CAL27 and A549 cell lines were seeded in 6-wells plate at a density of 1 x 10^5 cells/mL in a volume of 2 ml and allowed them to attach for 24 h. The day after seeding, the complete medium was removed, and medium with 0.05% of FBS was added for 24 h, with the aim of synchronizing the cells. Afterwards, it was replaced by 10% FBS complete media and cells were treated with the IC_{50} of compound **2** and

7 during 24 and 48 h. Cisplatin, cisdiamminedichloroplatinum (II) (CDDP), was used at 5 µM for 24 and 48 h.

After treatment, single cell suspension was collected in a 15 ml tube and centrifuged at 300 g for 5 min. After that, supernatant was discarded and cell pellet was washed with 1 x PBS. Cells in PBS were centrifuged at 300 g for 5 min, and the supernatant was discarded without disturbing the cell pellet. The pellet was resuspended in residual PBS by pipetting. Cell suspension was added drop by drop into a 50 ml tube containing 1 ml of cold 70% ethanol while vortexing at medium speed to fix cells. Fixed cells were stored at -20°C overnight. Ethanol-fixed cells (approximately 200 µL) were placed in a 12 x 75 mm polystyrene test tube and centrifuged at 300 g for 5 minutes at RT. The supernatant was discarded and the cell pellet was washed with PBS. Cell suspension was centrifuged at the same speed as before and the supernatant was removed. Afterwards, cell pellet was resuspended and incubated in 200 µL of Muse™ Cell Cycle Reagent (Merck Millipore, Darmstadt, Germany), which includes the nuclear DNA intercalating stain propidium iodide, for 30 minutes at RT and protected from light. Cells were analyzed by Muse™ Cell Analyzer and analysis software (Merck Millipore). The experiment was done in triplicate; the values shown are the mean ± its standard deviation.

7. Acridine Orange staining

Vital staining with acridine orange (AO) was used to evaluate pH changes in acidic organelles. A549 were seeded in a 12-well plate with 15 mm round sterile coverslips at a density of 1 x 10^5 cells/mL. The day after, once the cells are adhered, they were treated with the corresponding treatment for 1 h in DMEM supplemented with 10% FBS at 37 ºC.

A549 cells were treated with compounds **2** or **7** for 1 h at 10 µM. As a negative control, cells were treated with a non-transporter compound (**NT**) at 10 µM for 1 h. **NT** is a compound structurally related to 2 and 7 that displays modest activity as anion carrier. 1% DMSO (v/v) was added in control cells. After completion of the different treatments, the treatment was removed and the cells were washed twice with 1 x PBS, then the cells were stained with 200 µL of the AO solution (Sigma-Aldrich) at a concentration of 5 µg/mL for 30 min at RT and protected from light. Afterwards, cells were washed three times with 1 x PBS/10% FBS, mounted on a slide, and fluorescence was immediately examined in a Nikon eclipse E800 microscope (filter 330/380 nm) (Nikon Europe BV, Badhoevedorp, The Netherlands). Three independent experiments were conducted and representative images are shown.

8. Hoechst 33342 and propidium iodide staining

Hoechst 33342 (Sigma-Aldrich) and propidium iodide (PI) were used as nuclear counterstains to detect cells that underwent apoptotic or necrotic processes measuring morphological changes like chromatin condensation or loss of membrane integrity, respectively.

A549 cells were plated in a 12-well plate with 15 mm round sterile coverslips at a concentration of 1 x 10^5 cells per well. The cells were allowed to adhere to the coverslips for 24 h, afterwards cell

media was removed and fresh media with the corresponding drug dose was added. A549 cells were incubated in with the IC_{50} of compound **2** and **7** for 48 h. Control cells were incubated with DMSO. After this time, on one hand the media was collected and centrifuged twice at 700 g washing with 1 x PBS to pellet down the floating cells. At the same time, the attached cells were washed 3 times with 1 x PBS.

Cell pellet and cells on coverslips were stained with the nuclear counterstains Hoechst 33342 and PI at a concentration of 2 µg/mL and 25 µg/mL, respectively, for 20 min at 37ºC in dark conditions. Then, the staining solution was removed and cells were washed twice with 1 x PBS. Detached cells were centrifuged twice at 700 g and washed with 1 x PBS. PBS was discarded and cells were resuspended in 10 µL of glycerol:H_2O (9:1). Cells on glycerol were dropped in slides and the cells on the coverslips were placed over them. Mounts were examined fluorometrically with Cells were photographed using an inverted fluorescent microscope (Axio Observer Z1, Zeiss, Gottingen, Germany) and at least three representative images were acquired for each sample condition.

9. Phase contrast microscopy

In order to observe cytoplasmic vacuolization, 2 mL of A549 cells were seeded in a 6-well plate at a concentration of 1 x 10^5 cells/mL and were allowed to grow for 24 h. Subsequently, cells were treated with the IC_{75} values of compound **2** and **7,** or 10 µM of non-transporter compound, **NT**, during 6 h. Samples were observed under inverted phase contrast microscope (Axio Observer Z1). To monitor the vesicle formation process, A549 cells were seeded in 96-well microtiter plates at a density of 1 x 10^5 cells/mL and incubated for 24 h to allow cells to attach. Afterwards, they were treated for 24 h with 10 µM of each synthetic tambjamine analogue compound. Images were captured following a time course from0 (before adding drug) to 24 h with a Leica inverted phase contrast microscope DMIRBE equipped with digital capture software (Leica Microsystems, Wetzlar, Germany).

On the other hand, to record a video of the process of vacuolization, A549 cells were seeded in a µ-Slide chambered coverslip (Ibidi) at 5 x 10^3 cells/well. Cells were allowed to attach and grow during 72 h. Afterwards, cells were exposed to IC_{75} of the studied compound **2** for 16 h. 1% DMSO (v/v) was used as a control. The video was recorded using a Leica TCS-SL filter-free spectral confocal microscope (Leica Microsystems).

10. Immunofluorescence microscopy

Different cell markers were used by immunofluorescence to determine the origin of the observed vacuolization.

A549 cells were cultured in 12-well plates on 15 mm round sterile coverslips at 37°C, seeding 1 x 10^5 cells per well. 24 hours later, cells were treated at a confluence of 70-80% with the IC_{75} of compound **2** and **7** for 6 h. Control cells were treated with 1% (v/v) DMSO. Cells were then washed twice with 1 x PBS and fixed with approximately 500 µL of 4% paraformaldehyde for 20 min at RT. Then cells were permeabilized with 0.2% Triton™X-100 and then blocked with 1% BSA in 1 x PBS for 1 h. For cell

labeling, cells were incubated with the different primary antibodies diluted in blocking solution inside a wet chamber overnight at 4°C. Approximately, 40 µL of diluted antibody was placed inside the wet chamber covered with the coverslip, in contact with the side of the cells. The primary antibodies used are listed in this table 3:

Primary antibodies	Dilution	Produced in	Brand	Catalog number
Anti-Cytochrome C	1:50	Mouse	Santa Cruz Biotechnology (Santa Cruz, CA, USA)	6H2
Anti-EEA1	1:1000	Rabbit	Abcam (Cambridge, MA, USA)	ab2900
Anti-LC3	1:500	Rabbit	MBL international Corporation (Woburn, MA, USA)	PM036
Anti-LAMP1	1:1000	Rabbit	Abcam	ab24170
Anti-TOMM20	1:200	Rabbit	BD Biosciences	612278

Table 3. Specifications for primary antibodies used in immunofluorescence analysis.

In case of using anti-EEA1 (Early Endosomal Antigen 1) or anti-LAMP1, cells were permeabilized with 0.2% saponin in 1 x PBS, for 15 min, and then blocked with a solution of 0.2% gelatin-20% normal goat serum in 1 x PBS for 1 h at RT.

When the incubation time with the primary antibody ends, the wet chamber is placed at RT for 30 min. Afterwards, coverslips were placed face up in 12 well plate to perform washes with 1 x PBS twice. Cells were incubated at the same time with the fluorophore-conjugated secondary antibody and the nuclear marker (TO-PRO™-3 iodide) diluted in blocking solution. The incubation was carried out with the same procedure as the primary antibody, for one hour at RT. The secondary antibodies and the nuclear marker used are listed in the table 4:

Secondary antibodies& nuclear marker	Dilution	Brand	Catalog number
Alexa Fluor™ 555-conjugated donkey anti-mouse	1:400	MolecularProbes (Eugene, OR, USA)	A31570
Alexa Fluor™ 555-conjugated donkey anti-rabbit	1:400	Molecular Probes	A31572
TO-PRO™-3 iodide	1:400	Molecular Probes	T3605

Table 4. Specifications for secondary antibodies and nuclear marker used in immunofluorescence analysis.

After that, coverslips were placed in the 12 well plate, washed twice with 1 x PBS and rinsed in dH_2O. Finally, the samples were mounted on slides with a drop of Mowiol™ (Sigma- Aldrich) and allowed to dry at least 2 h before capturing images with Leica TCS-SL filter-free spectral confocal microscope (Leica Microsystems).

10.1. Synthetic tambjamine analogues emission spectra

Internalization of compound **2** and **7** in A549 cells was followed by Leica TCS-SL filter-free spectral confocal microscope (Leica Microsystems) with stable temperature and CO_2. Cells were irradiated with different excitation wavelengths with the aim of collecting the fluorescence emission spectra of each compound as it is shown in the figure 23. Maximum excitation for both compounds was at 488 nm.

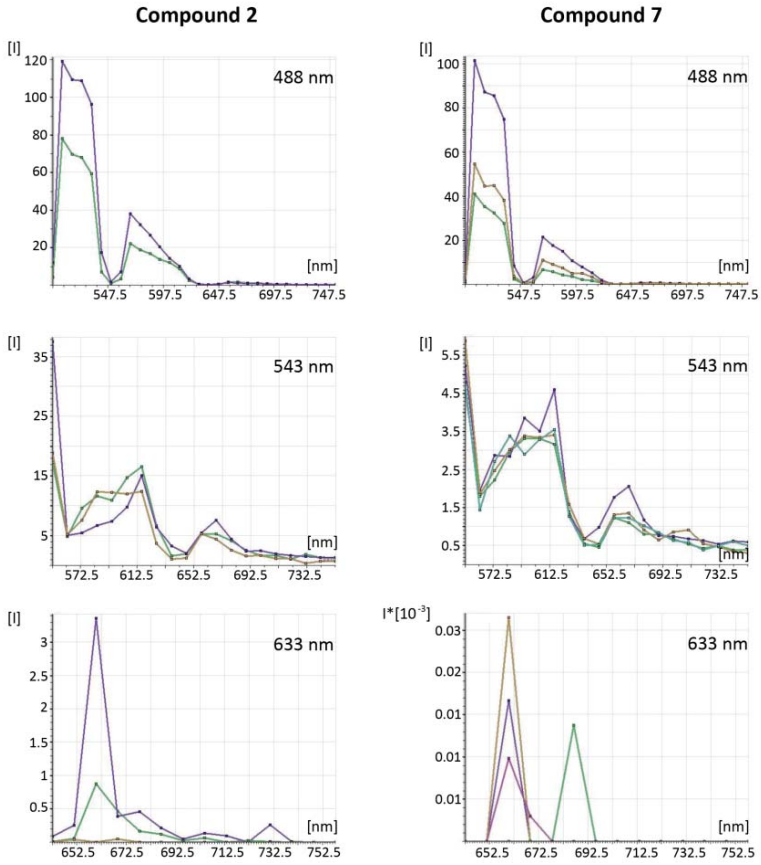

Figure 23. Compound 2 and 7 emission spectra.

In this regard, to avoid interference with the other fluorophores used in these experiments, especially when exciting at 488 nm, samples were irradiated for 2 min with 488 nm laser, to decrease fluorescence emission to non-significant values figure 24. This photobleaching procedure was performed prior to every capture of images with Leica TCS-SL filter-free spectral confocal microscope.

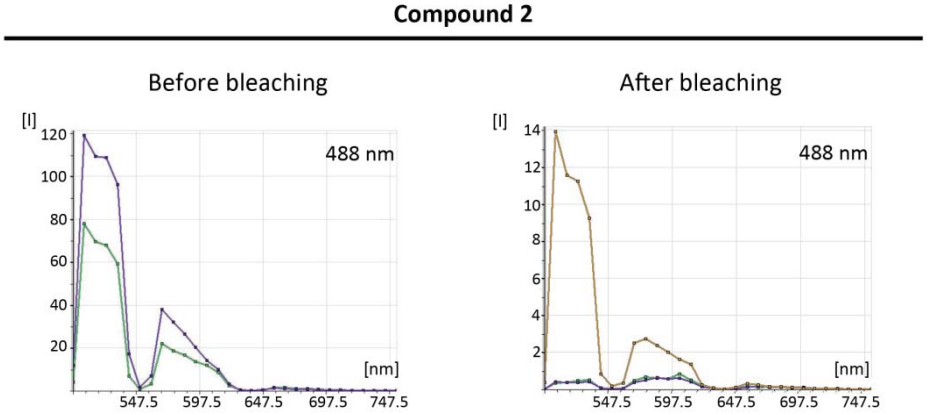

Figure 24. Emission spectra before and after photobleaching.

11. Dextran uptake

Fluorescently-labeled dextran, a fluid-phase marker, was used to study macropinocytosis process. A549 cells (10^4 cells/well) were seeded in aμ-Slide chambered coverslip (Ibidi, Martinsried, Germany), and allowed them to attach and grow during 72 h. Afterwards, cells were incubated with Dextran (ThermoFisher, D-1841) at 1 mg/mL diluted in culture media and 1 h later the studied compounds were added. Cells were treated for 6 h with the IC_{75} of compound **2** and with 10 μM MOMIPP compound, used as a positive control of the formation of macropinosomes. After the incubation time, the fluorescent images were captured using a Leica TCS-SL filter-free spectral confocal microscope (Leica Microsystems, Mannheim, Germany). Representative images from three independent experiments are shown.

12. mCherry-Mito7 stable cell transfection

The mCherry-Mito-7 plasmid DNA (figure 25), a gift from Michael Davidson (Addgene plasmid # 55102) (Olenych *et al.*, 2007), encodes a mitochondrial targeting sequence from subunit VIII of human cytochrome C oxidase (COX8A). In addition, it encodes a mCherry chromophore fusion protein, which excitation and emission wavelengths are 587 and 610 nm, respectively. This DNA construct used for transfection includes a selectable marker that confers resistance to neomycin (G418), to facilitate the selection of eukaryotic cells that stably express transfected plasmid.

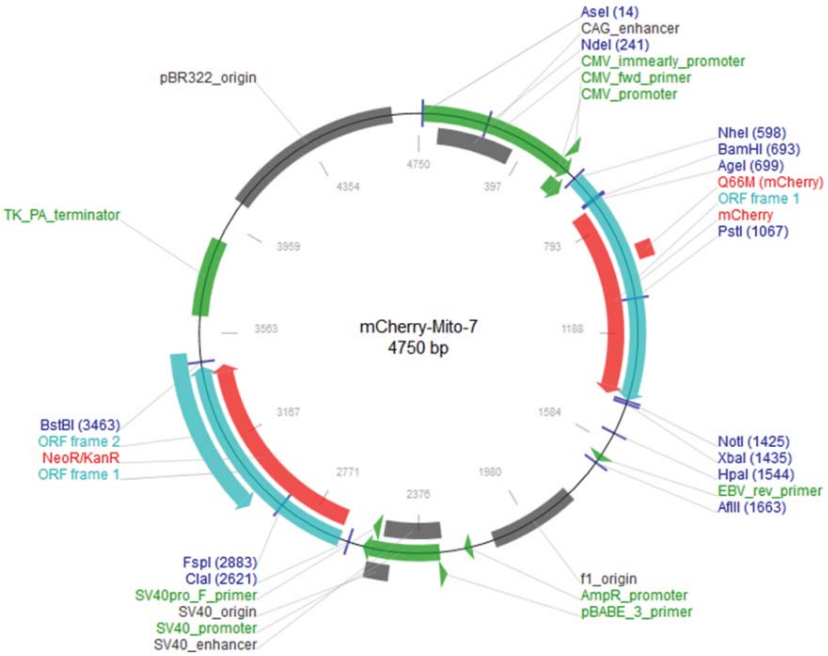

Figure 25. mCherry-Mito-7 plasmid

12.1. Plasmid purification

The plasmid was obtained as transformed bacteria in agar stab. First, bacteria were streaked in a Luria broth (LB) agar plate with kanamycin and allowed to grow overnight at 37 °C. A single colony of bacteria was isolated, and subsequently grown in a flask with 2 mL LB medium (1% NaCl, 1% Tripytone, 0.5%

yeast extract in dH_2O) containing the selective antibiotic, kanamycin (50 µg/mL) at 37 °C for 16 h with vigorous shaking to recover a high density of bacteria. After incubation, isolation of plasmid DNA was carried out with a QIAprep® Spin Miniprep kit (Qiagen, Hilden, Germany). Bacterial cells were harvested by centrifugation at 6800 g for 3 min at RT. All traces of supernatant were removed by inverting the tube until all medium was drained. Pelleted bacterial cells were resuspended in 250 µL Buffer P1 and transferred to a microcentrifuge tube. Then, 250 µL Buffer P2 were added and mixed thoroughly by inverting the tube 4-6 times until the solution became clear. Afterwards, 350 µL Buffer N3 were added and mixed as in the previous step. The microcentrifuge tube was centrifuged for 10 min at 17900 g. The supernatant (800 µL) was collected, transferred to the QIAprep 2.0 spin column by pipetting and centrifuged for 60 s. Once centrifuged, the flow-through was discarded and the column was washed by adding 0.75 mL Buffer PE and centrifuging for 60 s. Again, the flow-through was removed and the column was centrifuged at full speed for an additional 1 min to remove residual wash buffer.

To elute DNA, 50 µL Buffer EB (10 mM Tris-Cl, pH 8.5) were added to the center of the column, allowed to stand for 1 min and centrifuged for 1 min in a clean 1.5 mL microcentrifuge tube. Total DNA concentration and purity was checked by UV spectrophotometry in a nano spectrophotometer (Implen GmbH, München, Germany).

12.2. mCherry-Mito7 stable transfection

A549 cells were seeded in 60 mm plates and allowed to grow up to 80% confluence. Prior to transfection, the culture medium was changed to 4 ml/well of complete medium without FBS or antibiotics. For each transfection sample, the DNA - Lipofectamine™2000 (Invitrogen, Carlsbad, CA, USA) complexes were prepared. Both plasmid DNA (8 µg) and Lipofectamine™ 2000 (20 µL) were diluted in 500 µL of Opti-MEM® separately, and were incubated for 15 min at RT. After incubation time, the diluted DNA and the diluted Lipofectamine™ 2000 were combined and incubated for 25-30 minutes at RT to allow complexes to form. DNA-Lipofectamine™ 2000 complexes were gently dropped into each well and cells were incubated at 37°C in a humidified CO_2 incubator. After 5 h of transfection, the medium was replaced by complete medium. Two days after transfection, stable selection process was performed by adding G418 (Calbiochem, La Jolla, CA, USA) to the medium at 800 µg/mL final concentration. After 3 weeks culturing cells in selective medium, only those that had stably integrated the plasmid remained in the culture. The brightest cell population was selected by cell sorting using a MofloAstrios XPD Cell Sorter (Beckman Coulter, Miami, FL, USA). When a stable mCherry-Mito7 overexpressing A549 cell line was established, cells were seeded in a µ-Slide chambered coverslip (Ibidi), and allowed them to attach and grow during 72 h. Afterwards, cells were exposed to IC_{75} of the experimental compound 2. Control cells were treated with 1% (v/v) of DMSO. The images were captured every 20 min for 3 h using a Leica TCS-SL filter-free spectral confocal microscope (Leica Microsystems).

13. Mitotracker™ staining

MitoTracker Red CMXRos (ThermoFisher, M7512) is a red-fluorescent dye that is used to track and stain the mitochondria of living cells. Its accumulation depends on the mitochondrial membrane potential.

First, A549 cells (1 x 10^4 cells/well) were seeded in 8-well sterile µ-Slide chambered coverslip (Ibidi), and allowed to attach and grow during 72 h. Then, culture media was removed and cells were preincubated with 200 µL of MitoTracker™ Red CMXRox at 500 nM during 1 h, washed with 1 x PBS and exposed to IC_{75} value of compound **2** or to 1% (v/v) DMSO (used as a control) for 3 h. At the same time, a far-red nuclear counterstain, DRAQ5 (Abcam) was applied at a 1:5000 dilution. Subsequently, immunofluorescence images were captured using a Leica TCS-SL filter-free spectral confocal microscope (Leica Microsystems). Representative images from three independent experiments are shown.

14. ATP depletion measurement

CellTiter-Glo® luminescent assay was used to determine the amount of ATP present in cell culture after treatment with synthetic tambjamine analogues. A549 cells were seeded in opaque-walled 96-well plates at a concentration of 1 x 10^5 cells /mL in 90 µL per well. Cells were allowed to attach for 24 h. Then, cells were treated in time-course for 3, 6, 16, 24 and 48 h with the IC_{75} value of the compound **2**. Control cells were treated with 1% (v/v) of DMSO. Once the treatment finished, cell plates were equilibrated at RT for approximately 30 min. Afterwards, the CellTiter-Glo® reagent was added in an amount equal to the volume of cell culture medium present in each well. The content of the plate was mixed for 2 min on an orbital shaker to induce cell lysis. The plates were incubated at RT for 10 min to stabilize the signal. Luminescence signal was measured on a CLARIOstar® Microplate Reader (BMG LABTECH, Ortenberg, Germany). For each condition, at least three independent experiments were performed in duplicate. Amount of ATP was expressed as a percentage of control cells, and data are shown as the mean value ± S.D.

15. Transmission electron microscopy (TEM)

Electron microscopy was used to investigate the ultrastructure of cells treated with our experimental compounds thanks to its powerful magnification and resolution.

A549 cells were seeded in 100 mm plates at a concentration of 2 x 10^5 cells/mL. Twenty-four hours after plating, the cells were incubated with the IC_{75} of the compound **2** and **7** for 6 h. DMSO 1% (v/v) was used as a control. When the treatment ended, culture medium was removed and the cells were fixed in a solution containing 2% paraformaldehyde and 2.5% glutaraldehyde in 0.1 M phosphate buffer with a pH of 7.2. This procedure was carried out for one hour at RT. Then the cells were scraped very gently, harvested along with the fixative and centrifuged at 700 g to obtain cell pellets.

The obtained pellets were washed with phosphate buffer 0.1 M 3 times for 10 min at 4 °C. Subsequently, fixative solution was removed and pellets were kept in a post-fixed solution containing 1% osmium tetroxide, 0.8% potassium ferrocyanide in 0.1 M phosphate buffer (pH 7.2) at 4°C. One hour later, cells were dehydrated following a series of acetone washes at 4 °C as shown in the table 5.

Acetone percentage	Time	Temperature
25%	1x 10 min	4 °C
50%	1x 10 min	4 °C
70%	1x 10 min	4 °C
90%	3x 10 min	4 °C
96%	3x 10 min	4 °C
100%	3x 10 min	4 °C

Table 5. Dehydration steps in graded acetone

Thereafter, samples were embedded in Spurr's resin in a gradual process exposing samples to one or more mixtures of acetone and embedding medium, as shown in the table 6:

Mixture	Time
Acetone/spurr 3:1	3 h RT
Acetone/spurr 2:2	3 h RT
Acetone/spurr 1:3	3 h RT or overnight
Spurr	overnight
Spurr	2 h

Table 6. Steps of sample inclusion in the resin

Small drops of each sample-resin mixture were placed at the bottom of a mold. The molds were then filled with resin and cured at 60 °C for 48 hours. Afterwards, semithin sections (1 µm) were cut with a glass knife, mounted on slides, stained with 1% methylene blue and viewed using a light microscope to select the region of interest. Ultrathin sections (60–70 nm) were cut using a diamond knife, mounted on 200 mesh copper grids and double stained with 2% aqueous uranyl acetate for 30 min and Reynold's lead citrate for 10 min. Specimens were examined in a transmission electron microscope Jeol 1010 (Jeol, Tokyo, Japan) and digital images were acquired using a GatanOrius SC1000 CCD Digital Camera (Gatan, Inc., Pleasanton, California, USA). Two independent experiments were performed and photographs were taken from at least three different semithin sections from each experiment.

16. Immunoblot analysis

This analytical technique was employed to detect the expression of specific proteins in different cell extracts treated with synthetic tambjamine analogues. The procedure is divided into three steps that are detailed below.

16.1. Protein extract preparation

A549 cells were seeded at concentration of 1 x 10^5 cells/mL and allowed to grow for 24 h. Thereafter, they were exposed to IC_{25}, IC_{50} and IC_{75} values of compound **2** or **7** for 24 or 48 h. 1% (v/v) DMSO was used to treat control cells. After treatment, prior to protein extraction, the culture medium was collected

and cells were washed with 1 x PBS twice. Cells were collected by scraping and the wells or plates were washed again with 1 x PBS to acquire the maximum number of cells. The cell suspension with the media was centrifuged at 300 g and 4°C for 5 min. The supernatant was discarded and the cell pellet was washed with 1 x PBS and centrifuged again in the same conditions. The supernatant was discarded and the cell pellet was incubated for 15 min in lysis buffer (0.1% SDS, 1% NP-40, 0.5% sodium deoxycholate, 50 mM NaF, 40 mM β-glycerophosphate, 200 µM sodium orthovanadate, 1 mM phenylmethylsulfonyl fluoride, serine and cysteine protease inhibitor cocktail (Roche Mannheim, Germany) in 1 x PBS) at 4°C. Subsequently, the lysates were sonicated to degrade DNA. Protein concentration was determined by BCA protein assay (Pierce, Rockford, IL, USA) following manufacturer's instructions using BSA (bovine serum albumin) to create a standard curve that was taken as reference to calculate the protein concentration in our samples based on their absorbance. This procedure was performed in 96 well plates in duplicate and absorbance was read on a Multiskanmultiwell plate reader (Thermo Fisher) at 562 nm.

16.2. Gel electrophoresis and protein transfer

Laemmli buffer (Tris-HCl 250 mM pH 6.8; 10% SDS; 50% Glycerol; 0.01% Bromophenol Blue 25% 2-mercaptoethanol) was added to the samples and these were boiled at 95° C for 5 min. After that, 30-40 µg of protein extracts were loaded in SDS-polyacrylamide gel electrophoresis with different acrylamide percentages (8–15%) according to the size of the proteins that wanted to be studied. The gels were run at 120 V for approximately 90 min in Running Buffer (25 mM Tris; 192 mM Glycine; 0.1% SDS). Once the proteins were separated by size, they were transferred to Immobilon™-P PVDF membranes (Merk Millipore) using Mini Trans-Blot®Cell (Bio-Rad,Richmond, CA, USA) wet/tank system in Transfer Buffer (25 mM Tris; 192 mM Glycine; 20% Methanol) for 90 min at 100 V.

16.3. Detection of proteins

The membranes were blocked with blocking solution, 5% non-fat dry milk or 5% BSA, both diluted in 1 x TBS–Tween (20 mM Tris–HCl pH 7.5, 150 mM NaCl, 0.1% Tween 20) at RT for 1 h and then incubated with shaking overnight with primary antibodies (table 7), according to the manufacturer's instructions.

Antibody	Dilution	Produced in	Brand	Catalog number
Anti-actin	1:200	Goat	Santa Cruz Biotechnology	I-19, sc-1616
Anti-AKT	1:1000	Rabbit	Cell Signaling Technology (Beverly, MA, USA)	9272
Anti-caspase 3	1:1000	Rabbit	Cell Signaling Technology	9662
Anti-caspase 8	1:1000	Mouse	Cell Signaling Technology	9746
Anti-caspase 9	1:1000	Rabbit	Cell Signaling Technology	9502
Anti-LC3	1:1000	Rabbit	MBL International Corporation	PM036
Anti-p38 MAPK	1:1000	Rabbit	Cell Signaling Technology	8690
Anti-p62	1:1000	Rabbit	MBL International Corporation	PM045

Anti-PARP	1:1000	Rabbit	Cell Signaling Technology	9542
Anti-phospho AKT (Thr308)	1:1000	Rabbit	Cell Signaling Technology	9275
Anti-phospho MLKL (Ser358)	1:1000	Rabbit	Abcam	ab187091
Anti-phospho p38 MAPK (Thr180/ Tyr182)	1:1000	Rabbit	Cell Signaling Technology	4511
Anti-RIP	1:1000	Mouse	BD Bioscience	610459
Anti-vinculin	1:200	Mouse	Sigma-Aldrich	V-4505

Table 7. List of primary antibodies used in this thesis

The day after, the membranes were washed 3 times for 5 min each with TBS-Tween and then incubated with horseradish peroxidase (HRP) conjugated secondary antibodies diluted 1:1000 in blocking solution for 1 h at RT with shaking. The secondary antibodies used were: goat anti-mouse IgG-HRP (Cat#sc-2005), goat anti-rabbit IgG-HRP (Cat#sc-2004) and donkey anti-goat IgG-HRP (Cat#sc-2020), all from Santa Cruz Biotechnology. After 3 washes in TBS-Tween for 10 min each, the membranes were developed with the enhanced chemiluminescence detection kit, ECL reagent (Amersham, Buckinghamshire, UK) and with the ImageQuant LAS500 system (GE Healthcare, Germany). Actin or vinculin were used as gel loading controls. Densitometric analysis shows the fold-increase over control (untreated cells) in three different experiments (mean+SEM).

17. miRNA expression analysis

Evaluation of miRNA expression profiles through microarray analysis was performed to identify a specific subset of miRNAs expressed differently after treatment with synthetic tambjamine analogues versus untreated cells.

17.1. miRNA extraction

A549 cells were seeded in 100 mm plates at a concentration of 1 x 10^5 cells/ml and allowed to grow for 24 h. Subsequently, cells were incubated with the IC_{50} of compound **2** for 12 and 24 h. DMSO 1% (v/v) was added in control cells.

After treatment, prior to miRNA extraction with the miRNeasy Mini Kit (Qiagen, Hilden, Germany), culture media was collected and cells were washed with 1 x PBS twice. Then, cells were collected using a cell scraper and plates were washed again with 1 x PBS to recover the maximum number of cells. Cells were centrifuged at 300 g for 5 min, the supernatant discarded and pelleted cells were homogenized in 700 µL of QIAzol Lysis Reagent using a syringe and a 20G needle. The tube with the cell homogenate was placed on the benchtop at RT for 5 min. After that, 140 µL of chloroform was added and the tube was shaken vigorously for 15 s. In order to separate the homogenate into aqueous and organic phases, samples were centrifuged for 15 min at 12.000 g at 4 °C. After centrifugation, the

samples were separated into 3 phases: RNA partitions remained in the upper aqueous phase, DNA partitions in the interphase and proteins in the lower organic phase or the interphase. The upper aqueous phase was carefully transferred to a new collection tube and 1.5 volumes of 100% ethanol was added and mixed by pipetting to provide appropriate binding conditions for all RNA molecules from 18 nucleotides (nt) upwards. Samples were subsequently applied to RNeasy Mini spin columns and centrifuged at 8000 g for 15 s at RT. After that, on-column DNase digestion with the RNase-Free DNase Set was performed to remove residual DNA. First, 350 µL of Buffer RWT was added into the RNeasy Mini Spin Column and centrifuged for 15 s at 8000 g. The flow-through was discarded, and 80 µL of the DNase I incubation mix were directly placed onto the RNeasy Mini Spin Column membrane and allowed to incubate at RT for 15 min. Again Buffer RWT (350 µL) was added into the column and centrifuged for 15 s at 8000 g. The total RNA was attached to the membrane and contaminants were washed away using 500 µL of Buffer RPE and centrifuged at 8000 g for 2 min twice. Finally, high quality RNA was eluted in 30 µL of RNase-free water.

All the employed material was RNase free. Total RNA concentration and purity was checked by UV spectrophotometry in a nano spectrophotometer (Implen GmbH, München, Germany) and qualitative control was analyzed using an Agilent 2100 Bioanalyzer (Agilent Technologies, Santa Clara, CA, USA). Aliquots of each miRNA sample were run on the Agilent® Bioanalyzer using an RNA 6000 Nano LabChip®. All samples had RNA Integrity Number (RIN) greater than 9.

17.2. Gene expression analysis

For the reverse transcription of the mature miRNAs, 500 ng of total RNA was used for cDNA synthesis using the miScriptHiSpec Buffer and following the miScript II RT Kit protocol (Qiagen). In brief, the mature miRNAs are polyadenylated using a poly(A) polymerase and then reverse transcribed into cDNA using oligo-dT primers. This combination ensures that miScript miRNA PCR Arrays do not detect genomic DNA. Moreover, there is a kit's built-in control RNA that will be detected in the array using the miScript II RT Kit and will be used to access the reverse transcription performance.

Thus, each sample was gently mixed with the reverse-transcription reaction mix, prepared on ice according to table 8:

Component	Control	IC_{50} 12 h	IC_{50} 24 h
5x miScriptHiSpec Buffer	4 µL	4 µL	4 µL
10x miScriptNucleics Mix	2 µL	2 µL	2 µL
RNase-free water	11.48 µL	11.11µL	10.71 µL
miScript Reverse Transcriptase Mix	2 µL	2 µL	2 µL
Template RNA	0.52 µL	0.89 µL	1.29 µL
Total volume	20 µL	20 µL	20 µL

Table 8. Reverse-transcription reaction components

First, samples were incubated for 60 min at 37 °C, subsequently for 5 min at 95 °C to inactivate miScript Reverse Transcriptase Mix and placed on ice. After that, the cDNA was diluted with 200 µL

of RNase-free water and samples were stored at -20 °C overnight before beginning with the real-time PCR protocol.

For gene expression analysis, cDNAs of control and treated cells were combined with 2x QuantiTect SYBR Green PCR Master Mix, 10x miScript Universal Primerand RNase-free water at RT (Qiagen) according to table 9 and transferred into a loading reservoir.

Component	Volume
2x QuantiTect SYBR Green PCR Master Mix	550 µL
10x miScript Universal Primer	110 µL
RNase-free water	340 µL
TemplatecDNA	100 µL
Total volume	1100 µL

Table 9.Reaction mix for Pathway-Focused miScript miRNA PCR Arrays

PCR components mix were dispensed (10 µL/well) in theRT^2 Profiler PCR Array of Human Cancer PathwayFinder 384HC (MIHS-3102Z format E, Qiagen). This array profiles the expression of 372 miRNAs differentially expressed in tumors versus normal tissue *(the list of all cancer-related miRNAs included in the array can be found in supplementary data, table S1*). The array plate was tightly sealed with an optical adhesive film and centrifuged at 300 g for 2 min at RT to remove bubbles. Subsequently the Array was placed in an ABI PRISM 7900HTreal-time PCR system (Applied Biosystems, Thermo Fisher Scientific Inc.) and the analysis was carried out according to table 10.

Step	Duration	Temperature	Comments
PCR initial activation step	10 min	95°C	HotStart DNA *Taq*Polymerase was activated by temperature
3-step cycling:			
Denaturation	15 s	94 °C	
Annealing	30 s	55 °C	
Extension	30 s	70 °C	Performs fluorescence data collection
Cyclenumber	40 cycles		Cycle number depends on the amount of template cDNA and abundance of the target

Table 10. Cycling conditions for Applied Biosystems cycler

17.3. Data analysis

The average threshold cycle (CT) values obtained were analyzed in Qiagen Data Analysis Center (Qiagen) to retrieve the fold-regulation values for each miRNA gene. A selection of miRNA was made according to the following thresholds: more than 2-fold regulation between control and both treated conditions (12 h or 24 h) or more than 5-fold regulation between control and one group condition. These miRNAs will only be selected if at least one treated condition has an average threshold cycle below 30, when the control condition has an average threshold cycle below 35. In all selected miRNAs, regulation in both conditions should agree and the melting curves and amplification plots should be

well defined. Dissociation/melting curves and amplification plots were carefully analyzed using SDS software v2.3 and RQ Manager v1.2 (both from Applied Biosystems, Thermo Fisher Scientific Inc.). Experimentally validated miRNA-gene interactions databases as DIANA-TarBase v7.0 (http://www.microrna.gr/tarbase), miRTarBase v6.0 (http://mirtarbase.mbc.nctu.edu.tw/), the miRecords v4.0 (http://mirecords.umn.edu/miRecords/) and miRNAMapv2.0 (http://miRNAMap.mbc.nctu.edu.tw/) were employed to extract target genes for the selected miRNA (*the images of the modified miRNAs after treatment along with their target genes can be found in the supplementary data, figures S1-S16*). Finally, the open-source software, Cytoscape (Cytoscape Consortium, San Diego, CA, USA), was used to build a biomolecular interaction network with the most altered miRNAs after the compound treatment.

18. Computational methods

Computational methods such as molecular docking are widely used to predict possible drug targets or vice versa. This system uses different software of binding simulation to predict the most probable union between two molecules. In collaboration with Víctor Guallar's research group from Barcelona Supercomputing Center and using docking simulations of our compounds with more than 100 cancer-related proteins, the AKT enzyme was identified as one of the proteins to which the compound may bind with greater affinity.

18.1. System preparation

Coordinates for the AKT model were taken from the Protein Data Bank entry 3QKM (human AKT protein). Hydrogen atoms and side chains were optimized with the Protein Preparation Wizard tool from Schrodinger at physiological pH, and missing fragment (residues 452-456) was recovered and filled with Prime. Compound **2** ligand was built with the Maestro graphical interface and optimized with LigPrep.

18.2. Induced-fit docking simulations

Induced fit docking simulations were performed with PELE, software that combines a Monte Carlo stochastic approach with protein structure prediction algorithms (Borrelli *et al.*, 2005). PELE is capable of accurately reproducing long timescale processes (Cossins, Hosseini and Guallar, 2012) and conformational changes from protein-ligand recognition (Borrelli, Benjamin and Guallar, 2010; Grebner *et al.*, 2016; Kotev, Soliva and Orozco, 2016) PELE sampling algorithm is a consecutive iteration of three main steps: 1) ligand and protein (α-carbons) perturbations; 2) protein side-chains sampling; and 3) minimization.

The initial PELE structures were constructed by building 20 models where the compound **2** ligand (structure on Figure 53, A) was placed around AKT at distances varying from 10 to 30 Å to its approximate center (defined by Asn279); the ligand was allowed to explore all the space within 33 Å of this center. Ligand translation was switched between a larger step of 1.5 Å and a small one of 0.5 Å. Side chain sampling

was executed for all residues within 5 Å from the ligand and this was followed by the minimization of the full system. Recently, a similar protocol for global PELE exploration was applied successfully to EZH2 in complex with another derivatives from the tambjamine family (Kotev *et al.*, 2017). PELE simulations were carried out using 240 cores for 48 hours on the Marenostrum supercomputer; each color and shape in Figure 53B represents a single PELE trajectory running on a computing core (more details about PELE software and simulations can be found at https://pele.bsc.es).

Further rescoring of the PELE poses was done with Glide using the extra precision (XP) scoring function.

19. Surface Plasmon Resonance assays

Surface Plasmon Resonance (SPR) assays were performed using the Biacore T200 system. This technology makes possible to monitor and measure biomolecular interactions in real-time with high sensitivity. In this regard, it allows determining specificity, affinity and kinetic parameters during the binding of different pair of molecules including protein-protein, enzyme-substrate or inhibitor, receptor-drug or protein-small molecules, among others. The approach involves the immobilization of one interacting partner (ligand) to the surface of a sensor chip, and the injection of the sample in a continuous flow, containing the other interaction partner (analyte) over the surface. This chip is composed of a glass surface covered with a thin gold layer and over this layer, a coating which enables the attachment of the ligand.

The gold layer is a conducting film located at an interface between media of different refractive index, the glass of the sensor chip and the sample solution. SPR is a phenomenon that occurs when a polarized incident light hits the metal surface with certain incidence angle and wavelength. The electrons at the surface of the biochip absorb the energy of incident light photons and move generating plasmon waves due to the excitation. The light is reflected with a specific angle. Changes in molecular weight and solute concentration at the surface of the sensor chip, such as biomolecular interactions between ligand and analyte, cause changes in the refractive index of the solution (figure 25A), which in turn vary the reflected angle. Thus, the resonance angle shifts can be measured and are directly proportional to the concentration of biomolecules on the surface. The response or signal change is measured in resonance units (RU), where 1 RU is equivalent to a critical angle shift of 10^{-4} degree (Nguyen *et al.*, 2015). The system Biacore T200 tracks the changes in RU against time, showing the progress of the interaction in a plot known as sensorgram (figure 25B).

SPR assays were designed in order to monitor the interactions between ligand AKT2 (PV3184, Thermo Fisher) and compound **2** (analyte). AKT2 ligand was immobilized following Biacore T200 protocol in a sensor chip CM5 (GE Healthcare BioSciences AB, Uppsala, Sweden). This is coated with a carboxymethylated dextran matrix that allows a covalent protein attachment by amine coupling. Prior to immobilization, in order to determine the optimal pH for pre-concentrating the ligand over the matrix, a pH scouting was performed. The ligand was diluted to 1 µM in 10 mM acetate buffers with different pH ranging from 4.0 to 5.0, and injected during 180 s with a flow of 5 µL/min over an unmodified sensor chip. Then, the surface was regenerated with 50 mM NaOH to ensure no ligand remains bound to the surface. Once, the optimum pH was selected, the surface of the sensor chip

was activated with a mixture 1:1 of 1-ethyl-3-(3-dimethylaminopropyl)-carbodiimide (EDC) and N-hydroxysuccinimide (NHS) in order to form reactive ester groups on the surface. Subsequently, AKT2 protein was diluted to 0.75 **µM** in 10 mM acetate buffer with pH 4.5 and immobilized in flow-cell 2 up to 7500 RU. The immobilized ligand level was previously calculated according to the relative molecular weights of the ligand and the analyte and the maximum binding capacity of the surface with a theoretical R_{max} (maximal response) of 50 RU.

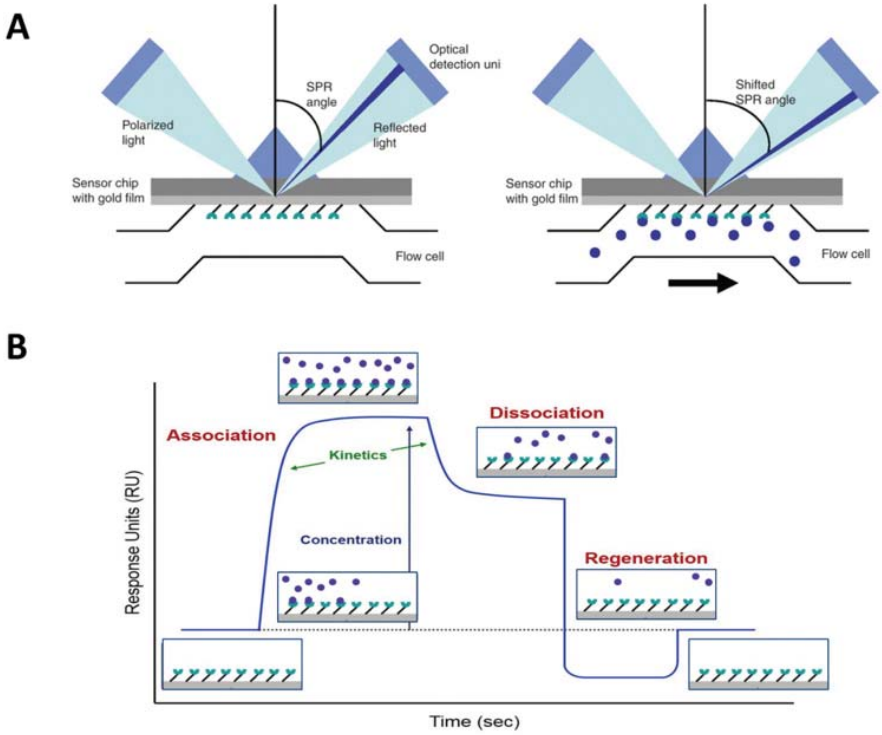

Figure 25. Principle of SPR from (Madeira *et al.*, 2009) and schematic sensorgram

The flow-cell 1 was activated and assigned as reference channel. Once the immobilization was performed, ethanolamine solution was injected in order to deactivate the remaining reactive groups of the surface (figure 26).

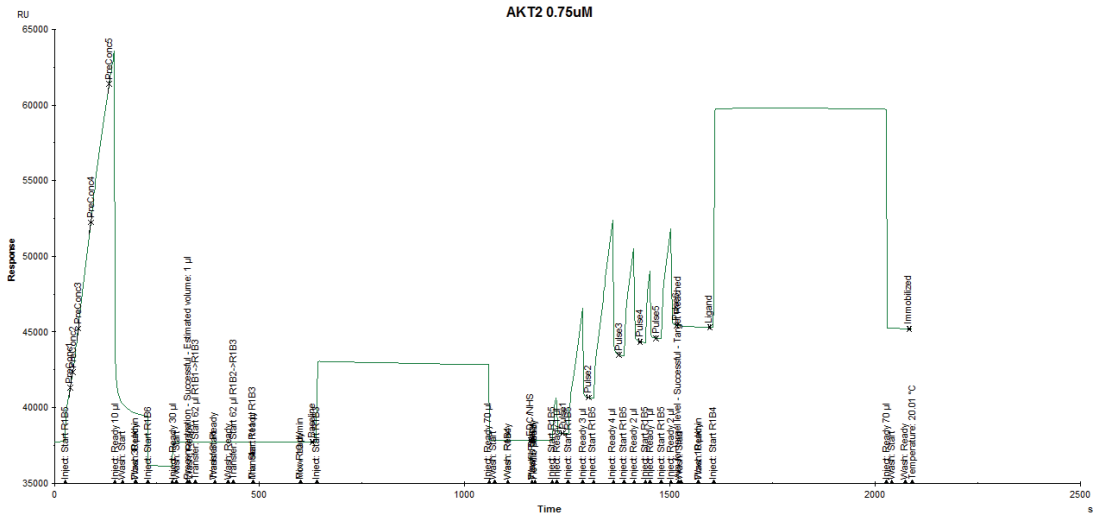

Figure 26. AKT2 immobilization

Compounds were stored as stock solutions in 100% DMSO at -20 °C. The compound was diluted with running buffer (1 x PBS-P 5% DMSO) at concentrations ranging from 0.15 µM to 10 µM. The run was started with 5 start-up cycles with running buffer. After that, samples were injected with a 30 µL/min flow for 60 s. Zero concentration samples were used as blanks. After every injection, the programmed dissociation phase was 120 s. The complexes were regenerated using 25 mM NaOH prior to every cycle series. Moreover, between sample series, a solvent correction with carefully prepared DMSO reference solutions ranging from 4.5% to 5.8% was run. Solvent correction was performed to adjust measured sample responses due to solvent effects on the bulk refractive index variations.

Experiments were performed with the instrument temperature (flow cell, sensor chip, and sample compartment temperature) set to 25 °C. For kinetic and affinity evaluations, Biacore T200 evaluation software was used for subtraction of reference and blank data, along with solvent correction as well as for curve fitting, using the 1:1 Langmuir model. Two independent experiments were performed and constant values are expressed as the mean ± SD.

20. *In vivo* evaluation of tambjamine-analogues therapeutic effect

Two murine models have been developed: the ectopic (subcutaneous) and the orthotopic model systems to evaluate the antitumor activity of the synthetic tambjamine analogues **2** and **7**.

All animal studies were approved by the Local Ethics Committee (Generalitat de Catalunya) under the protocol 9111. To generate the subcutaneous xenograft model, mice were subcutaneously implanted with 4.5×10^6 A549 cells suspended in a 1:1 solution of DMEM:Matrigel (BD Bioscience).

For the orthotopic model, subcutaneous xenografts of A549 in exponential growth from three different animals were aseptically isolated and placed at RT in DMEM supplemented with 10% FBS plus 50 U/mL penicillin and 50 mg/mL streptomycin and the surgical resection tumors were implanted in Crl:NU-Foxn1nu mice following previously reported procedures (Ambrogio *et al.*, 2014, 2016). Briefly, mice were anesthetized with a continuous flow of 1% to 3% isoflurane/oxygen mixture (2 L/minutes) and subjected to right thoracotomy. Mice were situated in left lateral decubitus position and a small transverse skin incision (around 5–8 mm) was made in the right chest wall. Chest muscles were separated by a sharp dissection and costal and intercostal muscles were exposed. An intercostal incision of 2–4 mm on the third or fourth rib on the chest wall was made and a small tumor piece of 2 to 4 mm^3 was introduced into the chest cavity. The tumor specimen was deposited between the second and the third lung lobule. Next, the chest wall incision was closed with surgery staples, and finally chest muscles and skin were closed. Mice were inspected twice a week, and monitored for the presence of breathing problems.

Mice bearing homogeneous subcutaneous tumors (approximately 150–200 mm^3) were randomly allocated to five treatment groups (n = 7/treatment). For A549 orthotopic-derived model, mice were randomly allocated to three groups (n = 4/treatment) and the treatment started 30 days after tumor implantation. Compounds **2** and **7** were diluted in 7.5% DMSO/0.8% Tween-80. All treatments were intraperitoneally administrated at a dose of 6 mg/kg in alternating days during 20 days. In the case of the subcutaneous model, we wanted to compare the effect of our compounds with the first-line

chemotherapeutic agent, CDDP. Mice were administrated with CDDP at a dose of 4 mg/kg days 0, 7 and 15 and sacrificed day 21.

Mice were weighed on the first day to determine the effects of compounds administration on their general health status. Mice weights of all groups were monitored over all the experimental period. Tumor growth was recorded two to three times per week starting from the first day of treatment (day 0) and tumor volume (in mm^3), estimated according to the formula V ¼ (ab2)/2, where “a” is the length or biggest diameter and “b” is the width or smallest diameter. After the final dose of the treatment, animals were sacrificed and tumors were dissected out and weighed. Liver and kidney samples were fixed in formalin overnight, embedded in paraffin, and cut into sections (5 µm). Paraffin-embedded sections were deparaffinized in xylene and gradually rehydrated for hematoxylin and eosin staining. Stained liver and kidney sections were gradually dehydrated and mounted for hepatotoxicity and nephrotoxicity examination, respectively.

21. Statistical analysis

Results are expressed as the mean ± SD or mean ± SEM of at least three independent experiments. One-way ANOVAs were carried out with the Statgraphics centurion statistical package and post hoc Tukey analyses were performed. Statistically significant differences, $p < 0.05$ and $p < 0.01$, are represented by * and **, respectively.

RESULTS

1. Anion transport screening

In the search of new molecules with anionophoric activity, the research group led by Dr. Roberto Quesada has designed and synthesised different batches of small molecules capable of facilitating the transmembrane transport of ions. Once synthesized, its capacity as anion carriers was tested in 1-palmitoyl-2-oleoyl-sn-glycero-3-phosphocholine (POPC) liposomes loaded with NaCl and dispersed in different buffers containing $NaNO_3$ or Na_2SO_4. Therefore, transmembrane anion transport activity of the aforementioned synthetic tambjamine analogues molecules was explored (*see figure 22, material and methods section 3*). The chloride efflux from chloride loaded vesicles was monitored over time and the EC_{50} values (the Effective Concentration of compound necessary to achieve 50% anion efflux at a particular time) were calculated (table 11). These tests revealed that synthetic tambjamines analogues are very efficient anion transporters since their EC_{50} values are in the nanomolar range.

Compound	EC_{50} (nM) NO_3^-/Cl^- [a]	EC_{50} (nM) HCO_3^-/Cl^- [b]
2	50 ± 8	240 ± 40
3	140 ± 6	890 ± 80
4	70 ± 5	460 ± 60
6	80 ± 10	370 ± 50
7	60 ± 3	880 ± 300
8	720 ± 70	11920 ± 1000
9	70 ± 3	430 ± 100
10	40 ± 2	170 ± 20

Table 11. Transport activities expressed as EC_{50} (nM) of synthetic tambjamine analogue compounds modified from (Hernando *et al.*, 2014)**.** a. Vesicles loaded with 488 mM NaCl dispersed in 488 mM $NaNO_3$ (5 mM phosphate buffer, pH 7.2). b. Vesicles loaded with 451 mM NaCl dispersed in 150 mM Na_2SO_4 (20 mM phosphate buffer, pH 7.2) upon addition of a $NaHCO_3$ pulse to make the extravesicular bicarbonate concentration 40 mM.

2. Anticancer effect evaluation

2.1. Assessment of anionophores cytotoxicity in oral and lung cancer cell lines

It has recently been described that the transport of ions causes, among other things, changes in the intracellular pH, which can induce cell death. Moreover, in recent years there has been considerable interest in natural tambjamines and their biological properties. In the literature there are several examples that characterize them as antimicrobial, cytotoxic or antitumor agents (Carbone *et al.*, 2010;

Pinkerton *et al.*, 2010). Therefore, we first decided to assess the effect of a synthetic tambjamine analogues batch on cell viability. This batch of synthetic tambjamines analogues consisted of eight compounds derived from the already known natural alkaloids tambjamines.

These molecules were characterized by the presence of aromatic groups as amine substituent, and either a methoxy or a benzyloxy group in the central heterocycle. On one hand, cell viability was evaluated after the treatment with synthetic tambjamine analogues in different lung cancer cell lines representative of the four major histological subtypes (A549, adenocarcinoma; SW900, squamous cell carcinoma; H460, large cell carcinoma; DMS53, small-cell carcinoma). Cells were treated with all the tested compounds in a single dose of 10 μM for 24 h and the MTT assay was employed to assess cell viability. On average, we found that after treatment, cell viability was reduced over 50% with the majority of compounds (figure 27A).

Among all compounds subjected to screening, we selected the most potent synthetic tambjamine analogues, compound **2**, along with its parent compound **7**. Both compounds bear the same aromatic substituent (4-tert-butylphenyl) in the enamine moiety, and compound **7** presents a benzyloxy group replacing the methoxy group characteristic of the natural tambjamine derivatives.

In order to compare the cytotoxic potential of both molecules and to evaluate the sensitivity of lung cancer cells to these compounds, A549 cells, representative of lung adenocarcinoma, were treated at different concentrations (a range between 0.78 and 100 μM) for 24 h. Moreover, dose-response experiments were also performed with cisplatin, a chemotherapeutic currently used in lung cancer treatment (figure 27B). Non-formulated cisplatin was tested with a range of concentrations between 2.34 and 300 μM, and commercial formulated cisplatin, CDDP, was tested in a range of concentrations from 1.56 to 200 μM.

The inhibitory concentrations (IC) values obtained are shown in table 12. Interestingly IC values of our compound pair were found below 5 μM. Compound **7** ICs were lower than **2**, making it the most potent of both for A549 cell line. Meanwhile the average values obtained with non-formulated cisplatin and CDDP exceed 20 μM. The values of the current drug were very high compared with synthetic tambjamine compounds ICs. These findings lend support to the idea that synthetic tambjamines analogues may have potential as future anticancer drugs.

A549							
Compound 2		**Compound 7**		**Cisplatin**		**CDDP**	
IC_{25}	0.99±0.46	**IC_{25}**	0.66±0.18	**IC_{25}**	25.76±2.29	**IC_{25}**	69.79±9.21
IC_{50}	3.38±0.98	**IC_{50}**	1.67±0.29	**IC_{50}**	>100	**IC_{50}**	>200
IC_{75}	4.88±1.59	**IC_{75}**	3.57±0.49	**IC_{75}**	>200	**IC_{75}**	>200

Table 12. Inhibitory concentrations (IC) values of compound 2 and 7, and the positive control, cisplatin (non-formulated) and CDDP (formulated), in A549 cell line. All the values are expressed as the mean ± SD in μM.

On the other hand, synthetic tambjamine analogues were tested in cell lines representative of squamous oral cancer, CAL27 and HN4. As in the previous case, first, the drugs were tested in a single dose of 10μM (figure 28) by MTT assay. This test revealed that the cellular viability drastically dropped with the majority of compounds.

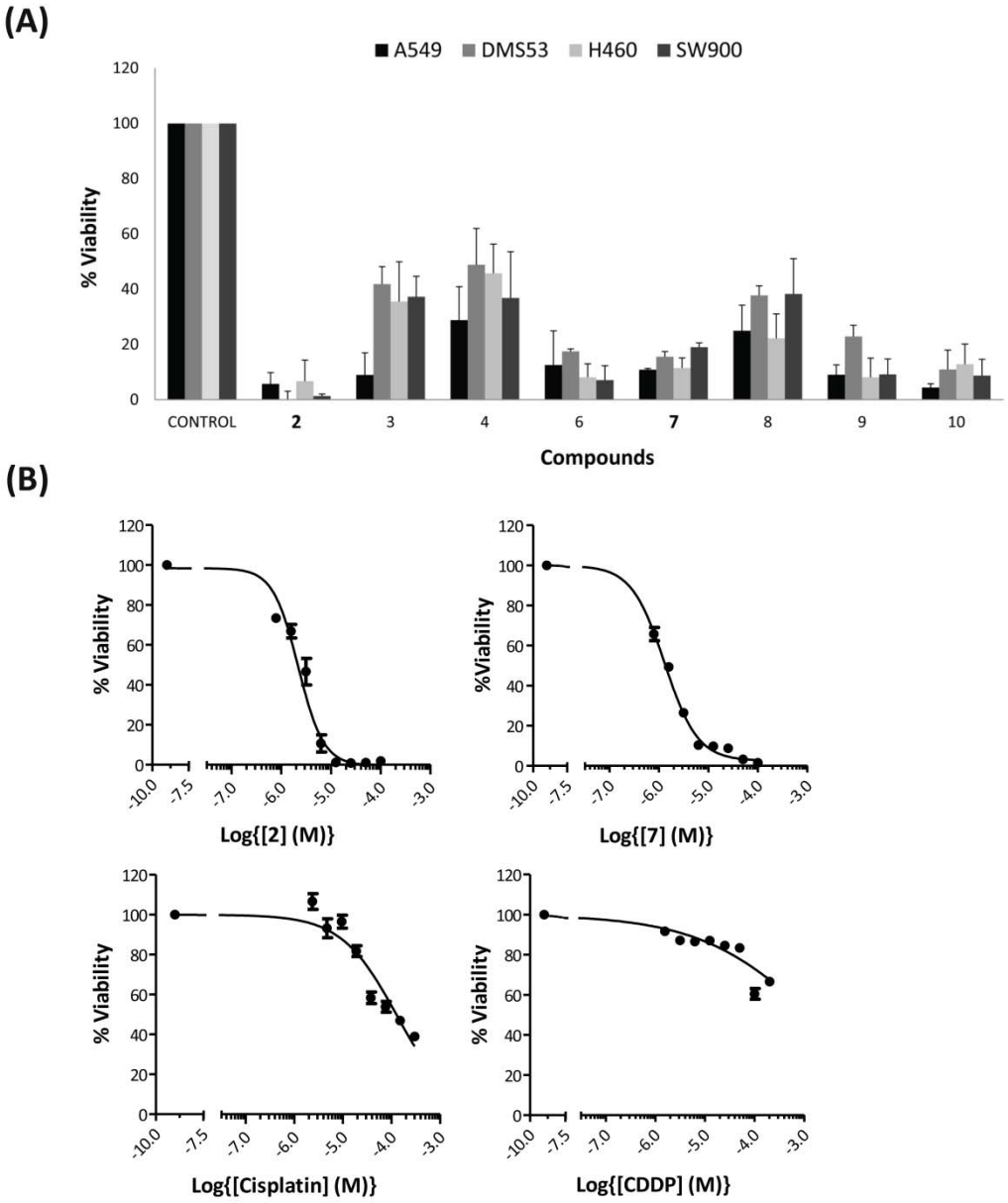

Figure 27. Synthetic tambjamine analogues significantly decrease cell viability. (A) MTT cell viability assay was performed after 24 h of treatment with synthetic tambjamine analogues at 10 µM in A549, DMS53, H460 and SW900 cell lines. (B) Concentrations ranging from 0.8 to 100 µM of compounds **2** and **7** were used in dose-response curve experiments in A549 cell line. Cisplatin (non-formulated) and CDDP (formulated) were used as a positive control at concentrations ranging from 2.34 to 300 µM or 1.6 to 200 µM, respectively. Results show the mean value ± SD of at least three independent experiments.

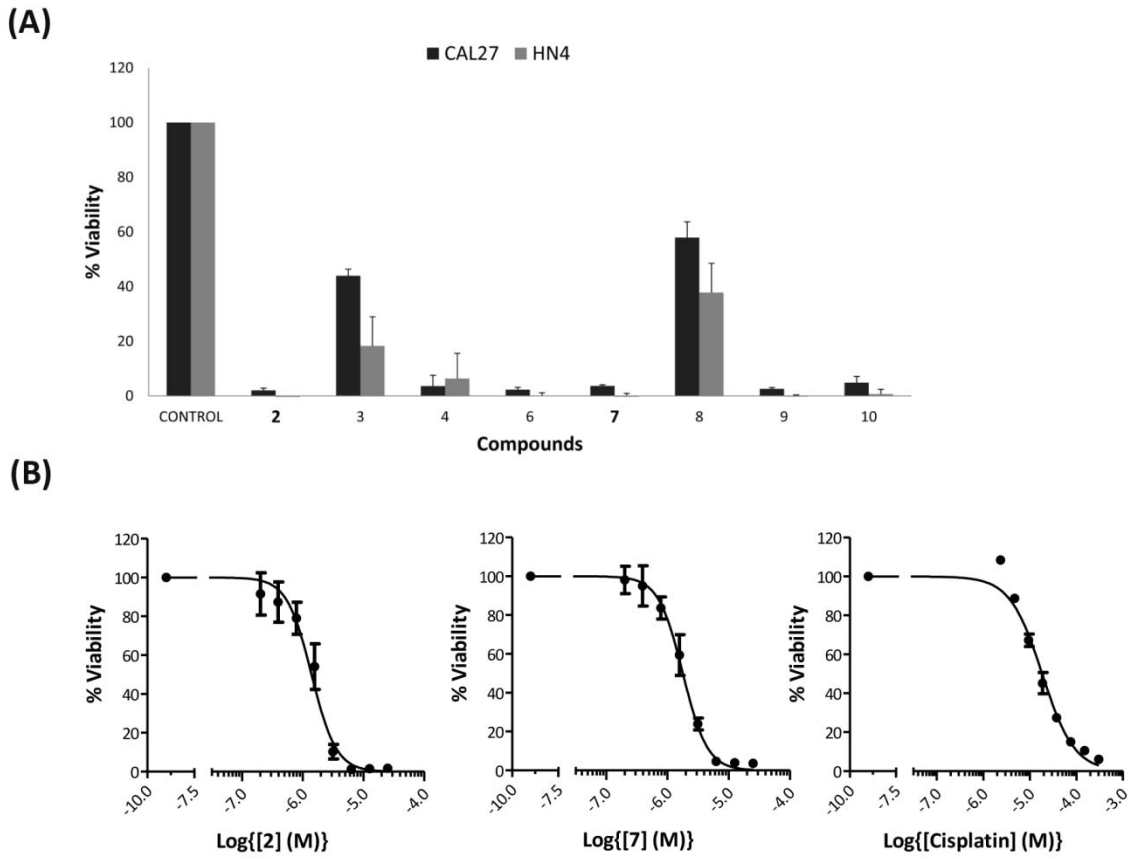

Figure 28. Inhibition of oral cancer cell lines proliferation by synthetic tambjamine analogues. (A) Changes in cell viability were measured by MTT assay after 24 h of incubation with synthetic tambjamine analogues at 10 µM in CAL27 and HN4 cell lines. (B) Compounds 2 and 7 were tested with concentrations ranging from 0.8 to 100 µM (dose-response) to calculate ICs value in CAL27 cell line. Cisplatin (non-formulated) was used as positive control with concentrations ranging from 2.34 to 300 µM. Results show the mean value ± SD of at least three independent experiments.

Compound **2** and **7** were selected among the most potent ones and ICs were calculated by MTT assay using different concentrations from 0.8 to 100 µM (figure 28 b). As a positive control non-formulated cisplatin was tested from 2.34 to 300 µM. The IC values are listed in the table 13, where it can be seen that compound **2** was slightly more potent than **7**, but both ICs were much lower than cisplatin IC values.

CAL27					
Compound 2		**Compound 7**		**Cisplatin**	
IC_{25}	0.79±0.69	**IC_{25}**	1.12±0.56	**IC_{25}**	37.02±4.21
IC_{50}	1.75±0.46	**IC_{50}**	1.95±0.56	**IC_{50}**	14.60±0.13
IC_{75}	2.36±0.59	**IC_{75}**	3.14±0.66	**IC_{75}**	7.23±0.35

Table 13. Inhibitory concentrations (IC) values of compound 2 and 7, and the positive control, cisplatin, in CAL27 cell line expressed in µM and shown as mean ± SD.

2.2. Compound effects on cancer stem cells derived from cell lines and patients tumor samples

Although our compounds proved to drastically reduce the viability in cancer cell lines, we wanted to check whether these compounds were active against cancer stem cells (CSC), which are usually an important resistance mechanism to conventional treatments. Thus, compound **2** and **7** were also tested on CSCs derived from patients or isolated from lung cancer cell lines.

Derived tumor spheres were deeply characterized, showing enrichment in stem cell surface markers as well as great tumorigenic properties in SCID mice transplantation experiments. On one hand, spheres derived from patients FIS302 and FIS303 and from A549 cell lines, were dissociated into single cells and cultured in suspension on non-adherent plates showing CSC properties. The expression level of cancer stem cell surface markers (Chen *et al.*, 2014) in the tumor spheres was analyzed by flow cytometry and is showed in the following table:

Cells	Marker expression %				
	EpCAM	CD44	CD166	CD90	CD133
A549	12.5	95	15		
FIS302	100	71	20		
FIS303	100	46	75		

Table 14. Expression of stem cell surface markers in tumor spheres from NSCLC cell lines and primary NSCLC tumors

On the other hand, primary lung tumor spheres derived from patients were dissociated into single cells and transplanted subcutaneously into NOD/SCID mice (from 2000 to 100000 cells, see figure 29). Both cell populations were able to form tumors in mice, suggesting that they are highly enriched in lung CSCs.

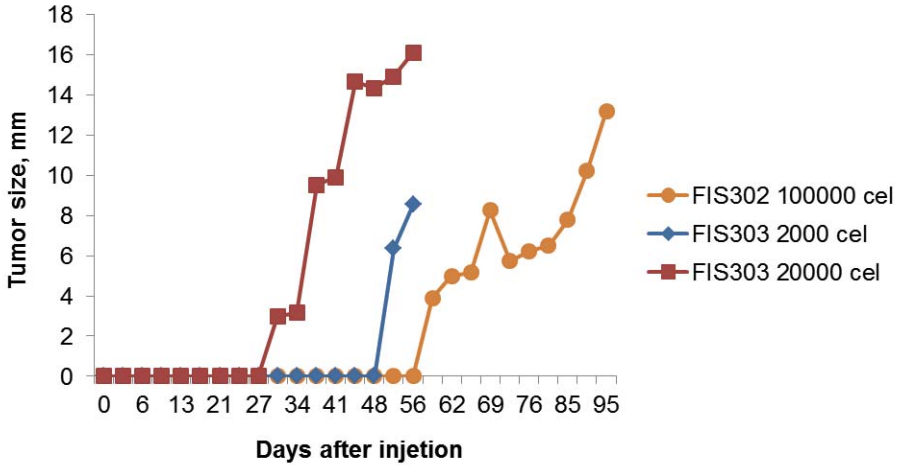

Figure 29. Tumor growth curves of FIS302 and FIS303 tumor spheres xenografts. NSCLC tumor spheres have tumor-initiating properties *in vivo*. Tumor growth curves of 1st generation xenografts derived from 2,000, 20,000 or 100,000 cells from FIS302 and FIS303 tumor spheres.

Cell viability was measured after 24 h of treatment with the evaluated compounds at 10 µM. Compound **2** showed a remarkable decrease in cell viability, either in CSC derived from cell lines or derived from the tumor patient samples (FIS302 and FIS303), whereas compound **7** reduced cell viability to 50% in most samples (figure 30). These results indicate that anion transporters are good

inhibitors of cancer cell viability even, in CSC. This ability gives them an advantage to be promising therapeutic candidates in comparison with other drugs, especially for treating patients with resistance to conventional treatments.

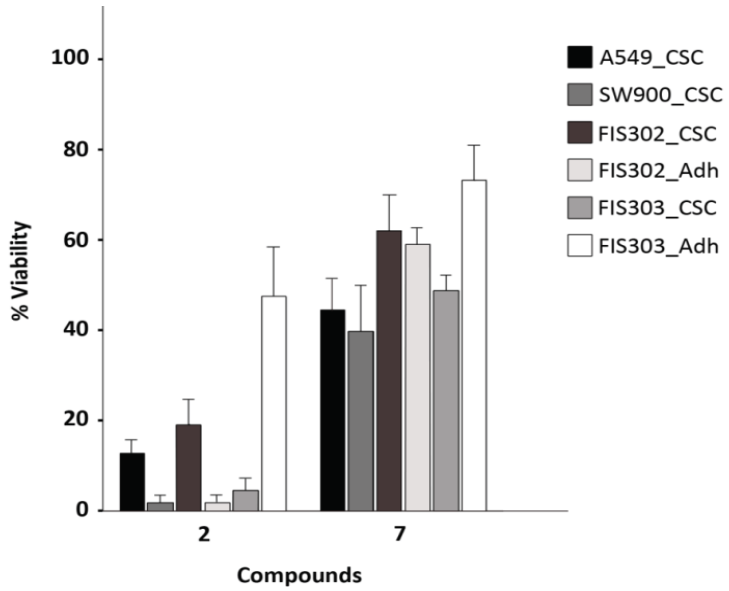

Figure 30. Synthetic tambjamine analogues decrease adherent (Adh) and cancer stem cells (CSC) viability. Cell viability was tested in adherent and cancer stem cells derived from lung cancer patients (FIS302, FIS303) or cancer cell lines (A549, SW900) after 10 µM of compound **2** and **7** for 24 h.

2.3. Study of the cytostatic effect of selected molecules

Viability assays report the number of remaining viable cells after the treatment but provide little information about the underlying mechanisms that may cause an antiproliferative or cytotoxic effect on cells. We performed flow cytometry analysis with propidium iodide stained cells to measure whether compound **2** and **7** could induce cell cycle alterations in lung and oral cancer cell lines. For this purpose, a representative cell line for each type of cancer, A549 and CAL27, was selected for lung and oral cancer, respectively.

Cell cycle phases were compared between A549 cells that had been incubated for 24 or 48 h with the IC_{50} of **2** and **7** (figure 31A), with respect to vehicle treated cells as control (DMSO), and cisplatin as a positive control of cell cycle arrest in G2/M phase (Mueller *et al.*, 2006). The distribution of the cells among the different phases of cell cycle (G_0/G_1, S, and G_2/M) was barely altered after the treatment with the IC_{50} of synthetic tambjamine analogues for 24 or 48 h. In this way, cell populations in each phase followed a similar pattern to the control cells. Approximately around a 60% of cells remained in G_0/G_1 phase, 10-15% in S phase and 20-25% in G_2/M phase. Remarkably, for cells exposed during 24 h to compound **7** it was found that proportion of cells in G_0/G_1 phase changed significantly, 76% compared to 61% in control cells, whereas cell cycle phases remained unaltered after 48 h.

As expected, the exposure to CDDP, a positive control, varied the proportion of cells in different phases of cell cycle. CDDP reduced the amount of cells that were in G_0/G_1, and increased the cells in phase S and G_2/M, 24 h after compound addition, leading to a great accumulation of cells in G_2/M

phase at 48 h (84% compared to 20% in untreated cells). The analysis did not identify any significant differences between control and treated cells, with the exception of a slight increase in G_0/G_1 phase of cells treated with the analogue **7** during 24 h. Therefore, taken as a whole, anion transporters do not remarkably affect cell proliferation on A549 cell line.

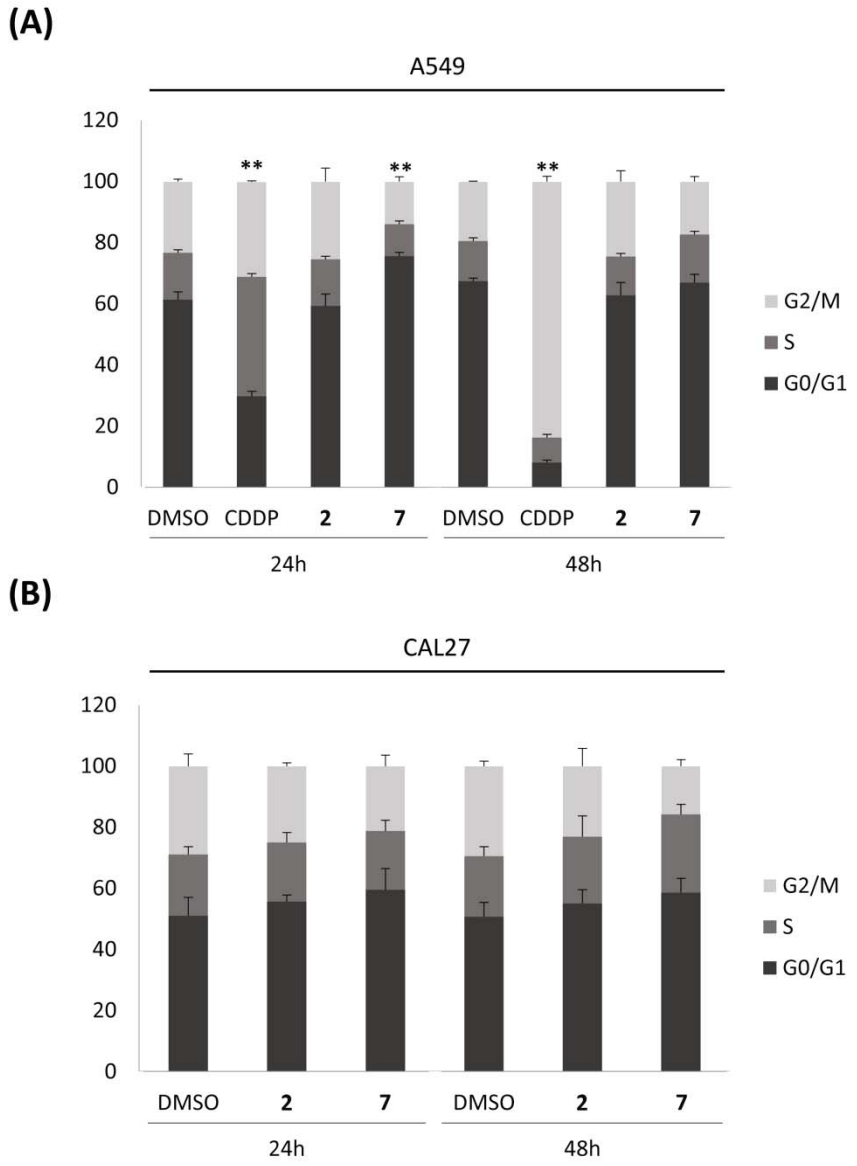

Figure 31. Cell cycle distribution in A549 and CAL27 cells exposed to synthetic tambjamine analogues. Cell cycle analysis of (A) A549 and (B) CAL27cells treated with compounds **2** or **7** for 24 or 48 h. CDDP was used as positive control. Quantification of different cell cycle phases was measured using the flow cytometry based MUSE™ cell cycle assay Kit. The bar graphs indicate the changes in the cell cycle progression as the mean ± S.D. of three independent experiments. **: Statistically significant differences between G_0/G_1 of cells treated with **7** and CDDP versus DMSO at 24 h, and between G_0/G_1 and G_2/M of CDDP versus DMSO at 48 h. Statistically significant results are indicated as *p< 0.05 and ** p< 0.01.

Squamous oral cancer cells were subjected to the same treatment, and after incubation with the IC_{50} of **2** and **7** for 24 or 48 h no change in distribution of cell cycle phase populations was observed with respect to control cells (figure 31B). Neither compound **2** or **7** causes a cell cycle arrest in CAL27 cells.

3. Anion transport in cells and its effect on intracellular pH

As shown above, the synthetic tambjamine analogues are good ion transporters. To assess more in detail the activity as transmembrane anion transporters of the two most cytotoxic compounds, **2** and **7**, *in vitro* experiments were performed on POPC liposome models.

Chloride loaded liposomes were suspended in an isotonic chloride free solution, and chloride efflux facilitated by these compounds was monitored using a chloride selective electrode. At the end of the experiments, vesicles were lysed by the addition of detergent and the final electrode reading considered as 100% chloride release. Quantification of the transport activity was carried out by repeating the experiments using several concentrations of the studied compounds and performing hill analyses of the results (figure 32A and 32B). The resulting EC_{50} value represents the amount of compound needed to release 50% of the encapsulated chloride in the time scale of the experiments (300 s). The EC_{50} values obtained for **2** and **7** were 50 nM and 60 nM respectively in the assay involving $NaNO_3$ as external solution and 240 nM and 880 nM respectively in the assay involving $NaHCO_3$ as external solution. The impact on the EC_{50} values of the external anion is consistent with an exchange mechanism in which chloride efflux from the interior of the vesicle is accompanied by influx of the external anion, thus precluding the formation of an electrochemical gradient. The relative higher lipophilicity of nitrate compared to bicarbonate makes this latter anion more difficult to extract into the membrane hydrophobic core and hence the higher EC_{50} observed. This transport mechanism has been studied by us in detail and the result demonstrates that **2** and **7** are very potent anionophores promoting effective transmembrane anion transport in vesicles at low loadings (Hernando *et al.*, 2014).

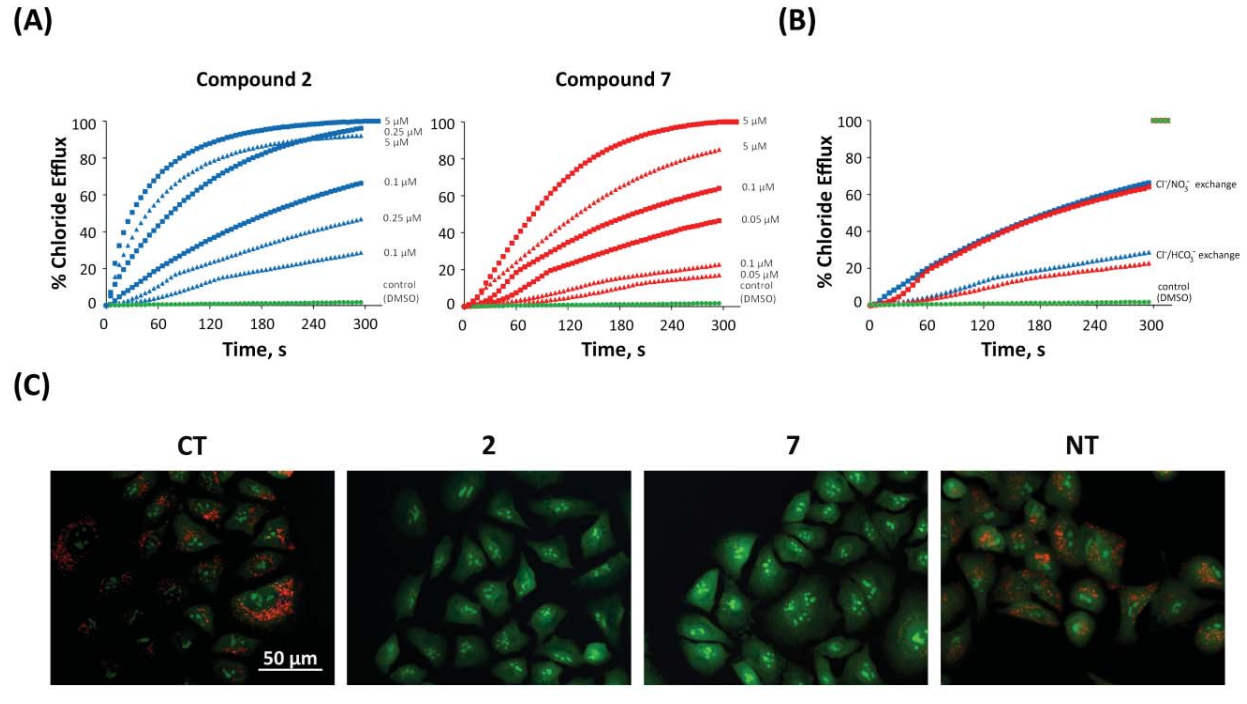

Figure 32. Potent transmembrane anion transport activity of synthetic tambjamine analogues in liposomes and cellular models. (A) Chloride efflux upon addition of compound **2** or **7** at different concentrations to vesicles composed of POPC. Squared symbols correspond to the results obtained using NaNO3 as external buffer, triangular symbols correspond to the results obtained using $NaHCO_3$/Na_2SO_4 as external buffer. Each trace represents an average of at least three different experiments (B) Impact of external buffer ($NaNO_3$, squared symbols, or $NaHCO_3$/Na_2SO_4, triangular symbols) in the chloride efflux promoted by **2** or **7** (0.1 µM, blue and red symbols, respectively). (C) Acridine orange staining on A549 cells treated with vehicle (DMSO), 10 µM compound **2, 7** and **NT**, non-transporter compound, for 1 h. Images are representative of three independent experiments. Scale bar 50 µm.

Once it was corroborated that both compounds, **2** and **7**, were good chloride anion carriers in liposome models, secondly acridine orange (AO) assays were performed in human lung adenocarcinoma cells (A549) to analyze modifications in cellular acidic compartments pH. The ability of anionophore **2** and **7** to modulate lysosomal pH was compared to a third compound that is structurally related to them, but which displays modest activity as anion carrier, and it will be considered as a non-transporter/negative-transporter **(NT)** in these assays. Since AO is a slightly cationic and lipophilic dye, it is capable of permeating cell and organelle membrane structure. Once it has penetrated into acidic intracellular organelles, like lysosomes or late endosomes, AO is protonated and trapped inside these compartments. As a result of its protonation under acidic pH conditions, when AO is excited with blue light, the protonated dye emits orange fluorescence. Meanwhile, the non-protonated fluorochrome emits green fluorescence in other parts of the cell.

Cells were treated with 10 µM of each compound for 1 h before staining with AO, and as it can be observed in the figure 32C, in those cells treated with the anion transporters the orange fluorescence in the acidic compartments disappeared, indicating an AO deprotonation and therefore an increase in the pH of these organelles. Meanwhile, in cells treated with **NT**, the orange dye corresponding to the acidic compartments remained as in control cells treated with the vehicle, DMSO. This result is in agreement with the ionophoric activity of these compounds that facilitate transport of anions like chloride and bicarbonate across the membrane of cellular compartments. This fact causes an alteration of the lysosomal pH, and in turn results in lysosomal dysfunction.

Therefore, these compounds have been characterized as good anion transporters in cellular membranes and subsequently, it has been proved that this transport is linked to an increase in lysosomal pH.

Beside this, after exposure to the IC_{75} of both compounds for 6 h, a massive vacuolization of the cytoplasm of A549 cells was observed through phase contrast microscopy (figure 33). These vesicles appeared in greater number after treatment with compound **2** than with **7**. However, after treatment with the **NT** hardly any vesicles were observed in the cytoplasm.

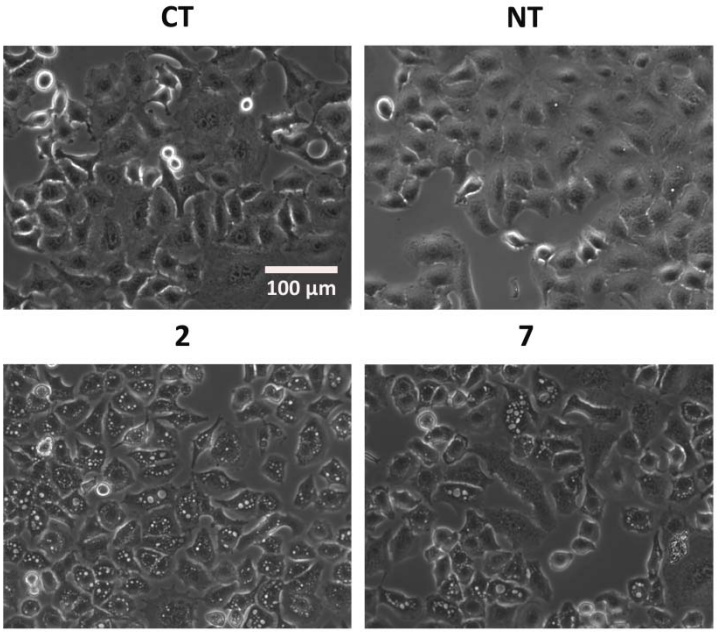

Figure 33. **Cytoplasmic vacuolization induced by synthetic tambjamine analogues.** Phase contrast microscopy images of A549 cells treated with IC_{75} of compounds **2** or **7** and 10 µM of **NT** for 6 h. Scale bar 100 µm. Images are representative of three independent experiments.

We decided to monitor this process for 24 h in order to study its evolution and observe which organelle was suffering vacuolization. As shown in figure 34, we had evidence of the presence of vacuoles from 3 h after addition of 10 µM of compound and these vesicles were then maintained over 24 h of treatment. At the endpoint of the experiment, especially in those cells exposed to compound **2**, cell death was observed suggesting that cell swelling or cell burst had occurred, both typical features of necrotic cell death. This finding reinforces the fact that the vacuolization event may depend on the osmotic imbalance caused by the compound anion-carrier capacity.

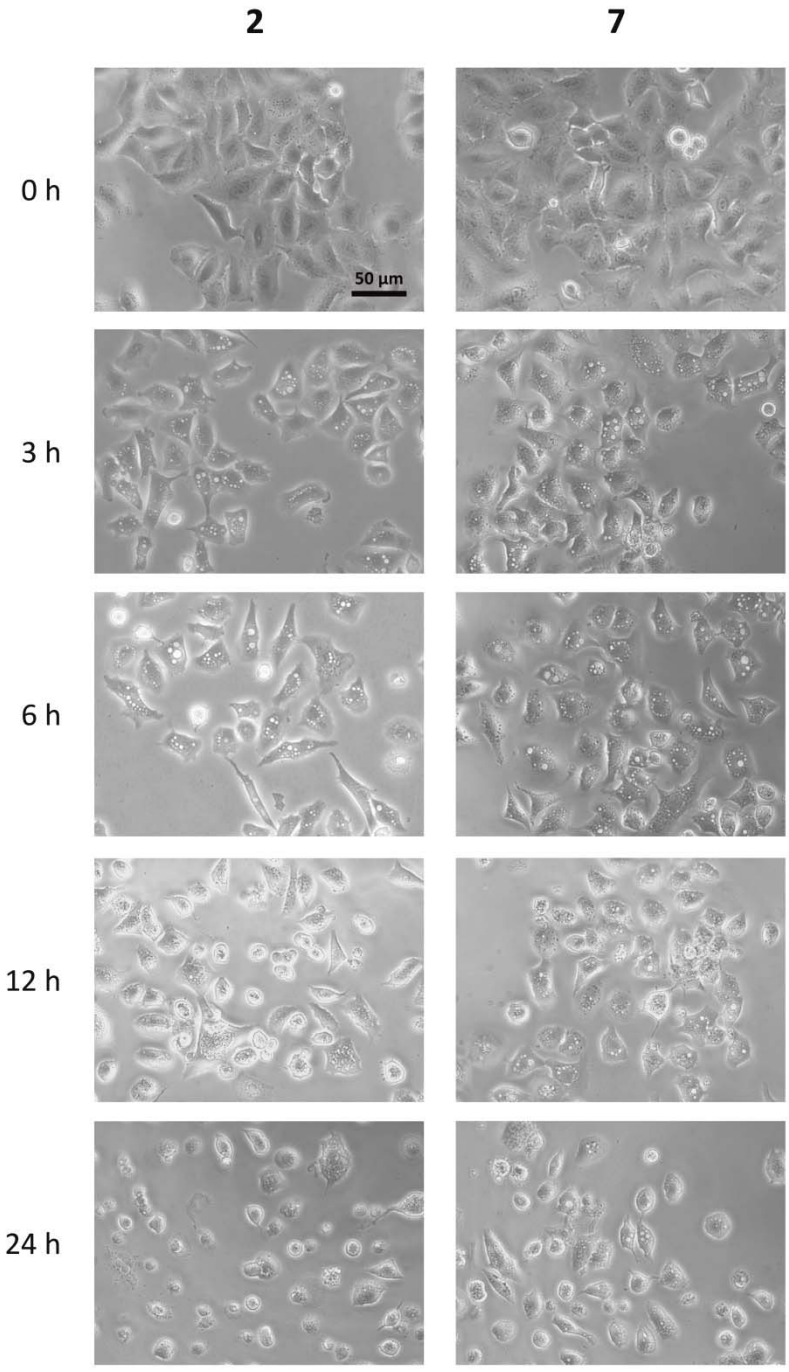

Figure 34. Cytoplasmic vacuolization after treatment. Time-course images of A549 cells treated with 10 µM of compound **2** or **7** during 24 h. Scale bar 50 µM.

3.1. Characterization of induced cytoplasmic vacuolization

The anionophores trigger a process of vacuolization in the cytoplasm. These vesicles may have different origin; on one hand they could arise inside the cell, from organelles or vesicles that swell, or on the other hand, they may come from the extracellular medium, as a vesicle derived from a pinocytic or endocytic process. In this regard, we tried first to identify which type of organelle was undergoing this vacuolization process. To assess this objective, cells were treated with the IC_{75} of each compound for 6 h and we tested several organelle markers by immunofluorescence. Among them, we first tested LC3, LAMP1 and EEA1, markers of autophagosomes, lysosomes and early endosomes, respectively.

Autophagy involves the engulfment of intracellular elements into double-membrane vesicles called autophagosomes. In this case, the microtubule-associated protein 1 light chain 3 (LC3) marker detects either cytosolic form called LC3-I or the autophagosome-associated form, LC3-II. In figures 35A and 36A, it can be observed how there was a massive increase of the LC3 marker after exposure to the ion-carrier compounds. In control cells, treated with the vehicle (DMSO), there was a slight dotting corresponding to the LC3-I cytosolic form and basal levels of autophagy, whereas there was a huge autophagy induction in treated cells, indicated by autophagosomes formation. However, this marker does not colocalize with the vacuoles formed after the treatment. Moreover, autophagy also involves autophagosomes delivery to the lysosomes for fusion and degradation of their cargo by the lysosomal hydrolases. In order to determine whether the vacuoles arise from lysosomes, we used an antibody against LAMP1 protein, which is located on the lysosome membrane. This marker was tested after the same treatment conditions, and as it can be observed in figure 35B and 36B, LAMP1 immunofluorescence revealed an increase and a change in the distribution of the marker compared to control cells, but as in the previous case, lysosomes did not colocalize with the generated vacuoles.

Eukaryotic cells are able to internalize macromolecules and fluids from the surrounding medium by endocytic trafficking pathways, including endocytosis and pinocytosis. The marker EEA1 identifies early endosomes, the first endocytic compartment that receives incoming cargo [Helenius et al, 1983]. The analysis of the immunofluorescence with EEA1 marker did not identify early endosomes as a possible organelle that underwent the process of vacuolization after treatment with our compounds. The dotted pattern of EEA1 was very similar between control and treated cells and there was also no overlap between the IF labeling and the vesicle in phase contrast images (figure 35C and 36C).

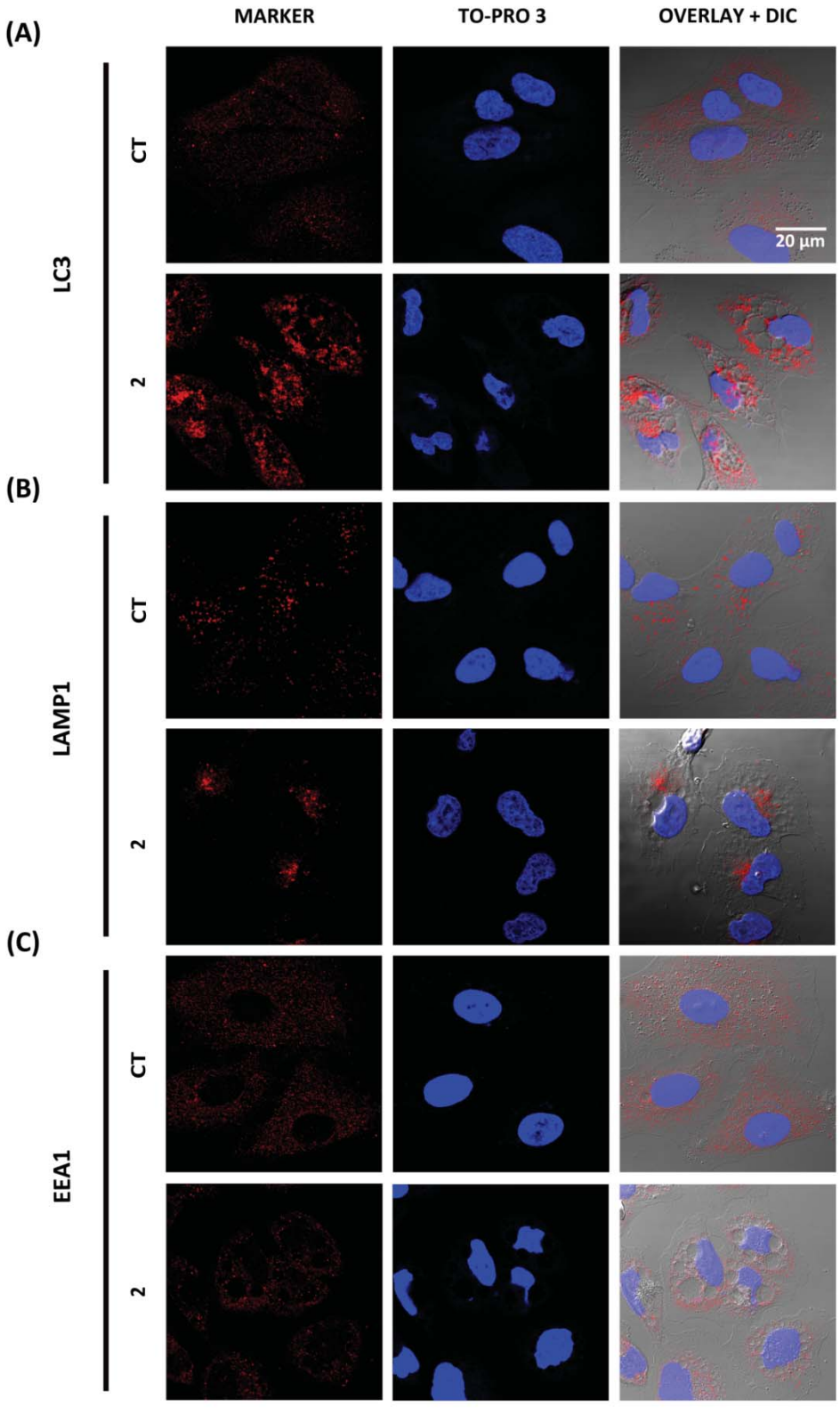

Figure 35. Synthetic tambjamine analogues treatment does not induce swelling of autophagosomes, lysosomes or early endosomes. Immunofluorescence in A549 cells treated with IC_{75} of compound **2** for 6 h. It was performed with different antibodies that recognize several cellular organelles (red) and were compared to the distribution of cytoplasmic vacuoles observed by phase contrast microscopy. (A) Distribution of the autophagosomal marker LC3, (B) distribution of lysosomal marker LAMP1 (C) distribution of the early endosome marker EEA1. The nucleus was counterstained with TO-PRO™-3 (blue). Scale bar 20 µm. Images are representative of at least three independent experiments.

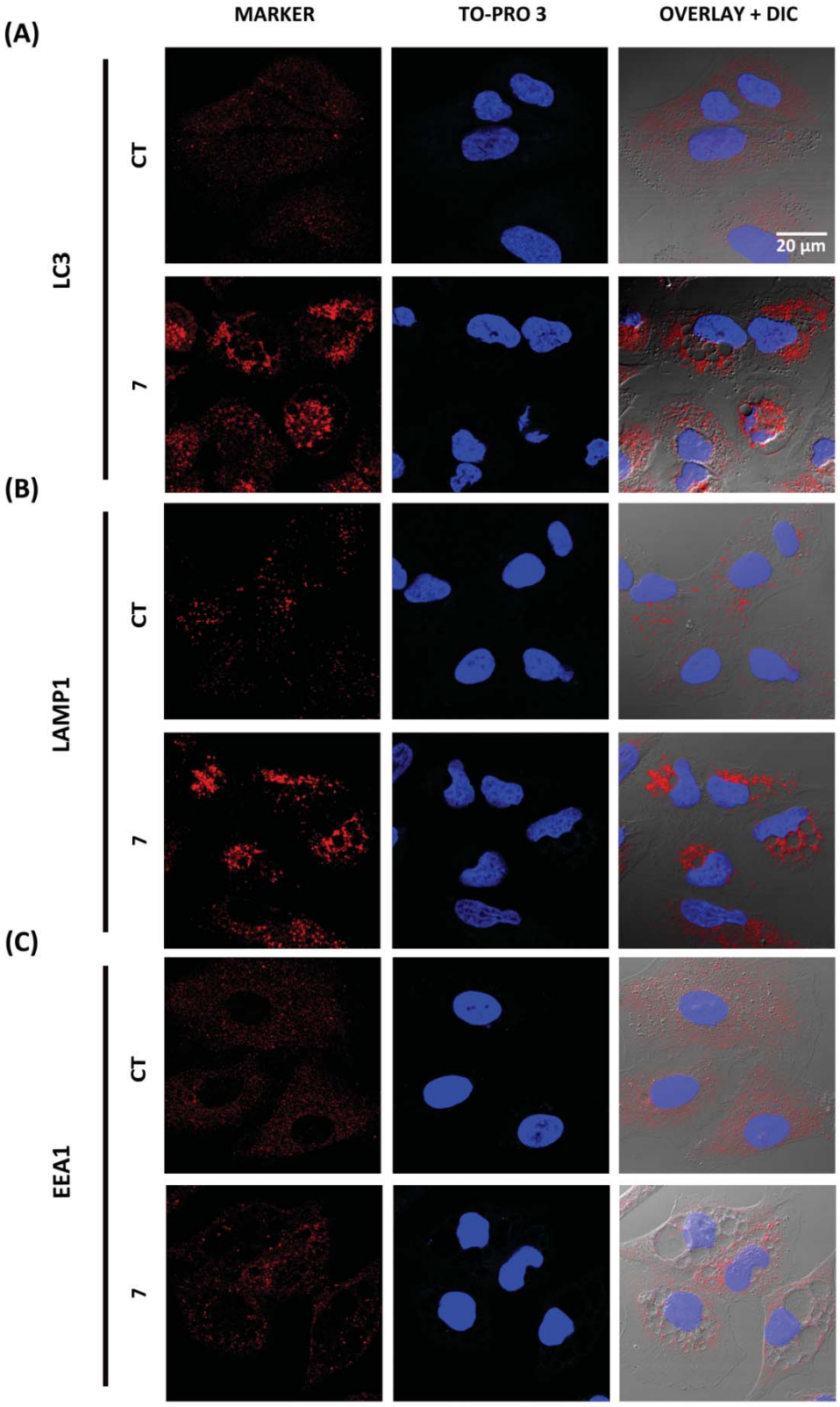

Figure 36. Exposure of A549 cells to compound 7 IC_{75} for 6 h does not induce swelling of autophagosomes, lysosomes or early endosomes. In red the distribution of different cellular organelles: (A) autophagosomal marker LC3, (B) lysosomal marker and (C) early endosome marker EEA1. The nucleus was counterstained with TO-PROTM-3 (blue). The location of the markers was compared to the disposition of cytoplasmic vacuoles observed by phase contrast microscopy. Scale bar 20 µm. Images are representative of at least three independent experiments.

Macropinocytosis is a type of endocytosis that involves the uptake of extracellular fluid and nutrients in vesicles known as macropinosomes. These vesicles arise from the fusion of formed lamellipodia with the plasma membrane. Once inside the cell they mature and fuse with the lysosome to degrade the contents, or are recycled back to the membrane. Dysregulation of this process can lead to cell death as occurs in methuosis. We analyzed whether vesicles caused by the treatment with anion transporters were formed by macropinocytosis. For this purpose, we used fluorescently-labeled dextran, a fluid-phase marker. The protocol is based on the incorporation of 70 kDa high molecular weight rhodamine B-labeled dextran from the extracellular medium into macropinosomes, which can be observed as fluorescent vesicles by microscopic methods. Therefore, A549 cells were incubated with dextran and then exposed to the IC_{75} of compound **2** for 6 h. MOMIPP, a reported methuosis inducer, was used to treat cells as a positive control. In the image (figure 37), it can be observed that MOMIPP produces vesicles just like compound **2**, with the difference that they are filled with red-labeled dextran, whereas vesicles formed by **2** are negative for red-labeled dextran staining. In cells treated with **2**, dextran appears to enter by diffusion but not by macropinocytosis. Therefore, the possibility that macropinocytosis is the mechanism that originates the vacuoles has been discarded.

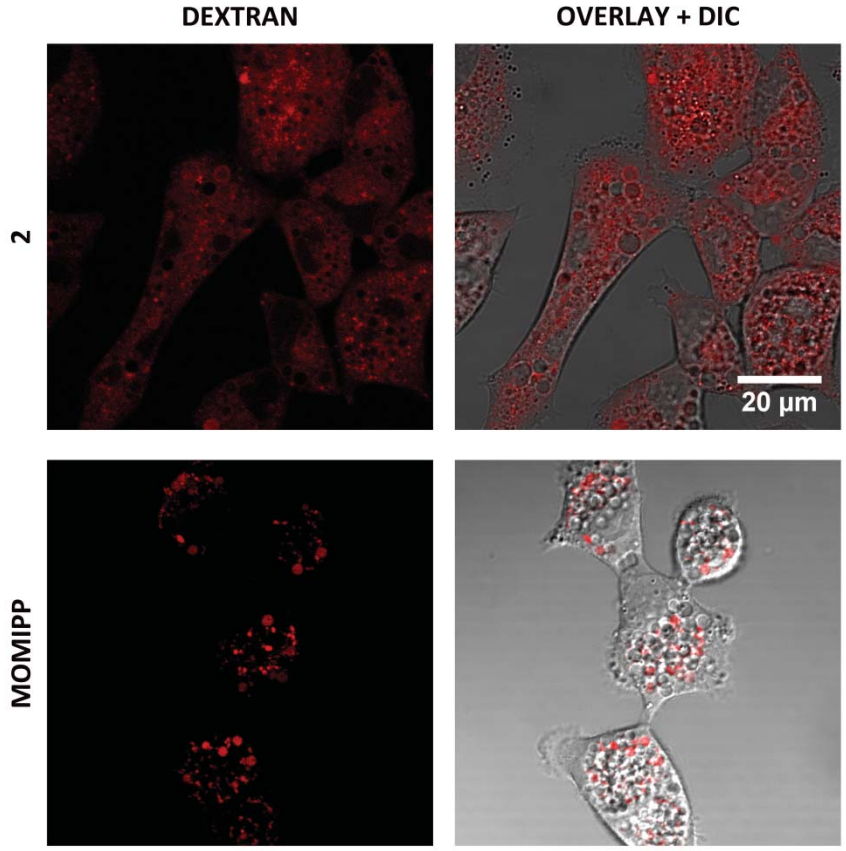

Figure 37. Tambjamine analogues treatment does not induce methuosis. A549 cells were exposed to labeled dextran 1 h prior treatment with IC_{75} of compound **2** or with 10 µM of MOMIPP, a methuosis inducer, for 6 h. The cells were examined after treatment and macropinosome-derived vacuoles induced by MOMMIPP were labeled with the fluid-phase tracer dextran, whereas vacuoles formed with compound **2** were not labeled. Scale bar 20 µm.

At the same time, we decided to try cytochrome C (CytC) marker since this highly conserved protein is normally localized to the mitochondrial inter-membrane space. To evaluate this, we performed an immunofluorescence with the anti-Cytochrome C antibody after treating A549 cells with the IC_{75} of our compounds for 6 h. In control cells CytC was located within the mitochondria which showed the typical morphology and distribution of these organelles in cultured cells (figure 38). In treated cells the marker seemed to be located enclosing the vesicles.

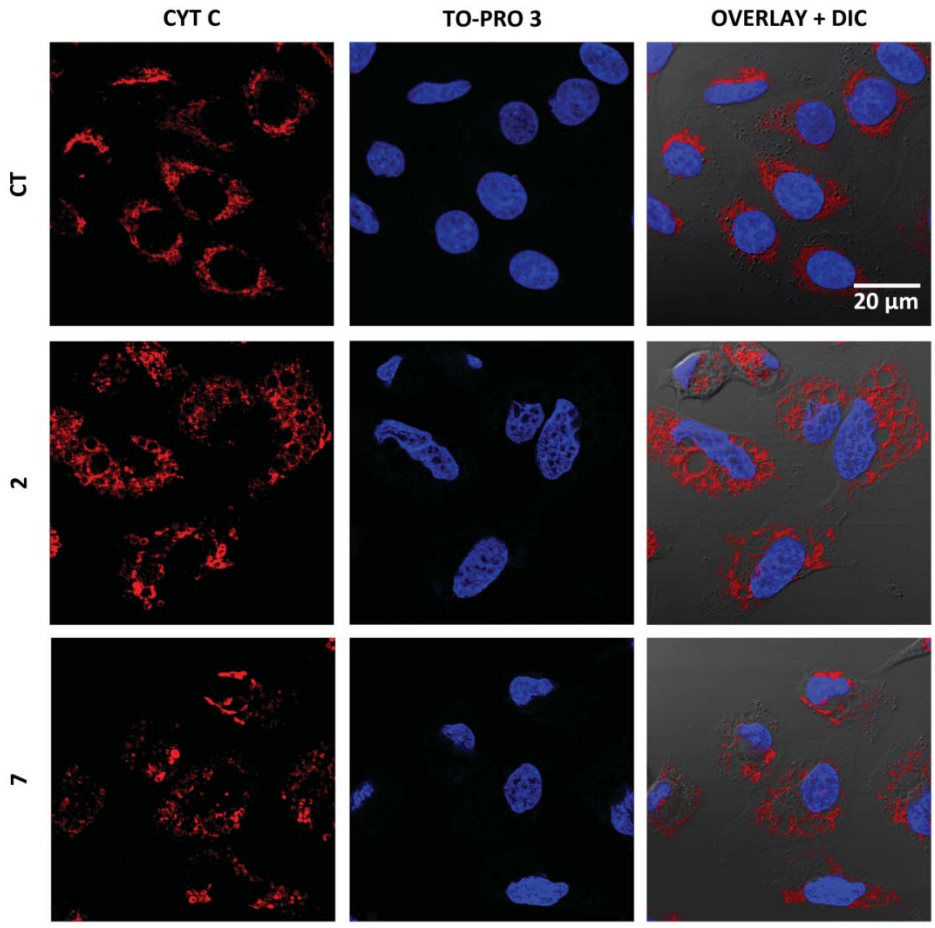

Figure 38. Cytochrome C immunofluorescence. A549 cells were exposed to IC_{75} of synthetic tambjamine analogues **2** and **7** for 6 h. The mitochondrial marker (in red) overlaps the vesicles observed in contrast phase images. Nucleus was stained with TO-PRO™-3. Scale bar 20 µm.

Therefore, the vesicles may be possible swollen mitochondria. Nevertheless, given the fact that CytC is a protein loosely associated to the inner mitochondrial membrane under normal physiological conditions and that, there are many stimuli that can cause its release into the cytoplasm, we used another marker to corroborate the previous result.

We chose an antibody against an outer membrane translocase of the mitochondria, TOMM20. This import receptor is responsible for the recognition and translocation of nuclear-encoded preproteins. As shown in the figure 39, TOMM20 proved to stain the membranes of the vacuoles in cells exposed to both compounds, whereas in cells treated with vehicle (DMSO) the marker showed the arrangement and structure typical of mitochondria. Therefore, it was possible to conclude that the treatment with anion transporters causes an extraordinary swelling of mitochondria in A549 cells.

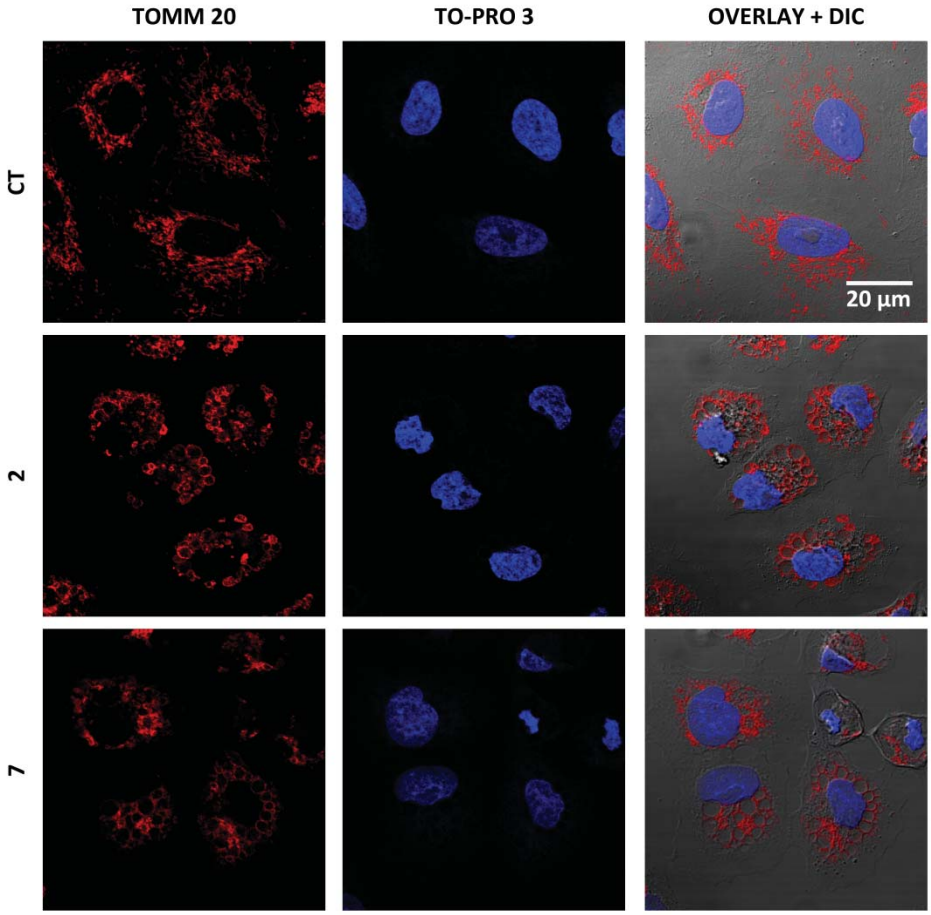

Figure 39. Immunofluorescence of mitochondrial marker TOMM20. A549 cells were treated with IC_{75} of compound **2** for 6 h. The antibody against the outer membrane translocase of the mitochondria (red) overlaps with the vesicles observed in contrast phase image. The nucleus was counterstained with TO-PRO™-3 (blue).

With the aim of further study the mitochondrial swelling process, we decided to track their changes in morphology during the first 3 hours after treatment. In order to perform the monitoring, we stably transfected A549 cells with the DNA plasmid mCherry-Mito-7, a mitochondrial targeting sequence from subunit VIII of the COX8A protein. The cells were then exposed to the IC_{75} of compound **2** for 3 h, and images were taken every 20 minutes. As a result, we could observe the evolution of mitochondrial swelling over time (figure 40). Before drug was added, Mito7 labeling in control and treated cells had the same pattern, mitochondria appeared unaltered with normal size and shape. As time progresses, the mitochondria of cells exposed to treatment began to increase in size, the red dotting relative to these organelles gradually became red vacuoles. It was possible to verify how the vacuoles observed in phase contrast overlap with the red vacuoles of the markerMito7. Meanwhile, mitochondria of control cells remained unaltered.

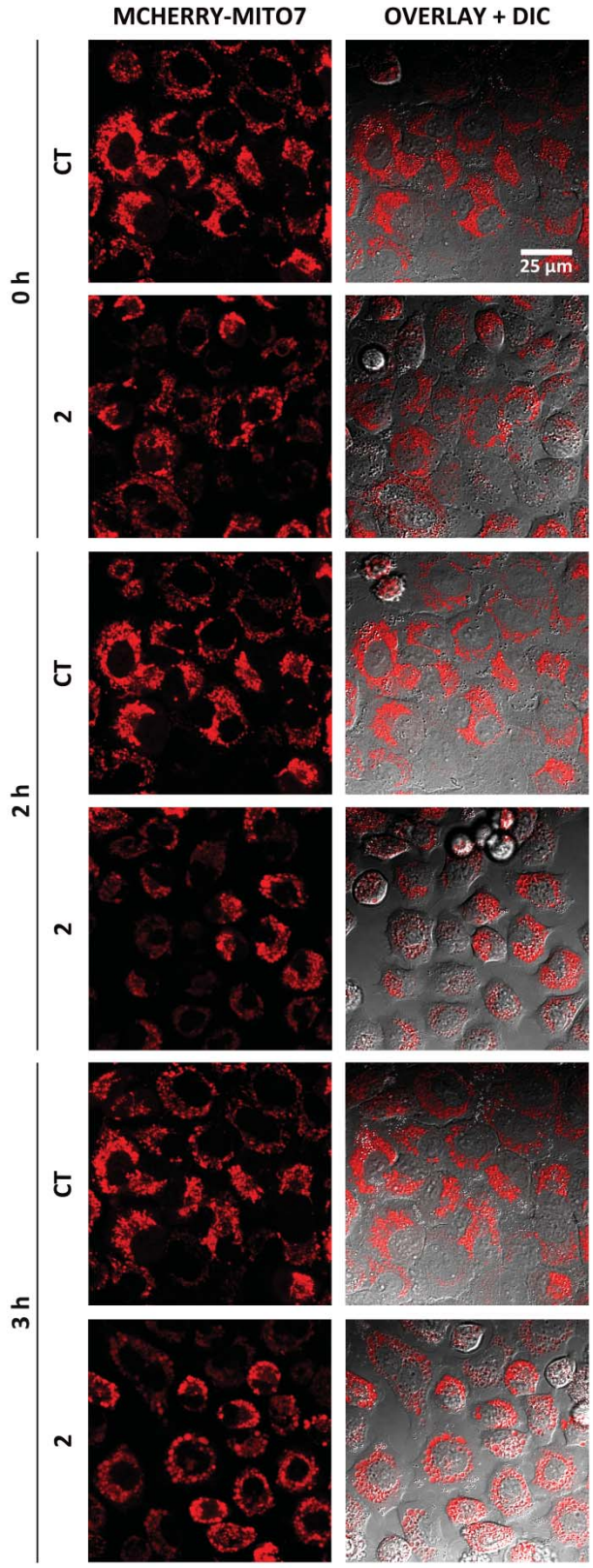

Figure 40. Mitochondrial swelling after synthetic tambjamine analogues treatment. A549 cells overexpressing mCherry-Mito7 plasmid, which targets mitochondria (red), were treated with IC_{75} of compound **2** for 3 h. Mitochondrial staining was compared to vacuolization observed in phase contrast photographs. Scale bar 25 µm.

In order to observe the mitochondrial swelling in more detail than in the previous time-course image, here we show another image (figure 40a) taken after exposure to the IC_{75} of the synthetic tambjamine analogue during 3 h, with an increase in magnification.

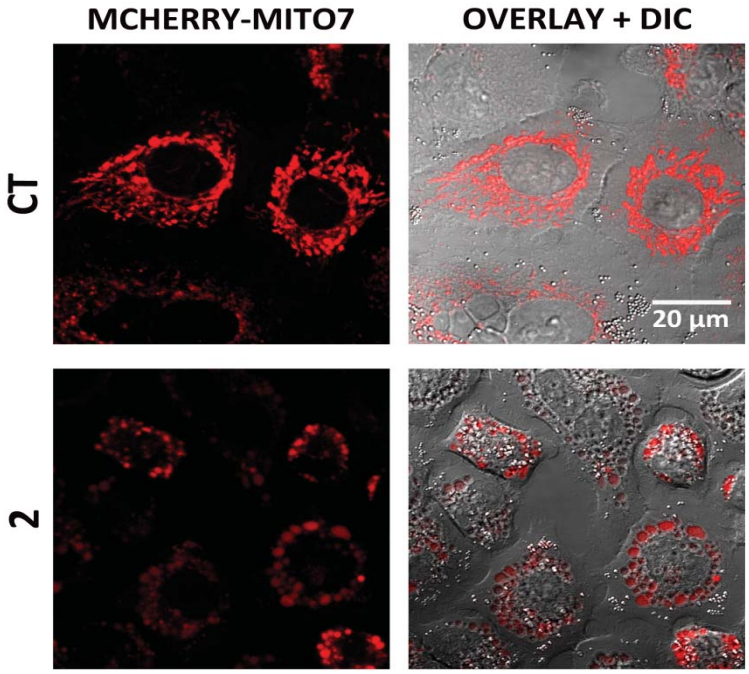

Figure 40a. Mitochondrial swelling after compound 2 treatment. mCherry-Mito7 stable A549 cells were treated with IC_{75} of compound **2** for 3 h. Mitochondrial staining overlaps the vacuolization observed in phase contrast images. Scale bar 20 µm.

An additional test was performed to determine the status of the mitochondrial membrane potential ($\Delta\Psi_m$) after treatment, which in turn is a key parameter for evaluating mitochondrial function. In this regard, we used MitoTracker™ Red CMXRos, a mitochondria-specific dye suitable to measure changes in $\Delta\Psi_m$, since its retention and fluorescence is dependent on a correct $\Delta\Psi_m$. Thereby, A549 cells were preincubated with MitoTracker for 1 h and treated with IC_{75} value of compound 2 or with 1% DMSO (used as a vehicle) for 3 more hours. The images were taken after the end of the treatment. Comparing control cells with treated cells images (figure 41), we could observe a remarkable difference in mitochondrial morphology. As on previous occasions, control cells showed filamentous or dotted mitochondria, while in treated cells mitochondria gradually swelled to a larger size vacuole. As mitochondria increases in size, the fluorescence of Mitotracker dissipated until it completely faded into the larger vacuoles. In addition, the experiment was carried out by altering the order of treatment, thus A549 cells were first treated with compound **2** for 3 h and then the MitoTracker was added. In these cases no fluorescence was observed, supporting that the synthetic tambjamine analogue alters the $\Delta\Psi_m$ and MitoTracker cannot be accumulated. Therefore, our findings indicate that $\Delta\Psi_m$ is lost during the swelling process after compound treatment.

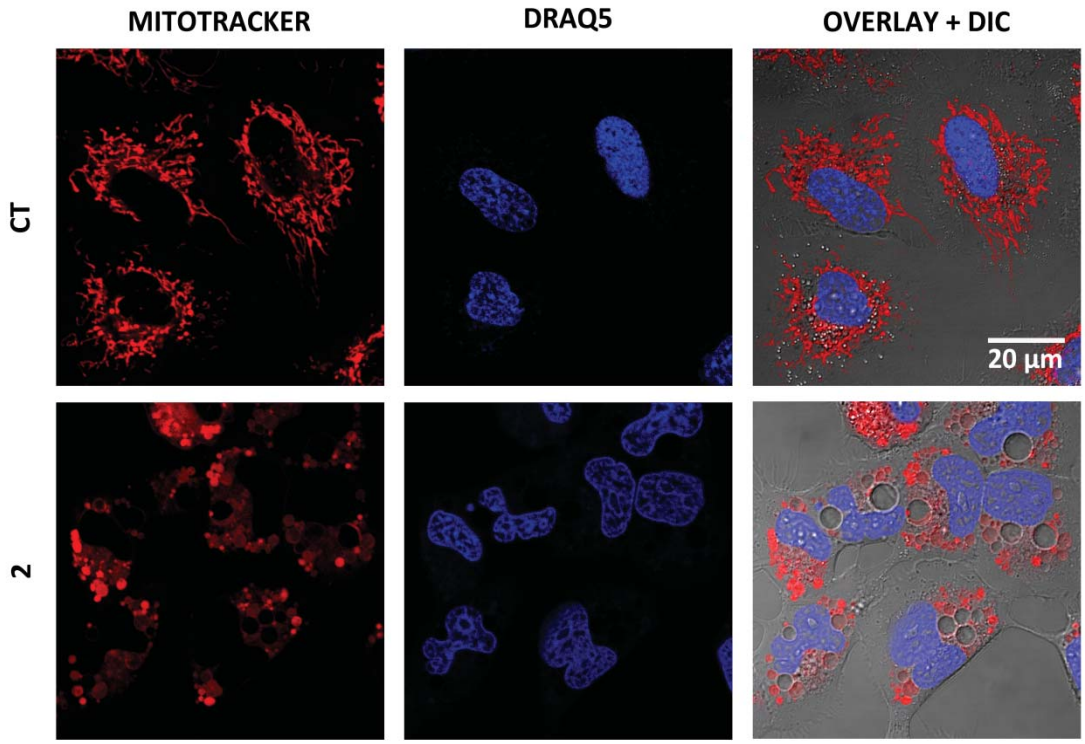

Figure 41. Mitochondrial swelling and loss of mitochondrial membrane potential ($\Delta\Psi_m$) after synthetic tambjamine analogues treatment. Confocal images of A549 cells treated with 500 nM MitoTrackerTM Red CMXRos during 1 h and then compound **2** for 3 h. Mitochondria with normal $\Delta\Psi_m$ are stained in red. Nucleus was counterstained with DRAQ5 (blue). Scale bar 20 µm. Images are representative of at least three independent experiments.

On the other hand, we performed an assay to evaluate whether mitochondrial activity was affected by the swelling after compounds treatment. Levels of adenosine-5'-triphosphate (ATP) define the energy state in living cells and are dependent mainly on mitochondrial function since this molecule is formed in these organelles. The analysis revealed (figure 42) an ATP decrease of 20% in the time interval of 3 - 6 h after treatment, and a drop of more than 50% from 24 h of treatment. Therefore, mitochondrial swelling leads to mitochondrial dysfunction, and is accompanied by a decrease in cellular ATP levels .

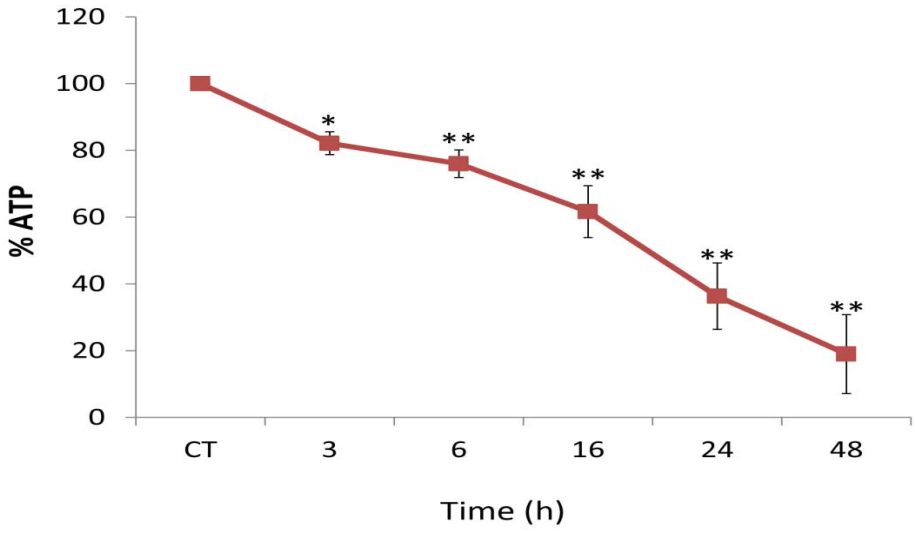

Figure 42. Intracellular ATP levels in treated A549 cells. Intracellular ATP content was determined after treatment with IC_{75} of compound **2** in a time-course experiment. Relative amounts were calculated as the ratio of luminescence of treatment group related to their respective control. Synthetic tambjamine analogue **2** causes ATP depletion. Experiments were carried out in triplicates, and results are shown as mean ± SD. *p< 0.05, ** p< 0.01.

In addition, in order to study this phenomenon more deeply, transmission electron micrographs were obtained from control and cells treated with compound **2** or **7**. Transmission Electron Microscopy (TEM) represents a useful technique to study the architecture of cells and the morphological phenomena that occurs after the treatment with synthetic tambjamine analogues. TEM produces images that have higher magnification and greater resolution than confocal microscopy, rendering this technology capable of determining a wide variety of cellular structures. TEM images revealed mitochondrial swelling (black arrows, figure 43) in those cells that had been treated with the IC_{75} of both compounds for 6 h, especially with compound **2**. Moreover, the accumulation of many autophagy-related structures such as autophagosomes, autolysosomes and dense lysosomes was also visualized in treated cells. These results correlate with the occurrence of mitochondrial swelling after treatment, as well as autophagosomes accumulation, which may be due to impairment in the autophagic flux caused by lysosomal dysfunction.

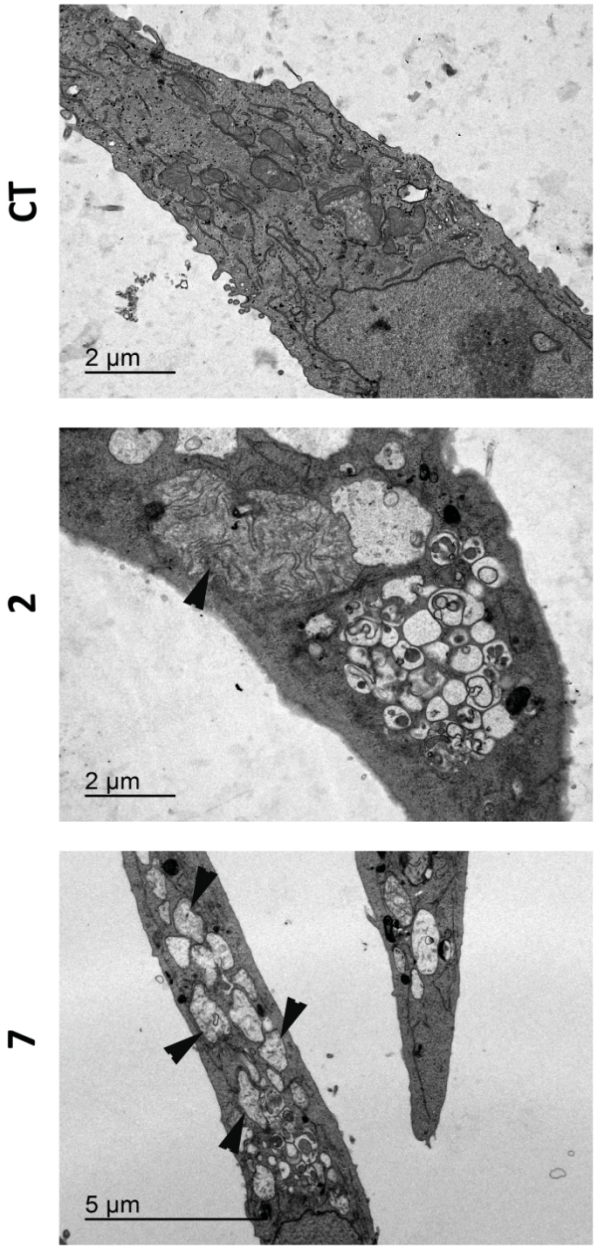

Figure 43. Transmission electron micrographs from control and treated A549 cells with compound 2 and 7 for 6 h. Mitochondrial swelling (black arrows) as well as double-membrane vesicles accumulation (autophagosomes and autolysosomes) were observed. Scale bar 2 and 5 µm.

4. Identification and characterization of the cell death mechanism induced by the selected molecules

Previously, as explained in the previous section, it was found that the anion transporters compounds decrease viability of different cancer cell lines as well as CSC derived from tumors of patients with lung cancer. In this regard, to understand the molecular cell death mechanisms triggered by these compounds, cells were exposed to the inhibitory concentration IC_{25}, IC_{50} and IC_{75} of compound **2** and **7** for 24 h and subsequently protein levels of different cell death markers were analyzed by western blot.

In first place, since these compounds cause mitochondrial dysfunction as well as pH modifications in acidic compartments, we checked whether the activity of proteins related to MAPKs family was modulated by drug treatment. In cells, members of the MAPK family, such as p38, can be activated by stress stimuli, which in turn can regulate cell death depending on the duration and magnitude of that stress. Figure 44 shows that treatment with both compounds greatly increased p38 phosphorylation in A549 cells in a dose-response manner. In the case of compound **2**, a significant activation (two and three-fold increase) of p38 could be observed from the IC_{50}, and in the case of compound **7**, with higher concentrations (IC_{75}) there was three-fold increase.

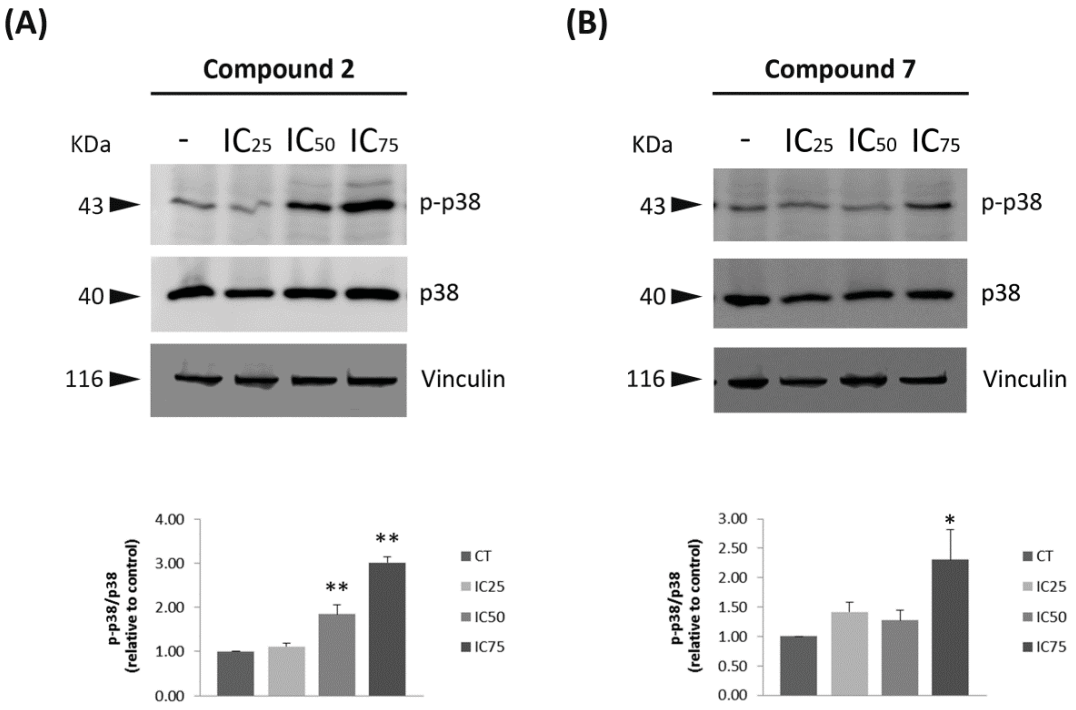

Figure 44. p38 MAPK activation. A549 cells were treated with synthetic tambjamine analogues at their IC_{25}, IC_{50} and IC_{75} values for 24 h and protein extracts were used to determine changes in stress kinase p38 MAPK and its phosphorylation protein levels. Protein levels were normalized with their respective loading controls (vinculin) in each blot. Fold changes in protein expression levels were quantified and referred to non-treated cells. Data show the mean ± SEM of three independent experiments. Statistically significant results are indicated as *$p < 0.05$ and **$p < 0.01$.

This kind of signal has been reported to activate apoptosis after some stresses (Dolado and Nebreda, 2007). In this sense, we checked whether the compounds elicit an apoptotic effect in A549 cells. According to results shown in figure 45 and figure 46, after 24 h of treatment with the different ICs of compound **2**, we were able to observe a light activation of caspase 9 and 3, and a significant cleavage of their substrate PARP with the $IC_{75,}$ which may have occurred in a caspase-independent manner. In the case of compound **7**, the decrease of the procaspase 9 and 3 as well as PARP cleavage are even more subtle. Since there was hardly any activation of the major markers of apoptosis after 24 h, we tried to check whether more potent apoptosis activation could be seen with the same treatment over time. Thus, A549 cells were incubated with the respective IC values of both compounds for 48 h. On one side, there was a slight drop of procaspases 9 and 3 after both compounds treatment. This decrease of the inactive forms was significant for both proteases in compound **2**, and just for procaspase 3 in compound 7. On the other side, their respective active forms, caspase 9 and 3 could be observed. Finally, the breakdown of the PARP substrate appeared after treatment with both compounds, significantly only with the highest dose of compound **2**.

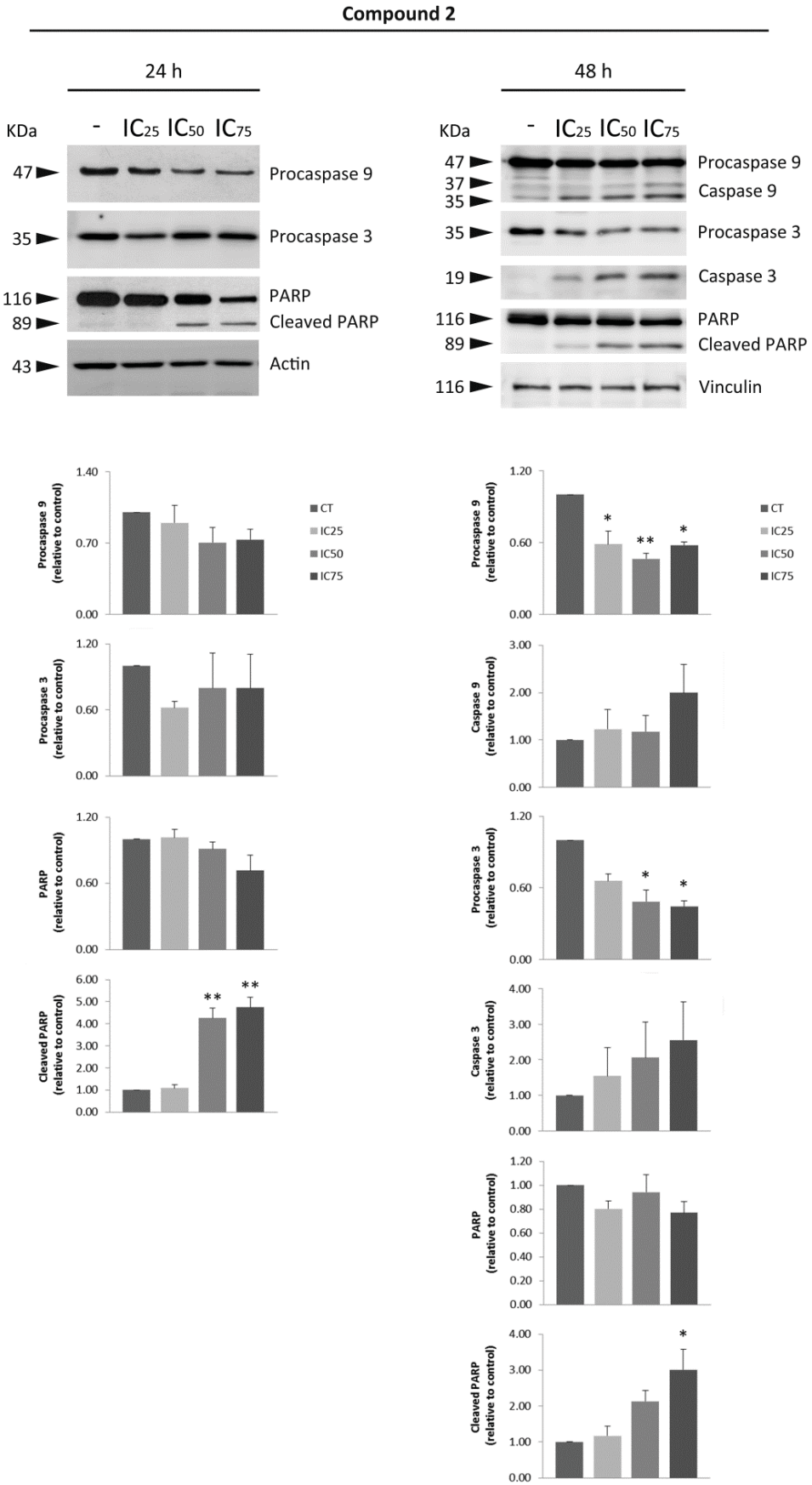

Figure 45. Apoptosis induction after compound 2 treatment. A549 cells were treated with compound **2** at their IC_{25}, IC_{50} and IC_{75} values for 24 and 48 h. Analysis of apoptotic proteins by Western blot. In each blot, protein levels were normalized with their respective loading controls. Fold changes in protein expression levels were quantified and referred to non-treated cells. Data show the mean ± SEM of three independent experiments. Statistically significant results are indicated as *$p < 0.05$ and **$p < 0.01$.

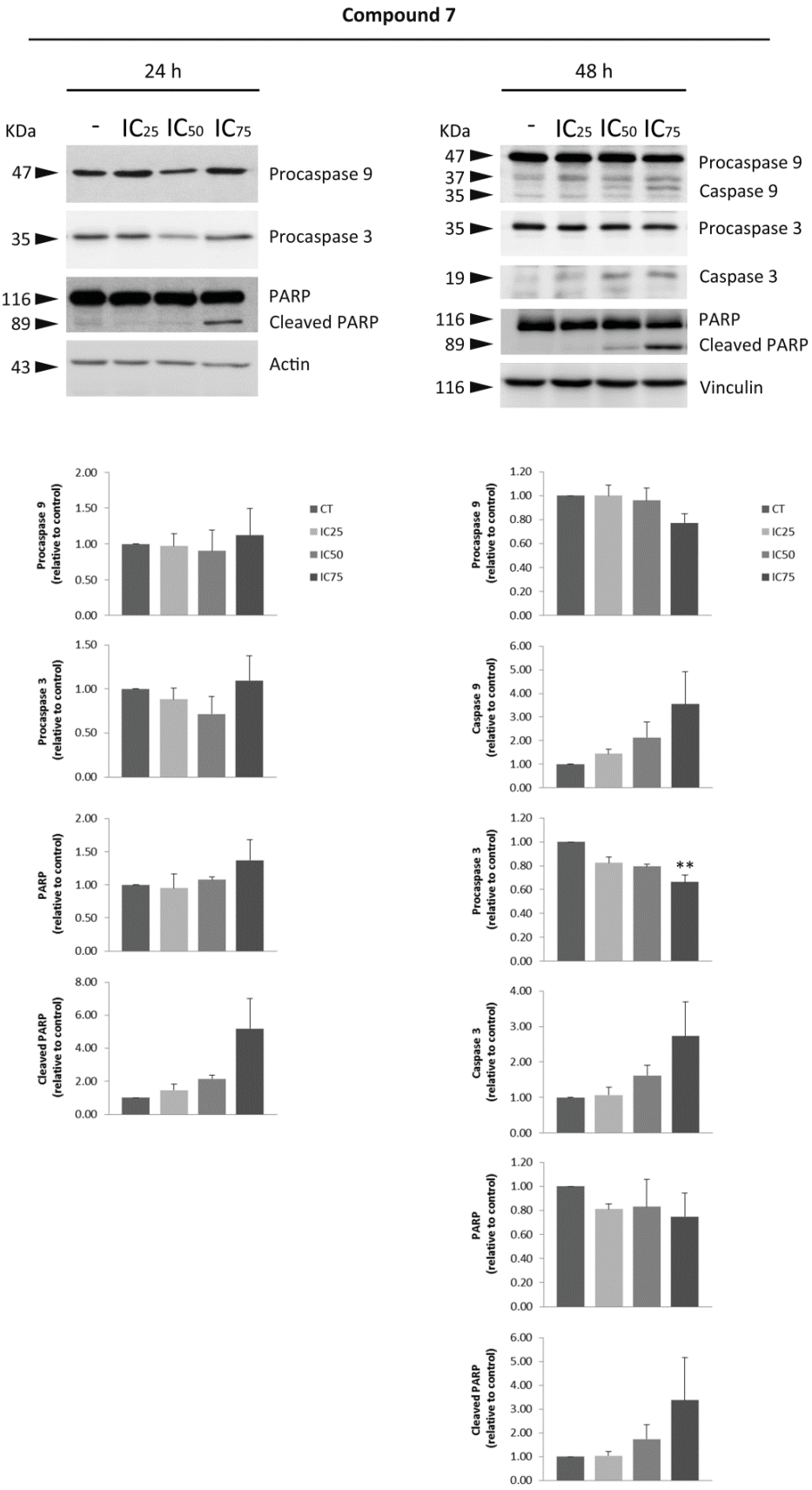

Figure 46. Apoptosis induction after compound 7 treatment. A549 cells were exposed to IC_{25}, IC_{50} and IC_{75} values of compound **7** for 24 and 48 h. Analysis of apoptotic proteins by Western blot. Actin or vinculin were used as loading controls to normalize proteins levels in each blot. Fold changes in protein expression levels were quantified and referred to non-treated cells. Data show the mean ± SEM of three independent experiments. Statistically significant results are indicated as *$p < 0.05$ and **$p < 0.01$.

In addition, we used Hoechst staining to detect chromatin condensation and apoptotic bodies formation, both hallmarks of apoptosis (figure 47). We carried out this experiment after 48 h of treatment with IC_{75}, point where we had observed a caspase activation peak in western blot analysis.

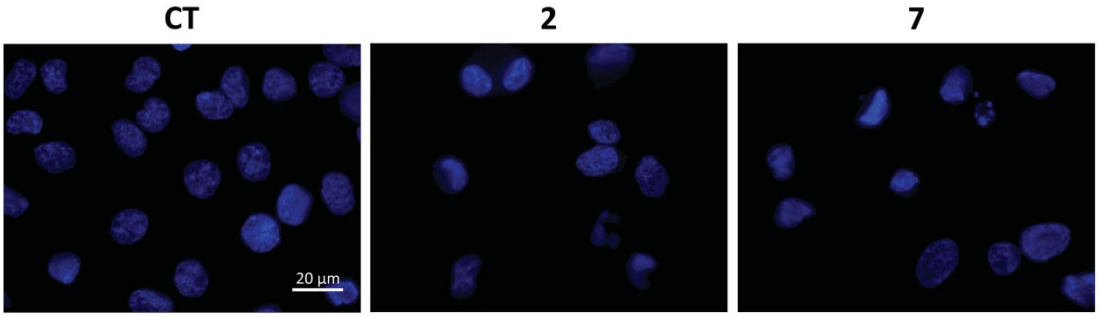

Figure 47. Morphological analysis of the nuclei induced by synthetic tambjamine analogues with Hoechst. A549 cells were treated with compound **2** and **7** at their IC_{75} for 48 h and stained with Hoechst. Nuclear or chromatin condensation and some apoptotic bodies with blue fluorescence were observed.

The results revealed that among the remaining cells, some of them kept the nucleus intact, and a small portion of treated cells showed chromatin condensation or apoptotic bodies. These facts indicate that treatment triggers the activation of the apoptotic process, and there is a cell subpopulation that dies by this mechanism. But on the other hand, in most treated cells, apoptosis does not end up being the only responsible for cell death.

Consequently, we decided to investigate whether another cell death process was involved in the observed cytotoxicity along with induced apoptosis. Considering that we had previously observed an increase in LC3 by immunofluorescence, indicative of autophagosome formation, we decided to evaluate the expression of proteins related to the process of autophagy.

Western blot analysis showed that the lipidated form of LC3 (LC3II) significantly augment from low concentrations of compound **2** (IC_{25}) (figure 48A). This great increase was also observed in cells treated in a dose-dependent manner with compound **7** (figure 48B). In addition, the p62 marker was examined. This protein facilitates the degradation of protein aggregates through autophagy and it is degraded during the process. As can be observed in the figure, p62 was not degraded but accumulated after treatment. Accumulation of p62 was observed in the treatment with both compounds, being statistically significant in the case of compound **7** (IC_{50} and IC_{75}). This result may indicate an accumulation of non-degraded autophagosomes, and therefore a blockade in the autophagic flow.

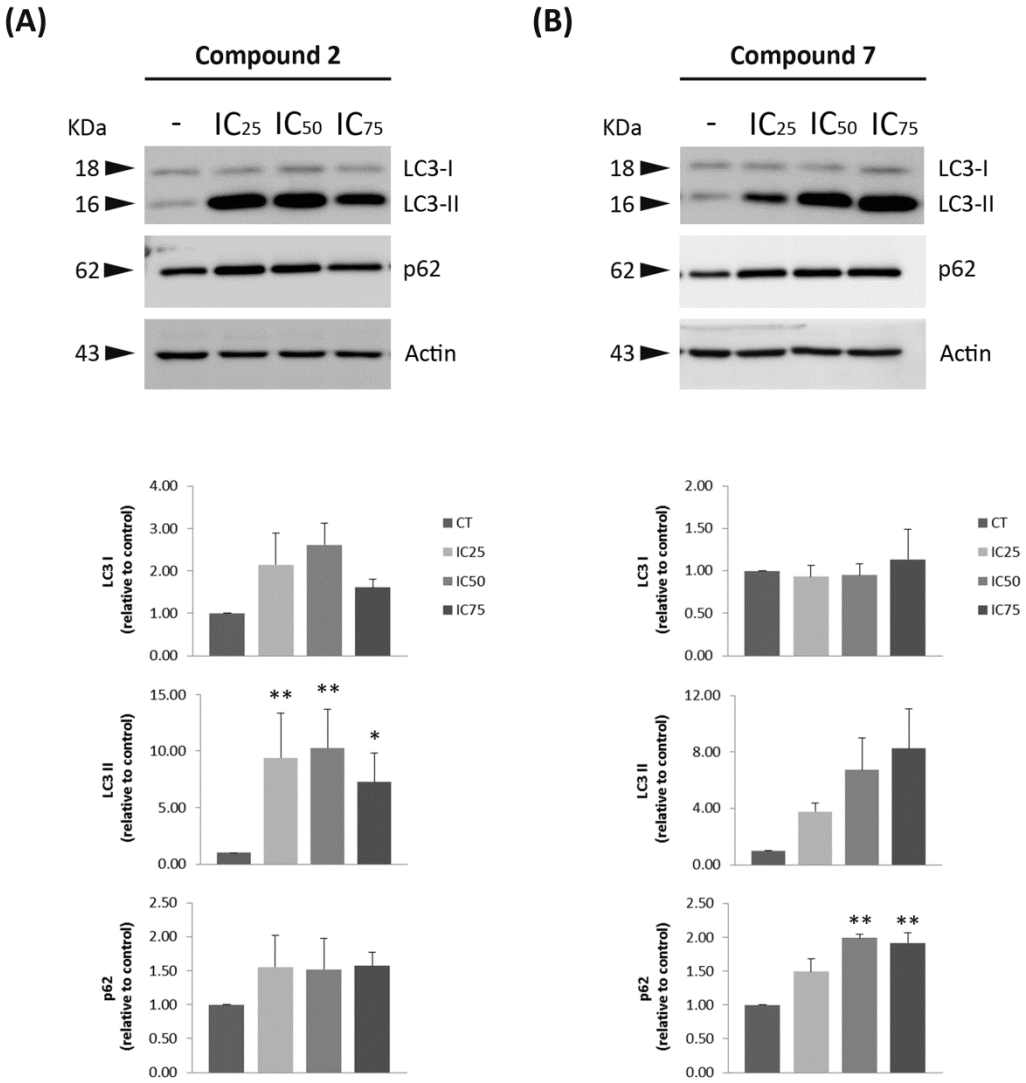

Figure 48. Expression of autophagic markers LC3II and p62. Rise of LC3II and the accumulation of p62 result in an increase in autophagosomes accumulation of and a blockade of the autophagic flux. A549 cells were treated with IC_{25}, IC_{50} and IC_{75} values of tambjamine analogues for 24 h. Actin was used as loading control to normalize protein levels in each blot. Fold changes in protein expression levels were quantified and referred to non-treated cells. Data show the mean ± SEM of three independent experiments. Statistically significant results are indicated as *p < 0.05 and **p < 0.01.

Analysis of apoptosis and autophagy markers revealed that, on one hand, there was activation of apoptotic cell death, and on the other hand, since the levels of some autophagic markers were increased, an autophagic mechanism of cell death might be plausible. To further analyze whether either mechanism was involved in the cytotoxic effect induced by synthetic tambjamine analogues, cell death inhibitors were used. In the case of apoptosis, a pan-caspase inhibitor, Z-VAD-FMK was added before treatment with different concentrations of compound **2** for 24 h. In the case of autophagy, an inhibitor of the PI3K involved in the early steps of autophagy activation, 3-MA, was added prior compound administration. However, these inhibitors failed to attenuate cell death under these conditions. Cell viability was not recovered (figure 49), suggesting that activation of caspases is not crucial for the cytotoxic effect induced by these compounds nor is the autophagosomes formation and their accumulation.

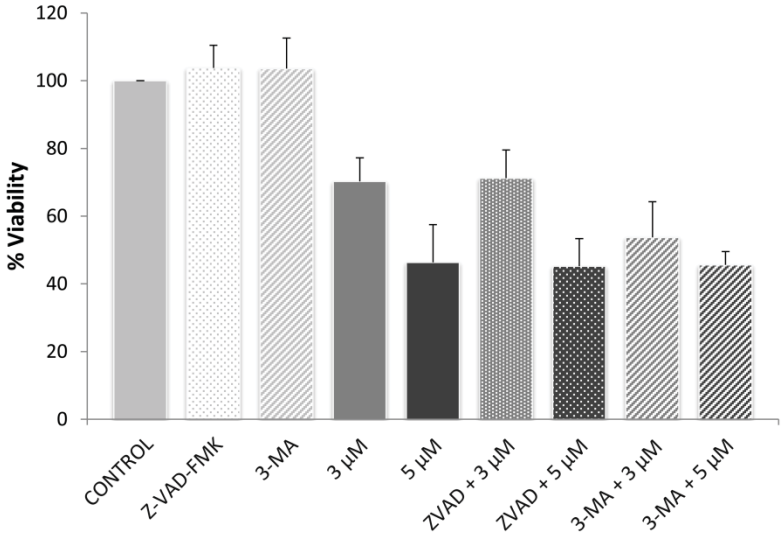

Figure 49. Cell viability after treatment with cell death inhibitors. A549 cells were pretreated with the cell death inhibitors Z-VAD (10 µM) and 3-MA (5 mM) for 1 h and then compound **2** was added at 3 and 5 µM. Cell viability was measured by MTT assay. Cell death inhibitors fail to recover cell viability.

Another possibility may be that treatment with our compounds may trigger a process of cell death like regulated necrosis, also known as necroptosis. Since RIP1 and MLKL are essential for the activation of the necroptosis pathway, we investigated their role after exposure to both compounds for 24 h. As can be observed in figure 50, there was a dose-response increase in RIP1 protein, statistically significant in the case of analogue **2**.

The major function of RIP1 kinase activity in necroptosis is to recruit RIP3, autophosphorylate, and form a functional necrosome, which in turn phosphorylates MLKL, an executioner of necroptosis. In this regard, we tried to discern whether the necrosome substrate was phosphorilated after treatment with our compounds, but anywestern blot band was detected with the p-MLKL antibody. Hence, although RIP1 increased after compounds treatment, the necrosome substrate MLKL was not activated. In addition we checked the presence of caspase 8, since necroptosis is inhibited by a supramolecular complex involving FADD, Caspase-8, and FLIP (Berghe et al., 2014). As can be seen in the figure 50, after treatment with our compounds, especially with **2**, there was activation of caspase 8 and thus necroptosis repression. Therefore, with these results, we discarded necroptosis as the possible mechanism of death.

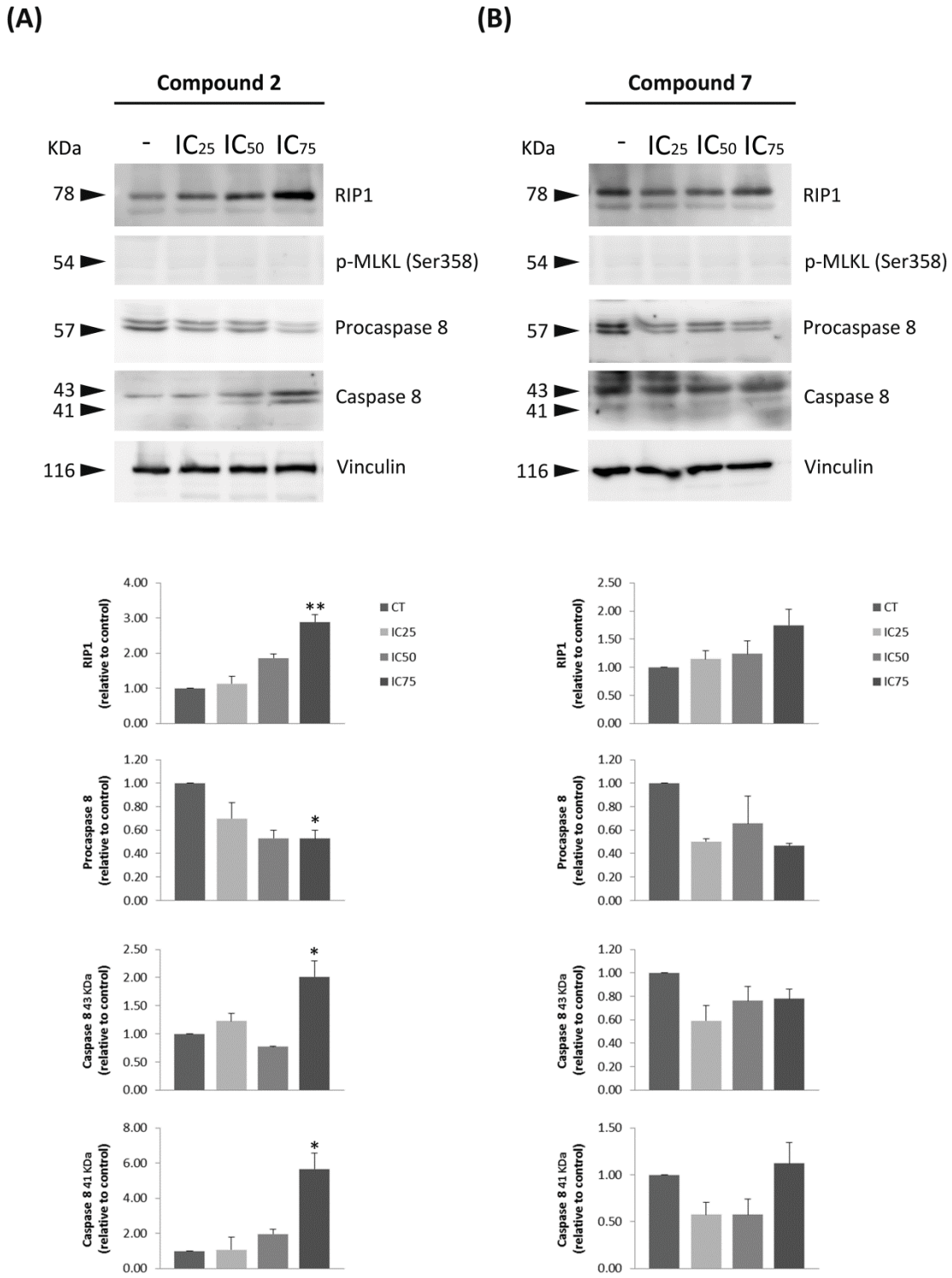

Figure 50. Expression of necroptosis related proteins and caspase 8. A549 cells were exposed to IC_{25}, IC_{50} and IC_{75} values of compound **2** or **7** for 24 h. Tambjamine analogues induced caspase 8 activation and therefore necroptosis repression. Protein levels were normalized with their respective loading controls (actin or vinculin) in each blot. Fold changes in protein expression levels were quantified and referred to non-treated cells. Data show the mean ± SEM of three independent experiments. Statistically significant results are indicated as *p < 0.05 and **p < 0.01.

Finally, we analyzed whether representative features of necrosis, such as irreversible plasma membrane damage or ROS production, were triggered after our treatment.

Hoechst staining, combined with the DNA-binding dye propidium iodide (PI), were used to measure necrosis and apoptosis in tandem after treatment with compound **2** or *7* with their respective IC_{50} value for 48 h (figure 51). Furthermore, Hoechst 33342 allows detecting changes in cell nucleus morphology, such as core condensation and formation of apoptotic bodies. This cell-permeant fluorochrome emits blue fluorescence when is intercalated into DNA. On the other hand, PI is permeable in cells that have lost plasma membrane integrity, such as necrotic cells. Nucleus of control cells retained Hoechst 33342 whereas PI was excluded by their intact cell membrane. In treated cells we could observe blue rounded nuclei in living cells, blue condensed nuclei in the case of apoptotic cells or red/purple nuclei (stained with both dyes) in those cells that have lost the integrity of their plasma membrane, hence necrotic cells. This indicates that part of cell population ends up dying by necrosis.

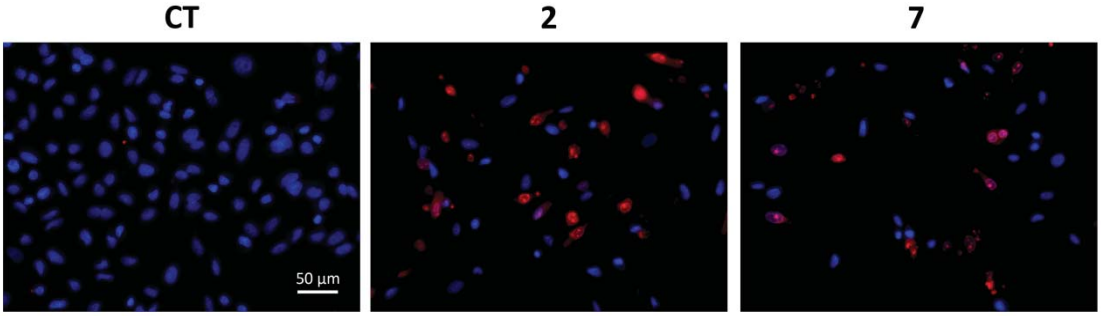

Figure 51. Hoechst and PI staining of A549 cells exposed to compound 2 and 7 IC_{50} for 48 h. Nucleus in blue represent viable cells or apoptotic bodies, depending on their condensation status. Necrotic cells appeared in red or purple due to the entry of PI after losing the integrity of the cell membrane. Scale bar 50 µm.

Otherwise, recording a video to examine cells treated at a higher dose of compound 2 with phase contrast microscopy, we could observe that synthetic tambjamine analogues also provoked cellular swelling, which finally led to plasma membrane breakdown, both typical features of necrosis. Full video appears in the supplementary information of Rodilla *et al.* paper. Here we present captures at different time points of the video (figure 52).

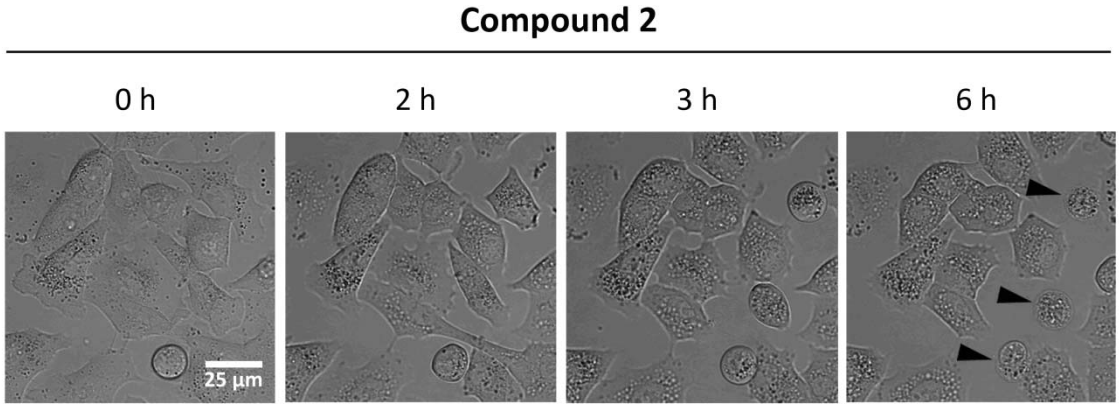

Figure 52. Contrast phase images of A549 cells plasma membrane breakdown. A video of A549 cells exposed to IC_{75} of compound 2 during 16 h was recorded. Captures at different times (0, 2, 3 and 6 h) represent the evolution of cell death process that culminates with the membrane rupture. Scale bar 25 µm.

Another factor involved in necrotic cell death is ROS production and accumulation. For its evaluation, we used The Muse® Oxidative Stress Kit based on dihydroethidium (DHE), reagent that has extensively

been used to detect ROS in cells (Gomes, Fernandes and Lima, 2005). Unfortunately, the emission wavelength of our compound interfered with this fluorescent probe and a clear results interpretation could not be obtained.

Taken together, these results support the idea that synthetic tambjamine analogues at first induce cell death by apoptosis accompanied by the activation of autophagy, but most cells end up collapsing in a necrotic cell death.

5. Molecular target identification

Our investigations so far have provided us broad information about the cell death mechanism of action of the synthetic analogues of tambjamines. These small molecules, whose cytotoxicity in cancer cells depends on their anion transport capacity, induce mitochondrial swelling and lysosomal dysfunction, which in turn lead to autophagy blockade and necrotic cell death in lung cancer cells. The identification of potential molecular targets within the cell would greatly enhance our understanding of the molecular mechanism of action of these compounds.

5.1. Identification of a potential molecular target of the synthetic tambjamine analogue

Computational methods, like molecular docking, are commonly used approaches in drug discovery. This methodology uses inputs of information about the molecular structure of any ligand (drug) or target (protein) and, through computational binding simulation, predicts potential targets for a given drug or *vice versa*. This simulation is based on the use of different algorithms by which two molecules interact with each other until they acquire the correct orientation and conformation to form an energetically favorable complex.

With the purpose of finding possible molecular targets for compound **2,** and in collaboration with Victor Guallar research group (Barcelona Supercomputing Center), PELE (Protein Energy Landscape Exploration methodology) software was used for studying protein-ligand interactions among more than one hundred cancer drug target proteins and our compound **2**. This software has the ability of mapping large conformational rearrangements stochastically over a large repertoire of protein structures. Among all the results, AKT2 appeared to be a good drug target candidate for compound **2**, since it showed very good binding results with this ligand.

Compound **2** (figure 53) has a similar structure as previously described for other anion transporters such as tambjamine or prodiginine derivatives (García-Valverde *et al.*, 2012; Soto-Cerrato *et al.*, 2015). The molecule has a conjugated π-system with a hydrophobic “outer shell” surrounding a hydrophilic “core” of three similar amino groups carrying one delocalized positive charge. All three -NH protons are capable to interact with anions such as chloride and bicarbonate ions (Soto-Cerrato *et al.*, 2015), or with a negatively charged protein group, from glutamate (Glu) or aspartate (Asp) residues, forming three hydrogen bonds as shown in figure 53A. Accordingly, our results show compound **2** preferably interacting (low protein-ligand binding energies) with Glu and Asp side chains.

PELE simulations show the ATP binding site as the energetically preferred one for compound **2** binding (figure 53B). In particular, two different ligand orientations were found for this pocket, both interacting with the carboxyl group in Asp292 (Figure 53C, molecules in purple and in ochre carbon atoms). However, four other possible pockets with favorable interaction energies were also discovered, as shown on figure 53B and 53C using blue circles. As in the ATP site, the additional pockets involve also the interaction of the ligand with an Asp or Glu. Besides the large ATP pocket, the other pockets are formed by smaller clefts that seem appropriate for the flat compound **2** π-system. Moreover, in all five sites compound **2** shows modes of binding with orientation where the bulkier tert-butyl group is pointing outward the binding cleft, and thus implying possibilities of disrupting interactions of AKT with other proteins (*see in discussion section 4.1*). In order to quantify the binding strength, Glide XP re-scoring was applied to the PELE derived best poses. The complexes showed scores between -7.0 to -9.0 kcal/mol, which should correspond from medium to low-μM experimental affinities.

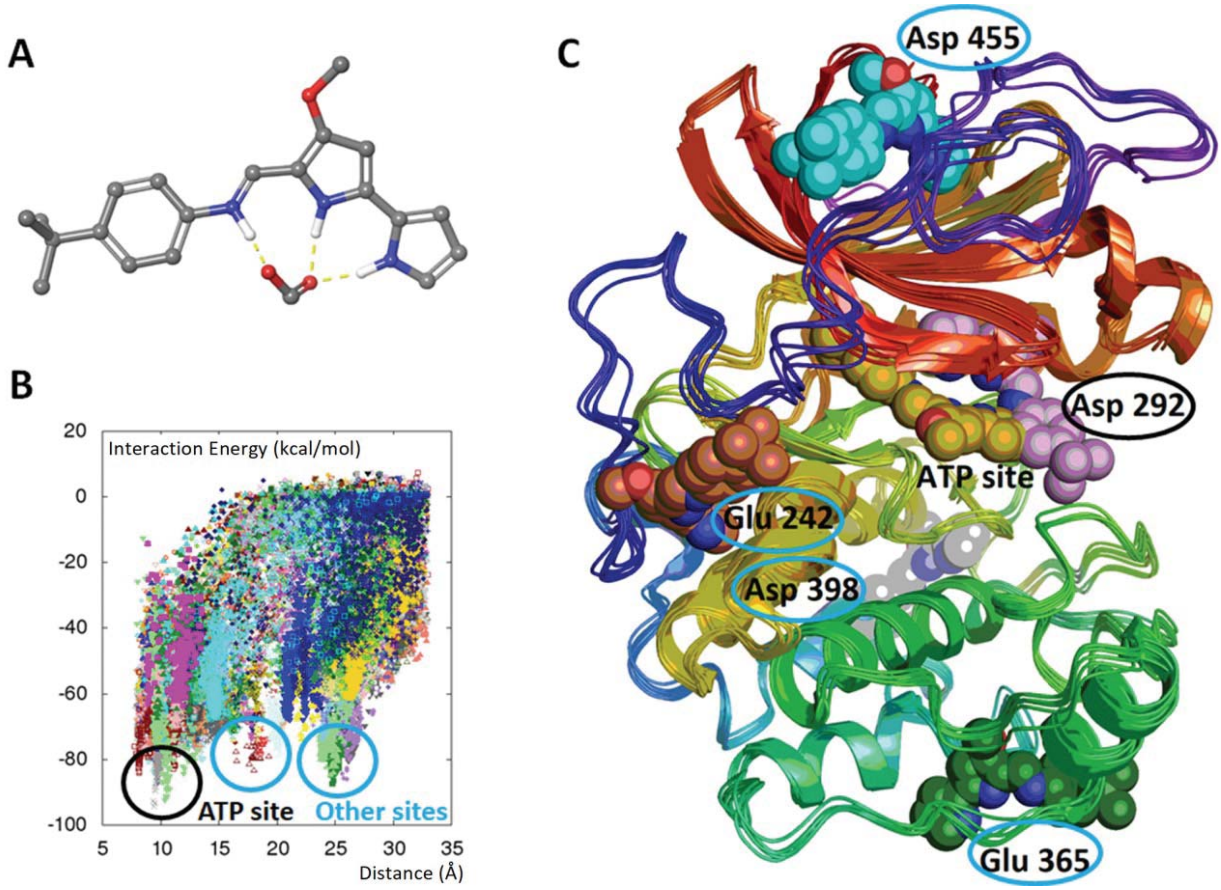

Figure 53. Induced fit docking for synthetic tambjamine analogue 2 with AKT2. A) Compound **2** molecule in complex with a carboxyl group from an Asp or Glu residue (H-bonds shown in yellow). B) Binding energy profile against the distance to the protein center obtained for the compound **2**/AKT PELE's simulation. The black and blue circles underline the best interaction energy complexes. C) Compound **2**/AKT best induced-fit docking poses (minima in B). All sites are located around a Glu or Asp residue, shown in circles. All circles use black color if located at the ATP binding site and blue color elsewhere. Compound **2** molecules are underlined using spheres with different carbon atom colors. Protein structures are shown in ribbons.

After obtaining good initial docking scores of our compound with the AKT protein through PELE and, in order to further characterize this potential binding, we decided to monitor the interaction between AKT and synthetic tambjamine analogue **2** by Surface Plasmon Resonance (SPR) assays. This real-time interaction analysis represents a valuable method which allows kinetic and affinity evaluation and determination of binding specificity between proteins and small molecules. Binding assays were performed using the Biacore system T200. We first immobilized the recombinant protein AKT2 on a

sensor surface and analyte (compound **2**) was injected in solution over the surface at concentrations ranging from 0.15 µM to 10 µM. Changes in SPR response were collected and analyzed using the software included in the system (Biacore T200 Evaluation Software). These changes, expressed in RU (resonance units), showed the association and dissociation curves of the interactions between AKT2 and compound **2** (figure 54A), allowing in turn to obtain the affinity curve (figure 54B) and kinetic and affinity constants (figure 54C).

(A)

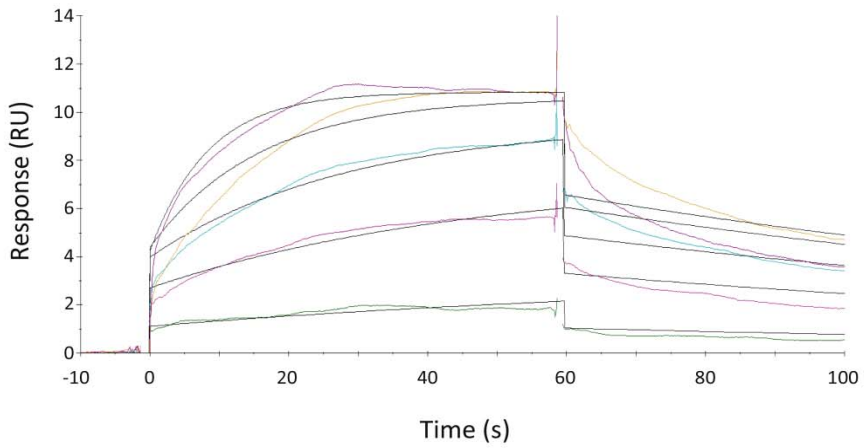

(B)

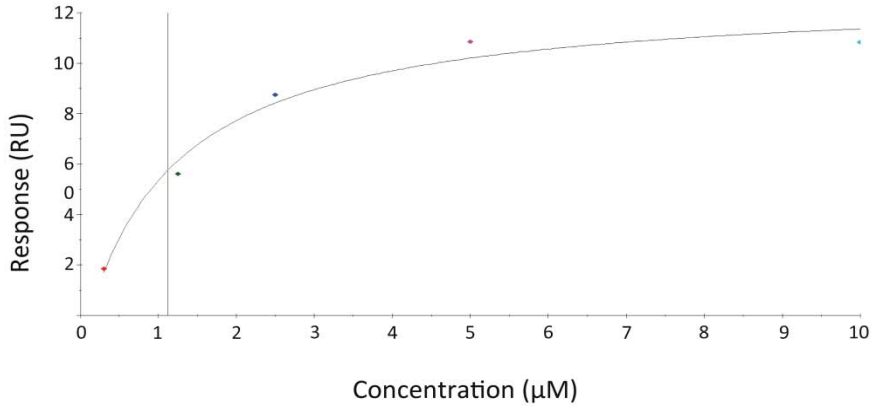

(C)

		Kinetic values			Affinity values
Ligand	**Analyte**	ka (1/M·s)	kd (1/s)	K_D (nM)	K_D (nM)
AKT2	Compound **2**	10398.5±1190	0.0064±0.0012	616.85±45.18	1206±113

Figure 54. Compound **2** binds to AKT. Binding of compound **2** (concentrations ranging from 0.15 µM to 10 µM) to immobilized AKT was analyzed by SPR as described in methods. A) Association and dissociation experimental curves are shown in color, and black traces represent the fitted data B) Affinity curve C) Kinetics and affinity data.

The data collected showed a binding constant (K_D), resulting from the relationship between the dissociation constant (Kd) and the association (Ka), of the order of nanomolar. From the affinity curve, we obtain a K_D of 1206 ± 113 nM. These values reflected the high affinity of compound **2** to the ligand, suggesting that the small molecule forms a complex with AKT2.

In order to determine whether this interaction affects its catalytic activity, we incubated A549 cells with increasing concentrations of the compound for 24 h to detect p-AKT levels by immunoblot. This test revealed that high doses of the compound not only decreased the expression of phosphorylated AKT but also caused a drop in total protein content (figure 55). This result suggest that anion transporter compound affects AKT pathway by direct binding to the protein, leading to a decrease in the total protein amount accompanied by a decrease of its activity. These data provide preliminary results about this anion transporter effect on the AKT pathway. Currently, our group is investigating in depth this important regulatory pathway in cancer as a possible target of the mechanism of action of the drug.

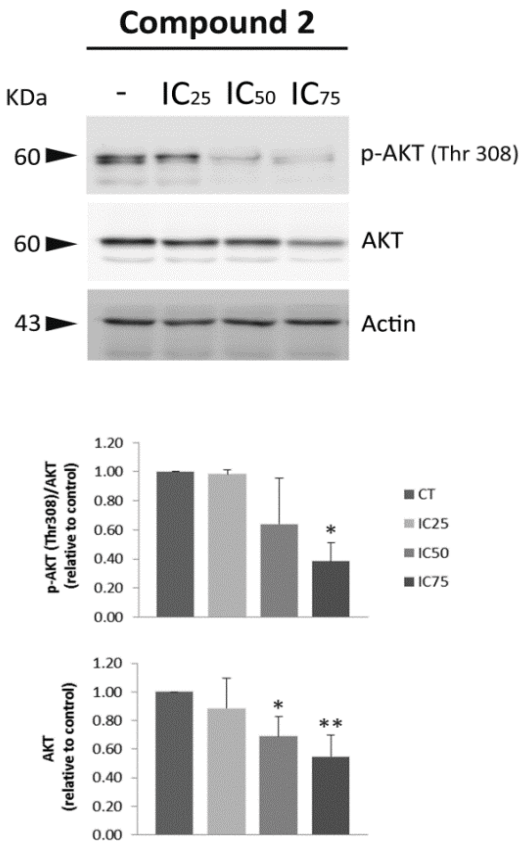

Figure 55. Decrease of phospho-AKT and total AKT. A549 cells were treated with increasing concentrations of compound **2** (IC_{25}, IC_{50} and IC_{75}) for 24 h. The activity and total amount of AKT was diminished after the treatment. Protein levels were normalized with their respective loading controls (actin) in each blot. Fold changes in protein expression levels were quantified and referred to non-treated cells. Data show the mean ± SEM of three independent experiments. Statistically significant results are indicated as *p < 0.05 and **p < 0.01.

5.2. miRNA expression analysis after compound treatment

MicroRNAs (miRNAs) are receiving much attention since they were found to be involved in the process of carcinogenesis and tumor progression. Irregular expression patterns of miRNA have been identified in several cancers, conferring adaptive advantages to cancer cells. Moreover, recent studies highlight that miRNA may influence responses of cancer cells to chemotherapy (Magee, Shi and Garofalo, 2015).

With the purpose of finding a set of miRNA involved in cancer that may be targeted by the synthetic tambjamine analogues, we used a cancer related miRNA array and studied the alteration of the miRNA expression profile in lung cancer cells after compound **2** treatment.

We decided to utilize Human Cancer Pathway Finder miRNA PCR array (MIHS-3102Z), which profiles the expression of 372 miRNAs already know to be differentially expressed in tumors versus normal tissue. This array is a useful tool to analyze the miRNAs most relevant to tumorigenesis and identify aberrantly expressed miRNAs between normal and cancer cells. In our case, the array detected expression changes in treated cancer cells compared to non-treated cancer cells.

According to our thresholds (*see material and methods section 18.3*) treatment with compound **2** altered a total of 17 miRNAs (table 15) with no change observed in the remaining 355 miRNAs of the array. Among the modified miRNA, we found some that have been reported to be specifically altered in lung cancer, including miR-21-3p, miR-30a-5p, miR-148a-3p and miR-205-5p.

miRNA Name	miRNA Previous Name	miRBase acession number
hsa-miR-7-5p	hsa-miR-7	MIMAT0000252
hsa-miR-18b-5p	hsa-miR-18b	MIMAT0001412
hsa-miR-20b-3p	hsa-miR-20b*	MIMAT0004752
hsa-miR-21-3p	hsa-miR-21*	MIMAT0004494
hsa-miR-23b-5p	hsa-miR-23b*	MIMAT0004587
hsa-miR-30a-5p	hsa-miR-30a	MIMAT0000087
hsa-miR-103a-3p	hsa-miR-103; hsa-miR-103a	MIMAT0000101
hsa-miR-106b-3p	hsa-miR-106b*	MIMAT0004672
hsa-miR-130a-5p	hsa-miR-130a*	MIMAT0004593
hsa-miR-146a-3p	hsa-miR-146a*	MIMAT0004608
hsa-miR-148a-3p	hsa-miR-148a	MIMAT0000243
hsa-miR-148a-5p	hsa-miR-148a*	MIMAT0004549
hsa-miR-205-5p	hsa-miR-205	MIMAT0000266
hsa-miR-212-3p	hsa-miR-212	MIMAT0000269
hsa-miR-224-3p	hsa-miR-224*	MIMAT0009198
hsa-miR-663a	hsa-miR-663	MIMAT0003326
hsa-miR-1287-5p		MIMAT0005878

Table 15. Differentially expressed miRNAs after treatment with compound 2. In red, those miRNAs whose expression decreased and in green those miRNAs overexpressed after treatment.

Secondly, to identify the target genes of these miRNAs, and hence the cancer pathways involved after the treatment, we used four experimentally validated miRNA-gene interactions databases (DIANA-TarBase v7.0, miRTarBase v6.0, miRecords v4.0 and miRNAMap v2.0). This bioinformatics analysis (*see material and methods section 18.3*) showed that these miRNAs regulate the expression of more than three hundred target genes. The open-source software Cytoscape was used to build a biomolecular interaction network with the most altered miRNAs and their corresponding target genes (figure 56). This network encompasses all the raw data generated from the bioinformatics analysis. The ellipses represent the altered miRNAs, in green or red as they are upregulated or downregulated, respectively, and the rectangles are the genes regulated by one, two or three miRNAs (blue, gray or green color, respectively).

Analysis of the altered gene-set revealed that cancer related pathways as PI3K/AKT/mTOR were the most affected by these miRNAs, particularly by miR-7-5p, miR-663a, miR-30a-5p, miR-205-5p, miR-18b-5p, miR-148a-3p and miR-103a-3p.

Moreover, many miRNAs were related to the regulation of apoptosis and autophagy pathways. For instance, miR-205-5p regulates 27 target genes involved in apoptosis, among which stands out BCL2 (B-cell lymphoma 2). Other miRNAs whose target genes participate in the apoptotic process are miR-7-5p, miR-30a-5p, miR-103a-3p, miR-148a-3p and miR-212-3p. Target genes implicated in autophagy are less abundant and are regulated mainly by miR-30a-5p and miR-205-5p.

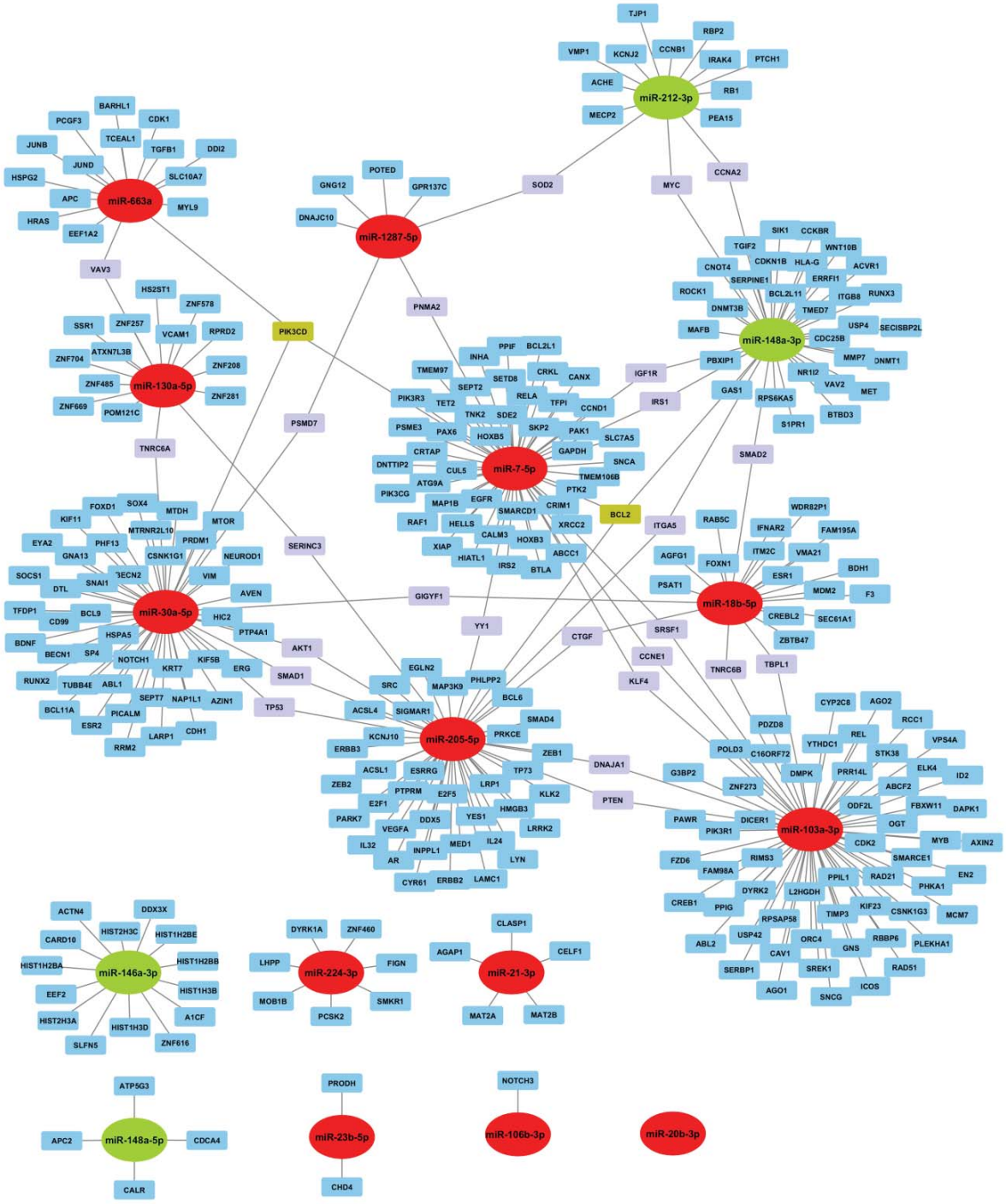

Figure 56. Network of target genes of the altered miRNAs upon compound 2 treatment. Target genes information was retrieved from 4 different databases. Network was build using the open-source software Cytoscape. The green and red ellipses indicate the up and downregulated miRNAs, respectively. The blue, lilac and gold rectangles indicate the target genes that are regulated by one, two or three miRNA, respectively.

Once we had all the data collected, we performed a more in-depth analysis focusing on the implication of these miRNAs in the above mentioned pathways related to cancer. First, by reviewing literature, we obtained information about how these miRNA are expressed in cancer. Therefore, it was possible to deduce the role that they exert as potential tumor suppressor genes or oncogenes. In this regard, we found that our compound decreased the expression of several miRNAs described as oncomirs or increased tumor suppressor miRNAs. We considered that in these cases, they may have

a role in the compound anticancer effect. On the other hand, we discarded from our analysis those miRNAs in which their potential role according to the bibliography would have an opposite effect from the observed anticancer results. Likewise, some miRNAs were excluded from further analysis due to the lack of information regarding its biological role in lung cancer.

The differentially-expressed miRNAs of the array that we managed to retrieve meaningful information regarding their regulation in lung cancer are stated in the following table:

miRNA name	miRBase accession number	Expression in cancer	Type	References
hsa-miR-103a-3p	MIMAT0000101	Up	Oncogene	(Sanfiorenzo *et al.*, 2013; Zhan *et al.*, 2014)
hsa-miR-106b-3p	MIMAT0004672	Up	Oncogene	(Z.-M. Lu *et al.*, 2014; Wang *et al.*, 2015)
hsa-miR-148a-3p	MIMAT0000243	Down	Tumor suppressor	(Yang *et al.*, 2015)
hsa-miR-148a-5p	MIMAT0004549	Down	Tumor suppressor	(J. Li *et al.*, 2015)
hsa-miR-18b-5p	MIMAT0001412	Same/Up	---	(Miko *et al.*, 2009; Dacic *et al.*, 2010; Sun *et al.*, 2013)
hsa-miR-205-5p	MIMAT0000266	Up	Oncogene	(Jiang *et al.*, 2013)
hsa-miR-212-3p	MIMAT0000269	Down	Tumor suppressor	(Rabinowits *et al.*, 2009; Incoronato *et al.*, 2010, 2011)
hsa-miR-21-3p	MIMAT0004494	Up	Oncogene	(Del Vescovo *et al.*, 2014)
hsa-miR-663a	MIMAT0003326	Up	Oncogene	(Zhang *et al.*, 2015)

Table 16. miRNAs selected according to their potential anticancer function. In red and green respectively, downregulated and upregulated miRNAs after treatment with compound **2**. These miRNAs are classified as potential oncogenes or tumor suppressor considering different studies that have reported their expression in lung cancer.

In the next step, we selected the genes, regulated by the aforementioned miRNA, that were involved in the pathways that can be related to the induction of an anticancer effect, which were apoptosis, macroautophagy and PI3K/AKT/mTOR. This was carried out using KEGG (Kyoto Encyclopedia of Genes and Genomes) pathway database (http://www. genome. jp/kegg/). This is a platform that collects multiple pathway maps representing experimental knowledge on molecular interactions, reaction and relation networks within the cells and organisms. Once the selection process was completed, we built a new network with Cytoscape software encompassing selected genes and their miRNAs (figure 57).

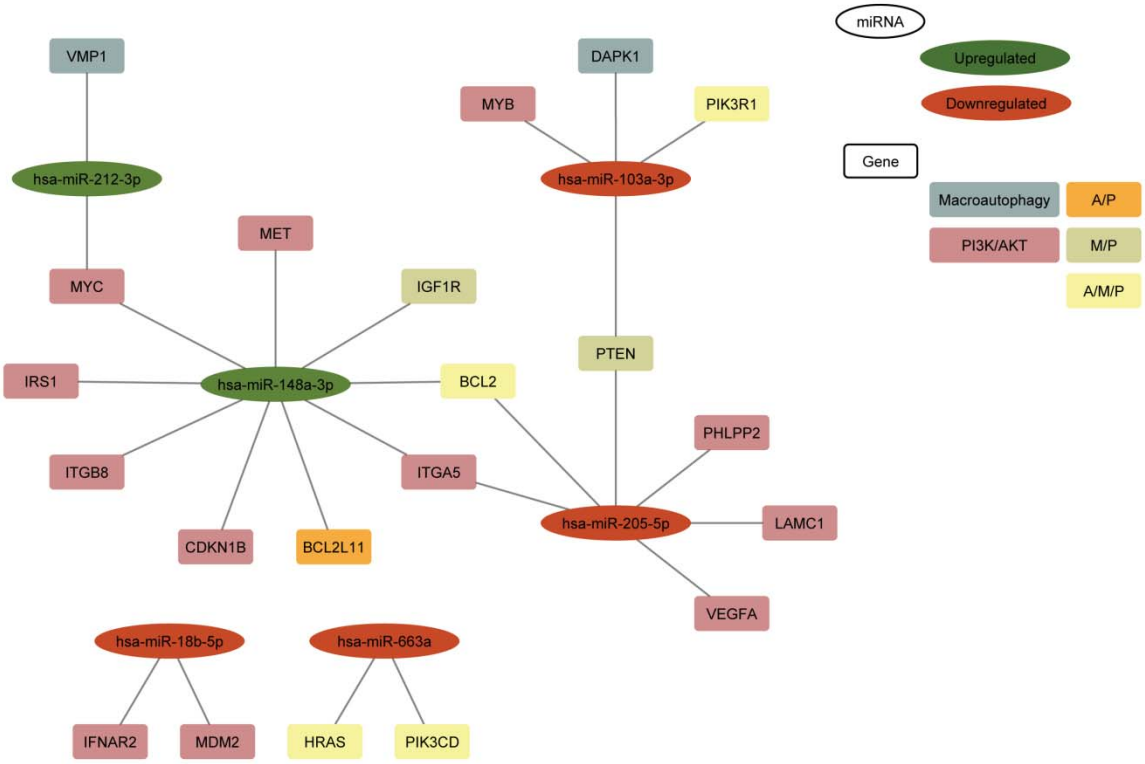

Figure 57. Differentially-expressed miRNAs and their target genes interaction network. Green and red ellipses stand for upregulated and downregulated miRNAs after compound **2** treatment, respectively. In rectangles, genes related to PI3K/AKT pathway, apoptosis and macroautophagy. Genes involved in macroautophagy are shown in light blue and PI3K/AKT in pink. Genes involved in two pathways are in orange or light green, representing apoptosis and PI3K/AKT (A/P), macroautophagy and PI3K/AKT (M/P). Those genes that are implicated in the three pathways are in yellow (A/M/P).

Attending to the target genes that appeared in the network, genes such as PTEN (phosphatase and tensin homolog) and PHLPP2 (PH domain and leucine rich repeat protein phosphatase 2), regulated by the downregulated miR-103a-3p and miR-205-5p, and genes like BCL2 or MYC (myelocytomatosis virus oncogene cellular homolog), regulated by the upregulation of miR-148a-3p and miR-212-3p must be highlighted. This miRNA expression profile generated after treatment with compound **2** might be related with the cytotoxic effect observed in A549 cell line.

In any case, these are preliminary results predicted by the observed miRNA modifications. To corroborate the implication of these genes in the cytotoxic effect induced by compound **2**, we would have to validate each of these potential target genes in further experiments.

6. Evaluation of compounds therapeutic effect in *in vivo* studies

Previous results with compound **2** and **7**, such as their high cytotoxicity in lung cancer cell lines and patient-derived CSC, suggested that these compounds may be potential antitumor drugs in cancer mice models. Accordingly, anti-tumor efficacy was first assessed in an ectopic xenograft model, using a subcutaneous model in collaboration with Dr. Villanueva (Institut d'Investigació Biomèdica de Bellvitge). Mice bearing subcutaneous A549 tumors were treated with compounds **2** or **7** (6 mg/kg

in saline with 7.5% of DMSO/0.8% Tween-80) or vehicle control (7.5% of DMSO/0.8% Tween-80) in alternating days during 20 days. At the same time, treatment with CDDP, standard chemotherapeutic drug, was carried out in order to compare their efficacy levels.

Figure 58 shows the results of treating mice bearing A549 tumors with compound **2** or **7** or/ and **CDDP**. Both compounds, at a dose of 6 mg/kg, produced a statistically significant ($P < 0.01$) reduction in tumor weight compared to the control group and it was similar to the CDDP induced reduction. However, the combination of our compounds with CDDP did not lead to a synergistic effect. Importantly, as a single agent, the treatment with compounds **2** or **7** did not produce any obvious toxicity (hepatotoxicity and nephrotoxicity) diarrhea or significant body weight loss.

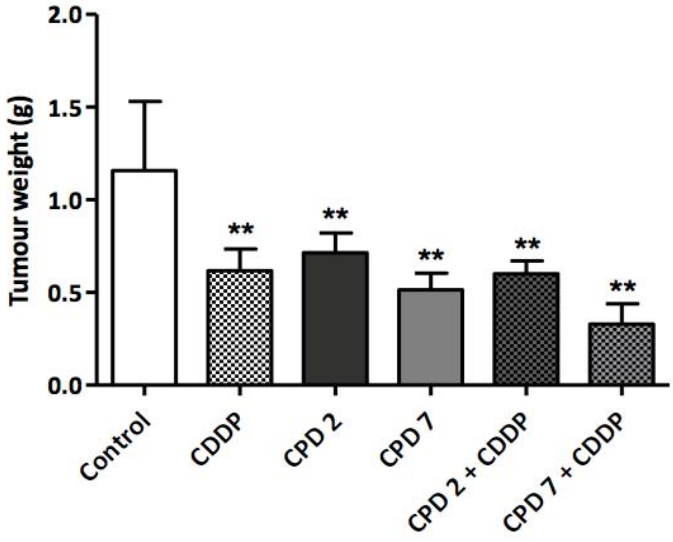

Figure 58. Effect of synthetic tambjamine analogues (2 and 7) in established A549 human adenocarcinoma subcutaneous tumors. Mice (7/group) were administered with compound **2** or **7** at 6 mg/kg in alternating days during 20 days or CDDP at 4 mg/kg day 0, 7 and 15. Significant differences in mean tumor weights compared to controls were observed with all single compounds treatments. No synergistic effect was observed in combination treatments. Statistically significant results are indicated as $*p < 0.05$ and $**p < 0.01$.

In a preliminary study, we tested our compounds in a murine orthotopic lung model developed by Dr. Villanueva. We selected this model since it reproduces the primary site of the common human lung cancer and is able to represent the common sites of metastasis. Unfortunately, due to technical difficulties, the groups were reduced to 3 or 4 animals per condition. Given that our findings are based on a limited number of animals, the results from this analysis should be treated with considerable caution. Despite this, it was observed that both compounds reduced tumor progression in this model, especially compound **7** (figure 59). Taken together, these preliminary results indicate the potential therapeutic effects of our compounds against lung cancer.

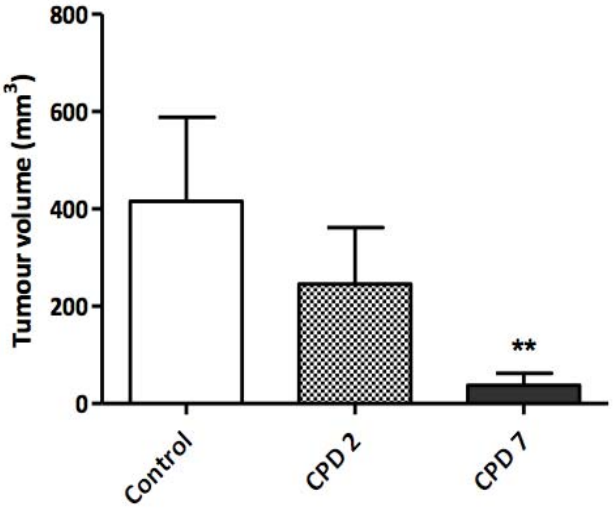

Figure 59. Antitumor effects of tambjamine analogues in an orthotopic model of human NSCLC. Bar graph showing the mean tumor volume in murine lung orthotopic model treated with 6 mg/kg of compound **2** and **7** for 20 days. Statistically significant results are indicated as *p < 0.05 and **p < 0.01 versus vehicle control.

DISCUSSION

1. Chemical structure, anion transport activity and cytotoxicity

Oral and lung cancer are listed among the most common respiratory diseases, being the latter one of the main causes of mortality in the world. Despite new advances in diagnosis and clinical care, the success of conventional treatments is still limited, especially in chemotherapy. Therefore, it is necessary to identify new molecules with different mechanisms of action and more effectiveness to fight against these types of cancers. Since cancer cells have a "reversed" pH gradient that supports their development, in the last years, the disruption of ionic homeostasis has been described as a new strategy against cancer (Webb *et al.*, 2011). Consequently, anion transport compounds such as prodigiosin, obatoclax and salinomycin, among others, are being studied as potential therapeutic agents for cancer (Perez-Tomas and Montaner, 2003; Gupta *et al.*, 2009; Perez-Tomas and Vinas, 2010; Goard and Schimmer, 2013). Natural tambjamines, secondary metabolites derived from marine invertebrates (Carte and Faulkner, 1983)(Soliev, Hosokawa and Enomoto, 2011), are also a family of anion carrier compounds with diverse biological activities (Carbone *et al.*, 2010). As a result of the search for novel compounds with efficient transporter activity, in collaboration with Roberto Quesada's research group (University of Burgos), new molecules derived from this family were synthesized. Structurally, the compounds in these series share a bipyrrole core, typical of natural compounds. These synthetic tambjamine analogues possess an aromatic enamine group bearing either electron donating or electron withdrawing substituents as well as a heteroaromatic (pyridine) group. Beside this, each analogue has a parent derivative, in which, in addition to the previous modifications, a benzyloxy group replacing the methoxy group characteristic of the natural compounds was introduced (Hernando *et al.*, 2014). The variability on the substituents confers a specific lipophilicity character to the compounds. This lipophilicity has a direct impact on the anion transport activity of these synthetic tambjamine analogues (Knight *et al.*, 2016).

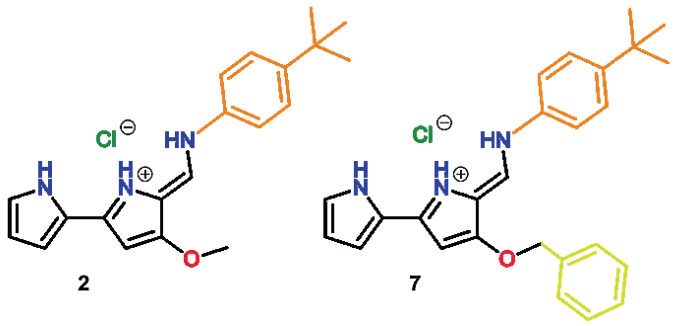

Figure 60. Chemical structure of synthetic tambjamine analogues

These compounds, as well as other natural tambjamines, have been described as potent transmembrane anion transporters in liposomal models, facilitating chloride and bicarbonate exchange across lipid membranes (Hernando *et al.*, 2014). The compounds form supramolecular complexes with anions through the formation of strong hydrogen bond interactions and are capable to promote chloride and bicarbonate transport through bilayers (figure 61).

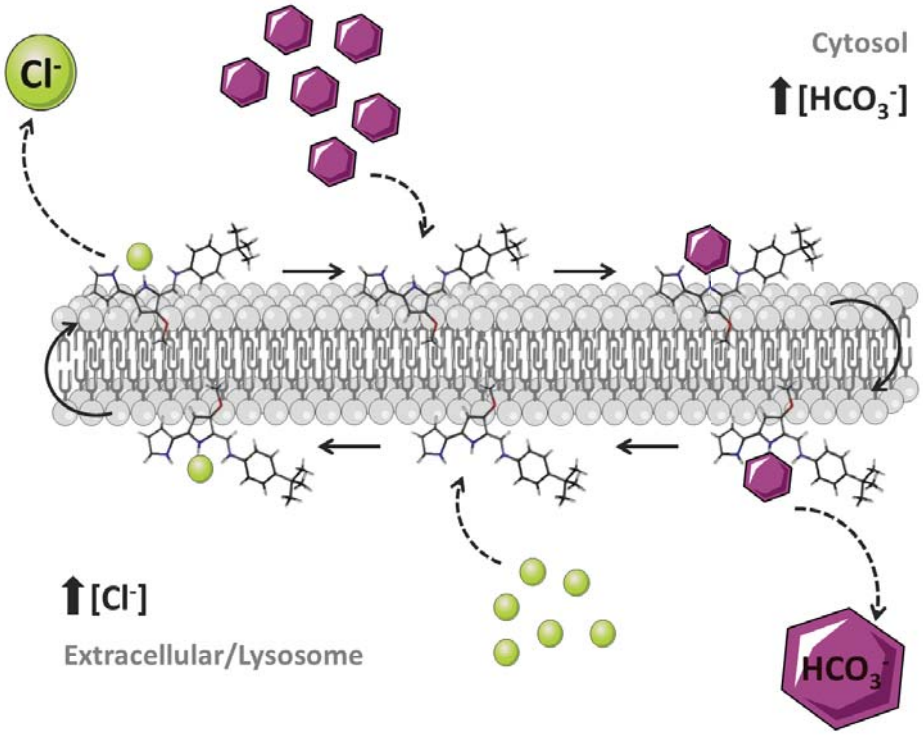

Figure 61. Model for anion transport mechanism induced by synthetic tambjamine analogues. This figure was produced using Servier Medical Art image bank.

Recently, as a result of its transport activity, several synthetic tambjamine analogues have shown potent anticancer activity in a panel of cancer cell lines, including human melanoma, lung carcinoma, colorectal adenocarcinoma and mammary adenocarcinoma cells (Hernández *et al.*, 2012; Hernando *et al.*, 2014). In this thesis, the results obtained related to their anticancer properties with those compounds bearing 4-alkoxy-2,20-bipyrrole moieties (Hernando *et al.*, 2014) are extended to several oral and lung cancer cell lines. Cell viability was reduced with the majority of the tested analogues in both oral and lung cancer cell lines. The most potent compound, analogue **2** was selected along analogue 7, its variant with benzyloxy group, as the most promising anticancer compounds. This pair of compounds showed IC_{50} values after 24 h of treatment below 5 µM in representative cell lines of both types of cancer. A third compound, **NT** or non-transporter, selected for further experiments due to its modest transport capacity, is structurally related to the synthetic tambjamine analogues and have showed significantly higher IC_{50} values. Hence, anion transport activity may be directly related to cellular cytotoxicity.

Similar studies carried out with indole-based tambjamine analogues, another batch of synthetic compounds derived from the natural marine alkaloids, showed higher IC_{50} values in lung cancer cell lines (Soto-Cerrato *et al.*, 2015). Hence, our compounds are the most potent among the different series of tambjamine analogues in terms of cytotoxicity for lung adenocarcinoma cells. Furthermore, our compounds have proved to be more effective than other anionophores since recently data published for the therapeutic cationophore salinomycin have showed IC_{50} values ranged from 5 to 10 µM for lung cancer A549 cell line (Arafat *et al.*, 2013). The comparison between IC_{50} values relative to these analogues with those obtained with cisplatin (standard chemotherapeutic agent used in the clinic for both oral and lung cancer) showed that compounds bearing 4-alkoxy-2,20-bipyrrole moieties are

more potent than cisplatin. The cisplatin IC_{50} value obtained in our group is consistent with previous published data (Yan *et al.*, 2009). In addition, synthetic tambjamine analogues are more efficient than gemcitabine *in vitro*, considering that it has an IC_{50} value around 10 μM after 72 h of treatment (Ikeda *et al.*, 2011; Li *et al.*, 2016). Therefore, tambjamine analogues *in vitro* values are in the range of the most currently used chemotherapeutics in the treatment of lung cancer.

Selected compounds were also tested in CSC (cancer stem cells) derived from patients or isolated from A549 cells and compound **2** showed to be especially potent against patient-derived CSC. This tumor subpopulation, involved in tumor initiation, possesses capacity for sustained self-renewal, contributes to metastatic dissemination as well as to acquired chemotherapy resistance in cancer (Valent *et al.*, 2012), thus these results are very encouraging for lung cancer treatment and the prevention of tumor recurrences. In this view, studies with indole-based tambjamine analogues have also demonstrated that they are able to severely reduce CSC viability (Soto-Cerrato *et al.*, 2015). Beside this, that kind of anion transporter induces cell membrane hyperpolarization, which in turn leads to CSC differentiation. This fact could increase CSC sensitivity to chemotherapy or radiation achieving greater efficacy and favorable clinical results (Soto-Cerrato *et al.*, 2015). In this regard, other anionophores such as the cation selective ionophore salinomycin has demonstrated that it has specific toxicity against CSCs in different types of human cancers *in vitro* (Gupta *et al.*, 2009; Wang, 2011), indicating that the application of these kind of compounds might be a very promising therapy.

All this work led us to conclude that selected synthetic tambjamine analogues demonstrate better capacity as cytotoxic compounds, both in cancerous cell lines and in patient-derived CSC, than first-line chemotherapy treatments, suggesting that they might be promising new chemotherapeutic agents.

2. Anionic unbalance and cellular stress

Cells are constantly subjected to different forms of endogenous and exogenous stimuli, many of which can induce stress. These insults that interfere with cellular homeostasis, such as hypoxia, DNA damage or ionic imbalance, initiate responses to maintain the balance that is needed for cell survival, and if this is not recovered, they may trigger cell death mechanisms.

2.1. Intracellular pH modifications

pH homeostasis and the maintenance of proton gradients across organellar membranes are key to cell survival, function and proliferation (Casey, Grinstein and Orlowski, 2009). On one hand, function of organelles is subjected to the establishment and preservation of an internal differentiated pH that provides optimal environmental conditions for the operation of certain metabolic pathways. On the other hand, all proteins depend on pH to preserve their structure and function. Moreover, different concentrations of protons among compartments and cytosol generate H^+ gradients essential to the generation and conversion of cellular energy, which in turn is an integral part of many metabolic reactions (Casey, Grinstein and Orlowski, 2009). This finely adjusted function, carried out mainly by transport proteins located on the cell membrane, can be modulated by endogenous or exogenous molecules, as well as, in some pathological situations, can lead to pH_i changes that have been implicated in both cell proliferation and cell death (Lagadic-Gossmann, Huc and Lecureur, 2004). Therefore, our

selected synthetic tambjamine analogues, as potent chloride/bicarbonate exchangers, could have direct consequences on both cytoplasmatic and organelle pH.

Lysosomes are acidic organelles responsible for the degradation of both intra- and extracellular components, via endocytosis or autophagy, respectively. For this reason, this organelle contains a large array of hydrolases designed to catabolize all types of macromolecules (Shen and Mizushima, 2014). Their catabolic activity depends on the highly acidic pH of the lysosomal lumen (pH 4.5-5.0). Acidic pH is mainly generated by V-ATPases, a large multimeric enzyme complex that couples the energy of ATP hydrolysis to pump protons across the lysosome membrane into the lysosome lumen. Considering that this proton accumulation generates a transmembrane voltage, another ion must move to dissipate this charge. In this regard, in addition to the proton pump, several ion channels have been identified in the lysosome membrane, for example Cl^-/H^+ antiporters (ClC-7) and Na^+/K^+ channels. Both contribute to acidification compensating lysosomal membrane charges through flux of counterions, such as K^+ or Cl^-, moving out or into the lysosome, respectively (Mindell, 2012) (Xu and Ren, 2015).

Once the cells internalize these synthetic tambjamine analogues, several cellular processes occur, converging in the potent cytotoxic effect observed. According to the temporal sequence of events that take place inside the cell, synthetic tambjamine analogues **2** and **7** cause the loss of acridine orange fluorescence from acidic organelles within the first hour of exposure, which indicate lysosomal deacidification. This increase in lysosomal pH is consistent with an anion carrier activity across cellular membranes, similarly to that observed in liposomal model. In acridine orange assay, as a negative control, we used another synthetic tambjamine analogue (**NT**) due to its modest anion carrier capacity. Even though **NT** is structurally similar to our compounds, it has lower lipophilic value, and therefore it does not have the same capacity to insert in the lipid membranes. For this reason, after treatment with **NT**, the acidic compartments maintain typical AO staining unlike those treated with **2** and **7** (*figure 32C, results section 3).*

Our suppositions to explain this phenomenon are based on transport activity assays. We presume that synthetic tambjamine analogues facilitate the entrance of bicarbonate into the lysosome and promote the efflux of chloride outside the lysosome, favoring electrochemical gradient (figure 62). On one hand, internalized HCO_3^- would combine with the H^+ present in the lysosome forming carbonic acid, which being unstable in aqueous solution, is transformed into water and carbon dioxide that can diffuse freely through the membrane. In this case, the bicarbonate entry would act as a buffering system, increasing the pH of the lysosome. On the other hand, after chloride output, the electrical potential across the membrane would be unbalanced. In this regard, this could cause a proton leakage trying to dissipate the electrical gradient (DiCiccio and Steinberg, 2011). Moreover, it could influence lysosome transporters, such as the chloride proton antiporter ClC-7, which might try to compensate the lack of chloride pulling out H^+.

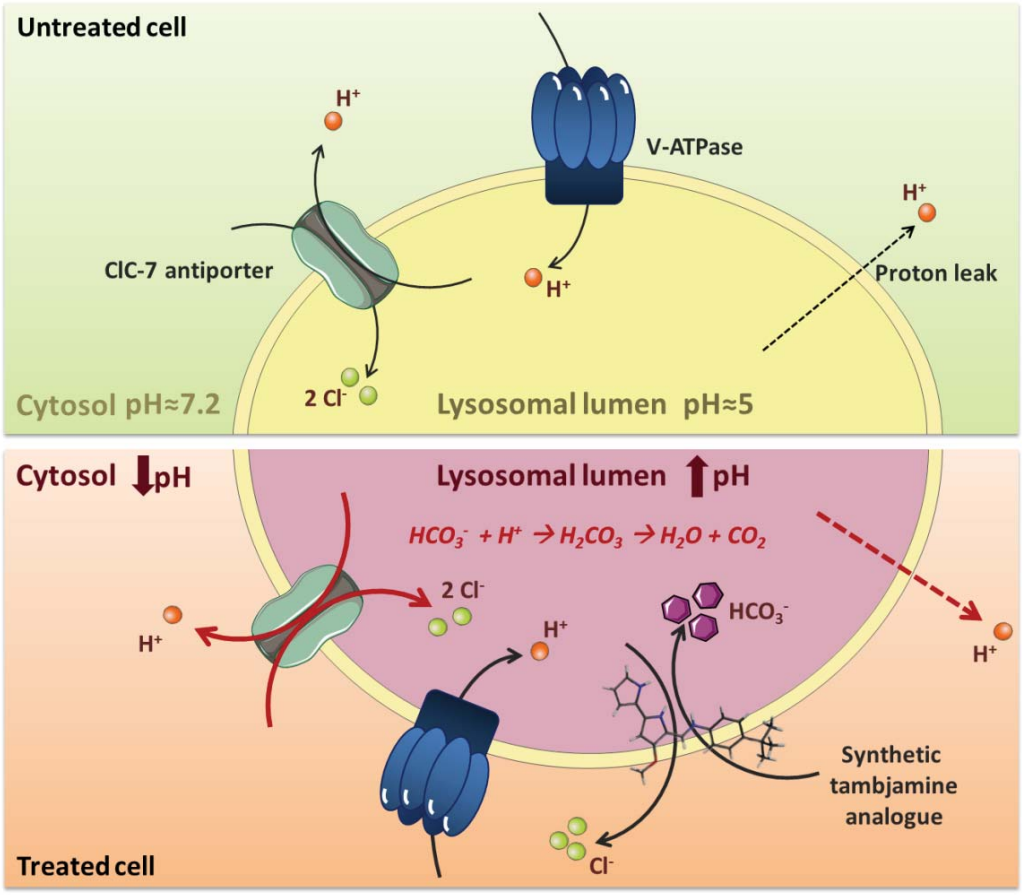

Figure 62. Lysosomal anion transport model induced by selected synthetic tambjamine analogues and its consequence on intracellular and lysosomal pH. This figure was produced using Servier Medical Art image bank.

Interestingly, it has recently been reported that obatoclax, another anionophore related to the prodiginine family that has been evaluated in clinical trials for different cancer conditions, rapidly localizes to the lysosomes and also induces lysosomal alkalization (Champa *et al.*, 2016; Stamelos et al., 2016). Typically, an increase in lysosomal pH could derive from H^+ leakage, a defective proton pump or lysosomal membrane permeabilization (LMP) (Boya, 2012). Beside this, it has recently been described that high luminal chloride in the lysosome is critical for lysosome function, being highly depleted in lysosomal storage disorders (Chakraborty, Leung and Krishnan, 2017). Therefore, defects in the normal functioning of the lysosome as a result of its alkalization may affect cellular homeostasis and are associated with several human diseases (Schneider and Cuervo, 2014; Serrano-Puebla and Boya, 2016). Moreover, it may lead to dysregulation of autophagic flux, which will be described in the following section.

On the other hand, lysosomal alkalization may also be derived from LMP, which is related to cell death (Boya and Kroemer, 2008; Galluzzi, Bravo-San Pedro and Kroemer, 2014). This process involves the release of lysosomal cathepsin proteases, and a partial drop of cytosolic pH that allows their activation. Depending on the cell type, and the nature and intensity of the stimulus, LPM can initiate or amplify different types of cell death. It has been reported that partial LMP can initiate apoptotic pathway through the cleavage of a variety of substrates (Kågedal *et al.*, 2001; Cirman *et al.*, 2004),

whereas extensive and rapid LMP results in necrosis (Galluzzi, Bravo-San Pedro and Kroemer, 2014; Repnik, Hafner Česen and Turk, 2014). In this sense, the increase in lysosomal pH may derive from LMP and be contributing to cell death.

On the other hand, synthetic tambjamine analogues may also induce a chloride/bicarbonate exchange at the plasma membrane, affecting to the intracellular pH. Attending to the typical ion concentration inside the cell, chloride is less abundant than bicarbonate (Lodish and A. Berk, S. L. Zipursky, P. Matsudaira, 2000), hence the movement of ions triggered by compounds would be the entry of chloride inside the cell and the expulsion of bicarbonate out of the cell. This would leave the cytosol with a low buffering capacity against the proton leakage from the lysosome, and therefore this would be acidified. Unfortunately, it was not possible to measure the decrease of pH_i caused by our selected compounds due to technical limitations of fluorescence interference. However, in recent studies with indol-based tambjamines (structurally related to our compounds), it has been proved that these compounds cause a significant intracellular acidosis (a drop of up to 0.70 pH units) as a consequence of the anion transport, and this might be responsible for initiating the process of cell death (Soto-Cerrato *et al.*, 2015; Manuel-Manresa *et al.*, 2017).

Interestingly, a recent research has been published in which they report how cisplatin, a first line treatment, induces acidification of the cytoplasm early after the treatment. In addition, their studies support the hypothesis that the ability to control and maintain an alkaline pH_i promote cell survival after treatment with cisplatin (Shirmanova *et al.*, 2017).

2.2. Mitochondrial swelling

Mitochondria are essential organelles that perform multiple functions in the cell. They are at the core of cellular energy metabolism, being the site of most ATP generation through the TCA cycle, OXPHOS and the electrochemical gradient generated across the inner of two membranes by the electron transport chain (ETC). However, mitochondria perform many roles beyond energy production; these organelles can contribute to cell death by shutting off the energy supply, producing damaging free radicals or releasing death-promoting proteins. Such processes can be part of a programmed process to eliminate those unneeded or abnormal cells, or they can derive from an unplanned response to an overwhelming stress (Green, Galluzzi and Kroemer, 2014).

Mitochondria volume regulation is a housekeeping cellular function essential for maintaining the structural integrity of the organelle (Kaasik *et al.*, 2007). Mitochondrial volume homeostasis is controlled by osmotic balance between cytosol and mitochondria. Increased colloidal osmotic pressure enhances the water influx leading to matrix swelling. Apparently, the flux of Ca^{2+} and K^+, which in turn may be associated with the movement of other ions, play a critical role in physiological and pathological swelling of mitochondria (Javadov, Chapa-Dubocq and Makarov, 2017). Changes in mitochondrial size within a physiological range stimulate mitochondrial function and metabolism (Halestrap, 1994). However, excessive mitochondrial swelling, resulted from alterations in ion homeostasis in the cytoplasm and mitochondrial matrix, compromises its function and integrity (Javadov, Chapa-Dubocq and Makarov, 2017).

In physiological conditions, the inner mitochondrial (IM) membrane is nearly impermeable to all ions, including protons. This allows the oxidative phosphorylation complexes to generate a proton gradient required to drive ATP synthesis. Beside this, this charge imbalance that results from the generation of an electrochemical gradient across the IM forms the basis of the mitochondrial transmembrane potential. Hence, maintenance of the proton gradient is crucial for cellular bioenergetics (Kroemer, Galluzzi, Brenner, et al., 2007). In addition, and overgeneration of ROS or intracellular calcium overload causes the opening of mitochondrial permeability transition pores (MPTP) in the IM. MPTP is accompanied by a drop of the mitochondrial membrane potential ($\Delta\Psi_m$), uncontrolled entry of solutes and water into the matrix, which causes organelle swelling and may culminate in the rupture of the outer membrane (Halestrap, 2009). When mitochondrial membrane permeabilization (MMP) occurs, proteins from the mitochondrial intermembrane space are released into the cytosol, where they promote cell death by multiple mechanisms (Kroemer, Galluzzi, Brenner, et al., 2007)(Galluzzi, Blomgren, & Kroemer, 2009).

Once the cells incorporate the synthetic tambjamine analogues, the following event that occurs within the cell is a huge cytoplasmic vacuolization due to mitochondrial swelling, as demonstrated by several specific markers of this organelle. Our hypothesis to explain this phenomenon is that ion transport carried out by our compounds could generate an osmotic imbalance between the cytosol and the mitochondria, triggering massive mitochondrial swelling and affecting its proper functioning. Moreover, after significant organelle swelling, loss of $\Delta\Psi_m$ was induced by compound **2**. According to literature, $\Delta\Psi_m$ occurs along with a bioenergetic crisis characterized by ROS overproduction and ATP synthesis arrest (Kroemer, Galluzzi, Brenner, et al., 2007). Usually, measurement of ATP is used to assess cell viability and cytotoxicity, since cells need ATP to sustain viability. In addition, the amount of ATP that remains in a cell is linked to the type of death that has been triggered, since apoptosis proceeds if cellular ATP levels are maintained, whereas necrosis can occur in an ATP-independent manner (Leist *et al*., 1997).

In this regard, it has also been characterized that in cells after other cellular stresses such as acute ischemic injury, mitochondrial depolarization and MMP occurs, which in turn led to a large amplitude swelling (Bosetti *et al.*, 2004) and cellular ATP depletion (Rouslin, Broge and Grupp, 1990). Moreover, it has been described that the increment in mitochondrial permeability induces ROS production (Batandier, Leverve and Fontaine, 2004).

Hence, we presume that mitochondrial dysfunction observed after tambjamine analogues treatment may cause an energetic failure and ROS production, contributing to their cytotoxic effect. In fact, treatment with compound **2** caused a decrease in the whole cellular amount of ATP, which coincides with mitochondrial swelling and the loss of the MMP. Therefore, tambjamine analogues may have similar effects thanmitochondrial uncoupler compounds, such as carbonyl cyanide p-(trifluoromenthoxy) phenyl hydrazone (FCCP), which causes depolarization of mitochondrial membrane and disruption of ATP synthesis since it transports protons across IM (Cheng *et al.*, 2003)(Kalbáčová *et al.*, 2003). In this regard, Tanigaki and colleagues studied the ionophoric activity of BE-18591, compound related to tambjamines, and they proved that uncouples H^+-ATPases at mitochondrial level due to H^+/Cl^- symport activity and leads to cell death by necrosis (Tanigaki *et al.*, 2002). Beside this, studies with salinomycin, cation transporter compound with anticancer properties, have recently demonstrated that induces mitochondrial membrane depolarization and ROS, which in turn led to apoptotic cell death in prostate cancer cells (Kim *et al.*, 2011).

In conclusion, synthetic tambjamine analogues cause mitochondrial destabilization, swelling and dysfunction, which is accompanied with energetic failure and ROS accumulation, and may promote cell death.

2.3. Stress sensor activation

MAPKs are signaling components that have important roles in the integration of stress signals and their conversion to cellular responses. These regulators play essential roles in various cellular processes such as cell growth, differentiation, development, cell cycle, survival, and cell death. In particular, the p38 MAPK cascade is activated by a wide range of environmental and genotoxic stresses (Wagner and Nebreda, 2009). Our results have shown robust p38 MAPK activation after treatment with compounds **2** and **7**. This increase can be consequence of multiple factors since, as discussed in the previous section, our tambjamine analogues disturb ion homeostasis and produce a mitochondrial dysfunction accompanied by swelling and loss of membrane potential, generating high levels of cellular stress. One type of stress that induces potential activation of p38 cascade is the oxidative stress caused by ROS (McCubrey, LaHair and Franklin, 2006)(Son *et al.*, 2011). ROS are highly active radicals, ions or molecules that have a single unpaired electron in the outermost shell of electrons. Under physiological conditions, ROS levels are tightly regulated by the activity of antioxidant systems (Sena and Chandel, 2012). Overproduction of ROS is extremely harmful since it induces irreversible damage to cellular components and lead to cell death by promoting the activation of the intrinsic apoptotic pathway (Schieber and Chandel, 2014). On the one hand, mitochondria are the largest contributor to cellular ROS as a result of its metabolism. Progressive accumulation of defects in mitochondria is accompanied by an increased generation of ROS (C.-H. Wang *et al.*, 2013; Zorov, Juhaszova and Sollott, 2014).

Since determining ROS production after treatment with our compounds was not possible due to technical limitations, we took as reference the related compounds indole-based tambjamines. Manuel-Manresa *et* al. demonstrated that these compounds cause an increase in ROS levels, probably linked to their anion transport capacity (Manuel-Manresa *et al.*, 2017). Similarly, several recent works have related the unbalanced ionic homeostasis, induced by ion carriers, with ROS generation (Ko *et al.*, 2014; Kim *et al.*, 2017). In conclusion, there is evidence to support the fact that our compounds generate cellular stress at different levels that are responsible for the activation of p38 MAPK.

3. Induced cell death mechanisms

Synthetic tambjamine analogues, as small ion exchanger molecules, do not have only one specific target but affect the cell at multiple levels that converge in the observed cytotoxicity. Likewise, the understanding of the cell death mechanism exerted by these compounds involves the activation of several cellular processes.

Apoptosis is the most widely recognized form of physiological programmed cell death. Depending on the stress stimuli, the initiation of apoptosis can be executed by two major pathways, the extrinsic or the intrinsic pathway, that ultimately lead to the activation of caspases that orchestrate the

demolition of the cell (Wong, 2011). Specifically in the intrinsic pathway, apoptotic signals converge on the mitochondria, where changes in membrane permeability lead to release of molecules that activate initiator caspase 9, which in turn, activates effector caspase 3, responsible for the cleavage of many cellular substrates, such as iCAD (inhibitor of caspase-activated DNase) or PARP (poly (ADP-ribose) polymerase 1), during cell death process (Wong, 2011)(Boulares *et al.*, 1999). The main morphological features associated with this kind of cell death include chromatin condensation, nuclear fragmentation and the appearance of membrane-associated apoptotic bodies (Wong, 2011).

Our results confirmed the activation of the apoptotic pathway with the consequent activation of caspases 9 and 3, as well as the cleavage of its substrate PARP in A549 cell line after 48 h of synthetic tambjamine analogues exposure. The activation of this pathway may be triggered by the MMP produced after the observed mitochondrial swelling (Kroemer, Galluzzi and Brenner, 2007), acting as other ionophores as it is the case of prodigiosin (Llagostera *et al.*, 2003), or by activating p38 MAPK pathway. This is supported by previous evidence that correlates activation of p38 MAPK with the induction of apoptosis in cells (L. Zhao *et al.*, 2015; Q. Li *et al.*, 2015; Feng *et al.*, 2017). In this regard, results obtained with the indol-based tambjamine analogues would be consistent with our initial findings, since these compounds induce apoptosis through p38 activation (Manuel-Manresa *et al.*, 2017).

However, the apoptosis inhibitor Z-VAD.fmk failed to reverse the cytotoxicity associated with these compounds, and besides that, the percentage of apoptotic bodies observed by Hoechst staining after exposure to the compounds during 48 h was a minority. Therefore, our compounds elicited apoptosis activation in a subpopulation of A549 cells, but it is not the responsible death mechanism for most of the cell population.

Autophagy is a catabolic process whereby cellular components are enclosed in double-membrane vesicles referred to as autophagosomes, targeting them for lysosomal degradation (White, 2015). This process is responsible for the degradation of old or malfunctioning organelles, and damaged or misfolded proteins to sustain metabolism and homeostasis. Basal levels of autophagy prevent the gradual accumulation of damaged elements containing p62 and ubiquitin, which are toxic over time. During nutrient deprivation, the induction of acute autophagy is critical to recycle intracellular components into metabolic pathways and survive (White, 2015). Besides this, this process serves as an essential cytoprotective response to pathologic stresses that occur during diseases such as cancer (Murrow and Debnath, 2013). During tumorigenesis, autophagy plays a dual role: it can be tumor-suppressing during the early stages, or it can be tumor-promoting in established tumors (Choi, 2012). It has been proposed to suppress malignant transformation by preserving genetic and genomic stability through the elimination of defective mitochondria, source of the highly genotoxic ROS (White, 2015). At the same time, removal of dysfunctional mitochondria preserves optimal bioenergetics functions. Moreover, it has been reported that autophagy avoid tumor initiation through degradation of oncogenic proteins (L. Galluzzi *et al.*, 2015). On the contrary, autophagy acts as a promoter of tumor growth in an established tumor, conferring stress tolerance and maintaining tumor cell survival. Tumor cells increase autophagy as a mechanism that permits obtaining higher amounts of both ATP and metabolic intermediates. Thereby, cells adapt to the environment poorly enriched in oxygen and nutrients, as well as to the high metabolic rate of the tumor (Ávalos *et al.*, 2014).

Accumulation of defective mitochondria triggers its selective degradation, process known as mitophagy, maintaining a healthy population of these organelles (Kim, Rodriguez-Enriquez and Lemasters, 2007; Kubli and Gustafsson, 2012). After treatment with synthetic tambjamine analogues for 24 h, a significant amount of the autophagosomal marker LC3II accumulates, even at very low concentrations. This indicates that the process of autophagy is being triggered by the treatment with these synthetic tambjamine analogues and that the induced mitochondrial damage may initiate the process of mitophagy in order to remove damaged organelles. This phenomenon, frequently found as a result of mitochondrial stress, have been also evidenced in the case of treatment with the mitochondrial chain uncoupler carbonyl cyanide m-chlorophenylhydrazone (CCCP) (Kwon, Viollet and Yoo, 2011), or ionophores such as salinomycin, which affects $\Delta\Psi_m$ (Jangamreddy *et al.*, 2013). Furthermore, it has recently been reported that pHi changes modulate both autophagy and mitophagy (Berezhnov *et al.*, 2016), thus possible changes in cellular pH caused by these compounds through anion exchange across membranes may also be contributing to trigger this pathway.

On the other hand, as it was explained in a previous section, tambjamine analogues molecules cause an increase in lysosomal pH, as a result of the ionic unbalance. The fact that lysosomal alkalization lead to a failure in their proper functioning, resulting in blockade of autophagy, has been widely addressed in literature (Y. Lu *et al.*, 2014)(Lu *et al.*, 2013). This feature mainly occurs because this organelle is essential in the final step of the autophagic process, wherein autophagosomes fuse with lysosomes and subsequent protein digestion occurs (Kroemer and Jäättelä, 2005). In this regard, the observed increase in lysosomal pH after exposure to our synthetic tambjamine analogues may inactivate its hydrolytic enzymes, and therefore it may block autophagy. This is in good agreement with another synthetic ion transporters, called squaramides, which disrupt autophagy and induce apoptosis by perturbing cellular chloride concentrations (Busschaert *et al.*, 2017).

Furthermore, the autophagic substrate p62, also known as SQSTM1, binds ubiquitinated proteins for subsequent degradation in lysosomes, where it is also degraded (Bjørkøy *et al.*, 2009). Apart from this, p62 accumulation associated to cellular waste induces cellular stress that may lead to disease (Mathew *et al.*, 2009; Rusten and Stenmark, 2010). Our results show that there is no significant p62 degradation, indicating an impairment in the autophagic flux and consequent accumulation of unprocessed autophagosomes or autolysosomes (Komatsu and Ichimura, 2010). Moreover, according to our results, autophagy inhibitor 3-MA, which inhibits autophagy by blocking autophagosomes formation via the inhibition of type III PI3K, is not able to reverse the cytotoxic effect induced by synthetic tambjamines. Consequently, activation of autophagy might be contributing to the cytotoxic effect, but it is not the main effector mechanism of cell death.

Loss of ion homeostasis, energy depletion or excessive ROS production can synergize in the induction of necrotic cell death. The cell dying by necrosis has been considered a victim overwhelmed by a stress that cannot control. However, there is evidence that indicates that death by necrosis involves inflammatory and reparative responses in the host that may serve to maintain organism homeostasis (Zong and Thompson, 2006). The fundamental feature that distinguishes most forms of necrosis is the rapid loss of cellular membrane potentials that results in membrane integrity rupture and cellular leakage (Zong and Thompson, 2006). In our case, necrosis was detected by measuring the permeability of the plasma membrane to a normally impermeable fluorescent dye (Cummings, Schnellmann and Schnellmann, 2004). The staining with Hoechst and PI after tambjamine compounds exposure for

48 h revealed that part of the cell population had lost their membrane integrity. Furthermore, a typical necrotic process encompasses swelling of organelles, followed by multiple organelle damage, and overproduction of ROS (Zong and Thompson, 2006). On one hand, as described in the previous section, our compounds produce mitochondrial swelling and lysosomal dysfunction and on the other hand, similarly to the indole-based tambjamines, our synthetic tambjamines are supposed to produce ROS (Manuel-Manresa *et al.*, 2017).

Regulated necrosis, necroptosis, requires the activation of RIPK1 and RIPK3, and the subsequent phosphorylation of MLKL (pseudokinase mixed lineage kinase domain-like) protein. Phosphorylated MLKL translocates to the plasma membrane where it induces its rupture and consequently cell death. Since activation of effector protein, MLKL, was not observed after treatment with the synthetic tambjamine analogues, necroptosis was discarded as possible induced cell death. In addition, our compounds activated caspase 8, which may inhibit necroptosis by proteolytic cleavage of RIPK1 and RIPK3, in the event that it is in a complex with FADD (Fas-associated protein with death domain) and FLIP (FLICE-like inhibitory protein) (Tummers and Green, 2017). Regarding RIP1, most papers relate their phosphorylation with necroptosis (De Almagro *et al.*, 2017). Although we have seen an increase in RIP1 levels, we have not observed its phosphorylation necessary for the activation of necroptosis.

Consequently, the imbalance in cellular ion homeostasis that triggers mitochondrial dysfunction and lysosomal alkalization causes an irreversible bioenergetic compromise, which ultimately induces cell death by necrosis. This lends support to previous findings in the literature in which it is shown that natural alkaloid tambjamine D, derived from marine organisms, displays cytotoxic activity on Chinese hamster lung fibroblast inducing apoptosis and necrosis (Cavalcanti *et al.*, 2008). Likewise, the H^+/Cl^- symporter compound BE-18591, from tambjamine family, also trigger necrosis in different cell lines (Tanigaki et al., 2002). Moreover, the lysosomal permeabilization induced by obatoclax, another ionophore, in apoptosis resistant anaplastic thyroid cells has been demonstrated to be sufficient to induce necrosis in this resistant model, representing an interesting therapeutic approach (Champa *et al.*, 2016).

These results shed light into the cellular and molecular mechanisms resulting from the action of these compounds. Taken as a whole, lysosomal and mitochondrial dysfunction, derived from ionic unbalance, activates apoptosis as well as the autophagic pathway. Moreover, mitochondrial dysfunction along with a defect in autophagy catabolism is detrimental to tumor cells, since they produce low rates of ATP and impaired recycling of nutrients for energy production, as well as an imbalance in vesicular biogenesis and turnover. This bioenergetic catastrophe determines that the cell ends up collapsing due to necrosis as the main death mechanism responsible for the cytotoxicity of the compounds.

4. Synthetic tambjamine analogues molecular mechanism of action

4.1. AKT as a molecular target of synthetic tambjamine analogues

The PI3K/AKT signaling pathway regulates multiple cellular processes including cell proliferation and survival, response to nutrient availability, transcription and protein synthesis (Manning and Toker, 2017). Activation of PI3K may be initiated by RTKs or GPCRs located at the cell surface, leading to

PIP3 generation at the plasma membrane. This event leads to recruitment of cytosolic AKT to the membrane, engaging PIP3 and its following activation through phosphorylation of T308 and S473 by PDK1 and mTORC2, respectively (Manning and Toker, 2017). Once fully active, AKT phosphorylates and inhibits downstream substrates such as glycogen synthase kinase 3 (GSK3), forkhead box O (FOXO) transcription factors, and BAD, thus suppressing apoptotic signals and activating cell cycle progression. In addition, AKT also phosphorylates and inhibits the tuberous sclerosis complex 1/2 (TSC1/2), which results in mTORC1 stimulation (Fumarola *et al.*, 2014). In particular, mTOR is responsible for cell growth and metabolism activating anabolic processes, including biosynthesis of proteins, lipids and organelles, and by limiting catabolic processes such as autophagy (Fumarola *et al.*, 2014).

Disruption of this tightly controlled system plays a critical role in the malignant transformation of human tumors and their subsequent growth, proliferation and metastasis. In the specific case of NSCLC, aberrant activation of PI3K/AKT cascade is associated with advanced stages of the disease (Scrima *et al.*, 2012). Thus, therapeutic agents that target the different components of this pathway, such as inhibitors of PI3K, AKT and mTOR, are in clinical development (Fumarola *et al.*, 2014). In particular, the inhibition of AKT as central node in PI3K signaling may have a significant impact on tumors that are dependent on PI3K/AKT pathway activity. For example, MK-2206, allosteric inhibitor of AKT, after showing significant anti-tumor activities either as single agent or used in combination with cytotoxic anti-cancer agents in preclinical models (Hirai *et al.*, 2010), had completed clinical trial phase II in patients with advanced NSCLC who had progressed after erlotinib treatment (Lara *et al.*, 2015). Similarly, it has recently been reported that targeting AKT is a good strategy to boost therapy efficacy and overcome acquired resistance to anti-EGFR agents in NSCLC (Jacobsen *et al.*, 2017; Le Grand *et al.*, 2017). On the other hand, anionophores such as prodigiosin and obatoclax have been shown to be inhibitors of this signaling pathway, decreasing AKT phosphorylation through the inhibition of the mTORC1 and mTORC2 complexes (Espona-Fiedler *et al.*, 2012).

In a preliminary experiment with SPR (Surface Plasmon Resonance), we could observe that compound **2** interacted with AKT with an affinity constant in the nanomolar range. Moreover, treatment of A549 cells with this small molecule produced a decrease in both, the total amount of protein and its phosphorylation. Mechanistically, inactivation of AKT could be due to inactivation of upstream elements of the pathway such as PI3K, PDK1 or mTORC2, or could be mediated by an increase in protein phosphatase 2A (PP2A) or PTEN (Liao and Hung, 2010). Otherwise, decrease in the total amount of protein could derive from of a loss of protein stability and consequent degradation. In this sense, heat-shock proteins (HSPs), such as HSP27, HSP70 or HSP90, are a class of proteins that guide the folding, intracellular disposition and proteolytic turnover of many of the key regulators of signal transduction processes (Calderwood and Gong, 2016). These molecular chaperones are overexpressed in cancer indicating a poor prognosis since they stabilize oncogenic mutations in proteins allowing tumor growth (Calderwood and Gong, 2016). It is well documented that HSP90 stabilizes AKT and prevents its inactivation mediated by PP2A (Sato, Fujita and Tsuruo, 2000). Saiori Sato and co-authors, in their study on AKT/HSP90 protein complex, mapped by deletion mutants the important surface regions for protein-protein interactions. They proved that AKT residues between 229 and 309 are responsible for binding with HSP90. They showed that inhibition of the AKT/HSP0 complex would lead to the dephosphorylation and inactivation of AKT (Sato, Fujita and Tsuruo, 2000). Moreover, it has been observed that blockade of the AKT-HSP-90 complex formation, after treatment with HSP90 specific inhibitors like 17-allyamino 17- demethoxy-geldanamycin (17-AAG), induces

AKT dephosphorylation and degradation (Münster *et al.*, 2001; Basso *et al.*, 2002). Interestingly, the results that we have obtained through computational methods showed that tambjamine analogue **2** can interact with AKT at five different sites, showing preference for the ATP binding site, where it may adopt two different orientations interacting with Asp292 residue (figure 53C). In the other possible union sites, tambjamine **2** also interacts with Asp or Glu residues. In addition, it is necessary to mention that in the five possible binding sites, our molecule is oriented with the tert-butyl group (more voluminous) pointing outward the binding cleft, involving possible disruptions of interaction with other proteins. Hence, compound **2** sites around residues Glu242, Asp292 and Asp398 (figure 53C) may disrupt such AKT/HSP90 interactions, since, as stated, the binding mode places the bulkier tert-butyl group in an area falling within the proposed protein-protein binding region.

Overall, these results suggest that tambjamine analogue **2** may be useful in tumors that have constitutively active AKT expression.

4.2. Effect of synthetic tambjamine analogues on cancer miRNA expression

MicroRNAs control gene expression at post-transcriptional level by translational repression or degradation of target mRNAs. These small noncoding RNAs are involved in the regulation of multiple cellular processes in animals, including differentiation, proliferation, and apoptosis. Therefore dysregulation of miRNA can have substantial physiological effects. These considerations, coupled with the fact that the literature gathers extensive evidence of gene expression studies displaying aberrant expression of miRNA in tumors, have established the participation of miRNAs in cancer (Herranz and Cohen, 2010). In this malignancy, altered miRNA can act as oncomiRs or tumor suppressor miRNAs, attending to their capability to repress the expression of tumor suppressor genes or oncogenes, respectively. One mRNA can be targeted by several miRNAs and a single miRNA can bind to hundreds of target mRNAs (Oliveto *et al.*, 2017). Moreover, miRNAs can play a dual role in tumorigenesis, exhibiting oncogenic or tumor suppressor activity depending on the tissue (Xiang and Wu, 2010). Therefore, to draw conclusions about the activity of a specific miRNA, it is important to consider the cellular context. In lung cancer, several studies have shown that certain microRNA expression profiles distinguish between lung cancer patients with better and worse prognosis (Inamura and Ishikawa, 2016). In addition, in the last decade, the expression profile of miRNA in response to anticancer treatments has become a subject of study since it might have biological relevance (Zhang and Dolan, 2010).

In our case, the aim of this preliminary study was the identification of dysregulated miRNA after tambjamine analogue **2** treatment and their potential role in the cytotoxic effect of this compound against the A549 lung cancer cell line. As a result, we found that treatment altered miRNA whose target genes are mainly involved in cancer related pathways, such as PI3K/AKT or apoptosis.

As explained in the results section, among modified miRNAs that appear in figure 56 (*results section 5.2*), we selected those miRNAs in which the treatment had a potential anticancer effect, and those miRNA in which the treatment might produce the opposite effect to the expected were not included in subsequent analyses. This is the case of miRNAs such as miR-7, miR-1287, miR-130a and miR-30a, with a role of potential tumor suppressor in cancer, but which have been downregulated by the treatment

(Acunzo *et al.*, 2012; Y. Wang *et al.*, 2013; J. Zhao *et al.*, 2015; Xu *et al.*, 2017; Zhu *et al.*, 2017). On one hand, this could be due to the fact that the bibliographic data are from other cellular models, and in our model these miRNAs may not have that role. On the other hand, the cancer cell may try to modulate miRNA expression as a mechanism of resistance.

On the other hand, papers sometimes show information concerning to the family or a particular form of miRNA. This happens with the miRNAs 146a-3p, 20b-3p, 224-3p and 23b-5p. According to literature, miR-146a has been reported as a tumor suppressor in several cancers (Li *et al.*, 2010; Chen *et al.*, 2013); Otherwise, miR-20b levels have been shown upregulated in tissues with secondary tumors derived from lung cancer (Hu *et al.*, 2014), miR-224 has been described as an oncomir (Cui *et al.*, 2015). Nevertheless, there is hardly any information related to the specific miRNA strands and its function in cancer. Taking into account that the 5p and 3p arm of the miRNA, derived from the same pre-miRNAs, have different expression patterns, abundance and targets, these miRNAs were also not included in the following analyses.

According to recent studies, miR-205 and miR-103 are considered biomarkers for the diagnosis of lung cancer cells since they are upregulated in lung cancer tissues when compared with the corresponding healthy lung tissues (Yanaihara *et al.*, 2006; Landi *et al.*, 2010; Jiang *et al.*, 2013). Our treatment with compound **2** inhibits their expression and might reduce A549 proliferation by negatively regulating the PI3K/AKT survival pathway (*figure 57, results section 5.2*). Their target genes, PTEN and PHLPP2, considered tumor suppressor genes, might be positively regulated and may antagonize the PI3K/AKT signaling pathway avoiding the activation of AKT. This is consistent with studies in NSCLC reporting that miR-205 increases AKT signaling and drives malignant phenotypes targeting PTEN and PHLPP2 (Li *et al.*, 2013). Moreover, there is evidence in other cancer types, such as colorectal cancer, where miR-103 promotes proliferation and migration due to PTEN loss of function (Geng *et al.*, 2014).

Likewise, upregulation of miR-148a-3p induced by compound 2, usually downregulated in lung cancer (Montani et al., 2015)(Incoronato et al., 2011), could directly repress the expression of genes that facilitates cancer development or correlate with bad prognosis, as for example the anti-apoptotic protein BCL2 (Zhang et al., 2011; He and Xue, 2017). Similarly, miR-148a target ITGA5 (integrin subunit alpha 5), a cell adhesion protein that can lead tumorigenesis and correlate with poor outcome in NSCLC (Adachi et al., 2000). In this sense, miR-148a-mediated down-regulation of ITGA5 and ITGB8 (integrin subunit beta 8) expression have resulted in the inhibition of malignant progression of tumor cells in gastric cancer (Tseng et al., 2011). In the same way, something similar could happen with miR-148a target genes IGF1R (insulin-like growth factor receptor) and IRS1 (insulin receptor substrate-1), which have been shown to play critical roles in the development and progression of various tumors (Denduluri et al., 2015). In this regard, Xu and colleagues have shown that overexpression of mir-148a in breast cancer cells could suppress proliferation, colony cell formation and tumor angiogenesis targeting IRS1 and IGF-IR (Xu et al., 2012). In hepatocellular carcinoma, miR-148a is significantly decreased as in lung cancer. A recent study, carried out with hepatocellular carcinoma in vitro and in vivo models, found that restoration of miR-148a expression significantly repressed the epithelial-mesenchymal transition and metastasis by targeting MET (N-methyl-N'-nitroso-guanidine human osteosarcoma transforming gene) signaling (Zhang et al., 2014). Moreover, miR-148a and miR-212 have been described as a negative regulator of MYC in hepatocellular and gastric carcinoma, respectively (Xu et al., 2011; Han et al., 2013). In this sense, MYC proteins are considered potential therapeutic targets in SCLC (Teicher,

2014). Hence, its inhibition thanks to miR-148a and miR-212 upregulation could help to suppress cancer development. These findings suggest that miR-148a as well as miR-212, upregulated in A549 cells after exposure to compound 2, may function as potential tumor suppressors through diverse mechanisms.

Altogether, this miRNA expression profile generated after tambjamine analogue **2** treatment might be related with the cytotoxic effect observed in A549 cell line. In any case, these are preliminary results predicted by the observed miRNA modifications after compound treatment. To corroborate the implication of these genes in the cytotoxic effect induced by compound **2**, we would have to validate each of these potential target genes in further experiments.

5. Therapeutic effect of synthetic tambjamine analogues in LC *in vivo* mouse models

Lung cancer is the leading cause of cancer-related death worldwide. According to statistical data, it is considered that it has poor prognosis. Over half of people diagnosed with lung cancer die within one year, and the 5-year survival is less than 18% (Zappa and Mousa, 2016). Lung cancer treatment is difficult due to its high complexity. In the past decades, there have been several contributions to the improved management of lung cancer. On one hand, the chemotherapy regimens have been optimized, and new therapeutic agents, against the same or different mechanisms, have been developed (Bao and Chan, 2011). In this sense, the most frequent current standard chemotherapeutic regimens are based on cisplatin combined with gemcitabine, vinorelbine, or etoposide (Hirsch *et al.*, 2017). Although platinum-based chemotherapy regimens have proved to be initially effective, significant relapse rates are still observed due to drug-resistance appearance (Amable, 2016). On the other hand, the emergence of targeted therapies, as a result of better understanding of cancer biology, has been a significant advantage to the overall outcome for this disease (Bao and Chan, 2011). Inevitably, patients have developed resistance because of the emergence of an insensitive cellular tumor subpopulation, selected by pharmacologic pressure (Facchinetti *et al.*, 2017; Neel and Bivona, 2017). In this sense, there is growing evidence supporting that CSCs form a chemoresistant subpopulation that possess the ability to regenerate the heterogeneous tumor mass (MacDonagh *et al.*, 2016). Thus, the development of new cytotoxic agents that are also targeted to the CSC remains an important area of clinical research in lung cancer.

Before starting anticancer drug trials, pharmaceutical companies and independent researchers conduct extensive preclinical studies. Animal models have been essential in cancer research to examine preliminary efficacy, toxicity and pharmacokinetics. To date, a variety of mouse models that mimic human lung cancer have been developed. Xenograft models require the transplantation of primary human cancer tissue fragments or cells into lungs of immunocompromised mice, either subcutaneously or orthotopically (Kellar, Egan and Morris, 2015). Orthotopic model, compared to the subcutaneous one, shows advantages since it provides the proper microenvironment for transplanted cells and reflects closely lung cancer clinical pathology (Kellar, Egan and Morris, 2015).

In preliminary studies, the therapeutic capacity of our compounds **2** and **7** was tested in both an ectopic and an orthotopic mouse model. In mice bearing A549 cells subcutaneously injected, both compounds significantly reduced tumor size as **CDDP** did, the first-line treatment. Surprisingly, no

better outcome was observed with simultaneous treatment, **CDDP** plus tambjamine analogues **2** or **7**. In the orthotopic mice model, a decrease in tumor growth was observed, especially with compound **7**. Given that our findings are based on a limited number of animals, the results from these analyses should consequently be interpreted with care. Nevertheless, both compounds corroborate their cytotoxic effect observed *in vitro*, and have promising therapeutic effect against lung cancer. Likewise, these compounds have been shown to reduce viability in CSCs derived from patient tumors and from cell lines. This can be considered an advantage for our compounds, since effectiveness of standard therapy is limited due to properties of CSC population, such as drug resistance and self-renewal (Dragu *et al.*, 2015). Eradicating CSCs with synthetic tambjamine analogues may reduce the occurrence of drug resistance and the incidence of tumor relapse, thus achieving better results with conventional treatments.

In addition, tambjamine analogues could be a convenient alternative therapeutic strategy to overcome the resistance to proapoptotic chemotherapeutic agents, which are most of the conventional chemotherapeutic agents available at the moment. Different approaches that are able to induce necrotic cell death have been reported. For example, photodynamic treatment (PDT) involves the generation of ROS by a photosensitizing molecule previously accumulated in the tumor through the irradiation of neoplastic area with a specific wavelength (Robertson, Evans and Abrahamse, 2009). Produced ROS activate necrosis and necroptosis mechanisms among other signaling pathways (Soriano *et al.*, 2014) which accumulates preferentially in tumor cells. Subsequent irradiation of the neoplastic area triggers a cascade of photochemical reactions that leads to the formation of highly reactive oxygen species responsible for cell inactivation. Photodynamic treatments in vitro are performed with the PS, zinc-phthalocyanine (ZnPc being able to induce cell death even in breast cancer xenograft lacking caspase-3 (Whitacre *et al.*, 2002). Likewise, in literature has also been described how other chemical agents promote necrosis or regulated necrosis that can be used as an alternative way to eradicate apoptosis-resistant cancer cells, this is the case of honokiol, shikonin or the small molecule Obatoclax (Li *et al.*, 2007)(Xuan and Hu, 2009)(Basit, Cristofanon and Fulda, 2013).

Although targeting necroptosis and other types of programmed necrosis has been proposed as an anti-tumor treatment strategy, necrotic and necroptotic cancer cells release damage-associated molecular patterns (DAMPs) that may act as inducers of inflammation. On one hand, DAMPs may have a protective function by alerting the immune system of the presence of dying tumor cells and triggering the immunogenic tumor cell death (Hernandez, Huebener and Schwabe, 2016). On the other hand, it has been described that cell death linked to the release of DAMPs may also trigger chronic inflammation and thereby promote the development and progression of tumors (Mantovani *et al.*, 2008). It is therefore necessary to explore and clarify these concerns to facilitate the development and administration of these therapeutics with a new mechanism of action. Taken together, synthetic tambjamine analogues may be an attractive anti-tumor treatment strategy in those cases that do not respond to conventional chemotherapy, and especially for apoptotic resistant patients.

Altogether, these synthetic tambjamine analogues have been characterized as potent anion transporters and, may be promising antitumor molecules. These compounds trigger massive mitochondrial swelling and lysosomal alkalization, which in turn leads to autophagy blockade. These phenomena cause cell stress that leads to the activation of cell death mechanisms, such as apoptosis and necrosis, being the latter the main responsible for the induced cytotoxicity. In addition, at the molecular level these compounds target AKT pathway, frequently altered in human cancers.

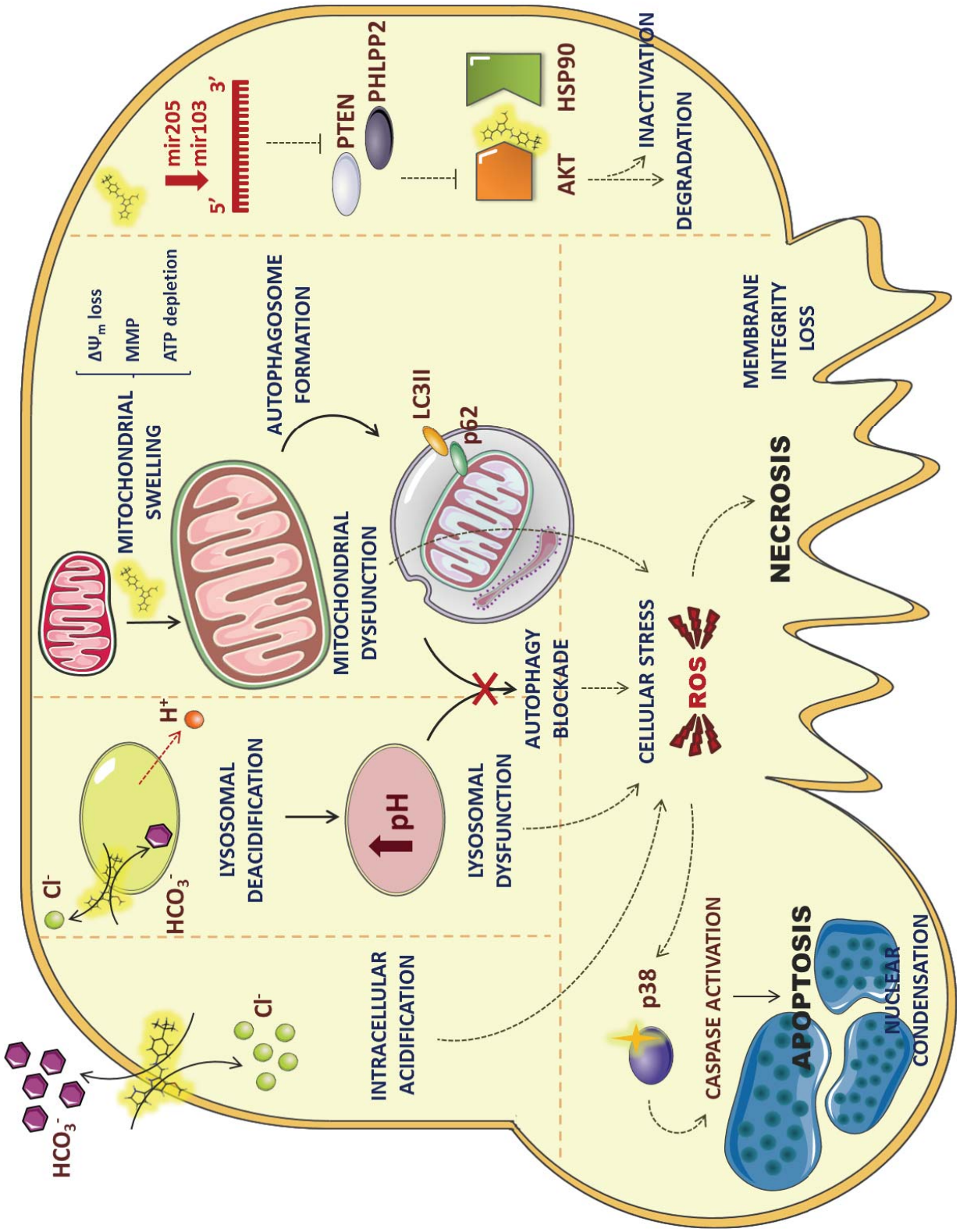

Figure 63. **Model for the mechanism of action of selected synthetic tambjamine analogues on LC *in vitro* model.** This figure was produced using Servier Medical Art image bank.

CONCLUSIONS

1. Synthetic tambjamine analogues are potent anion transporter compounds with a potent cytotoxic effect in oral and lung cancer cell lines. Selected analogues (compounds **2** and **7**) also produce toxicity in lung cancer stem cells derived from patient tumors.

2. Selected synthetic tambjamine analogues cause massive swelling of mitochondria and lysosomal deacidification. These phenomena generate the dysfunction of both organelles. Mitochondria lose their membrane potential and consequently a cellular depletion of ATP. At the same time, lysosomal dysfunction leads to a blockade of autophagy.

3. Cellular stress generated by synthetic tambjamine analogues induces an increase in the activity of the stress sensor protein p38-MAPK.

4. Selected synthetic tambjamine analogues induce the activation of apoptosis along with the autophagy process, although cells end up collapsing into a necrotic cell death as the main death mechanism responsible for the cytotoxicity of the compounds.

5. AKT has been identified as a potential molecular target of the synthetic tambjamine analogue **2**, and it induces a decrease in protein activity and in the total amount of AKT protein.

6. Selected synthetic tambjamine analogues, **2** and **7**, proved to be effective therapeutic compounds showing a significant decrease in tumor growth in a subcutaneous mice model as well as in an orthotopic lung cancer mice model.

SUPPLEMENTARY INFORMATION

Table S1. miRNA list of Human Cancer PathwayFinder 384HC miRNA PCR Array

miRNA Mature Table			
Position	**miRBase or NCBI Accession No.**	**Mature miRNA ID or Gene Symbol**	**miScript Primer Assay Catalog #**
A01	MIMAT0004481	hsa-let-7a-3p	MS00008274
A02	MIMAT0000062	hsa-let-7a-5p	MS00031220
A03	MIMAT0004482	hsa-let-7b-3p	MS00008281
A04	MIMAT0000063	hsa-let-7b-5p	MS00003122
A05	MIMAT0000064	hsa-let-7c-5p	MS00003129
A06	MIMAT0000065	hsa-let-7d-5p	MS00003136
A07	MIMAT0004485	hsa-let-7e-3p	MS00008316
A08	MIMAT0000066	hsa-let-7e-5p	MS00031227
A09	MIMAT0000067	hsa-let-7f-5p	MS00006489
A10	MIMAT0000414	hsa-let-7g-5p	MS00008337
A11	MIMAT0004585	hsa-let-7i-3p	MS00008351
A12	MIMAT0000415	hsa-let-7i-5p	MS00003157
A13	MIMAT0000416	hsa-miR-1-3p	MS00008358
A14	MIMAT0004512	hsa-miR-100-3p	MS00008365
A15	MIMAT0000098	hsa-miR-100-5p	MS00031234
A16	MIMAT0000099	hsa-miR-101-3p	MS00008372
A17	MIMAT0000101	hsa-miR-103a-3p	MS00031241
A18	MIMAT0000102	hsa-miR-105-5p	MS00031248
A19	MIMAT0004517	hsa-miR-106a-3p	MS00008393
A20	MIMAT0004672	hsa-miR-106b-3p	MS00008400
A21	MIMAT0000680	hsa-miR-106b-5p	MS00003402
A22	MIMAT0000104	hsa-miR-107	MS00031255
A23	MIMAT0004555	hsa-miR-10a-3p	MS00008407
A24	MIMAT0000253	hsa-miR-10a-5p	MS00031262
B01	MIMAT0000254	hsa-miR-10b-5p	MS00031269
B02	MIMAT0005868	hsa-miR-1204	MS00014161
B03	MIMAT0005872	hsa-miR-1207-3p	MS00014182
B04	MIMAT0000421	hsa-miR-122-5p	MS00003416
B05	MIMAT0005583	hsa-miR-1228-3p	MS00042385
B06	MIMAT0005582	hsa-miR-1228-5p	MS00016387
B07	MIMAT0000422	hsa-miR-124-3p	MS00006622
B08	MIMAT0004602	hsa-miR-125a-3p	MS00008554
B09	MIMAT0000443	hsa-miR-125a-5p	MS00003423
B10	MIMAT0004592	hsa-miR-125b-1-3p	MS00008561
B11	MIMAT0000423	hsa-miR-125b-5p	MS00006629
B12	MIMAT0000445	hsa-miR-126-3p	MS00003430
B13	MIMAT0000444	hsa-miR-126-5p	MS00006636
B14	MIMAT0000446	hsa-miR-127-3p	MS00003437

B15	MIMAT0005929	hsa-miR-1275	MS00037786
B16	MIMAT0004604	hsa-miR-127-5p	MS00008575
B17	MIMAT0000424	hsa-miR-128-3p	MS00008582
B18	MIMAT0005876	hsa-miR-1285-3p	MS00031367
B19	MIMAT0005878	hsa-miR-1287-5p	MS00014497
B20	MIMAT0000242	hsa-miR-129-5p	MS00006643
B21	MIMAT0000425	hsa-miR-130a-3p	MS00003444
B22	MIMAT0004593	hsa-miR-130a-5p	MS00008603
B23	MIMAT0000691	hsa-miR-130b-3p	MS00003451
B24	MIMAT0000426	hsa-miR-132-3p	MS00003458
C01	MIMAT0004594	hsa-miR-132-5p	MS00031409
C02	MIMAT0000427	hsa-miR-133a-3p	MS00031423
C03	MIMAT0000770	hsa-miR-133b	MS00031430
C04	MIMAT0000447	hsa-miR-134-5p	MS00031437
C05	MIMAT0004595	hsa-miR-135a-3p	MS00042259
C06	MIMAT0000428	hsa-miR-135a-5p	MS00008624
C07	MIMAT0004698	hsa-miR-135b-3p	MS00031444
C08	MIMAT0000758	hsa-miR-135b-5p	MS00003472
C09	MIMAT0000448	hsa-miR-136-5p	MS00003479
C10	MIMAT0000429	hsa-miR-137	MS00003486
C11	MIMAT0000430	hsa-miR-138-5p	MS00006657
C12	MIMAT0004552	hsa-miR-139-3p	MS00008666
C13	MIMAT0000250	hsa-miR-139-5p	MS00003493
C14	MIMAT0004597	hsa-miR-140-3p	MS00008673
C15	MIMAT0000431	hsa-miR-140-5p	MS00003500
C16	MIMAT0000432	hsa-miR-141-3p	MS00003507
C17	MIMAT0004598	hsa-miR-141-5p	MS00008680
C18	MIMAT0000434	hsa-miR-142-3p	MS00031451
C19	MIMAT0000433	hsa-miR-142-5p	MS00006671
C20	MIMAT0000435	hsa-miR-143-3p	MS00003514
C21	MIMAT0000436	hsa-miR-144-3p	MS00020328
C22	MIMAT0004600	hsa-miR-144-5p	MS00008701
C23	MIMAT0004601	hsa-miR-145-3p	MS00008708
C24	MIMAT0000437	hsa-miR-145-5p	MS00003528
D01	MIMAT0004608	hsa-miR-146a-3p	MS00008715
D02	MIMAT0000449	hsa-miR-146a-5p	MS00003535
D03	MIMAT0004766	hsa-miR-146b-3p	MS00008722
D04	MIMAT0002809	hsa-miR-146b-5p	MS00003542
D05	MIMAT0000251	hsa-miR-147a	MS00003549
D06	MIMAT0000243	hsa-miR-148a-3p	MS00003556
D07	MIMAT0004549	hsa-miR-148a-5p	MS00008736
D08	MIMAT0000759	hsa-miR-148b-3p	MS00031458
D09	MIMAT0004699	hsa-miR-148b-5p	MS00008743
D10	MIMAT0004609	hsa-miR-149-3p	MS00037702
D11	MIMAT0000450	hsa-miR-149-5p	MS00003570

D12	MIMAT0000451	hsa-miR-150-5p	MS00003577
D13	MIMAT0000757	hsa-miR-151a-3p	MS00007665
D14	MIMAT0000438	hsa-miR-152-3p	MS00003591
D15	MIMAT0000439	hsa-miR-153-3p	MS00008771
D16	MIMAT0000453	hsa-miR-154-3p	MS00031479
D17	MIMAT0000452	hsa-miR-154-5p	MS00003598
D18	MIMAT0004658	hsa-miR-155-3p	MS00008778
D19	MIMAT0000646	hsa-miR-155-5p	MS00031486
D20	MIMAT0000068	hsa-miR-15a-5p	MS00003178
D21	MIMAT0004586	hsa-miR-15b-3p	MS00008799
D22	MIMAT0000417	hsa-miR-15b-5p	MS00008792
D23	MIMAT0000069	hsa-miR-16-5p	MS00031493
D24	MIMAT0000071	hsa-miR-17-3p	MS00006524
E01	MIMAT0000070	hsa-miR-17-5p	MS00029274
E02	MIMAT0000270	hsa-miR-181a-3p	MS00006692
E03	MIMAT0000256	hsa-miR-181a-5p	MS00008827
E04	MIMAT0022692	hsa-miR-181b-3p	MS00042252
E05	MIMAT0000257	hsa-miR-181b-5p	MS00006699
E06	MIMAT0000258	hsa-miR-181c-5p	MS00008841
E07	MIMAT0002821	hsa-miR-181d-5p	MS00031500
E08	MIMAT0000260	hsa-miR-182-3p	MS00008862
E09	MIMAT0000259	hsa-miR-182-5p	MS00008855
E10	MIMAT0004560	hsa-miR-183-3p	MS00008869
E11	MIMAT0000261	hsa-miR-183-5p	MS00031507
E12	MIMAT0000454	hsa-miR-184	MS00003640
E13	MIMAT0004611	hsa-miR-185-3p	MS00008876
E14	MIMAT0000455	hsa-miR-185-5p	MS00003647
E15	MIMAT0000456	hsa-miR-186-5p	MS00003654
E16	MIMAT0000262	hsa-miR-187-3p	MS00003661
E17	MIMAT0002891	hsa-miR-18a-3p	MS00006538
E18	MIMAT0000072	hsa-miR-18a-5p	MS00031514
E19	MIMAT0001412	hsa-miR-18b-5p	MS00031521
E20	MIMAT0000458	hsa-miR-190a-5p	MS00008911
E21	MIMAT0001618	hsa-miR-191-3p	MS00031528
E22	MIMAT0000440	hsa-miR-191-5p	MS00003682
E23	MIMAT0004543	hsa-miR-192-3p	MS00008925
E24	MIMAT0000222	hsa-miR-192-5p	MS00003689
F01	MIMAT0000459	hsa-miR-193a-3p	MS00031542
F02	MIMAT0004614	hsa-miR-193a-5p	MS00008932
F03	MIMAT0002819	hsa-miR-193b-3p	MS00031549
F04	MIMAT0004767	hsa-miR-193b-5p	MS00008939
F05	MIMAT0004671	hsa-miR-194-3p	MS00031556
F06	MIMAT0000460	hsa-miR-194-5p	MS00006727
F07	MIMAT0004615	hsa-miR-195-3p	MS00008953
F08	MIMAT0000461	hsa-miR-195-5p	MS00003703

F09	MIMAT0004562	hsa-miR-196a-3p	MS00008960
F10	MIMAT0000226	hsa-miR-196a-5p	MS00031563
F11	MIMAT0001080	hsa-miR-196b-5p	MS00031570
F12	MIMAT0000227	hsa-miR-197-3p	MS00008967
F13	MIMAT0000228	hsa-miR-198	MS00033824
F14	MIMAT0000232	hsa-miR-199a-3p	MS00007602
F15	MIMAT0000231	hsa-miR-199a-5p	MS00006741
F16	MIMAT0000263	hsa-miR-199b-5p	MS00003731
F17	MIMAT0000073	hsa-miR-19a-3p	MS00003192
F18	MIMAT0004490	hsa-miR-19a-5p	MS00008988
F19	MIMAT0000074	hsa-miR-19b-3p	MS00031584
F20	MIMAT0000682	hsa-miR-200a-3p	MS00003738
F21	MIMAT0001620	hsa-miR-200a-5p	MS00009009
F22	MIMAT0000318	hsa-miR-200b-3p	MS00009016
F23	MIMAT0004571	hsa-miR-200b-5p	MS00009023
F24	MIMAT0000617	hsa-miR-200c-3p	MS00003752
G01	MIMAT0004657	hsa-miR-200c-5p	MS00009030
G02	MIMAT0002811	hsa-miR-202-3p	MS00009037
G03	MIMAT0000264	hsa-miR-203a-3p	MS00003766
G04	MIMAT0022693	hsa-miR-204-3p	MS00037821
G05	MIMAT0000265	hsa-miR-204-5p	MS00003773
G06	MIMAT0009197	hsa-miR-205-3p	MS00016793
G07	MIMAT0000266	hsa-miR-205-5p	MS00003780
G08	MIMAT0000462	hsa-miR-206	MS00003787
G09	MIMAT0004493	hsa-miR-20a-3p	MS00009065
G10	MIMAT0000075	hsa-miR-20a-5p	MS00003199
G11	MIMAT0004752	hsa-miR-20b-3p	MS00009072
G12	MIMAT0001413	hsa-miR-20b-5p	MS00003206
G13	MIMAT0000267	hsa-miR-210-3p	MS00003801
G14	MIMAT0022694	hsa-miR-211-3p	MS00042210
G15	MIMAT0000268	hsa-miR-211-5p	MS00003808
G16	MIMAT0000269	hsa-miR-212-3p	MS00003815
G17	MIMAT0004494	hsa-miR-21-3p	MS00009086
G18	MIMAT0000271	hsa-miR-214-3p	MS00031605
G19	MIMAT0000272	hsa-miR-215-5p	MS00003829
G20	MIMAT0000076	hsa-miR-21-5p	MS00009079
G21	MIMAT0000273	hsa-miR-216a-5p	MS00009100
G22	MIMAT0004959	hsa-miR-216b-5p	MS00009107
G23	MIMAT0000274	hsa-miR-217	MS00003843
G24	MIMAT0000275	hsa-miR-218-5p	MS00006769
H01	MIMAT0000276	hsa-miR-219a-5p	MS00006776
H02	MIMAT0000278	hsa-miR-221-3p	MS00003857
H03	MIMAT0000279	hsa-miR-222-3p	MS00007609
H04	MIMAT0004569	hsa-miR-222-5p	MS00009177
H05	MIMAT0000280	hsa-miR-223-3p	MS00003871

H06	MIMAT0004570	hsa-miR-223-5p	MS00009184
H07	MIMAT0000077	hsa-miR-22-3p	MS00003220
H08	MIMAT0009198	hsa-miR-224-3p	MS00031626
H09	MIMAT0000281	hsa-miR-224-5p	MS00003878
H10	MIMAT0004495	hsa-miR-22-5p	MS00009142
H11	MIMAT0000078	hsa-miR-23a-3p	MS00031633
H12	MIMAT0004496	hsa-miR-23a-5p	MS00031640
H13	MIMAT0000418	hsa-miR-23b-3p	MS00031647
H14	MIMAT0004587	hsa-miR-23b-5p	MS00031654
H15	MIMAT0000080	hsa-miR-24-3p	MS00006552
H16	MIMAT0000081	hsa-miR-25-3p	MS00003227
H17	MIMAT0004498	hsa-miR-25-5p	MS00009212
H18	MIMAT0000082	hsa-miR-26a-5p	MS00029239
H19	MIMAT0004500	hsa-miR-26b-3p	MS00009233
H20	MIMAT0000083	hsa-miR-26b-5p	MS00003234
H21	MIMAT0000084	hsa-miR-27a-3p	MS00003241
H22	MIMAT0004501	hsa-miR-27a-5p	MS00009240
H23	MIMAT0000419	hsa-miR-27b-3p	MS00031668
H24	MIMAT0004588	hsa-miR-27b-5p	MS00009247
I01	MIMAT0000085	hsa-miR-28-5p	MS00003255
I02	MIMAT0000690	hsa-miR-296-5p	MS00016401
I03	MIMAT0004450	hsa-miR-297	MS00031675
I04	MIMAT0004901	hsa-miR-298	MS00009275
I05	MIMAT0000086	hsa-miR-29a-3p	MS00003262
I06	MIMAT0004503	hsa-miR-29a-5p	MS00009282
I07	MIMAT0000100	hsa-miR-29b-3p	MS00006566
I08	MIMAT0000681	hsa-miR-29c-3p	MS00003269
I09	MIMAT0004673	hsa-miR-29c-5p	MS00009303
I10	MIMAT0000688	hsa-miR-301a-3p	MS00009317
I11	MIMAT0000684	hsa-miR-302a-3p	MS00009331
I12	MIMAT0000715	hsa-miR-302b-3p	MS00003906
I13	MIMAT0000714	hsa-miR-302b-5p	MS00007644
I14	MIMAT0000717	hsa-miR-302c-3p	MS00003913
I15	MIMAT0000718	hsa-miR-302d-3p	MS00003920
I16	MIMAT0000088	hsa-miR-30a-3p	MS00009352
I17	MIMAT0000087	hsa-miR-30a-5p	MS00007350
I18	MIMAT0004589	hsa-miR-30b-3p	MS00009359
I19	MIMAT0000420	hsa-miR-30b-5p	MS00003276
I20	MIMAT0000244	hsa-miR-30c-5p	MS00009366
I21	MIMAT0004551	hsa-miR-30d-3p	MS00009394
I22	MIMAT0000245	hsa-miR-30d-5p	MS00009387
I23	MIMAT0000693	hsa-miR-30e-3p	MS00009408
I24	MIMAT0000692	hsa-miR-30e-5p	MS00009401
J01	MIMAT0000089	hsa-miR-31-5p	MS00003290
J02	MIMAT0000510	hsa-miR-320a	MS00014707

J03	MIMAT0000755	hsa-miR-323a-3p	MS00037219
J04	MIMAT0004696	hsa-miR-323a-5p	MS00031717
J05	MIMAT0004505	hsa-miR-32-3p	MS00021063
J06	MIMAT0000761	hsa-miR-324-5p	MS00006825
J07	MIMAT0000771	hsa-miR-325	MS00003941
J08	MIMAT0000090	hsa-miR-32-5p	MS00003297
J09	MIMAT0000756	hsa-miR-326	MS00003948
J10	MIMAT0000752	hsa-miR-328-3p	MS00081472
J11	MIMAT0000751	hsa-miR-330-3p	MS00031738
J12	MIMAT0000760	hsa-miR-331-3p	MS00003969
J13	MIMAT0004700	hsa-miR-331-5p	MS00031745
J14	MIMAT0004703	hsa-miR-335-3p	MS00009464
J15	MIMAT0000765	hsa-miR-335-5p	MS00003976
J16	MIMAT0000754	hsa-miR-337-3p	MS00007651
J17	MIMAT0000763	hsa-miR-338-3p	MS00003990
J18	MIMAT0000764	hsa-miR-339-5p	MS00003997
J19	MIMAT0004506	hsa-miR-33a-3p	MS00009492
J20	MIMAT0000091	hsa-miR-33a-5p	MS00003304
J21	MIMAT0003301	hsa-miR-33b-5p	MS00007819
J22	MIMAT0000750	hsa-miR-340-3p	MS00004004
J23	MIMAT0004692	hsa-miR-340-5p	MS00031759
J24	MIMAT0000753	hsa-miR-342-3p	MS00004011
K01	MIMAT0022698	hsa-miR-345-3p	MS00041860
K02	MIMAT0000772	hsa-miR-345-5p	MS00031766
K03	MIMAT0000773	hsa-miR-346	MS00031773
K04	MIMAT0004557	hsa-miR-34a-3p	MS00009534
K05	MIMAT0000255	hsa-miR-34a-5p	MS00003318
K06	MIMAT0004676	hsa-miR-34b-3p	MS00008190
K07	MIMAT0004677	hsa-miR-34c-3p	MS00009548
K08	MIMAT0000686	hsa-miR-34c-5p	MS00003332
K09	MIMAT0000703	hsa-miR-361-5p	MS00004032
K10	MIMAT0000707	hsa-miR-363-3p	MS00009576
K11	MIMAT0000710	hsa-miR-365a-3p	MS00031801
K12	MIMAT0000719	hsa-miR-367-3p	MS00009583
K13	MIMAT0000722	hsa-miR-370-3p	MS00004053
K14	MIMAT0000723	hsa-miR-371a-3p	MS00004060
K15	MIMAT0000724	hsa-miR-372-3p	MS00004067
K16	MIMAT0000726	hsa-miR-373-3p	MS00031815
K17	MIMAT0004688	hsa-miR-374a-3p	MS00009611
K18	MIMAT0000727	hsa-miR-374a-5p	MS00009604
K19	MIMAT0000728	hsa-miR-375	MS00031829
K20	MIMAT0000729	hsa-miR-376a-3p	MS00007392
K21	MIMAT0002172	hsa-miR-376b-3p	MS00007399
K22	MIMAT0000720	hsa-miR-376c-3p	MS00004046
K23	MIMAT0000730	hsa-miR-377-3p	MS00004095

K24	MIMAT0000732	hsa-miR-378a-3p	MS00006909
L01	MIMAT0004690	hsa-miR-379-3p	MS00009660
L02	MIMAT0000733	hsa-miR-379-5p	MS00009653
L03	MIMAT0000736	hsa-miR-381-3p	MS00004116
L04	MIMAT0000737	hsa-miR-382-5p	MS00031836
L05	MIMAT0000738	hsa-miR-383-5p	MS00004130
L06	MIMAT0001639	hsa-miR-409-3p	MS00006895
L07	MIMAT0001638	hsa-miR-409-5p	MS00006902
L08	MIMAT0002171	hsa-miR-410-3p	MS00004144
L09	MIMAT0003339	hsa-miR-421	MS00004165
L10	MIMAT0001339	hsa-miR-422a	MS00004172
L11	MIMAT0001340	hsa-miR-423-3p	MS00004179
L12	MIMAT0004748	hsa-miR-423-5p	MS00009681
L13	MIMAT0001341	hsa-miR-424-5p	MS00004186
L14	MIMAT0003393	hsa-miR-425-5p	MS00009695
L15	MIMAT0001536	hsa-miR-429	MS00004193
L16	MIMAT0002814	hsa-miR-432-5p	MS00031850
L17	MIMAT0001627	hsa-miR-433-3p	MS00004214
L18	MIMAT0001541	hsa-miR-449a	MS00004228
L19	MIMAT0003327	hsa-miR-449b-5p	MS00004235
L20	MIMAT0001631	hsa-miR-451a	MS00004242
L21	MIMAT0001635	hsa-miR-452-5p	MS00031871
L22	MIMAT0004784	hsa-miR-455-3p	MS00009744
L23	MIMAT0003150	hsa-miR-455-5p	MS00031878
L24	MIMAT0002173	hsa-miR-483-3p	MS00009751
M01	MIMAT0004761	hsa-miR-483-5p	MS00009758
M02	MIMAT0002174	hsa-miR-484	MS00004277
M03	MIMAT0002175	hsa-miR-485-5p	MS00006972
M04	MIMAT0004762	hsa-miR-486-3p	MS00031892
M05	MIMAT0002177	hsa-miR-486-5p	MS00004284
M06	MIMAT0003180	hsa-miR-487b-3p	MS00004298
M07	MIMAT0004763	hsa-miR-488-3p	MS00009772
M08	MIMAT0002805	hsa-miR-489-3p	MS00007700
M09	MIMAT0002807	hsa-miR-491-5p	MS00031899
M10	MIMAT0002812	hsa-miR-492	MS00004333
M11	MIMAT0003161	hsa-miR-493-3p	MS00006979
M12	MIMAT0002813	hsa-miR-493-5p	MS00009800
M13	MIMAT0002816	hsa-miR-494-3p	MS00033754
M14	MIMAT0002817	hsa-miR-495-3p	MS00004347
M15	MIMAT0004768	hsa-miR-497-3p	MS00031906
M16	MIMAT0002820	hsa-miR-497-5p	MS00004361
M17	MIMAT0002824	hsa-miR-498	MS00004368
M18	MIMAT0002870	hsa-miR-499a-5p	MS00004375
M19	MIMAT0004773	hsa-miR-500a-5p	MS00023751
M20	MIMAT0002874	hsa-miR-503-5p	MS00033838

M21	MIMAT0002875	hsa-miR-504-5p	MS00004410
M22	MIMAT0002878	hsa-miR-506-3p	MS00009856
M23	MIMAT0022701	hsa-miR-506-5p	MS00038738
M24	MIMAT0002879	hsa-miR-507	MS00031934
N01	MIMAT0002880	hsa-miR-508-3p	MS00009863
N02	MIMAT0002808	hsa-miR-511-5p	MS00006993
N03	MIMAT0002823	hsa-miR-512-3p	MS00007000
N04	MIMAT0002883	hsa-miR-514a-3p	MS00031948
N05	MIMAT0002852	hsa-miR-517a-3p	MS00004459
N06	MIMAT0002844	hsa-miR-518b	MS00004466
N07	MIMAT0002848	hsa-miR-518c-3p	MS00004473
N08	MIMAT0002869	hsa-miR-519a-3p	MS00033852
N09	MIMAT0002832	hsa-miR-519c-3p	MS00010003
N10	MIMAT0002853	hsa-miR-519d-3p	MS00004508
N11	MIMAT0002829	hsa-miR-519e-3p	MS00010017
N12	MIMAT0002843	hsa-miR-520b	MS00033859
N13	MIMAT0002846	hsa-miR-520c-3p	MS00007413
N14	MIMAT0002825	hsa-miR-520e	MS00004536
N15	MIMAT0002858	hsa-miR-520g-3p	MS00031955
N16	MIMAT0002850	hsa-miR-524-3p	MS00004550
N17	MIMAT0003389	hsa-miR-542-3p	MS00010073
N18	MIMAT0003340	hsa-miR-542-5p	MS00007147
N19	MIMAT0003215	hsa-miR-552-3p	MS00010164
N20	MIMAT0003235	hsa-miR-570-3p	MS00007791
N21	MIMAT0003249	hsa-miR-584-5p	MS00037198
N22	MIMAT0003252	hsa-miR-586	MS00010248
N23	MIMAT0003255	hsa-miR-588	MS00004886
N24	MIMAT0003260	hsa-miR-592	MS00004914
O01	MIMAT0003264	hsa-miR-596	MS00016359
O02	MIMAT0003269	hsa-miR-601	MS00004970
O03	MIMAT0003273	hsa-miR-605-5p	MS00004998
O04	MIMAT0003275	hsa-miR-607	MS00005012
O05	MIMAT0003276	hsa-miR-608	MS00005019
O06	MIMAT0004805	hsa-miR-616-3p	MS00010339
O07	MIMAT0003291	hsa-miR-622	MS00005117
O08	MIMAT0003294	hsa-miR-625-5p	MS00033894
O09	MIMAT0004810	hsa-miR-629-5p	MS00010395
O10	MIMAT0003299	hsa-miR-630	MS00005173
O11	MIMAT0003305	hsa-miR-635	MS00005208
O12	MIMAT0003307	hsa-miR-637	MS00005222
O13	MIMAT0003320	hsa-miR-650	MS00005313
O14	MIMAT0003322	hsa-miR-652-3p	MS00010451
O15	MIMAT0022709	hsa-miR-652-5p	MS00037905
O16	MIMAT0003324	hsa-miR-661	MS00005390
O17	MIMAT0003326	hsa-miR-663a	MS00037247

O18	MIMAT0004926	hsa-miR-708-5p	MS00010521
O19	MIMAT0004945	hsa-miR-744-5p	MS00010549
O20	MIMAT0000252	hsa-miR-7-5p	MS00032116
O21	MIMAT0003945	hsa-miR-765	MS00021812
O22	MIMAT0004948	hsa-miR-885-3p	MS00010661
O23	MIMAT0004947	hsa-miR-885-5p	MS00010668
O24	MIMAT0000092	hsa-miR-92a-3p	MS00006594
P01	MIMAT0003218	hsa-miR-92b-3p	MS00032144
P02	MIMAT0000093	hsa-miR-93-5p	MS00003346
P03	MIMAT0000442	hsa-miR-9-3p	MS00006510
P04	MIMAT0000094	hsa-miR-95-3p	MS00010906
P05	MIMAT0000441	hsa-miR-9-5p	MS00010752
P06	MIMAT0004510	hsa-miR-96-3p	MS00010913
P07	MIMAT0000095	hsa-miR-96-5p	MS00003360
P08	MIMAT0000096	hsa-miR-98-5p	MS00003367
P09	MIMAT0004511	hsa-miR-99a-3p	MS00010920
P10	MIMAT0000097	hsa-miR-99a-5p	MS00032158
P11	MIMAT0004678	hsa-miR-99b-3p	MS00032172
P12	MIMAT0000689	hsa-miR-99b-5p	MS00032165
P13	MIMAT0000010	cel-miR-39-3p	MS00019789
P14	MIMAT0000010	cel-miR-39-3p	MS00019789
P15		SNORD61	MS00033705
P16		SNORD68	MS00033712
P17		SNORD72	MS00033719
P18		SNORD95	MS00033726
P19		SNORD96A	MS00033733
P20		RNU6-6P	MS00033740
P21	SA_miRNA_005	miRTC	
P22	SA_miRNA_005	miRTC	
P23	SA_00104	PPC	
P24	SA_00104	PPC	

Images of altered miRNAs after compound 2 treatment and their target genes:

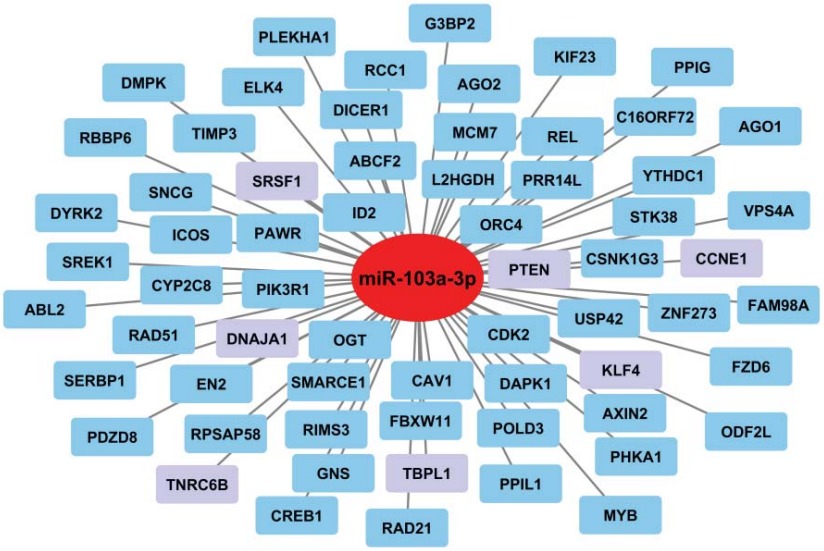

Figure S1. miR-103a-3p and its target genes in detail

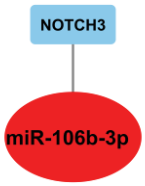

Figure S2. miR-106b-3p and its target gene in detail

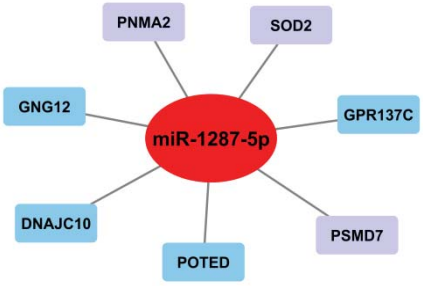

Figure S3. miR-1287-5p and its target genes in detail

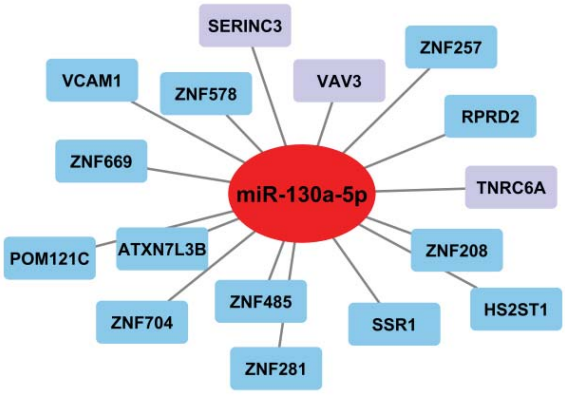

Figure S4. miR-130-5p and its target genes in detail

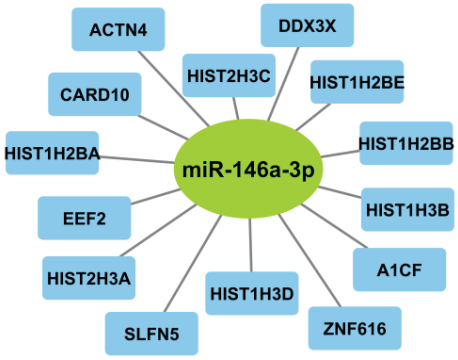

Figure S5. miR-146a-3p and its target genes in detail

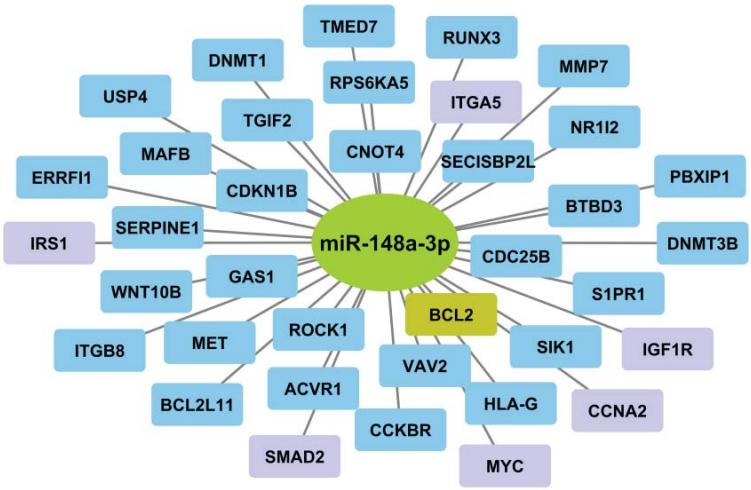

Figure S6. miR-148a-3p and its target genes in detail

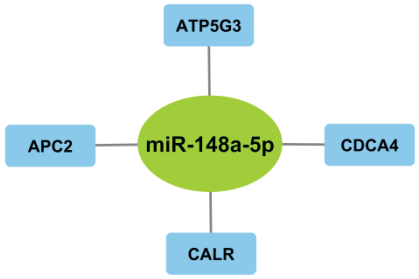

Figure S7. miR-148a-5p and its target genes in detail

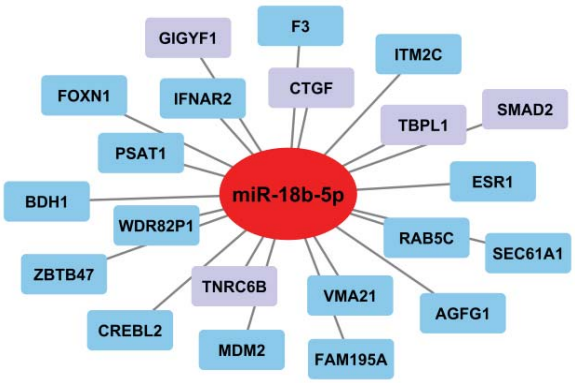

Figure S8. miR-18b-5p and its target genes in detail

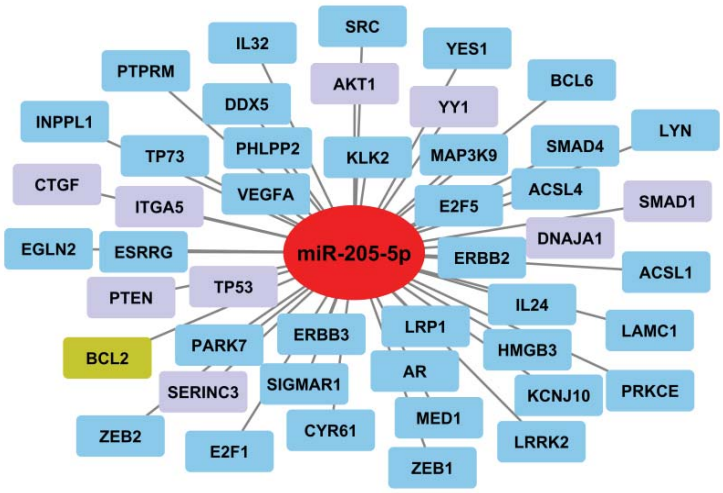

Figure S9. miR-205-5p and its target genes in detail

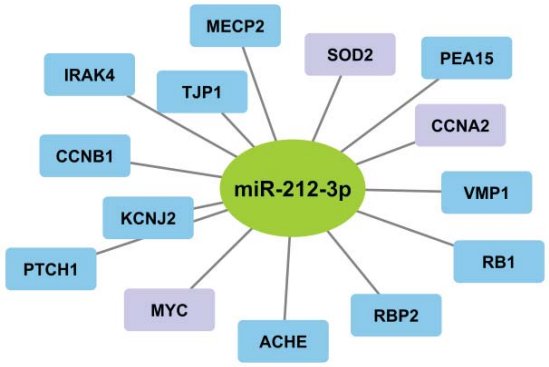

Figure S10. miR-212-3p and its target genes in detail

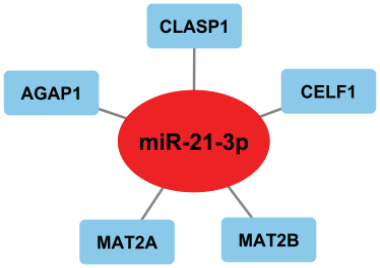

Figure S11. miR-21-3p and its target genes in detail

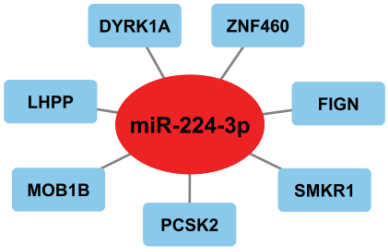

Figure S12. miR-224-3p and its target genes in detail

Figure S13. miR-23b-5p and its target genes in detail

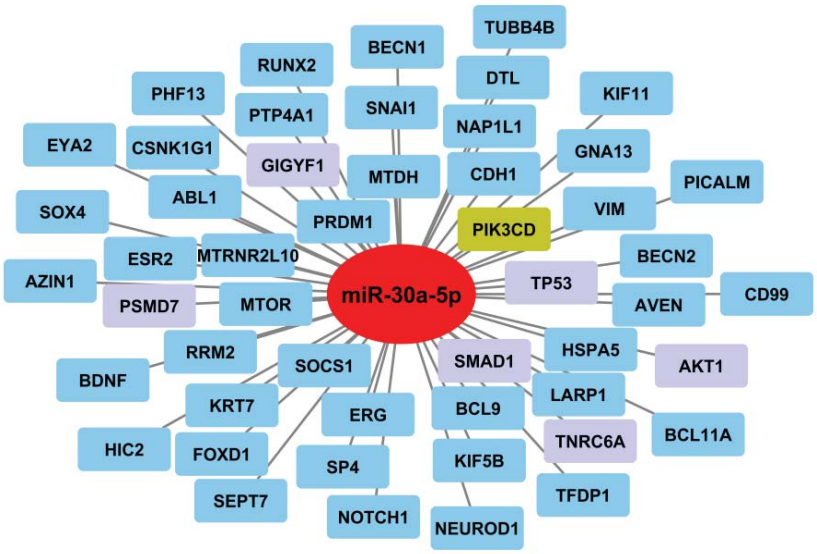

Figure S14. miR-30a-5p and its target genes in detail

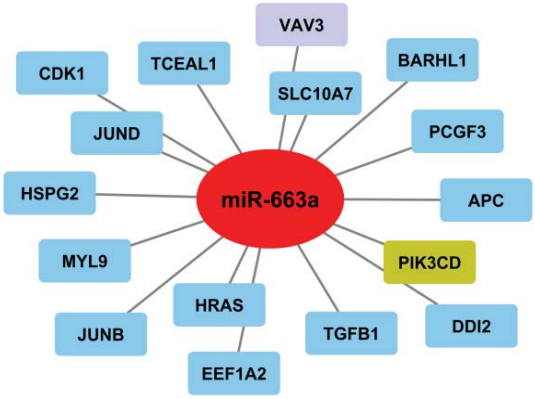

Figure S15. miR-663a and its target genes in detail

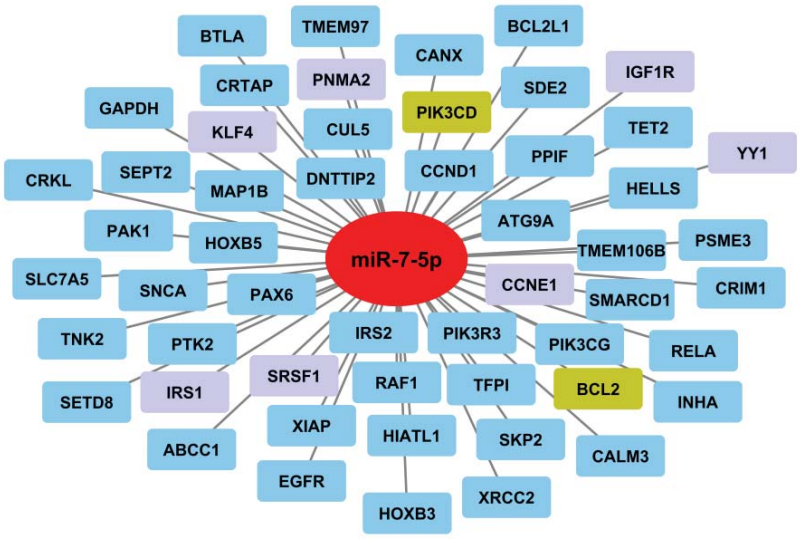

Figure S16. miR-7-5p and its target genes in detail

ANNEX I

In collaboration with the group of Professor Phillip Gale (University of Southampton, UK), we perform a series of in vitro studies with anionophore compounds, squaramides and thiosquaramides. This will be published along with in silico transmembrane transport studies of these compounds.

ABSTRACT

The transport of biologically relevant ions across phospholipid bilayers membranes is a vital process that relies on channel proteins. Alterations in their expression or activity are related to a wide range of pathologies. Series of squaramide and thiosquaramide derivatives with different fluorination degrees, have been synthesized. The *in vitro* activity of these anion transporters has been studied. The most cytotoxic squaramides trigger apoptosis in melanoma cell lines with IC_{50} values in the low micromolar range as well as modify the intracellular pH, inducing the basification of acidic organelles. This preliminary study provides a basis for understanding the mechanism of action of these potential anticancer compounds.

INTRODUCTION

The ion transport in biological systems, particularly chloride and bicarbonate, is very important as it controls multiple processes. The ionophores called squaramides and thiosquaramides have been developed given the growing demand for anion carrier molecules that overcome the effect of defective ion channels in some diseases.

On one hand, squaramides molecules are formed by four-membered ring systems derived from squaric acid. The design and incorporation of drugs with these chemical entities into medicinal chemistry programs has been quite scarce so far. Despite this, squaramide compounds have been investigated for a range of targets and have shown potential therapeutic effects against a variety of pathologies like Changas disease (parasitic illness) (Olmo *et al.*, 2014) or chronic obstructive pulmonary disorder (Martin *et al.*, 2015). In addition, some molecules containing squaramides moieties have been promoted to the clinic for instance for the treatment of gastroduodenal ulcers (Ian Storer, Aciro and Jones, 2011).

On the other hand, compounds with thiourea groups had previously shown to work as potent chloride-bicarbonate exchange agents in liposomal models (Busschaert *et al.*, 2010). Therefore, thiosquaramides have been generated from the combination of squaramides and thioureas (Busschaert *et al.*, 2014). Moreover, some molecules that belong to this new group of anion carriers display a pH-switchable transport behavior. This means that under physiological conditions these compounds have low transport capacity across lipid bilayers, whereas at lower pH become active transporters. This feature may serve as a potential tool to activate chloride transport within acidic environments, and to be able to act favorably in diverse diseases like cancer (Busschaert *et al.*, 2014).

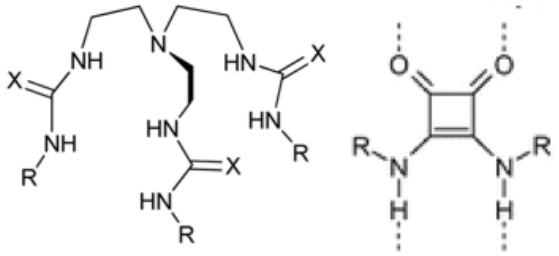

Figure A1. Structures of a tripod thiourea and squaramide

In this preliminary study, we decided to explore the antiproliferative activities of these anion transporter with a set of *in vitro* experiments in different cancer lines, which will serve as a basis for understanding the mechanism of action.

MATERIAL AND METHODS

Evaluated compounds

The set of squaramides and thiosquaramides with different fluorination degrees were synthesized by Dr. Philip Gale and colleagues from the Department of Chemistry, University of Southampton, UK.

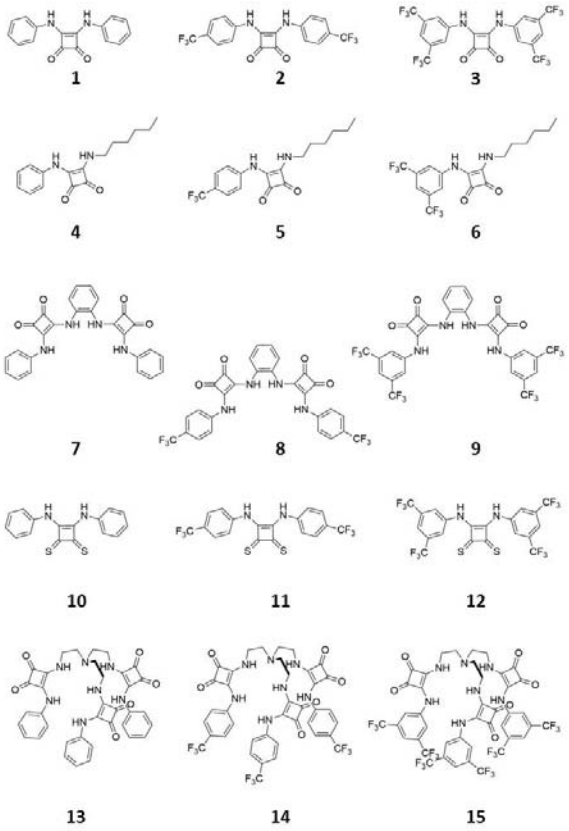

Figure A2. Structures of mono- and bis-squaramides (1-12) and thiosquaramides (13-15) tested in this thesis.

Cell lines and culture conditions

Human lung adenocarcinoma cell line (A549), human melanoma cell line (A375) and human prostatic carcinoma cell line (PC3) were purchased from the American Type Culture Collection, and were cultured in DMEM. Culture medium was supplemented with 10% FBS, 100 U/ml penicillin, 100 µg/ml streptomycin, and 2 mM L-glutamine. Cells were grown in a humidified atmosphere of air containing 5% CO_2 at 37 ºC.

Cell viability assay

Cell viability was determined by the MTT assay. Adherent cell lines were plated in 96-well microtiter plates 24 h before treatment at a concentration of $1x10^4$ in 100 µL of growth medium per well. For single dose experiments, cells were incubated in the absence or in the presence 10 µM of the 15 synthetic

squaramides. Control cells were incubated only with drug diluent, DMSO. A range of concentrations from 0.99 to 25 µM of the most cytotoxic squaramides, **2** and **9**, or a range from 5.93 to 100 µM, in the case of squaramide **7,** were used for dose response experiments. After 24 hours incubation, 10mM of MTT (3-(4,5-dimethylthiazol-2-yl)-2,5-diphenyltetrazolium bromide) diluted in 1 x PBS was added to each well for an additional 4 hours. The medium was removed and a 100 µL of DMSO was added to each well in order to dissolve the MTT formazan precipitate. Absorbance was measured at 570 nm on a Multiskan multiwell plate reader. Cell viability was expressed as a percentage of control and IC_{50} represents the concentration of drug causing 50% inhibition of the increase in absorbance compared with control cells. Data are shown as the mean value ± S.D. of three independent experiments. The IC values were calculated with GraphPad Prism™ 5 software.

Vital fluorescence microscopy – Acridine Orange staining

The living cultured cells were stained with acridine orange (AO). A375 cells (2 x 10^3 cells/mL) grown in a 12-well plate with cover slips for 24 h and were incubated with or without the squaramides **2**, **7** and **9** at their IC_{50} dose for 1 h or at the IC_{75} dose for 1 h (DMSO was used for control cells). Afterwards cells were washed twice with 1 x PBS and incubated with 5 µg/mL AO solution for 30 min at RT and protected from light. Finally, cover slips were washed three times with 1 x PSB supplemented with 10% FBS and then examined with a NIKON eclipse E800 microscope (filter 330/380 nm).

Hoechst 33342 staining

A375 cells were seeded in a 12-well plate with 15 mm round sterile coverslips at a concentration of 2 x 10^5 cells/mL 24 h before the treatment. Afterwards, cell media was removed and fresh media with the corresponding drug dose was added. A375 cells were incubated in the absence (control cells) or in the presence of 10 µM of thiosquaramides **2, 7** and **9** for 48 h. After this time, media was centrifuged twice at 700 g washing with 1 x PBS to collect the floating cells, whereas the attached cells were washed 3 times with 1 x PBS.

Cells (floating and attached) were stained with the nuclear counterstain Hoechst 33342 at a concentration of 2 µg/mL for 30 min at 37ºC in dark conditions. Then, cells were washed twice with 1 x PBS. Detached cells were centrifuged twice at 700 g and washed with 1 x PBS. PBS was discarded and cells were resuspended in 10 µL of glycerol:H_2O (9:1). Cells in glycerol were deposited in slides and the cells on the coverslips were placed over them. Mounts were examined fluorometrically with a Nikon elipse E800microscope (Nikon) using the 330-380 nm filter.

Assessment of cell cycle arrest

A375 cells were synchronized maintained in normal culture condition with only 0.5% FBS for a period of 24h before initiate the experiment. Then cells treated without and with the squaramides **2** and **9** at the IC_{50} dose for 6 h, 24 h and 48 h. Cells were collected and then fixed in 70% ethanol at -20ºC overnight. Afterwards, cells were washed in 1 x PBS and cell pellet was then resuspended with 200 µl of Muse™ cell cycle reagent for 30 min at RT in dark conditions. Fluorescence was measured by flow cytometry on a FACSCalibur fitted with a 488 nm Ar laser, and data were analyzed using CellQuest Pro software (Becton Dickinson, San Jose, CA) and ModFit LT cell cycle analysis software (Verity software, Topsham, ME).

RESULTS

Compounds cytotoxic effect on cancer cell lines

Squamides had been classified in previous papers as good anion transporters. To determine the effects of perturbing ion homeostasis on organelles and cells, we carried out cell viability studies in three different cancer cell lines. The *in vitro* cytotoxic activity of squaramides 1 to 12 and thiosquaramides 13-15 was tested on a collection of different cancer cell lines from diverse origin: human lung adenocarcinoma cell line (A549), human melanoma cell line (A375) and human prostatic carcinoma cell line (PC3). First of all, we used a single point screening assay with all the above mentioned compounds at 10 µM (figure A3). Through the colorimetric test of MTT, the levels of formazan salts produced were measured and quantified in order to evaluate cell viability. Squaramides **2** and **9** were particularly cytotoxic in A375 cell line being the most sensitive one, while no significant effect was observed after treatment with the other squaramides or thiosquaramides at the same dose and time.

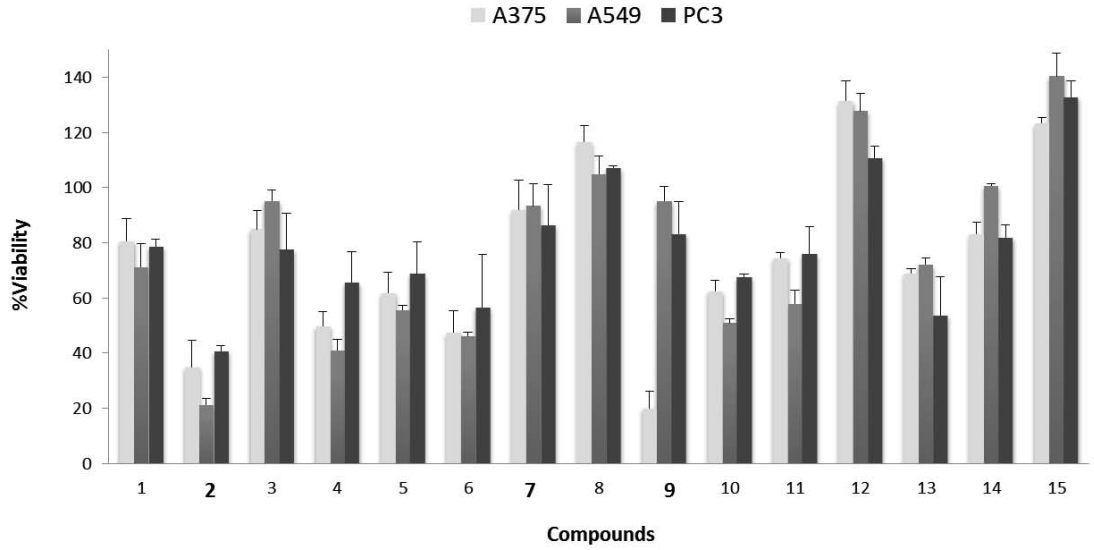

Figure A3. Cell viability measured by MTT assay after 24 h of squaramide compounds treatment. Single-point screening of compounds 1–15 (10 µM) on a collection of different cancer cell lines, from right to left, A375, A549 and PC3.

Dose-response experiments were performed and IC values were calculated for cytotoxic compounds (squaramides **2** and **9**) as well as for the non-cytotoxic one, squaramide **7**. These experiments were carried out in A375, A549 and PC3 cell lines for 24 h. The obtained results corroborate how squaramide **2** is the most potent compound; showing IC_{50} values below 10 µM in the three cell lines studied. Compound **9** showed values close to 10 µM, being A375 the most sensitive cell line to this compound. In the case of compound **7**, with higher IC values, the most sensitive cell line to this compound was PC3.

A375					
Squaramide 2		Squaramide **7**		Squaramide **9**	
IC_{25}	3.77±1.89	$\mathbf{IC_{25}}$	10.52±3.71	$\mathbf{IC_{25}}$	6.63±1.12
IC_{50}	8.86±0.63	$\mathbf{IC_{50}}$	16.60±2.38	$\mathbf{IC_{50}}$	8.03±1.19
IC_{75}	9.79±0.42	$\mathbf{IC_{75}}$	21.15±1.10	$\mathbf{IC_{75}}$	9.59±1.51

A549					
Squaramide 2		Squaramide **7**		Squaramide **9**	
IC_{25}	1.29±0.23	$\mathbf{IC_{25}}$	21.13±1.63	$\mathbf{IC_{25}}$	8.74±0.60
IC_{50}	5.56±0.78	$\mathbf{IC_{50}}$	49.13±4.11	$\mathbf{IC_{50}}$	11.13±2.65
IC_{75}	8.94±0.24	$\mathbf{IC_{75}}$	63.99±2.20	$\mathbf{IC_{75}}$	13.09±0.13

PC3					
Squaramide 2		Squaramide **7**		Squaramide **9**	
IC_{25}	1.55±0.56	$\mathbf{IC_{25}}$	8.67±0.71	$\mathbf{IC_{25}}$	12.13±2.50
IC_{50}	3.03±0.57	$\mathbf{IC_{50}}$	12.79±0.88	$\mathbf{IC_{50}}$	15.90±1.12
IC_{75}	19.44±2.16	$\mathbf{IC_{75}}$	24.40±1.66	$\mathbf{IC_{75}}$	18.11±0.70

Table A1. IC values (μM) of squaramides **2**, **7** and **9** on A375, A549 and PC3 cancer cell lines.

Dysregulation of lysosomal pH

Since these compounds showed anion transport activity in the liposome assays through Cl^-/NO_3^- antiport or H^+/Cl^- symport (Busschaert *et al.*, 2012, 2014) we sought to determine whether they could show transport activity inside cells, contributing to their cytotoxicity. The *in vitro* ionophoric activity of the cytotoxic compounds was studied in A375, melanoma cell line, using vital staining with acridine orange (AO). This cell permeable dye, as a weak base, accumulates in acidic compartments, such as lysosomes, where it is protonated and shows orange fluorescence emission, whereas it emits green fluorescence at higher pH (Allison and Young, 1969). When A375 cells were stained with AO, granular orange fluorescence was observed in the cytoplasm (Figure A4 a,b), suggesting that the orange fluorescence is due to acidic organelles, such as lysosomes and endosomes. Cells treated with non-cytotoxic squaramide **7** showed no changes (figure A4 e,f). Surprisingly, cells treated with the cytotoxic squaramides **2** and **9** also did not show a significant disappearance of orange emission when administered at their IC_{50} value (figure A4 c,g), but at higher concentrations (IC_{75} values) the orange colour did disappear (figure A4 d,h). These results indicate that both compounds were capable of inducing pH discharge across the lysosomal membrane.

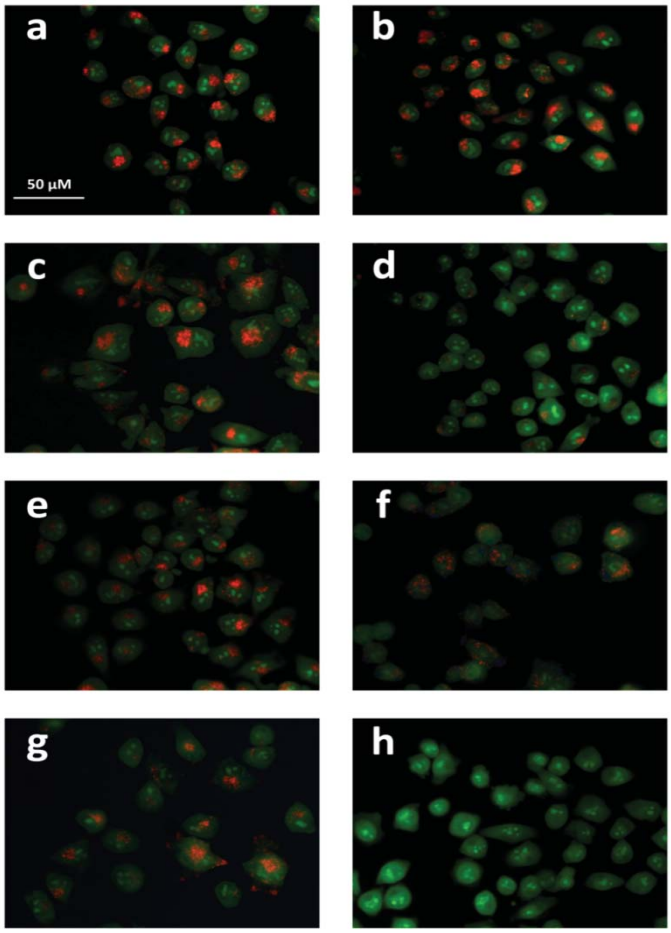

Figure A4. Acridine Orange staining of melanoma A375 cells after exposure to squaramides 2, 7 and 9 at the IC_{50} for 1h or IC_{75} dose for 3 h. (a, b) untreated cells, (c) **2** at IC_{50} concentration, (d) **2** at IC_{75} concentration, (e) **7** at IC_{50} concentration, (f) **7** at IC_{75} concentration, (g) **9** at IC_{50} concentration, (h) **9** at IC_{75} concentration. Cells with cytoplasmic granular orange fluorescence were observed (a, b, e and f), cells with disappearance of cytoplasmic orange fluorescence were detected in (d and h).

Cytotoxic squaramide compounds induce apoptotic cell death

As has been seen in previous sections the compounds are cytotoxic. Therefore, we wanted to analyze the cell death induced by these squaramides. Apoptosis is a tightly regulated form of cell death in which cells actively participate in their own destruction. This cell death can be triggered by different stimulus such as sustained changes in pHi (De Milito *et al.*, 2007). A cell that is undergoing apoptosis demonstrates, among other morphological characteristics, nuclear condensation and DNA fragmentation, which can be detected by staining with Hoechst 33342 and fluorescence microscopy. Through this technique we tried to examine all these nuclear alterations after the exposure to the different squaramides in A375 cells (figure A5).

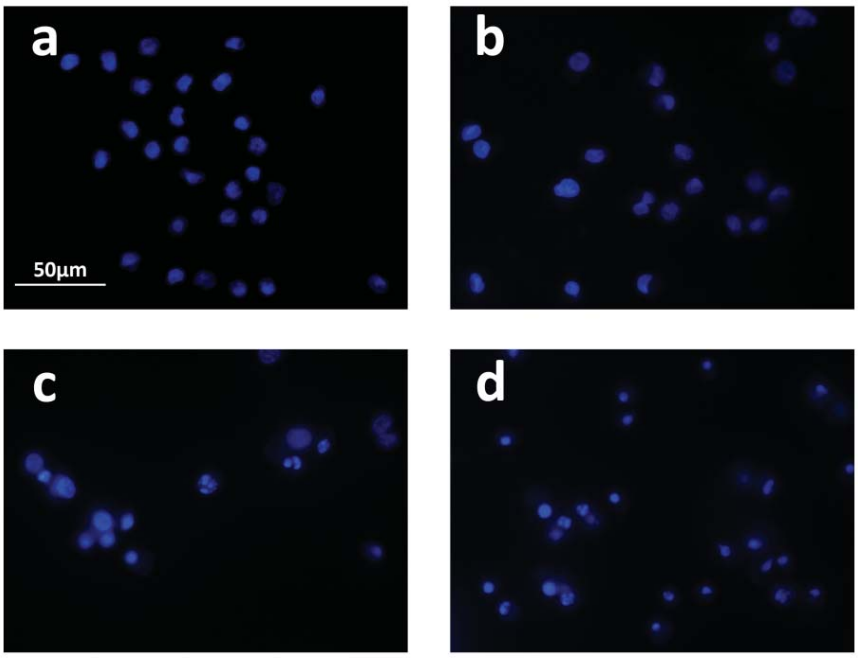

Figure A5. Hoechst 33342 staining of A375 cells after exposure with squaramides 2, 7 and 9 at 10 µM: (a) untreated cells, (b) squaramide **7**, (c) squaramide **2** and (d) squaramide **9**. Cells with normal nuclear morphology were observed in figure A5a and A5b, cells with nuclear condensation and apoptotic bodies were showed in figure A5 c and d.

In figure A5 untreated A375 cells have typical rounded nuclei (Figure A5a). Following treatment with the squaramides **2** and **9** (10 µM for 48 hours) the cells showed nuclear condensation (figure A5c and d) and the formation of apoptotic bodies was observed, confirming that these compounds induce apoptotic cell death. However, with the non-cytotoxic squaramide **7** the appearance of the nucleus was normal (figure A5b).

Cell cycle phases distribution after treatment

In case the drop in viability observed in previous experiments was caused by cell cycle arrest, we further analyzed the squaramides **2** and **9** effects on cell cycle distribution. Cultured A375 cells were treated at different times with the most potent compounds and analyzed by flow cytometry (figure A6). A slight modification in the proportion of cells in G_1 and S phases was detected with both squaramides at 24 and 48 h. However, the most significant changes were observed in the percentage of apoptotic population with an increase of 15.78% and 51.78% at 48 h of treatment with squaramides **2** and **9** respectively. These results indicate that the compounds are essentially cytotoxic since they do not cause cell cycle arrest. Consequently, taking into account the previous results, the observed decrease in viability would be caused mainly by apoptotic cell death.

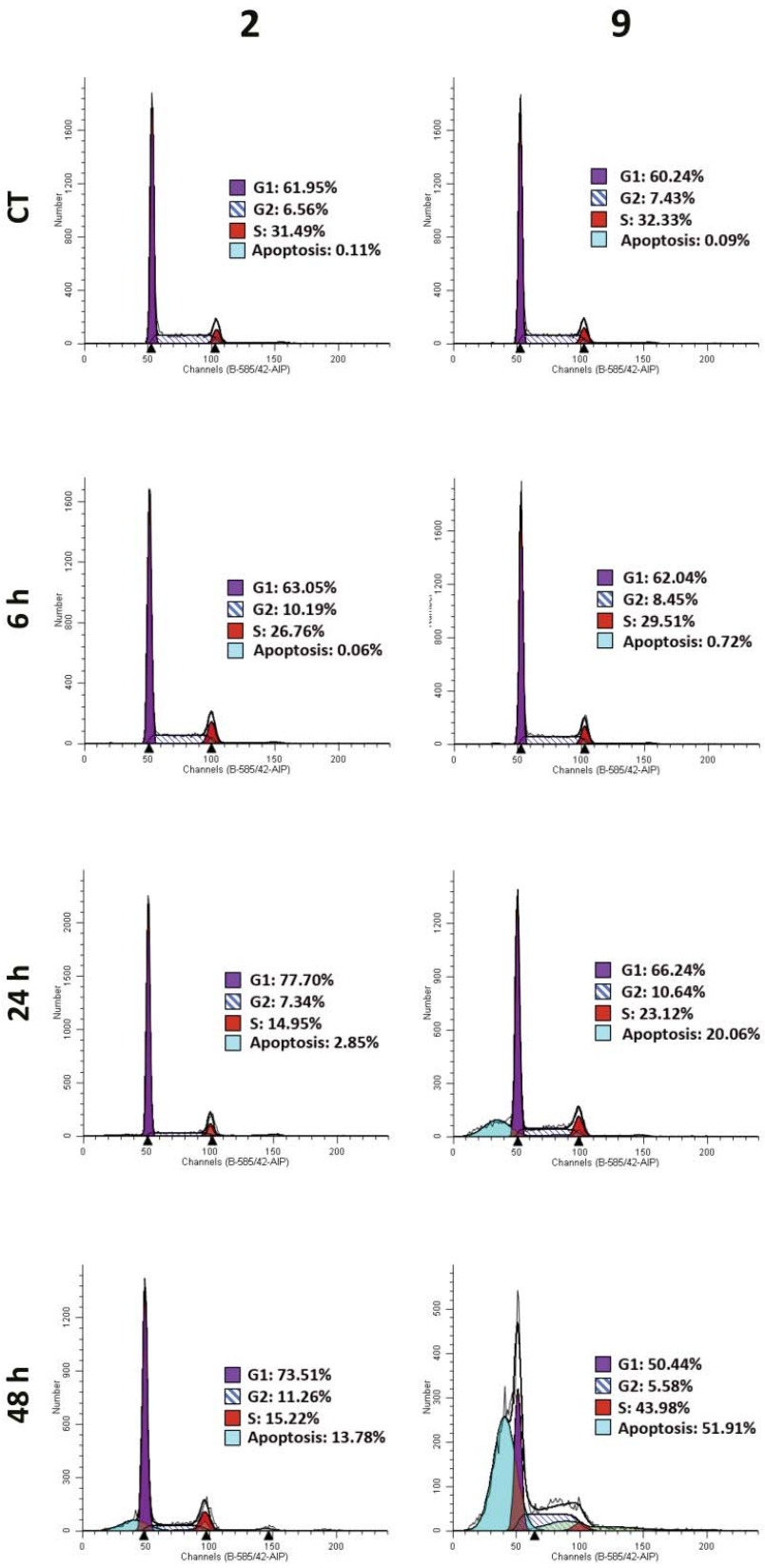

Figure A6. Flow cytometry analysis of the of A375 cells without treatment (control) or after 6 h, 24 h and 48 h squaramides **2** and **9** treatment at the IC_{50} dose. Numbers represent the percentage of cells in each cell cycle phase. Violet color percentage of cells in G_1 phase; striped bars percentage in G_2/M phase; red color percentage of cells in S phase and blue color percentage of apoptotic cells. Data shown are representative of three independent experiments with similar results obtained in each.

DISCUSSION

The transport of anion chloride across cell membranes regulates multiple biological processes such as intracellular pH, membrane potential and cellular volume that are essential in multiple physiological processes such as cell migration, proliferation and differentiation (Gale, Pérez-Tomás and Quesada, 2013)(Habela et al., 2009). This important process is normally regulated by transmembrane ion channels. Malfunction of any of these channels results in the development of diseases known as channelopathies, as in the case of cystic fibrosis (Ashcroft, 2000). Therefore, interest in developing anionophores that can restore chloride permeability has recently increased (Li et al., 2017). In addition, in the last decades, ion channels and transporters have emerged as drivers of the cancer progression since cancer cells suffer a metabolic shift associated with increased acid production and upregulation of acid-extruding transporters in plasma membrane (Neri and Supuran, 2011). This altered transport results in alkalization of pHi in cancer cells comparing to normal ones. In this sense, it has been shown how anionophores that are able to modify pH and ionic gradients between intracellular compartments cause cytotoxicity in cancer cells, affording the possibility of using these molecules as anticancer agents (Soto-Cerrato et al., 2015).

Our set of squaramides and thiosquaramides have been identified as potent anion transporters in liposomal model by Nathalie Busschaert and colleagues (Busschaert et al., 2012, 2014). Disturbing ion homeostasis on organelles and cells can trigger cell death (Yu, Canzoniero and Choi, 2001; Ko et al., 2014). In this regard, compound 2 and 9 decreased cell viability, especially in human melanoma cell line, whereas the rest of compounds exhibited reduced toxicity. Thus, the most potent ones, presenting IC values below 10 µM in all tested cell lines, might have a potential function as anticancer compounds, as well as prodigiosin or synthetic tambjamine analogues, anion transporters that have shown in vitro anticancer activity (Jonathan L. Sessler et al., 2005; Soto-Cerrato et al., 2015); and those that barely affect cell viability might be suitable candidates as potential drugs for the treatment of channelopathies (Li et al., 2017).

On the other hand, the treatment of the A375 cell line with the most cytotoxic squaramides, **2** and **9**, caused a loss of the orange punctate characteristic of AO, which is associated with acidic organelles such as lysosomes or endosomes. Lysosomes, essential organelles for degradation and cellular homoeostasis, regulate the final steps of the catabolic autophagic process. It has been described that changes in lysosomal pH, related to an impairment of lysosomal enzyme activity, result in diverse pathological situations (Boya, 2012). In this sense, altered lysosomal pH, caused by squaramide compounds, might generate an autophagy impairment that may contribute to the observed cytotoxicity. Philip Gale research group have performed additional analysis with squaramides that are focused on lysosomal pH alteration and its corresponding function. Results obtained in these tests confirmed that some squaramides disrupt autophagy raising lysosomal pH and inhibiting cathepsins function (lysosomal enzymes) (Busschaert et al., 2017). This effect would be consistent with recent studies carried out with synthetic tambjamine analogues, chloride/bicarbonate transporters with anticancer capacity that cause lysosomal alkalization and autophagic blockade (Rodilla et al., 2017).

In literature, there are previous papers where it is shown that dysregulation of ionic homeostasis, particularly through chloride influx, can prompt cell death by apoptosis (Saha *et al.*, 2016). After treatment with the most potent compounds, **2** and **9**, it was possible to detect characteristic elements

of apoptotic dell death in A375 cells, such as apoptotic bodies and sub-G1 peak by Hoechst staining and flow cytometry, respectively. More in-depth studies revealed that the movement of ions caused by squaramides results in cytochrome *c* release from the mitochondria into the cytosol, promoting caspase-dependent apoptosis (Busschaert *et al.*, 2017).

Overall, this initial study propose that squaramides **2** and **9** exert cytotoxic activity inducing apoptosis along with alkalization of cellular acidic compartments in a melanoma cell line. These findings suggest that these synthetic anion transporters may have a role as novel anticancer agents.

ANNEX II

Rodilla, A. M.; Korrodi-Gregório, L.; Hernando, E.; Manuel-Manresa, P.; Quesada, R.; Pérez-Tomás, R.; Soto-Cerrato, V. "Synthetic tambjamine analogues induce mitochondrial swelling and lysosomal dysfunction leading to autophagy blockade and cell death in lung cancer". Biochemical Pharmacology, 2017.

Article that includes part of this doctoral thesis work.

Biochemical Pharmacology 126 (2017) 23–33

Contents lists available at ScienceDirect

Biochemical Pharmacology

journal homepage: www.elsevier.com/locate/biochempharm

Synthetic tambjamine analogues induce mitochondrial swelling and lysosomal dysfunction leading to autophagy blockade and necrotic cell death in lung cancer

Ananda M. Rodilla [a], Luís Korrodi-Gregório [a,b], Elsa Hernando [c], Pilar Manuel-Manresa [a], Roberto Quesada [c], Ricardo Pérez-Tomás [a,*], Vanessa Soto-Cerrato [a,*]

[a] Cancer Cell Biology Research Group, Department of Pathology and Experimental Therapeutics, Faculty of Medicine, University of Barcelona, Barcelona, Spain
[b] Laboratory of Signal Transduction, Department of Medical Sciences, Institute for Research in Biomedicine – iBiMED, Health Sciences Program, University of Aveiro, Aveiro, Portugal
[c] Department of Chemistry, University of Burgos, Burgos, Spain

ARTICLE INFO

Article history:
Received 7 October 2016
Accepted 22 November 2016
Available online 24 November 2016

Keywords:
Anionophores
Synthetic tambjamine analogues
Lysosomal dysfunction
Autophagy blockade
Necrosis

ABSTRACT

Current pharmacological treatments for lung cancer show very poor clinical outcomes, therefore, the development of novel anticancer agents with innovative mechanisms of action is urgently needed. Cancer cells have a reversed pH gradient compared to normal cells, which favours cancer progression by promoting proliferation, metabolic adaptation and evasion of apoptosis. In this regard, the use of ionophores to modulate intracellular pH appears as a promising new therapeutic strategy. Indeed, there is a growing body of evidence supporting ionophores as novel antitumour drugs. Despite this, little is known about the implications of pH deregulation and homeostasis imbalance triggered by ionophores at the cellular level. In this work, we deeply analyse for the first time the anticancer effects of tambjamine analogues, a group of highly effective anion selective ionophores, at the cellular and molecular levels. First, their effects on cell viability were determined in several lung cancer cell lines and patient-derived cancer stem cells, demonstrating their potent cytotoxic effects. Then, we have characterized the induced lysosomal deacidification, as well as, the massive cytoplasmic vacuolization observed after treatment with these compounds, which is consistent with mitochondrial swelling. Finally, the activation of several proteins involved in stress response, autophagy and apoptosis was also detected, although they were not significantly responsible for the cell death induced.

Altogether, these evidences suggest that tambjamine analogues provoke an imbalance in cellular ion homeostasis that triggers mitochondrial dysfunction and lysosomal deacidification leading to a potent cytotoxic effect through necrosis in lung cancer cell lines and cancer stem cells.

1. Introduction

Correct ion exchange through cellular membranes is an essential process for maintaining osmotic balance and intracellular pH (pHi) [1], which are key parameters controlling many biological processes. In fact, variations in cellular concentrations of certain ions coordinate the signals that converge on cell cycle checkpoints [2], regulating the proliferative capacity of cells and their differentiation. Similarly, the triggering of the apoptotic programmed cell death also depends on ion fluxes mediated by cellular ion channels [3]. Therefore, when cellular pH is not preserved at a favourable level, different pathologies may appear, as it is the case of cancer. Cancer cells undergo a pH deregulation during the process of carcinogenesis, resulting in the acidification of the extracellular pH (pHe) and the alkalinisation of the pHi. This adaptive reversed pH gradient is decisive for survival and propagation of tumours, promotes metabolic adaptation, evasion of apoptosis and facilitates the metastatic dissemination of tumour cells. Consequently, pH is recently being considered as another hallmark of cancer [4].

Among different cancers, lung cancer remains a major public health problem since it is the leading cause of mortality related to this disease, accounting for more than 1.5 million deaths in 2012 [5]. Early diagnosis and advances in first-line treatments

* Corresponding authors at: Cancer Cell Biology Research Group, Department of Pathology and Experimental Therapeutics, Faculty of Medicine, University of Barcelona, C/Feixa Llarga s/n, 08907 L'Hospitalet de Llobregat, Barcelona, Spain.
E-mail addresses: ananda.rodilla@ub.edu (A.M. Rodilla), korrodi@ub.edu (L. Korrodi-Gregório), ehsanta@ubu.es (E. Hernando), pilarmanuel@ub.edu (P. Manuel-Manresa), rquesada@ubu.es (R. Quesada), rperez@ub.edu (R. Pérez-Tomás), vsoto@ub.edu (V. Soto-Cerrato).

http://dx.doi.org/10.1016/j.bcp.2016.11.022
0006-2952/

are not entirely effective in reducing this high mortality since conventional treatments have limited success. Therefore, the identification of novel anticancer compounds focused on different mechanisms of action is eagerly needed [6,7].

Based on the specific altered pH of cancer cells, modulation of intracellular pH has recently been proposed as a new therapeutic strategy against cancer. In this regard, a diverse group of anionophores, lipid soluble compounds that facilitate the transport of anions across cell membranes, have recently emerged as promising anticancer compounds [8,9]. Indeed, prodigiosin, a tripyrrolic natural product with anticancer properties, represents one of the first described anionophores [10–13]. It has been reported that its biological activity is partly due to its ability to deacidify acidic compartments within cells, which may cause a drop in pHi, and therefore the onset of apoptosis in cancer cells [9,11,14]. Emulating that characteristic, different anionophores have been designed and evaluated [15]. We have focused our attention on the bioactive marine alkaloids tambjamines, a class of natural anionophores that has shown interesting cytotoxic effects [16,17]. We have recently synthesized novel synthetic tambjamine analogues bearing aromatic substituents in the enamine moiety, as well as explored different substitution patterns on characteristic alkoxy group of the central pyrrole ring. These compounds proved to be very efficient anion exchangers in liposome models, promoting both chloride and bicarbonate transport [18–20]. As a result of this anionophoric activity, compounds bearing 4-alkoxy-2,2′-bipyrrole moieties have shown to possess interesting anticancer activities in a wide panel of cancer cell lines [19]. Moreover, a different type of tambjamine analogues, in which the characteristic 2,2′-bipyrrole unit is replaced by a 2-pyrrolylindole, have recently shown the ability to hyperpolarize the cellular membrane as well as differentiate and induce cell death in lung cancer stem cells [20], which are promising properties for their potential use in cancer therapy.

Despite the identification of this class of anion selective ionophores as novel potential anticancer drugs, very little is known about the effects at the cellular level of the facilitated anion transport and the implications of unbalanced homeostasis and pH deregulation in the cytotoxicity exhibited by anionophores. In the present work, we analyse in detail for the first time the cellular and molecular mechanisms of action that lead to the cell death triggered by these potent anionophores in several lung cancer cell lines and cancer stem cells (CSC).

2. Materials and methods

2.1. Compounds synthesis

Tambjamine analogues (Fig. 1a) were synthesized as previously reported [19]. Drugs were dissolved at 10 mM in DMSO and stored at −20 °C. Subsequent dilutions for biological assays were made in culture medium.

2.2. Cell lines and culture conditions

Human lung cancer cell lines A549 (adenocarcinoma), DMS53 (small cell carcinoma), H460 (large cell carcinoma) and SW900 (squamous carcinoma) were obtained from the American Type Culture Collection (ATCC, Manassas, VA, USA), and maintained in DMEM (A549) or RPMI medium (Biological Industries, Beit Haemek, Israel). All media were supplemented with 100 U/mL penicillin, 100 μg/mL streptomycin, and 2 mM L-glutamine, all from Biological Industries and 10% foetal bovine serum (FBS; Gibco, Paisley, UK). Cancer stem cells were obtained from resected patient tumour samples or isolated from cancer cell lines and characterized through evaluation of stem cell surface markers (CD166, CD44, CD90, CD133 and EpCAM) by flow cytometry. Moreover, tumorigenic properties of tumour spheres were assessed through subcutaneous transplantation in NOD.CB17-Prkdc^{scid}/NcrCrl mice (Jackson Laboratories, Bar Harbor, ME, USA) and tumour growth curves were monitored. For detailed procedures and results see Supplementary information in Ref. [20]. CSC were cultured as a cell suspension in RPMI medium supplemented with 50 μg/mL Epidermal Growth Factor, 20 μg/mL basic Fibroblast Growth Factor, 1× Insulin-Transferrin-Selenium, 0.4% BSA and 2% B27™ (Gibco). Cells at passage 10–25 were grown at 37 °C under a 5% CO_2 atmosphere.

2.3. Cell viability assay

Cell viability was determined by the MTT assay [21]. Cells (1×10^5 cells/mL) were seeded in 96-well microtiter plates and incubated for 24 h to allow cells to attach. Afterwards, they were treated for 24 h with 10 μM of each compound for single point experiments and dose-response curves were performed ranging from 0.78 to 100 μM to calculate the inhibitory concentrations (IC) of 25%, 50% and 75% of cell population. The drug concentrations corresponding toIC_{25}, IC_{50}, and IC_{75} values were used in subsequent experiments. Cisplatin and DMSO were used as positive and negative controls, respectively. In the case of positive control, concentrations ranging from 1.56 to 200 μM were tested. For inhibition assays, the apoptotic inhibitor Z-VAD-FMK (10 μM) (BD Biosciences, San Jose, CA, USA) or the autophagic inhibitor 3-Methyladenine (3-MA) (5 mM) from Sigma-Aldrich (St Louis, MO, USA) was added 30 min prior to compound **2** addition. After 24 h, 10 μM of 3-(4,5-dimethylthiazol-2-yl)-2,5-diphenyltetrazolium bromide diluted in 1× PBS (MTT, Sigma-Aldrich) was added to each well for an additional 4 h. The medium was removed and the MTT formazan precipitate was dissolved in 100 μL of DMSO. Absorbance was read on a Multiskan multiwell plate reader (Thermo Fisher Scientific Inc., Waltham, MA, USA) at 570 nm. For each condition, at least three independent experiments were performed in triplicate. Cell viability was expressed as a percentage of control cells, and data are shown as the mean value ± S.D. The IC_{25}, IC_{50} and IC_{75} values were calculated with GraphPad Prism™ 5 software (Graph Pad Software, San Diego, CA, USA).

For single-point cell viability assays in monolayer cells (passage 10–20) and sphere-forming cells (passage 1–2), they were plated at the desired density ($1–2 \times 10^3$ or $2–3.5 \times 10^3$, respectively) in 200 μL per well in 96-well plates. One day (24 h) after seeding, compound **2** was added in three replicates at 10 μM for each cell line or patient's derived cultures. Patient samples acquisition protocol and informed consent were approved by the local ethics committee. Cell viability was measured after 24 h, using the CellTiter 96™ AQueous One Solution Cell Proliferation Assay (Promega, Madison, WI, USA) and following the manufacturer's instructions. Absorbance at 490 nm was detected using a VICTOR3™ Multilabel Plate Reader (Perkin Elmer-Cetus, Norwalk, CT, USA). Cell viability was normalized to the respective control cells and presented as a percentage of them. For each condition, three independent experiments were performed and mean ± SD is shown.

2.4. Ion-selective electrode transport assays

A chloroform solution (20 mg/mL) of 1-palmitoyl-2-oleoyl-*sn*-glycero-3-phosphocholine (POPC) (Sigma-Aldrich) was evaporated in vacuo using a rotary evaporator and the resulting lipid film was dried under vacuum for at least 2 h. After that, it was rehydrated by addition of a sodium chloride solution (489 mM NaCl and 5 mM phosphate buffer, pH 7.2 or 451 mM NaCl and 20 mM phosphate buffer, pH 7.2) followed by careful vortexing. The obtained lipid suspension was subjected to nine freeze-thaw cycles and twenty-nine extrusions through a 200 nm polycarbonate Nucleopore

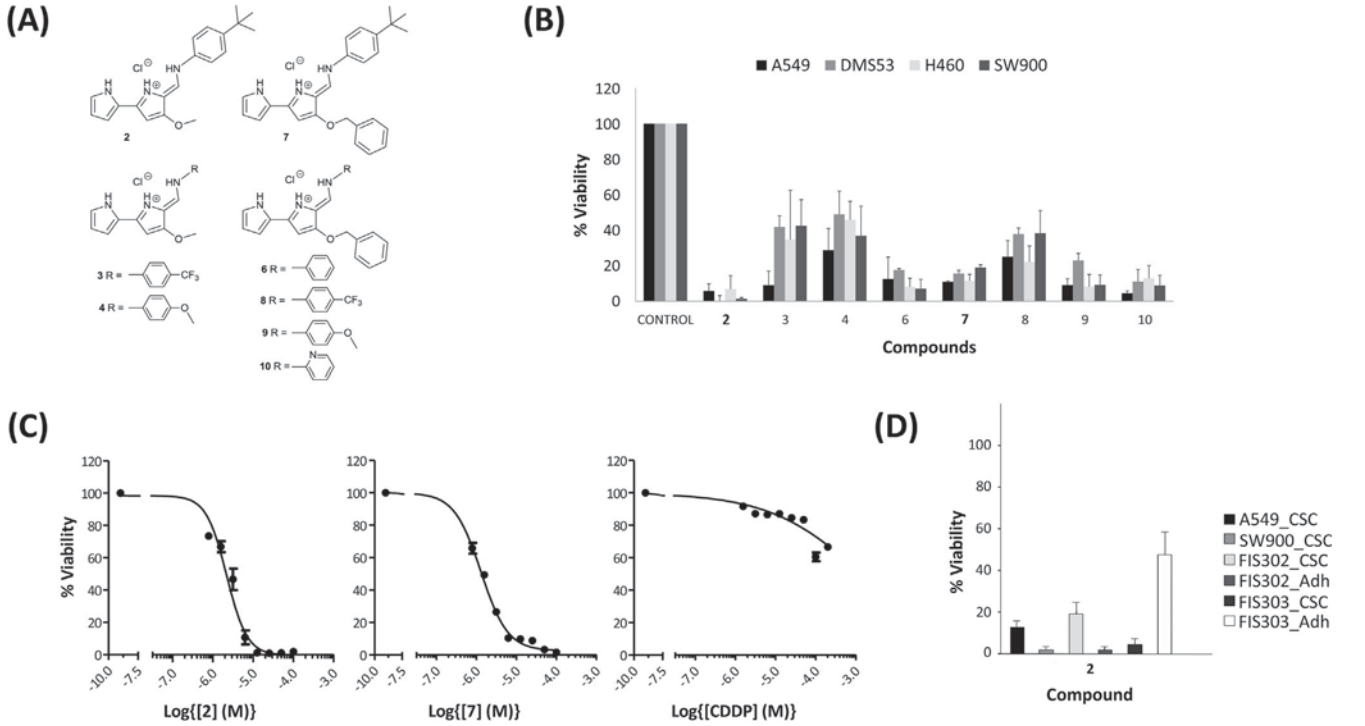

Fig. 1. Synthetic tambjamine analogues significantly decrease cell viability. (A) Chemical structure of synthetic tambjamine analogues. (B) MTT cell viability assay was performed after 24 h of treatment with synthetic tambjamine analogues at 10 μM in A549, DMS53, H460 and SW900 cell lines. (C) Concentrations ranging from 0.8 to 100 μM of compounds **2** and **7** were used in dose-response curve experiments for IC_s value calculation in A549 cell line. At the same time, in case of positive control, concentrations ranging from 1.6 to 200 μM of cisplatin (CDDP) were tested. (D) Cell viability was tested in adherent (Adh) and cancer stem cells (CSC) derived from lung cancer patients (FIS302, FIS303) or cancer cell lines (A549, SW900) after 10 μM of compound **2** for 24 h. Results show the mean value ± SD of at least three independent experiments.

membrane using a LiposoFastBasic extruder (Avestin Inc., Ottawa, Canada). In order to remove the unencapsulated chloride, the obtained vesicles were dialyzed against a $NaNO_3$ solution (489 mM $NaNO_3$ and 5 mM phosphate buffer, pH 7.2) or a Na_2SO_4 solution (150 mM Na_2SO_4 and 20 mM phosphate buffer, pH 7.2), respectively. For the NO_3^-/Cl^- assays, vesicles prepared as described above (rehydrated with 489 mM NaCl), were suspended in a solution 489 mM $NaNO_3$ and 5 mM phosphate buffer, pH 7.2 to a final lipid concentration of 0.5 mM in a total volume of 5 mL. Using a chloride selective electrode (CRISON 96 52 C I.S.E. electrode) the chloride efflux was monitored over time. After 60 s, an aliquot of the transmembrane anion carrier in DMSO was added (the amount of DMSO was always less than 20 μL in order to avoid influence of the solvent molecules in the assay). After five minutes (t = 360 s), a pulse of detergent was added (Triton™ X-100 10% dispersion in water, 20 μL), thus vesicles were lysed. The obtained final reading was considered as the 100% of the chloride encapsulated and used as such. For (HCO_3^-/Cl^-) assays, the vesicles were rehydrated with 451 mM NaCl and suspended in the Na_2SO_4 solution. Again, the final lipid concentration in each experiment was 0.5 mM and the total volume in each experiment 5 mL. A volume of the carrier molecule was added at the beginning of the experiment (t = 0 s). A minute later (t = 60 s), an aliquot of $NaHCO_3$ (in 150 mM Na_2SO_4 buffered to pH 7.2 with 20 mM sodium phosphate salts) was added for a final concentration of 40 mM. The chloride efflux was measured during 5 min and then the detergent was added (t = 360 s). The data were used as described previously.

2.5. Acridine orange staining

A549 cells (1×10^5 cells/well) grown in a 12-well plate with cover slips for 24 h were treated with or without the IC_{50} value of the studied compounds for 1 h (DMSO was added in control cells). Afterwards, cells were washed twice with 1× PBS and stained with 5 μg/mL acridine orange (AO) solution for 30 min at room temperature. Finally, they were washed three times with 1× PBS/10% FBS and fluorescence was immediately examined in a NIKON eclipse E800 microscope (filter 330/380 nm) (Nikon Europe BV, Badhoevedorp, The Netherlands). Three independent experiments were conducted and representative images are shown.

2.6. Phase contrast microscopy

For cytoplasmic vacuolization, A549 cells (1×10^5 cells/mL) were seeded in a 6-well plate and allowed to grow for 24 h. Subsequently cells were treated with the IC_{75} values of each compound during 6 h and images were observed under inverted phase contrast microscope (Axio Observer Z1, Gottingen, Germany). For cell monitoring, A549 cells (1×10^5 cells/mL) were seeded in 96-well microtiter plates and incubated for 24 h to allow cells to attach. Afterwards, they were treated for 24 h with 10 μM of each compound. Then, images were captured following a time course from 0 (before adding drug) to 24 h with a Leica inverted phase-contrast microscope DMIRBE equipped with digital capture software (Leica Microsystems, Wetzlar, Germany).

2.7. Immunofluorescence microscopy

A549 cells (2×10^5 cells/mL) were cultured in a 12-well plate containing glass coverslips and were incubated with the IC_{75} of the studied compounds for 6 h. Cells were then washed twice with 1× PBS and fixed with 4% paraformaldehyde for 20 min. Fixed cells were permeabilized with 0.2% Triton™ X-100 and then blocked with 1% BSA in 1× PBS for 1 h. Cells were incubated overnight at 4 °C with anti-LC3 (1:500 dilution, Cat#PM036) from MBL Interna-

tional Corporation (Woburn, MA, USA) or anti-TOMM20 (1:200 dilution, Cat#612278) from BD Biosciences. In case of using anti-EEA1 (1:1000 dilution, Cat#ab2900) and anti-LAMP1 (1:1000 dilution, Cat#ab24170) both from Abcam (Cambridge, MA, USA) cells were permeabilized with 0.2% Saponin, for 15 min, and then blocked with 0.2% gelatin-20% normal goat serum in 1× PBS for 1 h at room temperature.

Cells were then washed with 1× PBS and incubated with Alexa Fluor™ 555-conjugated donkey anti-mouse (Cat#A31570, Molecular Probes, Eugene, OR, USA) or Alexa Fluor™ 555-conjugated donkey anti-rabbit (Cat#A31572, Molecular Probes) at 1:400 dilution for 1 h at room temperature. At the same time, the nuclear marker TO-PRO™-3 iodide (1:400, Cat#T3605, Molecular Probes) was added. Afterwards, coverslips were washed with 1× PBS and were placed on the slides using Mowiol™ (Sigma-Aldrich). The immunofluorescence images were captured using a Leica TCS-SL filter-free spectral confocal microscope (Leica Microsystems). Representative images from three independent experiments are shown.

2.8. mCherry-Mito7 stable transfection in A549 cells

A549 cells (3×10^5 cells/mL) were seeded in 60 mm plates and allowed to grow up to 80% confluence. Before transfection, growth medium was replaced by Opti-MEM™ medium without FBS (Gibco) and 8 μg of plasmid DNA (mCherry-Mito-7 was a gift from Michael Davidson (Addgene plasmid # 55102) [22] was transfected using 20 μL of lipofectamine™ reagent (Invitrogen, Carlsbad, CA, USA) per condition. After 5 h of transfection, the medium was replaced by complete medium. Stable selection was performed by adding G418 (Calbiochem, La Jolla, CA, USA) to the medium at 800 μg/mL final concentration 2 days after the transfection. After 3 weeks, the brightest cell population was selected by cell sorting using a Moflo Astrios XPD Cell Sorter (Beckman Coulter, Miami, FL, USA). When a stable mCherry-Mito7 overexpressing A549 cell line was established, cells were seeded in a μ-Slide chambered coverslip (Ibidi, Martinsried, Germany), and allowed them to attach and grow during 72 h. Afterwards, cells were exposed to IC_{75} of the studied compounds and a far-red nuclear counterstain, DRAQ5 (Abcam) was applied at a 1:5000 dilution. The images were captured every 20 min for 3 h using a Leica TCS-SL filter-free spectral confocal microscope (Leica Microsystems). Representative images from three independent experiments are shown.

2.9. Transmission electron microscopy

A549 cells (2×10^5 cells/mL) grown in 100 mm plates and were incubated with the IC_{75} of the studied compounds for 6 h. Cells were fixed in a solution containing 2% paraformaldehyde, 2.5% glutaraldehyde in 0.1 M phosphate buffer (pH 7.2) at room temperature for 1 h and then collected as cell pellets. Pellets were kept in a post-fixed solution containing 1% osmium tetroxide, 0.8% potassium ferrocyanide in 0.1 M phosphate buffer (pH 7.2) at 4 °C. After that, cells were dehydrated in graded acetone, embedded in Spurr's resin and cured at 60 °C for 48 h. Semithin sections (1 μm) were cut with a glass knife, mounted on slides, stained with 1% methylene blue and viewed using a light microscope to select the region of interest. Ultrathin sections (60–70 nm) were cut using a diamond knife, mounted on 200 mesh copper grids and double-stained with 2% aqueous uranyl acetate for 30 min and Reynold's lead citrate for 10 min. Specimens were examined in a transmission electron microscope Jeol 1010 (Jeol, Tokyo, Japan) and digital images were acquired using a Gatan Orius SC1000 CCD Digital Camera (Gatan, Inc., Pleasanton, California, USA). Two independent experiments were performed and photographs were taken from at least three different semithin sections from each experiment.

2.10. Mitotracker™ staining

A549 cells (1×10^4 cells/well) were seeded in 8-well sterile μ-Slide (chambered coverslip) (Ibidi), and allowed to attach and grow during 72 h. Then, cells were preincubated with MitoTracker™ Red CMXRox 500 nM during 1 h, washed with 1× PBS and exposed to IC_{75} value of compound **2** for 3 h. Immunofluorescence images were captured using a Leica TCS-SL filter-free spectral confocal microscope (Leica Microsystems). Representative images from three independent experiments are shown.

2.11. Immunoblot analysis

A549 cells (1×10^5 cells/mL) were seeded and allowed to grow for 24 h. Afterwards, they were exposed to compounds (IC_{25}, IC_{50} and IC_{75} values) for 24 or 48 h. Total protein extracts were obtained from cells by the addition of lysis buffer (0.1% SDS, 1% NP-40, 0.5% sodium deoxycholate, 50 mM NaF, 40 mM β-glycerophosphate, 200 μM sodium orthovanadate, 1 mM phenylmethylsulfonyl fluoride, serine and cysteine protease inhibitor cocktail (Roche Mannheim, Germany) in 1× PBS). Protein concentration was determined by BCA protein assay (Pierce, Rockford, IL, USA) using BSA as a standard. After that, 40 μg of protein extracts were separated by 8–15% SDS-polyacrylamide gel electrophoresis and transferred to Immobilon™-P membranes (Millipore, Bedford, MA, USA). Membranes were blocked in 5% dry milk or 5% BSA, both diluted in 1× TBS–Tween (50 mM Tris–HCl pH 7.5, 150 mM NaCl, 0.1% Tween 20) for 1 h and then incubated overnight with primary antibodies, according to the manufacturer's instructions. Antibodies were obtained from the following sources: anti-caspase 3 (Cat#9662), anti-caspase 9 (Cat#9502), anti-PARP (Cat#9542), anti-phospho-p38 MAPK (Thr180/Tyr182, Cat#4511), anti-p38 MAPK (Cat#8690), from Cell Signaling Technology (Beverly, MA, USA); anti-LC3 (Cat#PM036) and anti-p62/SQSTM1 (Cat#PM045) both from MBL International Corporation; anti-actin (I-19, Cat#sc-1616) from Santa Cruz Biotechnology (Santa Cruz, CA, USA) and anti-vinculin (Cat#V-4505) from Sigma-Aldrich. Antibody binding was detected with goat anti-mouse IgG-HRP (Cat#sc-2005), goat anti-rabbit IgG-HRP (Cat#sc-2004) and donkey anti-goat IgG-HRP (Cat#sc-2020) all from Santa Cruz Biotechnology, and the ECL detection kit (Amersham, Buckinghamshire, UK). Actin or vinculin was used as gel loading controls. Results shown are representative of Western blot data obtained from at least three independent experiments with similar observations. Images were captured on an Image Quant™ LAS 500 (GE Healthcare Little Chalfont, UK) and band densitometries were retrieved using the software ImageJ version 1.43u software (National Institutes of Health, Bethesda, Maryland, USA).

2.12. Statistical analyses

Results are expressed as the mean ± SEM of at least three independent experiments. One-way ANOVAs were carried out with the Statgraphics centurion statistical package and post hoc Tukey analyses were performed. Statistically significant differences, $p < 0.05$ and $p < 0.01$, are represented by * and **, respectively.

3. Results

3.1. Compounds cytotoxic effects on cancer cell lines and cancer stem cells

The effect on cell viability of several tambjamine analogues (Fig. 1a), selected from a previous screening [19], was evaluated in different lung cancer cell lines representative of the four major

histological subtypes (A549, adenocarcinoma; SW900, squamous cell carcinoma; H460, large cell carcinoma; DMS53, small-cell carcinoma) (Fig. 1b). Cell viability was measured by the MTT assay and a significant decrease (more than 50%) was observed after 24 h with 10 μM of all the tested compounds. From these experiments two derivatives (compounds **2** and **7**) were selected as the most potent compounds. Then, dose-response experiments were conducted in A549 cells and compared to a positive control, cisplatin as a current chemotherapeutic treatment in lung cancer. The IC_{50} values obtained for compound **2** and **7** were 3.38 ± 0.98 and 1.67 ± 0.29 μM and IC_{75} values were 4.72 ± 0.76 and 3.57 ± 0.49 μM, respectively; while IC_{50} value for cisplatin (CDDP) was more than 200 μM (Fig. 1c).

Cell viability after treatment with the most potent compound, tambjamine **2**, was also evaluated in cancer stem cells (CSC) derived from patients or isolated from cancer cell lines (Fig. 1d). The derived tumour spheres were deeply characterized, showing enrichment in stem cell surface markers as well as great tumorigenic properties in scid mice transplantation experiments (see Supplementary information Ref. [20]). Our results show a significant decrease in cell viability, either in CSC derived from cell lines (A549 and SW900) or derived from tumour patient samples (FIS302 and FIS303).

3.2. Tambjamine derivatives are effective anion transporters that deregulate lysosomal pH

The activity as transmembrane anion carriers of the two most cytotoxic compounds, **2** and **7**, was assayed in model POPC liposomes. Chloride loaded liposomes were suspended in an isotonic chloride free solution, and chloride efflux facilitated by these compounds was monitored using a chloride selective electrode. At the end of the experiments, vesicles were lysed by the addition of detergent and the final electrode reading considered as 100% chloride release. Quantification of the transport activity was carried out by repeating the experiments using several concentrations of the studied compounds and performing hill analyses of the results (Fig. 2a and b). The resulting EC_{50} value represents the amount of compound needed to release 50% of the encapsulated chloride in the time scale of the experiments (300 s). The EC_{50} values obtained for **2** and **7** were 50 nM and 60 nM respectively in the assay involving $NaNO_3$ as external solution and 240 nM and 880 nM respectively in the assay involving $NaHCO_3$ as external solution. The impact on the EC_{50} values of the external anion is consistent with an exchange mechanism in which chloride efflux from the interior of the vesicle is accompanied by influx of the external anion, thus precluding the formation of an electrochemical gradient. The relative higher lipophilicity of nitrate compared to bicarbonate makes this latter anion more difficult to extract into the membrane hydrophobic core and hence the higher EC_{50} observed. This transport mechanism has been studied by us in detail and the result demonstrates that **2** and **7** are very potent anionophores promoting effective transmembrane anion transport in vesicles at low loadings [19].

On the other hand, lysosomal pH modifications in A549 cells were analysed using acridine orange staining [23]. This dye accumulates into acidic organelles, like lysosomes or late endosomes, and emits orange fluorescence as a result of its protonation under

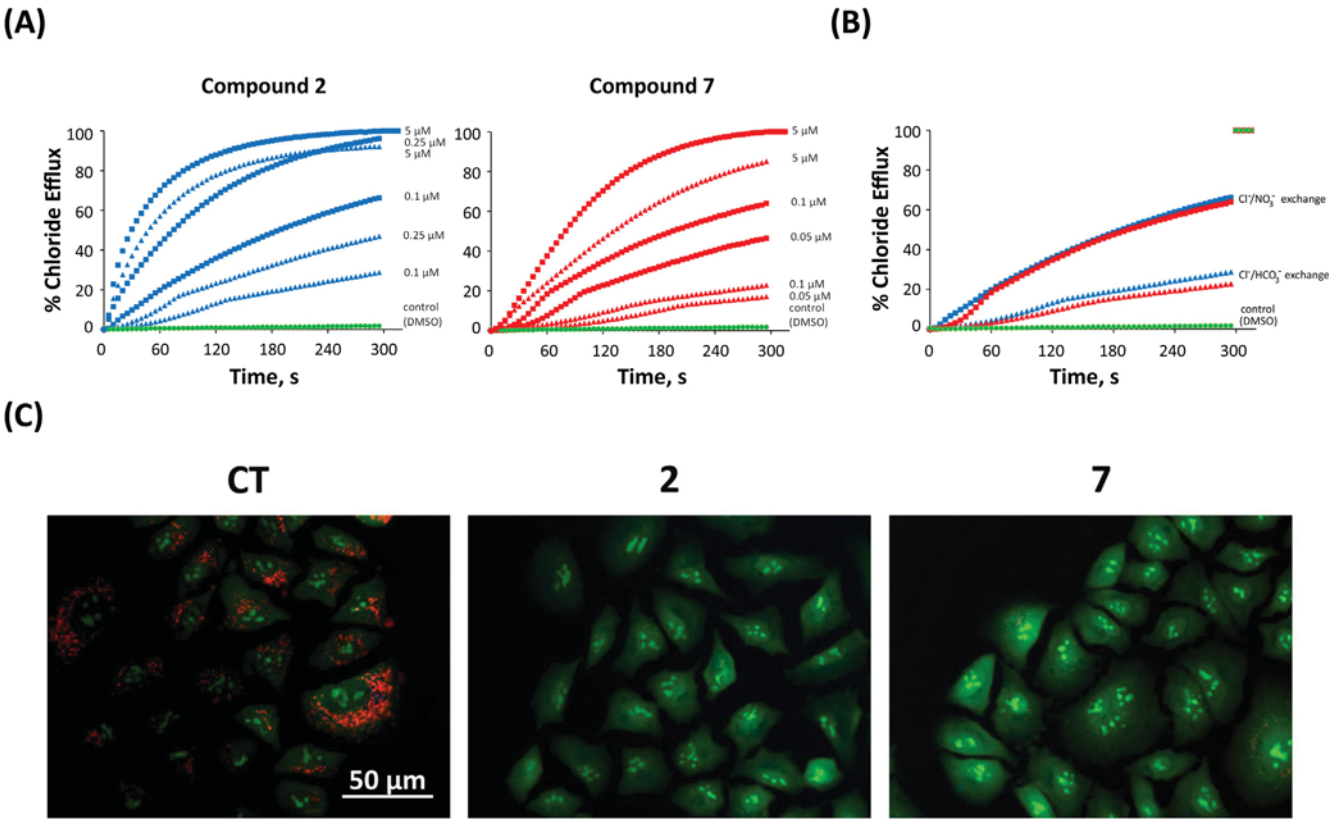

Fig. 2. Potent transmembrane anion transport activity of tambjamine analogues in liposomes and cellular models. (A) Chloride efflux upon addition of compound **2** or **7** at different concentrations to vesicles composed of POPC. Squared symbols correspond to the results obtained using $NaNO_3$ as external buffer, triangular symbols correspond to the results obtained using $NaHCO_3$/Na_2SO_4 as external buffer. Each trace represents an average of at least three different experiments (See Section 2.2. for details). (B) Impact of external buffer ($NaNO_3$, squared symbols, or $NaHCO_3$/Na_2SO_4, triangular symbols) in the chloride efflux promoted by **2** or **7** (0.1 μM, blue and red symbols, respectively). (C) Acridine orange staining on A549 cells treated with vehicle (DMSO), 10 μM compound **2** or **7** for 1 h. Images are representative of three independent experiments. (For interpretation of the references to colour in this figure legend, the reader is referred to the web version of this article.)

these acidic pH conditions, whilst it emits green fluorescence in other parts of the cell, as observed in control cells (Fig. 2c). When A549 cells were treated with IC_{50} values of compounds **2** or **7** for 1 h, the orange fluorescence in the vesicle compartments disappeared, indicating an increase in the pH of these organelles. This result is in agreement with the ionophoric activity of these compounds facilitating the transmembrane transport of anions such as bicarbonate across cellular membranes and this pH alteration should result in lysosomal dysfunction.

3.3. Cytoplasmic vacuolization due to mitochondrial swelling induced by tambjamine analogues

After treatment with compounds **2** or **7**, massive cytoplasmic vacuolization was observed by phase contrast microscopy after 6 h exposure with their IC_{75} values (Fig. 3a). To better understand this phenomenon, cells were monitored during 24 h after 10 μM treatment with each compound (Fig. 3b). Cytoplasmic vacuolization was observed as soon as 3 h of compounds addition and was maintained up to 24 h. In the case of compound **2**, cell death due to cellular swelling and/or burst was observed within the 24 h period. This is indicative of necrotic cell death reflecting the potent cytotoxic activity of this compound.

In order to determine which cellular organelle was undergoing this vacuolization process, several subcellular markers were used for immunofluorescence detection (Figs. 4 and 5). First of all, the autophagosomal marker LC3 was evaluated and, although a high increase on protein levels was observed, it did not colocalize with the vacuoles (Fig. 4a). Then, the lysosomal marker LAMP1 and the early endosomal marker EEA1 were used and different protein localization was observed in treated cells, but again neither colocalized with the vacuolated organelle (Fig. 4b and c). Moreover, the hydrophilic polysaccharide dextran-red was administered to treated cells to monitor macro/pinocytosis, but we did not obtain vesicle staining (data not shown). Finally, a mitochondrial protein called TOMM20 was employed and proved to stain the membranes of the vacuoles, indicating that mitochondrial swelling was occurring after compound treatment (Fig. 5a) and ruling out vacuolization of autophagosomes, lysosomes or endosomes.

To further characterize that the vacuolated organelle was mitochondria, a plasmid with the mitochondrial targeting sequence from subunit VIII of human cytochrome *c* oxidase was transfected into cells in order to monitor mitochondria. Control cells showed typical red mitochondrial staining, whereas in cells treated with compound **2**, mitochondrial swelling was clearly observed (Fig. 5b). Transmission electron micrographs were obtained from control and cells treated with compounds **2** or **7** to analyse these results in deep, and mitochondrial swelling was also observed (black arrows, Fig. 5c). Moreover, many autophagy-related structures such as autophagosomes, autolysosomes and dense lysosomes are also visualized in treated cells. This process was also studied using MitoTracker™ Red CMXRos, a fluorescent dye whose accumulation depends on mitochondrial membrane potential [24], to track mitochondria (Fig. 6). Control cells showed typical filamentous mitochondria, but in treated cells mitochondria gradually swelled to a larger size structure and finally lost fluorescence. This indicates that mitochondrial membrane potential is lost during the swelling process after compound treatment.

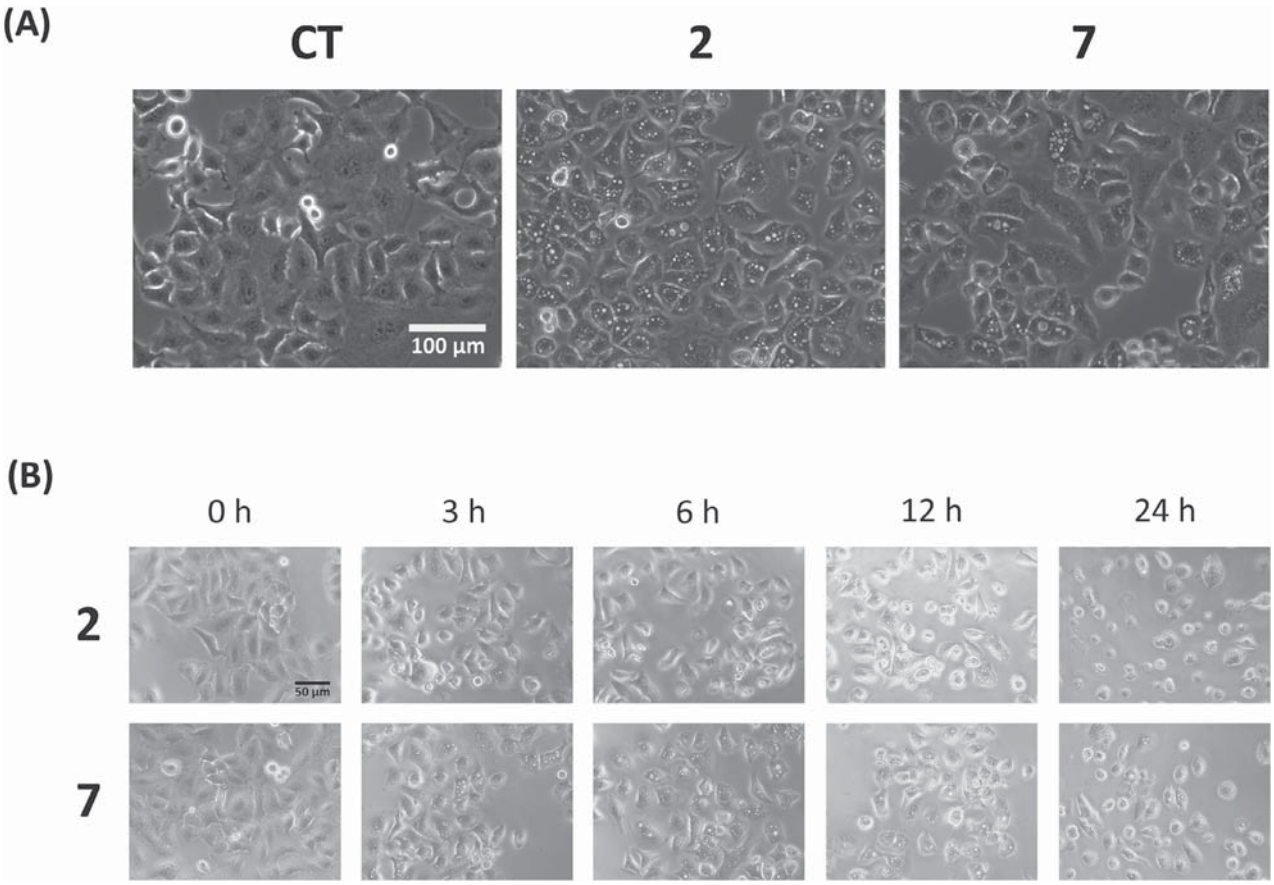

Fig. 3. Cytoplasmic vacuolization induced by tambjamine analogues. (A) Phase contrast microscopy images of A549 cells treated with IC_{75} of compounds **2** or **7** for 6 h. (B) Time-course photographs of A549 cells treated with 10 μM of compound **2** or **7** during 24 h. Scale bars 100 μm (A) and 50 μm (B). Images are representative of three independent experiments.

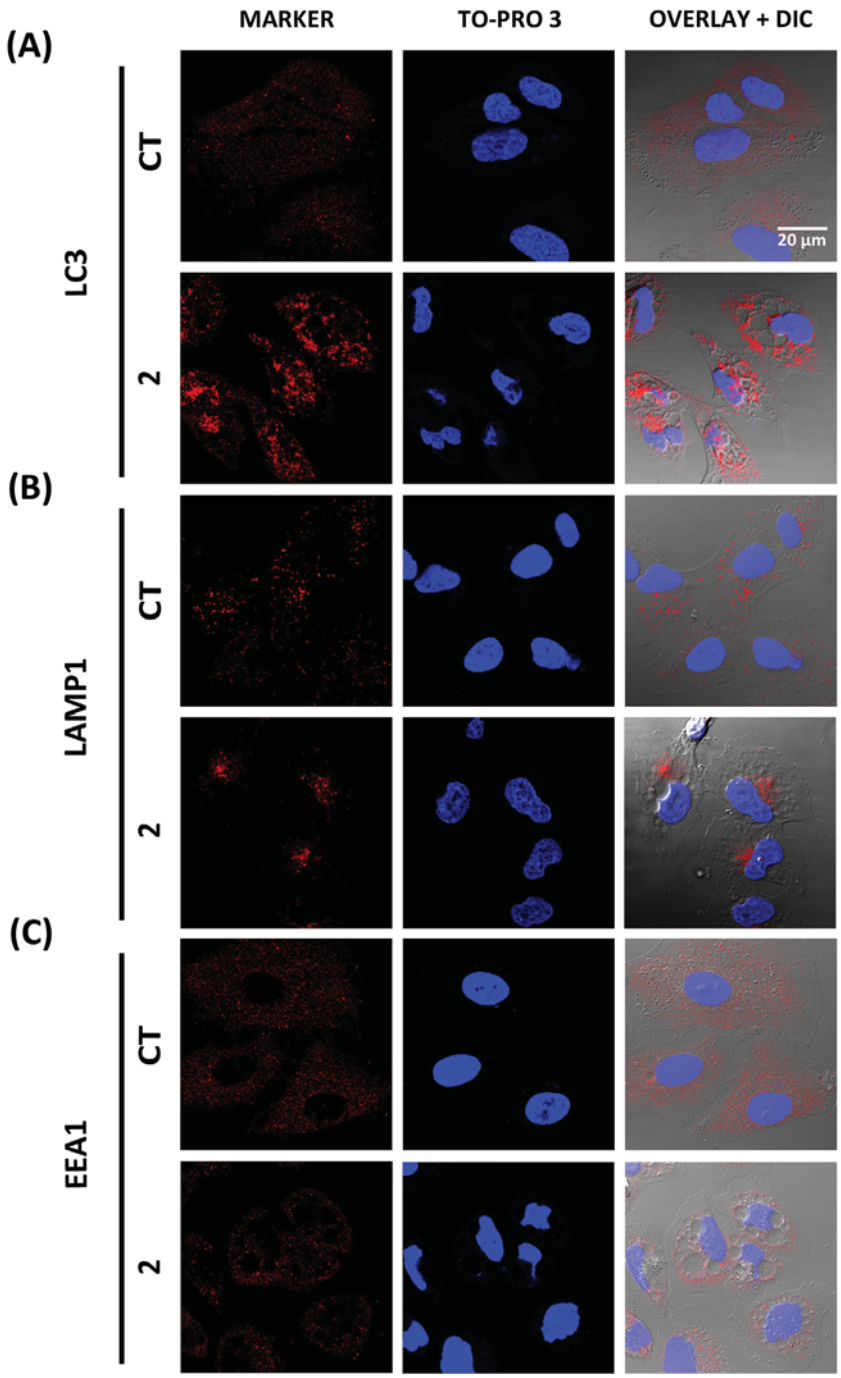

Fig. 4. Tambjamine analogues treatment did not induce swelling of autophagosomes, lysosomes or early endosomes. Immunofluorescence in A549 cells treated with IC_{75} of compound **2** for 6 h. It was performed with different antibodies that recognize several cellular organelles (red) and were compared to the distribution of cytoplasmic vacuoles observed by phase contrast microscopy. (A) Distribution of the autophagosomal marker LC3, (B) distribution of lysosomal marker LAMP1 (C) distribution of the early endosome marker EEA1. The nucleus was counterstained with TO-PRO™-3 (blue). Scale bar 20 µm. Images are representative of at least three independent experiments. (For interpretation of the references to colour in this figure legend, the reader is referred to the web version of this article.)

3.4. Molecular cell death mechanisms

Finally, to understand the molecular cell death mechanisms triggered by these compounds, cells were treated with compound **2** and several proteins involved in stress response, autophagy and apoptosis were analysed. Activation of p38 Mitogen-Activated Protein Kinase (MAPK) in A549 cells was observed in a dose-response manner (Fig. 7a). This signal has been reported to activate apoptosis after some stresses. After 24 h of treatment with high concentrations of compound **2**, we were able to observe a small activation of caspase 9 and 3, as well as PARP cleavage (Fig. 7b). Likewise, small activation of apoptotic markers was observed after 48 h treatment. To further analyse whether this apoptotic activation was involved in the cytotoxic effect induced by tambjamines, a pan-caspase inhibitor (10 µM Z-VAD-FMK) was added before treatment with compound **2**. Under these conditions, cell viability was not recovered (data not shown). Therefore, this result suggested that although apoptosis is being triggered by these tambjamine analogues, this process is not entirely responsible for the cytotoxic effect induced by these compounds.

This led us to study the autophagic process after compound treatment and to investigate whether it was involved in the

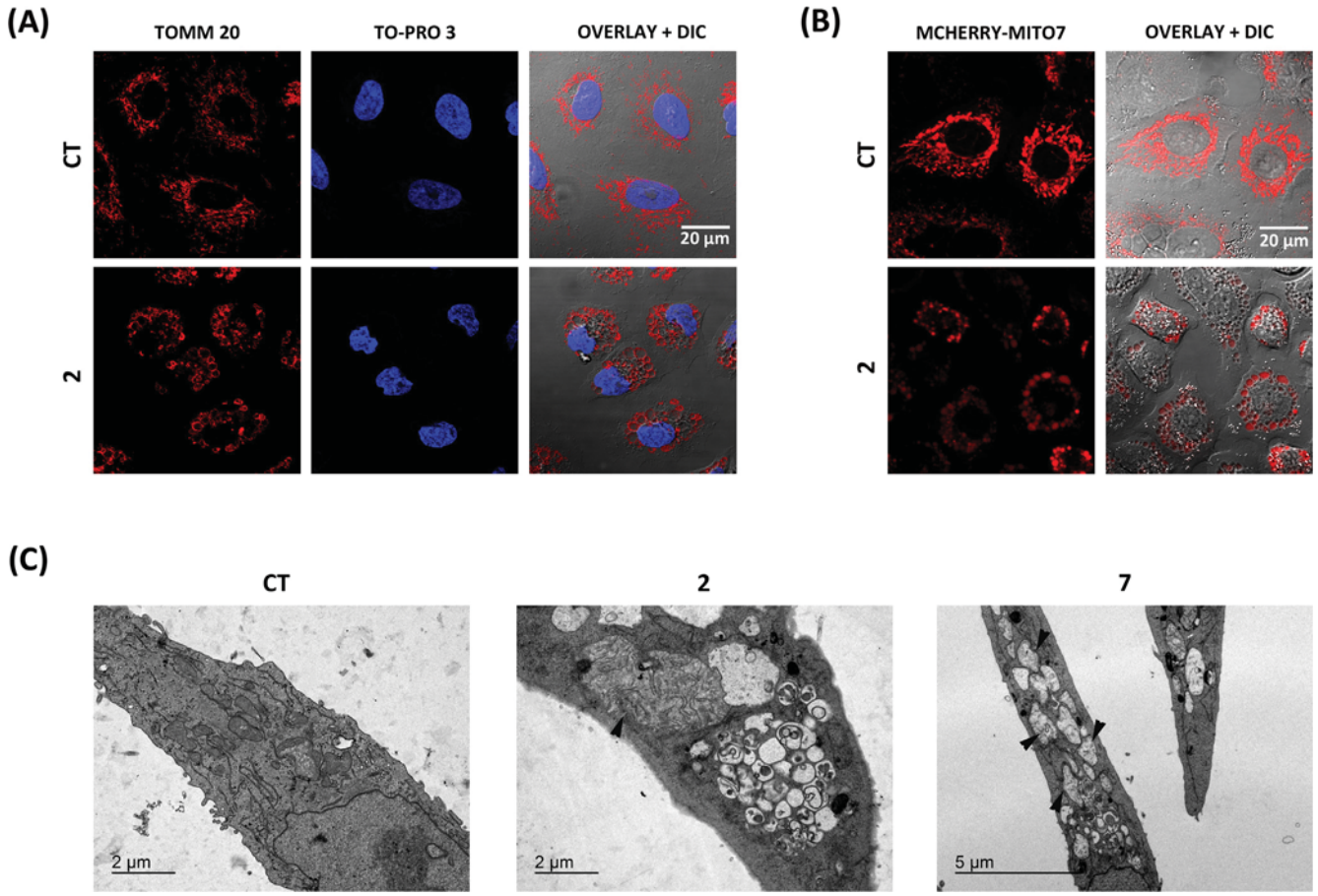

Fig. 5. Mitochondrial swelling after tambjamine analogues treatment. (A) Immunofluorescence of mitochondrial marker TOMM20 in A549 cells treated with IC_{75} of compound **2** for 6 h. The nucleus was counterstained with TO-PRO™-3 (blue). (B) A549 cells overexpressing mCherry-Mito7 plasmid, which targets mitochondria (red), were treated with IC_{75} of compound **2** for 3 h. Mitochondrial staining was compared to vacuolization observed in phase contrast photographs. Scale bar 20 µm. (C) Transmission electron micrographs from control and treated A549 cells with compound **2** and **7** for 6 h. Mitochondrial swelling (black arrows) as well as double-membrane vesicles accumulation (autophagosomes and autolysosomes) were observed. Scale bar 2 and 5 µm. Images are representative of at least three independent experiments. (For interpretation of the references to colour in this figure legend, the reader is referred to the web version of this article.)

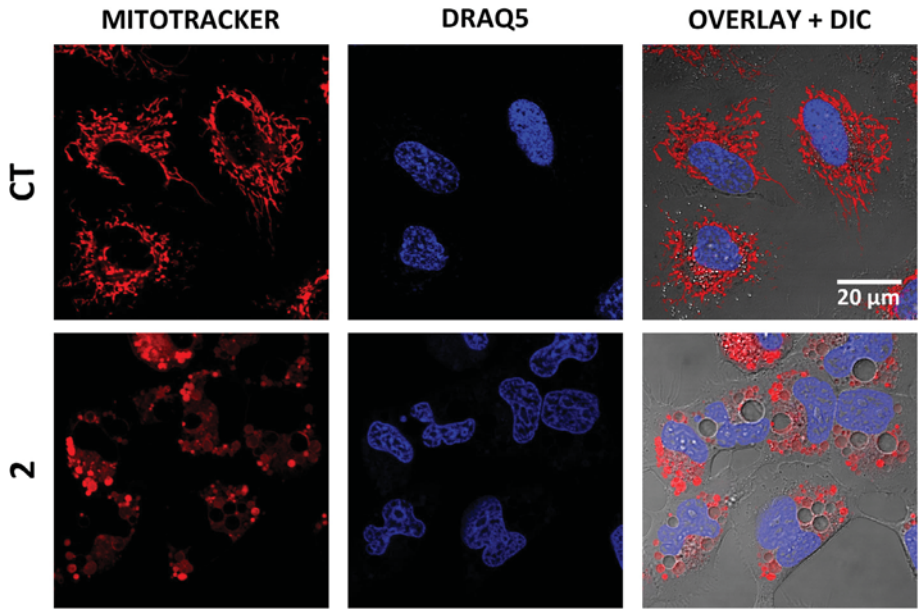

Fig. 6. Mitochondrial swelling and loss of mitochondrial membrane potential after tambjamine analogues treatment. Confocal images of A549 cells treated with 500 nM MitoTracker™ Red CMXRos during 1 h and then compound **2** for 3 h. Mitochondria with normal membrane potential are stained in red. Nucleus was counterstained with DRAQ5 (blue). Scale bar 20 µm. Images are representative of at least three independent experiments. (For interpretation of the references to colour in this figure legend, the reader is referred to the web version of this article.)

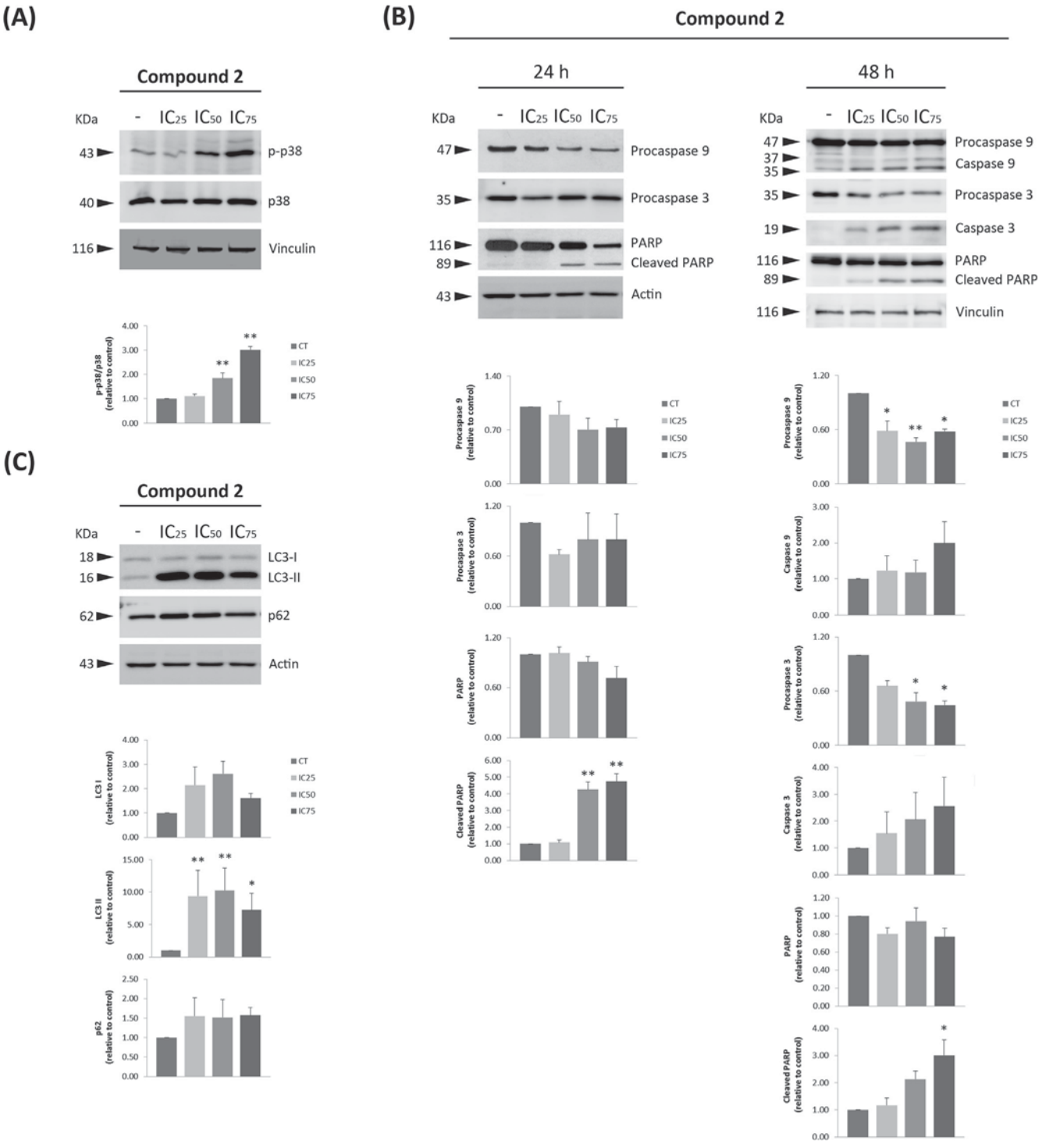

Fig. 7. p38 MAPK activation, apoptosis induction and autophagy blockade after tambjamine analogues treatment. A549 cells were treated with compound **2** IC_{25}, IC_{50} and IC_{75} values for 24 h and protein extracts were used to determine changes in protein levels. Detection and quantification of: (A) the stress kinase p38 MAPK and its phosphorylation levels; (B) apoptotic markers caspase 9, 3 and PARP substrate and (C) autophagic markers LC3II and p62. Protein levels were normalized with their respective loading controls (actin or vinculin) in each blot. Fold changes in protein expression levels were quantified and referred to non-treated cells. Data show the mean ± SEM of three independent experiments. Statistically significant results are indicated as $^{*}p < 0.05$ and $^{**}p < 0.01$.

observed cytotoxicity. At very low concentrations of compound **2** (IC_{25}), an impressive appearance of the lipidated LC3 form (LC3-II), indicative of autophagosome formation (Fig. 7c), was detected. On the other hand, p62, a protein that is itself degraded by autophagy, was not degraded but accumulated after treatment, indicating a blockade of the autophagic flux. To elucidate whether autophagy was involved in the induced cell death, an inhibitor of autophagosomes formation (5 mM 3-MA) was added prior compound administration (data not shown). Cell viability was not recovered after 3-MA administration, suggesting that autophagosomes formation and their accumulation are not crucial for the cytotoxic effect induced by tambjamines. Finally, at higher doses and 24 h of treatment, tambjamines also provoked cytoplasmic swelling, which finally led to plasma membrane breakdown

indicative of necrosis, as observed in the phase contrast images (Fig. 3b) and the Supplementary video.

4. Discussion

Diverse synthetic tambjamine analogues have recently shown potent anticancer activity in a panel of cancer cell lines, including human melanoma, lung carcinoma, colorectal adenocarcinoma and mammary adenocarcinoma cells [19,20]. In this study, we extend the results obtained with those compounds bearing 4-alkoxy-2,2′-bipyrrole moieties [19] to several lung cancer cell lines and CSC, as well as characterize in deep for the first time the cellular and molecular events that are participating in the cell death induced by these potent compounds.

Cell viability was significantly reduced by most of the tested compounds in all human lung cancer cell lines studied, and compound **2** showed to be especially potent against patient-derived CSC. This tumour subpopulation possesses tumour-initiating and self-renewal capacities, and contributes to acquired chemotherapy resistance in cancer [25], thus these results are very promising for lung cancer treatment and the prevention of tumour recurrences. In this view, other anionophores such as the recently reported 2-pyrrolylindole tambjamine analogues or the cation selective ionophore salinomycin, also induce CSC-specific toxicity [20,26], indicating that the application of these kind of compounds might be a very promising therapy.

Once the cells internalize these synthetic tambjamine analogues, several cellular processes occur, converging in the potent cytotoxic effect observed. On one hand, a huge cytoplasmic vacuolization was detected after compound treatment, which was due to mitochondrial swelling, as demonstrated by several specific markers of this organelle. Moreover, after significant organelle swelling, loss of mitochondrial membrane potential was induced by compound **2**. Mitochondria in eukaryotic cells are the essential machinery to provide energy with an aerobic environment. It has previously been described in cells with acute cellular injury that mitochondrial depolarization and mitochondrial membrane permeabilization lead to a large amplitude swelling and cellular ATP depletion [27,28]. Therefore, mitochondrial dysfunction observed after tambjamine analogues treatment may cause an energetic failure contributing to their cytotoxic effect.

Autophagy is a catabolic process whereby cellular components are enclosed in double-membrane vesicles referred to as autophagosomes, targeting them for lysosomal degradation. This process serves as an essential cytoprotective response to pathologic stresses [29]. Accumulation of defective mitochondria triggers its selective degradation, process known as mitochondrial autophagy or mitophagy, maintaining a healthy population of these organelles [30,31]. A very significant amount of the autophagosomal marker LC3II protein accumulates after treatment with tambjamine analogues, even at very low concentrations. This indicates that the process of autophagy is being triggered by the treatment with these tambjamine analogues and that the induced mitochondrial damage may launch the process of mitophagy in order to remove damaged organelles. This phenomenon is frequently found as a result of mitochondrial stress, such is the case of treatment with the mitochondrial chain uncoupler carbonyl cyanide m-chlorophenylhydrazone (CCCP)[32], or salinomycin, an ionophore which affects mitochondrial potential [33]. On the other hand, it has recently been reported that pHi changes modulate both autophagy and mitophagy [34], thus the changes in cellular pH caused by these compounds could also be contributing to trigger this pathway [20].

The loss of the typical acridine orange fluorescence in acidic organelles after exposure to our compounds indicates lysosomal alkalization. This increase in lysosomal pH is consistent with an anion carrier activity across cellular membranes, similarly to that observed in model liposomes. Interestingly, it has recently been reported that obatoclax, another anionophore related to the prodiginine family which has been evaluated in clinical trials for different cancer conditions, rapidly localizes to the lysosomes and also induces lysosomal alkalization [35,36].

Lysosomes contain many different types of hydrolytic enzymes that usually exert their maximal enzymatic activity at low pH [37]. Typically, an increase in lysosomal pH could derive from H^+ leakage, a defective proton pump or lysosomal permeabilization [38]. This could lead to a failure in their proper functioning, resulting in blockade of autophagy [39,40]. After tambjamine analogues treatment, increase in the lysosomal pH derived from lysosomal membrane permeabilization may inactivate its hydrolytic enzymes and therefore it may block autophagy. This feature mainly occurs because this organelle is essential in the final step of the autophagic process, wherein autophagosomes fuse with lysosomes and subsequent protein digestion occurs [41]. The autophagic substrate, p62, also known as sequestosome 1 (SQSTM1), binds ubiquitinated proteins for subsequent degradation in lysosomes, where it is also degraded [42]. Our results show that there is no p62 degradation, indicating an impairment in the autophagic flux and consequent accumulation of unprocessed autophagosomes or autolysosomes [43]. Moreover, the autophagy inhibitor 3-MA, which inhibits autophagy by blocking autophagosomes formation via the inhibition of type III phosphatidylinositol 3-kinases (PI3K), is not able to reverse the cytotoxic effect induced by tambjamines. Thus this autophagy might be contributing to the cytotoxic effect, but it is not responsible for it. Nevertheless, mitochondrial dysfunction along with a defect in autophagy catabolism due to lysosomal deacidification might be detrimental to tumour cells since they produce low rates of ATP and impaired recycling of nutrients for energy production, as well as an imbalance in vesicular biogenesis and turnover. This cellular stress is reflected by p38 MAPK activation, which may initiate apoptosis [44], although again this process is not crucial for the observed cytotoxicity elicited by these compounds. Therefore, the imbalance in cellular ion homeostasis that triggers mitochondrial dysfunction and lysosomal deacidification may be inducing cell death by necrosis after tambjamine analogues treatment. In this regard, the lysosomal permeabilization induced by obatoclax in apoptosis-resistant anaplastic thyroid cells has been demonstrated to be sufficient to induce necrosis in this resistant model, representing an interesting therapeutic approach [36].

Overall, these new tambjamine analogues show promising anticancer properties in lung cancer and could represent a good therapeutic option for apoptosis-resistant tumours. These results shed light into the cellular and molecular mechanisms resulting from the action of these compounds. Lysosomal and mitochondrial dysfunction led to necrosis as the main cell death mechanism responsible for the cytotoxicity of these compounds, which might be shared by other active small molecule anionophores.

Conflict of interest

The authors declare no conflict of interest.

Acknowledgements

This work was supported by a grant from the Spanish government and the EU (FIS PI13/00089), a grant from La Marató de TV3 Foundation (20132730), Consejería de Educación de la Junta de Castilla y León (BU340U13 and BU092U16). The authors would

like to thank Dr. Jantus-Lewintre and Dr. Calabuig-Fariñas for their assistance with cancer stem cell cultures. Moreover, the authors also thank Benjamín Torrejón from CCiT (Centres Científics i Tecnològics, Campus de Bellvitge, Universitat de Barcelona) for his technical support. E.H. thanks the Junta de Castilla y León (Consejería de Educación) and Fondo Social Europeo for a PIRTU contract.

Appendix A. Supplementary data

Supplementary data associated with this article can be found, in the online version, at http://dx.doi.org/10.1016/j.bcp.2016.11.022.

References

[1] C.A. Hübner, T.J. Jentsch, Ion channel diseases, Hum. Mol. Genet. 11 (2002) 2435–2445.
[2] A. Becchetti, Ion channels and transporters in cancer. 1. Ion channels and cell proliferation in cancer, Am. J. Physiol. Cell Physiol. 301 (2011) C255–C265.
[3] V. Lehen'kyi, G. Shapovalov, R. Skryma, N. Prevarskaya, Ion channels and transporters in cancer. 5. Ion channels in control of cancer and cell apoptosis, Am. J. Physiol. Cell Physiol. 301 (2011) C1281–C1289.
[4] B.A. Webb, M. Chimenti, M.P. Jacobson, D.L. Barber, Dysregulated pH: a perfect storm for cancer progression, Nat. Rev. Cancer 11 (2011) 671–677.
[5] J. Ferlay, I. Soerjomataram, M. Ervik, R. Dikshit, S. Eser, C. Mathers, GLOBOCAN 2012 v1.0, Cancer Incidence and Mortality Worldwide: IARC CancerBase No. 11, International Agency for Research on Cancer, Lyon, France, 2013. Available from: <http://globocan.iarc.fr> (accessed on 25/07/2016).
[6] S. Cooper, S.G. Spiro, Small cell lung cancer: treatment review, Respirology 11 (2006) 241–248.
[7] R. Rosell, F. Cecere, M. Santarpia, N. Reguart, M. Taron, Predicting the outcome of chemotherapy for lung cancer, Curr. Opin. Pharmacol. 6 (2006) 323–331.
[8] N. Busschaert, P.A. Gale, Small-molecule lipid-bilayer anion transporters for biological applications, Angew. Chem. Int. Ed. 52 (2013) 1374–1382.
[9] P.A. Gale, R. Pérez-Tomás, R. Quesada, Anion transporters and biological systems, Acc. Chem. Res. 46 (2013) 2801–2813.
[10] E. Llagostera, V. Soto-Cerrato, B. Montaner, R. Perez-Tomas, Prodigiosin induces apoptosis by acting on mitochondria in human lung cancer cells, Ann. N. Y. Acad. Sci. 1010 (2003) 178–181.
[11] R. Pérez-Tomás, B. Montaner, E. Llagostera, V. Soto-Cerrato, The prodigiosins, proapoptotic drugs with anticancer properties, Biochem. Pharmacol. 66 (2003) 1447–1452.
[12] V. Soto-Cerrato, E. Llagostera, B. Montaner, G.L. Scheffer, R. Perez-Tomas, Mitochondria-mediated apoptosis operating irrespective of multidrug resistance in breast cancer cells by the anticancer agent prodigiosin, Biochem. Pharmacol. 68 (2004) 1345–1352.
[13] N.R. Williamson, P.C. Fineran, T. Gristwood, S.R. Chawrai, F.J. Leeper, G.P. Salmond, Anticancer and immunosuppressive properties of bacterial prodiginines, Future Microbiol. (2007).
[14] J.L. Sessler, L.R. Eller, W.S. Cho, S. Nicolaou, A. Aguilar, J.T. Lee, et al., Synthesis, anion-binding properties, and in vitro anticancer activity of prodigiosin analogues, Angew. Chem. Int. Ed. 44 (2005) 5989–5992.
[15] N. Busschaert, C. Caltagirone, W. Van Rossom, P.A. Gale, Applications of supramolecular anion recognition, Chem. Rev. 115 (2015) 8038–8155.
[16] M. Carbone, C. Irace, F. Costagliola, F. Castelluccio, G. Villani, G. Calado, et al., A new cytotoxic tambjamine alkaloid from the Azorean nudibranch Tambja ceutae, Bioorg. Med. Chem. Lett. 20 (2010) 2668–2670.
[17] B.C. Cavalcanti, H.V. Júnior, M.H. Seleghim, R.G. Berlinck, G.M. Cunha, M.O. Moraes, et al., Cytotoxic and genotoxic effects of tambjamine D, an alkaloid isolated from the nudibranch Tambja eliora, on Chinese hamster lung fibroblasts, Chem-Biol. Interact. 174 (2008) 155–162.
[18] P.I. Hernández, D. Moreno, A.A. Javier, T. Torroba, R. Pérez-Tomás, R. Quesada, Tambjamine alkaloids and related synthetic analogs: efficient transmembrane anion transporters, Chem. Commun. 48 (2012) 1556–1558.
[19] E. Hernando, V. Soto-Cerrato, S. Cortes-Arroyo, R. Perez-Tomas, R. Quesada, Transmembrane anion transport and cytotoxicity of synthetic tambjamine analogs, Org. Biomol. Chem. 12 (2014) 1771–1778.
[20] V. Soto-Cerrato, P. Manuel-Manresa, E. Hernando, S. Calabuig-Fariñas, A. Martinez-Romero, V.c. Fernández-Dueñas, et al., Facilitated anion transport induces hyperpolarization of the cell membrane that triggers differentiation and cell death in cancer stem cells, J. Am. Chem. Soc. 137 (2015) 15892–15898.
[21] M.B. Hansen, S.E. Nielsen, K. Berg, Re-examination and further development of a precise and rapid dye method for measuring cell growth/cell kill, J. Immunol. Methods 119 (1989) 203–210.
[22] S.G. Olenych, N.S. Claxton, G.K. Ottenberg, M.W. Davidson, The fluorescent protein color palette, Curr. Protoc. Cell Biol. (2007) (Chapter 21, Unit 21.5).
[23] A. Allison, M. Young, Vital staining and fluorescence microscopy of lysosomes, Lysosomes Biol. Pathol. 2 (1969) 600–628.
[24] W. Pendergrass, N. Wolf, M. Poot, Efficacy of MitoTracker Green™ and CMXRosamine to measure changes in mitochondrial membrane potentials in living cells and tissues, Cytometry Part A 61 (2004) 162–169.
[25] P. Valent, D. Bonnet, R. De Maria, T. Lapidot, M. Copland, J.V. Melo, et al., Cancer stem cell definitions and terminology: the devil is in the details, Nat. Rev. Cancer 12 (2012) 767–775.
[26] P.B. Gupta, T.T. Onder, G. Jiang, K. Tao, C. Kuperwasser, R.A. Weinberg, et al., Identification of selective inhibitors of cancer stem cells by high-throughput screening, Cell 138 (2009) 645–659.
[27] J.J. Lemasters, A.-L. Nieminen, T. Qian, L.C. Trost, S.P. Elmore, Y. Nishimura, et al., The mitochondrial permeability transition in cell death: a common mechanism in necrosis apoptosis and autophagy, Biochim. Biophys. Acta, Bioenerg. 1366 (1998) 177–196.
[28] J.-S. Kim, L. He, J.J. Lemasters, Mitochondrial permeability transition: a common pathway to necrosis and apoptosis, Biochem. Biophys. Res. Commun. 304 (2003) 463–470.
[29] L. Murrow, J. Debnath, Autophagy as a stress response and quality control mechanism—implications for cell injury and human disease, Annu. Rev. Pathol. 8 (2013) 105.
[30] D.A. Kubli, Å.B. Gustafsson, Mitochondria and mitophagy the yin and yang of cell death control, Circ. Res. 111 (2012) 1208–1221.
[31] I. Kim, S. Rodriguez-Enriquez, J.J. Lemasters, Selective degradation of mitochondria by mitophagy, Arch. Biochem. Biophys. 462 (2007) 245–253.
[32] K.-Y. Kwon, B. Viollet, O.J. Yoo, CCCP induces autophagy in an AMPK-independent manner, Biochem. Biophys. Res. Commun. 416 (2011) 343–348.
[33] J.R. Jangamreddy, S. Ghavami, J. Grabarek, G. Kratz, E. Wiechec, B.-A. Fredriksson, et al., Salinomycin induces activation of autophagy, mitophagy and affects mitochondrial polarity: differences between primary and cancer cells, Biochim. Biophys. Acta, Mol. Cell Res. 2013 (1833) 2057–2069.
[34] A.V. Berezhnov, M.P. Soutar, E.I. Fedotova, M.S. Frolova, H. Plun-Favreau, V.P. Zinchenko, et al., Intracellular pH modulates autophagy and mitophagy, J. Biol. Chem. (2016), http://dx.doi.org/10.1074/jbc.M115.691774.
[35] V.A. Stamelos, N. Fisher, H. Bamrah, C. Voisey, J.C. Price, W.E. Farrell, et al., The BH3 mimetic obatoclax accumulates in lysosomes and causes their alkalinization, PLoS ONE 11 (2016) e0150696.
[36] D. Champa, A. Orlacchio, B. Patel, M. Ranieri, A.A. Shemetov, V.V. Verkhusha, et al., Obatoclax kills anaplastic thyroid cancer cells by inducing lysosome neutralization and necrosis, Oncotarget 5 (2016).
[37] J. Coffey, C. de Duve, The digestion of proteins by extracts of rat liver lysosomes, J. Biol. Chem. 243 (1968) 3255–3263.
[38] P. Boya, Lysosomal function and dysfunction: mechanism and disease, Antioxid. Redox Signal. 17 (2012) 766–774.
[39] B. Levine, G. Kroemer, Autophagy in the pathogenesis of disease, Cell 132 (2008) 27–42.
[40] M. Mrschtik, K.M. Ryan, Lysosomal proteins in cell death and autophagy, FEBS J. 282 (2015) 1858–1870.
[41] G. Kroemer, M. Jäättelä, Lysosomes and autophagy in cell death control, Nat. Rev. Cancer 5 (2005) 886–897.
[42] G. Bjørkøy, T. Lamark, S. Pankiv, A. Øvervatn, A. Brech, T. Johansen, Monitoring autophagic degradation of p62/SQSTM1, Methods Enzymol. 452 (2009) 181–197.
[43] M. Komatsu, Y. Ichimura, Physiological significance of selective degradation of p62 by autophagy, FEBS Lett. 584 (2010) 1374–1378.
[44] T. Wada, J.M. Penninger, Mitogen-activated protein kinases in apoptosis regulation, Oncogene 23 (2004) 2838–2849.

ANNEX III

-"Facilitated anion transport induces hyperpolarization of the cell membrane that triggers differentiation and cell death in cancer stem cells". Journal of the American Chemical Society, 2015.

-"Novel indole-based tambjamine-analogues induce apoptotic lung cancer cell death through p38 mitogen-activated protein kinase activation". Molecular Cancer Therapeutics, 2017.

Collaboration articles in which I have participated characterizing the mechanisms of action at cellular and molecular level of indole-based tambjamines analogues.

JACS
JOURNAL OF THE AMERICAN CHEMICAL SOCIETY

Article

pubs.acs.org/JACS

Facilitated Anion Transport Induces Hyperpolarization of the Cell Membrane That Triggers Differentiation and Cell Death in Cancer Stem Cells

Vanessa Soto-Cerrato,[†,●] Pilar Manuel-Manresa,[†,●] Elsa Hernando,[‡] Silvia Calabuig-Fariñas,[§,¶] Alicia Martínez-Romero,[∥] Víctor Fernández-Dueñas,[⊥] Kristoffer Sahlholm,[⊥,○] Thomas Knöpfel,[#] María García-Valverde,[‡] Ananda M. Rodilla,[†] Eloisa Jantus-Lewintre,[§,◆] Rosa Farràs,[∥] Francisco Ciruela,[⊥,▽] Ricardo Pérez-Tomás,*[,†] and Roberto Quesada*[,‡]

[†]Cancer Cell Biology Research Group, Department of Pathology and Experimental Therapeutics, Faculty of Medicine, University of Barcelona, 08007 Barcelona, Spain

[‡]Departmento de Química, Universidad de Burgos, 09001 Burgos, Spain

[§]Fundación de Investigación Hospital General Universitario de Valencia, 46014 Valencia, Spain

[∥]Centro de Investigación Príncipe Felipe, 46012 Valencia, Spain

[⊥]Unitat de Farmacologia, Departament Patologia i Terapèutica Experimental, Facultat de Medicina, IDIBELL, Universitat de Barcelona, L'Hospitalet de Llobregat, 08007 Barcelona, Spain

[▽]Department of Biochemistry and Microbiology, Faculty of Sciences, University of Ghent, 9000 Gent, Belgium

[○]Department of Neuroscience, Karolinska Institute, 171 77 Solna, Stockholm, Sweden

[#]Division of Brain Sciences, Imperial College London, London SW7 2AZ, United Kingdom

[¶]Department of Pathology, Universitat de València, 46010 Valencia, Spain

[◆]Department of Biotechnology, Universitat Politècnica de València, 46022 Valencia,Spain

Supporting Information

ABSTRACT: Facilitated anion transport potentially represents a powerful tool to modulate various cellular functions. However, research into the biological effects of small molecule anionophores is still at an early stage. Here we have used two potent anionophore molecules inspired in the structure of marine metabolites tambjamines to gain insight into the effect induced by these compounds at the cellular level. We show how active anionophores, capable of facilitating the transmembrane transport of chloride and bicarbonate in model phospholipid liposomes, induce acidification of the cytosol and hyperpolarization of plasma cell membranes. We demonstrate how this combined effect can be used against cancer stem cells (CSCs). Hyperpolarization of cell membrane induces cell differentiation and loss of stemness of CSCs leading to effective elimination of this cancer cell subpopulation.

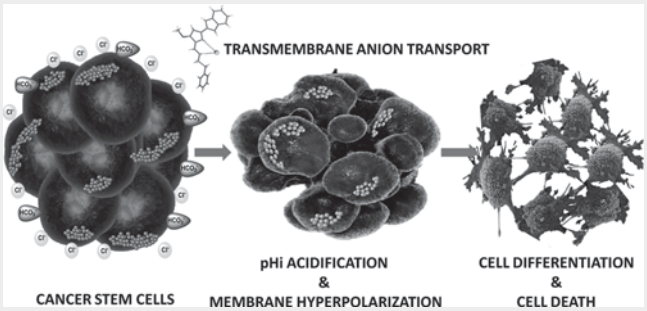

INTRODUCTION

Transmembrane ion channels and pumps are sophisticated cellular machineries involved in many biological processes. As such, ion channels constitute one of the main drug targets in medicinal chemistry. An estimated 13% of currently approved drugs have ion channels as their main therapeutic target, being used for the treatment of a variety of disease conditions.[1] The most successful strategy to modulate transmembrane ion flux is to use small molecules activators or blockers of endogenous proteins. Nevertheless, there is an intense interest in designing artificial ion channels and ionophores.[2,3] In particular, cation selective ionophores are widely used as antibiotics and research tools. In the past few years, the development of small molecules capable of facilitating the transmembrane transport of anions has emerged as an active research field.[4−6] A number of molecules inspired by naturally occurring anionophores such as prodiginines or by synthetic molecules containing amide, (thio)urea, or (thio)squaramide hydrogen-bond donors have been characterized as efficient anion transporters.[7−10] The potential biological applications of these compounds have been less explored. In a seminal work, Magda, Sessler et al. linked the

Received: September 22, 2015
Published: December 3, 2015

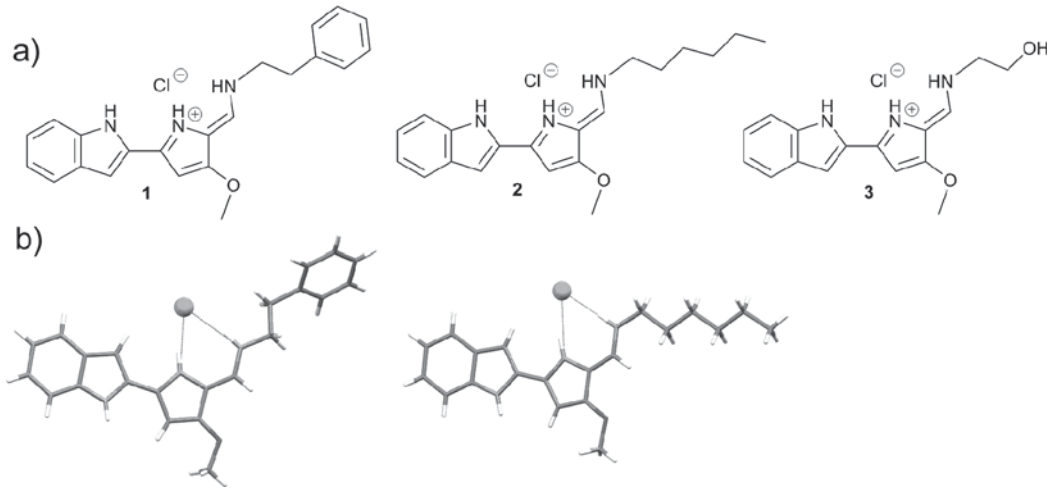

Figure 1. Studied compounds. (a) molecular structures of compounds **1**−**3**. (b) X-ray structures of compounds **1** and **2** as hydrochloride salts.

anionophoric activity of prodigiosin-like molecules with their anticancer activity.[11] Further work by different research groups delineated relationships between the transmembrane transport of anions and the cytotoxicity induced by some of these compounds.[12] Very recently, Gale, Sessler, Shin, and co-workers have demonstrated how diamide-strapped calix[4]-pyrroles induced apoptosis via a caspase-dependent pathway as a result of the facilitated sodium and chloride influx promoted by these derivatives.[13]

Potentially, facilitated transmembrane transport of chloride and bicarbonate (the most abundant anions in biological environments) could impact on cellular ion homeostasis, pH levels, and membrane potentials. These are key parameters for cell survival, and there is a growing body of evidence showing their relationships with cancer development and progression.[14] Dysregulated pH has been recognized as a hallmark of cancer. Cancer cells show a reversed pH gradient compared to normal differentiated cells, with intracellular pH (pHi) higher than extracellular pH.[15] This reversed gradient is regulated by ion channels and pumps and facilitates cancer progression being permissive for some of the acquired characteristics of cancer cells, such as sustained proliferative signaling or resistance to cell death.[16] Membrane potential (Vm) also plays key roles in cancer development and cell differentiation.[17] Nonproliferating, terminally differentiated somatic cells, such as muscle cells and neurons, are characterized by their hyperpolarized Vm, whereas proliferative cells, especially rapidly proliferating tumor cells, displayed depolarized Vm. Interestingly, cancer stem cells (CSCs), a tumor cell subpopulation that exhibits tumor-initiating capacity, self-renewal in serial transplantation assays and contributes to acquired chemotherapy resistance in cancer,[18] need to maintain a depolarized Vm in order to preserve their stemness capacities.[19,20] Therefore, pH modulation to avoid cancer cells acquired advantages as well as suppression of stemness properties through the modulation of plasma membrane potential might be promising new therapeutic strategies for cancer treatment. High-throughput screening of selective inhibitors of CSC growth and survival has identified the potassium ionophore salinomycin as a promising drug candidate, although its mechanism of action is unclear.[21] The potential of a synthetic chloride channel to regulate cell membrane potential has also been reported.[22]

Here we report the biological activity of transmembrane anion transporters inspired in the structure of marine metabolites tambjamines. We demonstrate how these molecules induce pHi acidification and cytotoxicity related to their anion transport abilities. We also show how the facilitated transport activity triggers plasma membrane hyperpolarization leading to cancer stem cell differentiation and effective elimination of this cell population.

■ RESULTS AND DISCUSSION

Synthesis and Anion Transport through Lipid Bilayers. Compounds **1**−**3** (Figure 1) were selected for this study. These compounds are inspired in the structure of marine secondary metabolites tambjamines.[23] They are readily prepared by acid-catalyzed condensation of 5-(1H-indol-2-yl)-3-methoxy-1H-pyrrole-2-carbaldehyde and the appropriate amine. These compounds are isolated as stable yellow-orange solids in good yields as hydrochloride salts and fully characterized (see Supporting Information for details). The spectroscopic data evidenced the strong hydrogen-bond interaction between these compounds and the chloride anion. These interactions are also evident in the solid-state structures of compounds **1** and **2** (Figure 1). The two heterocycles and the enamine moiety are essentially coplanar. A chloride anion is found interacting with the pyrrole and enamine N−H groups, whereas the indole moiety is found rotated 180° and interacting with a second chloride anion. A conformational analysis of these molecules both in solution and computationally is provided in the Supporting Information. In their preferred conformation these molecules bind the anion through the hydrogen-bond cleft involving the three N−H groups of the molecule.

The chloride anion binding ability of **1** and **2** was explored by means of ^{1}H NMR titration experiments using perchlorate salts of these derivatives and tetrabutylammoniun chloride in DMSO-d_6. Under these conditions chloride readily replaces the less coordinating perchlorate anion, and association constants could be calculated at 3301 and 3778 M^{-1} for **1**·$HClO_4$ and **2**·$HClO_4$ respectively. Treatment of DMSO-d_6 solutions of **1**·$HClO_4$ and **2**·$HClO_4$ with tetraethylammonium bicarbonate resulted in deprotonation of the compounds. Lack of solubility prevented the study of these processes in pure water. Nevertheless, the apparent pK_a values of **1** and **2** were calculated in DMSO:water 1:1 mixtures at 9.64 and 9.62. This result as well as computational studies suggested that

deprotonation is not likely to occur under physiological conditions (see Figures S89–S92). On the other hand, in their neutral form, these derivatives are also able to bind anions under these conditions albeit with lower affinity (see Figures S49–S53).

The anion transport properties of **1**–**3** were assayed in 1-palmitoyl-2-oleoyl-*sn*-glycero-3-phosphocholine (POPC) vesicles using a chloride selective electrode to evaluate the chloride efflux promoted by these compounds. Thus, liposomes loaded with NaCl were suspended in an isotonic, chloride-free external medium. Chloride release promoted by **1**–**3** was monitored over time, and at the end of the experiment the vesicles were lysed by the addition of detergent, being the final electrode reading used as 100% release of chloride. Repeating these assays in the presence of variable amounts of compound allowed Hill analyses and calculation of EC_{50} values (the concentration of carrier needed to achieve the release of 50% of encapsulated chloride) for comparative purposes (Table 1).

Table 1. Transport Activities for Compounds 1–3

	EC_{50} NO_3^-/Cl^{-a}		
compound	(μM)	(mol %)[d]	Hill coefficient
1	0.101 ± 0.007	0.020 ± 0.001	1.12 ± 0.10
2	0.041 ± 0.003	0.008 ± 0.001	1.17 ± 0.14
3	17.212 ± 1.172	3.442 ± 0.234	1.13 ± 0.10
	EC_{50} HCO_3^-/Cl^{-b}		
compound	(μM)	(%)	Hill coefficient
1	0.243 ± 0.023	0.048 ± 0.005	1.16 ± 0.15
2	0.137 ± 0.004	0.027 ± 0.001	1.49 ± 0.07
3	n.d.[c]	n.d.[c]	n.d.

[a]Vesicles loaded with 489 mM NaCl dispersed in 489 mM $NaNO_3$ (5 mM phosphate buffer, pH 7.2). [b]vesicles loaded with 451 mM NaCl dispersed in 150 mM Na_2SO_4 (20 mM phosphate buffer, pH 7.2) upon addition of a $NaHCO_3$ pulse to make the extravesicular bicarbonate concentration 40 mM. [c]not determined (carrier loadings over 5% promoted <50% chloride efflux). [d]molar percentage carrier:POPC

Compounds **1** and **2** proved to be extremely active transmembrane transporters, whereas compound **3** displayed modest activity as anion carrier. This difference in transmembrane transport activity is likely due to the significantly lower calculated lipophilicity of **3** with respect to **1** and **2** (See Table S3). The key role of lipophilicity in the design of effective anion transporters has been studied in several families of compounds including tambjamine analogs.[24,25]

Compounds **1** and **2** were selected as their calculated lipophilicity matched the optimal log *P* range for these compounds in order to maximize their transport activity. Compound **3** was predicted to display very limited activity. The experimental results fully supported this hypothesis. The nature of the external anion impacted dramatically in the rate of chloride efflux promoted by these compounds (see Figures S122–S123). Both a Hill parameter close to 1 and the differences in EC_{50} values found when the chloride efflux is measured in the presence of nitrate, bicarbonate, or sulfate suggested that these compounds function as discrete carriers promoting anion exchange through the lipid bilayer. The relatively higher hydrophilicity of bicarbonate compared with nitrate resulted in lower chloride efflux at higher carrier loadings. This was unsurprising as anion exchange has already been reported as the main mechanism accounting for the activity as anion carriers for tambjamine derivatives. Experiments using different metal chlorides such as KCl, RbCl, and CsCl were also performed, and no significant differences were observed (Figures S124–S126). Thus, influence of the metal cation in the transmembrane transport event can be ruled out. Carboxyfluorescein leakage assays also rule out the possibility of these compounds functioning as membrane disruptors promoting unspecific chloride leakage (Figure S136). This set of assays demonstrated that **1** and **2** are very efficient transmembrane transporters. Compound **3** represents an adequate control molecule, being structurally very similar to **1** and **2** yet displaying significantly lower level of transmembrane transport activity (Table 1).

Anionophores Induce Intracellular pH Changes and Cellular Toxicity. In order to evaluate the ability of anionophores **1**–**3** to modulate pHi, first vital staining with acridine orange (AO) was used. When this cell-permeable dye accumulates in acidic compartments, such as lysosomes, it shows a characteristic orange fluorescence emission, while it emits green fluorescence at higher pH, such as in the cytosol. Human lung adenocarcinoma (A549) cells were stained with AO, and typical granular orange fluorescence was observed, corresponding to cellular acidic compartments (Figure 2a). Treatment with active anion transporters **1** and **2** induced complete loss of orange fluorescence, whereas treatment with compound **3** did not modify AO emission, compared to nontreated cells. These results evidenced an increase in the pH of acidic organelles upon treatment with the active anion transporters **1** and **2**, as opposite to control compound **3**.

We were also interested in studying variations in cytoplasmic pH levels. This parameter has been claimed to modulate cell proliferation and apoptosis.[26] Therefore, it could be more relevant to gain insight into the mechanisms accounting for the cytotoxicity of these compounds. Thus, changes in pHi of A549 cells after treatment with **1**–**3** were quantified using the pH-sensitive fluorescent dye SNARF-1. In its ester form, 5-(and-6)-carboxy seminaphthorhodafluor-1-acetoxymethylester (SNARF-1-AM) can diffuse across the cellular membrane into the cytoplasm. Hydrolyzation of this compound by cellular esterases yields the cell-impermeable fluorescent dye carboxy-SNARF-1. This dye can be used for quantitative determinations of pHi because it exhibits a significant pH-dependent emission shift in the appropriate range. First, fluorescent signal ratios at 576 and 664 nm were determined under different pH conditions, which allowed us to construct a calibration curve. Then, fluorescence of SNARF-1 was measured in A549 cells. Upon treatment with 10 μM concentration of active anionophores **1** and **2**, pHi dropped significantly. A lowering of 0.33 ± 0.10 and 0.70 ± 0.22 pH units was measured for compound **1** and **2**, respectively, after 1 h (Figure 2b). Such change of pHi is known to be sufficient to trigger apoptotic processes in cells.[26] Under these conditions, compound **3** only induced minor changes of pHi inducing an increase of 0.02 ± 0.14 pH units. These results are in agreement with the involvement of the transmembrane transport activity in the lowering of pHi observed.

To assess whether chloride transport participated in the cytotoxic effect exhibited by **1** and **2**, cell viability was measured in A549 cells resuspended in Hank's balanced salt solution (HBSS) either containing chloride or without this anion (Figure 2c,d). Moderate yet significant differences between cell viability in both buffers upon treatment with **1** and **2** were observed, with reduced cytotoxicity in absence of chloride.

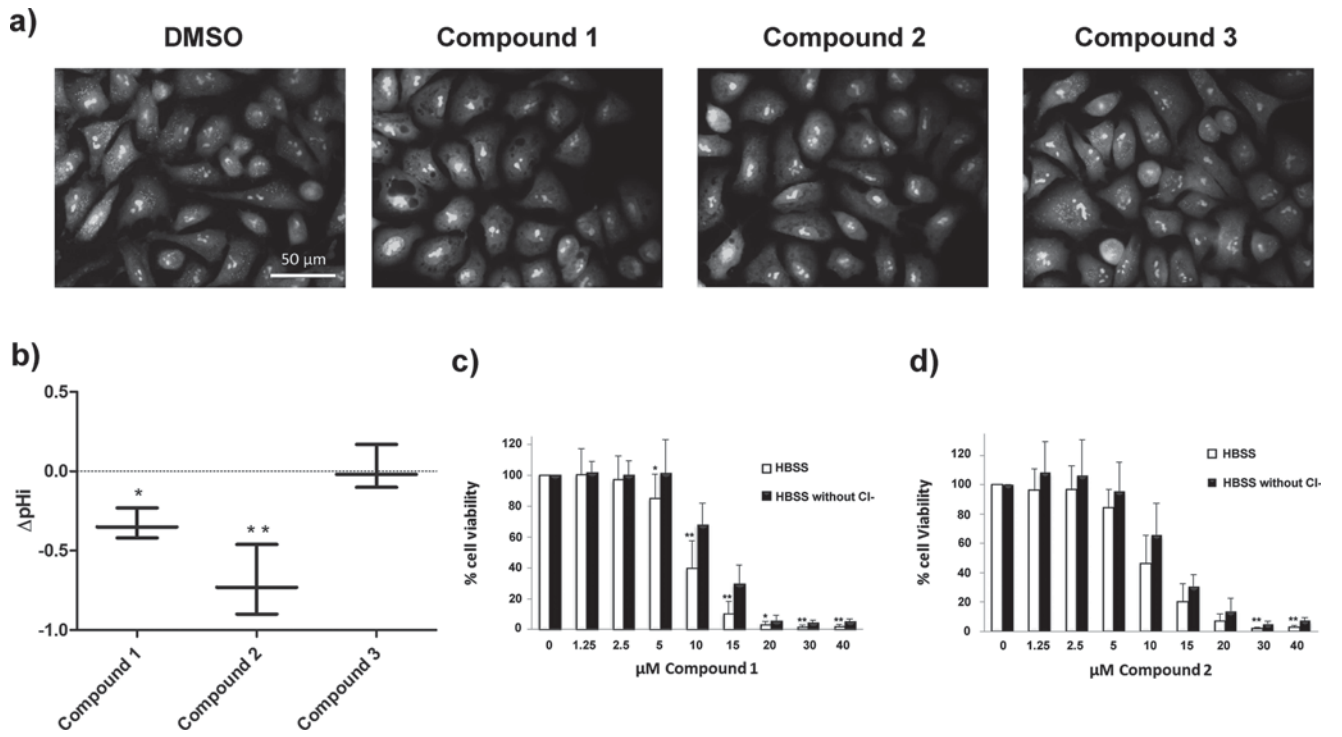

Figure 2. Transmembrane anion transport impact intracellular pH (pHi) levels and reduce cell viability. (a) AO staining on human lung adenocarcinoma (A549) cells. From left to right: Untreated (control) cells; cells treated with compounds **1**, **2**, and **3** (10 μM). Disappearance of orange fluorescence due to basification of acidic organelles is evident upon treatment with active anionophores. (b) pHi measurements using SNARF-1 staining. A significant decrease in pHi is observed after treatment with 10 μM of compound **1** or **2**. * $p < 0.05$; ** $p < 0.01$. (c,d) Cell viability after treatment with compound **1** and **2** in the presence (HBSS) or absence (HBSS without Cl^-) of chloride ion. Higher cytotoxicity is observed in the presence of chloride ion. * $p < 0.05$; ** $p < 0.01$.

Under these conditions, calculated inhibitory concentration 50 (IC_{50}) values in the presence of chloride dropped to 8.8 and 9.6 μM from the calculated 12.4 and 12.11 μM in HBSS without chloride for compounds **1** and **2**, respectively. This result as well as the reduced toxicity of inactive transporter **3** (see Figure S136) again supported the involvement of anion transport in the cytotoxic effect exerted by **1** and **2**.

Membrane Potential Changes in Liposomes and Voltage Changes in Single A549 Cells. We decided to explore the potential of these compounds to induce changes in the membrane polarization. We first explore this possibility in model liposomes. Thus, membrane potential-sensitive dye safranin O was used. The fluorescence of this compound is affected by changes in membrane potential.[27] POPC vesicles containing NaCl were suspended in a Na_2SO_4 solution. As demonstrated using chloride-selective electrode assays, compounds **1**−**3** are unable to promote sulfate transport (see Figures S119 and S120), and under these conditions only chloride permeation can occur. Addition of active transporters **1** and **2** at 0.1% molar carrier:lipid resulted in a marked decrease in safranin O fluorescence (Figure 3b). Control experiments using the essentially inactive transporter **3** or DMSO resulted in no significant change of fluorescence. These results are consistent with a decrease of the membrane potential induced by **1** and **2**. Likewise, little change in safranin O fluorescence was observed when these experiments were carried out with no chloride electrochemical potential (Figure 3a).

We next aimed to assess the ability of anion transporters to induce voltage changes in A549 cells. A549 cells were transfected with the VSFP2.32 genetically encoded voltage indicator, which permits monitoring membrane voltage changes by recording changes in FRET efficacy between a pair of fluorescent proteins.[28,29] To determine the voltage range within VSFP2.32 reports, voltage changes in A549 cells, VSFP2.32 expressing cells, were patch-clamped, and a voltage ramp (from 130 to −170 mV) was applied. A progressive decrease in FRET was observed as the cell membrane was hyperpolarized to negative voltages from −30 mV and down to −170 mV (Figure 3c). We next evaluated the effects of compounds **1**−**3** on membrane voltage. The superfusion of transporter **1** induced a robust decrease in the FRET signal (Figure 3d). The decrease in the FRET signal indicates that treatment with this compound hyperpolarized A549 cells. These cells normally exhibit a resting Vm close to 0 mV that upon facilitated influx of anions shifts to more negative values. Similar to the transporter **1**, transporter **2** also produced a decrease on FRET signal (Figure S141), although with slightly different kinetics. Thus, transporter **1** had a higher magnitude of the signal (0.18 ± 0.03 vs 0.15 ± 0.02) and faster τ time constant (5.16 ± 0.79 vs 7.65 ± 0.58 s) than transporter **2**. Finally, we attempted to demonstrate that the critical feature of these compounds in order to induce Vm changes was their anion transport abilities. Thus, transporter **3**, possessing much reduced potency as transmembrane anion transporter, was then assayed in the FRET illumination protocol, in order to monitor possible voltage alterations (Figure 3e). This compound induced significantly lower decreases in the FRET signal (0.03 ± 0.01) than transporter **1** and **2**, thus demonstrating again that hyperpolarization of the cell membrane was induced as a result of the transmembrane transport facilitated by active anion transporters.

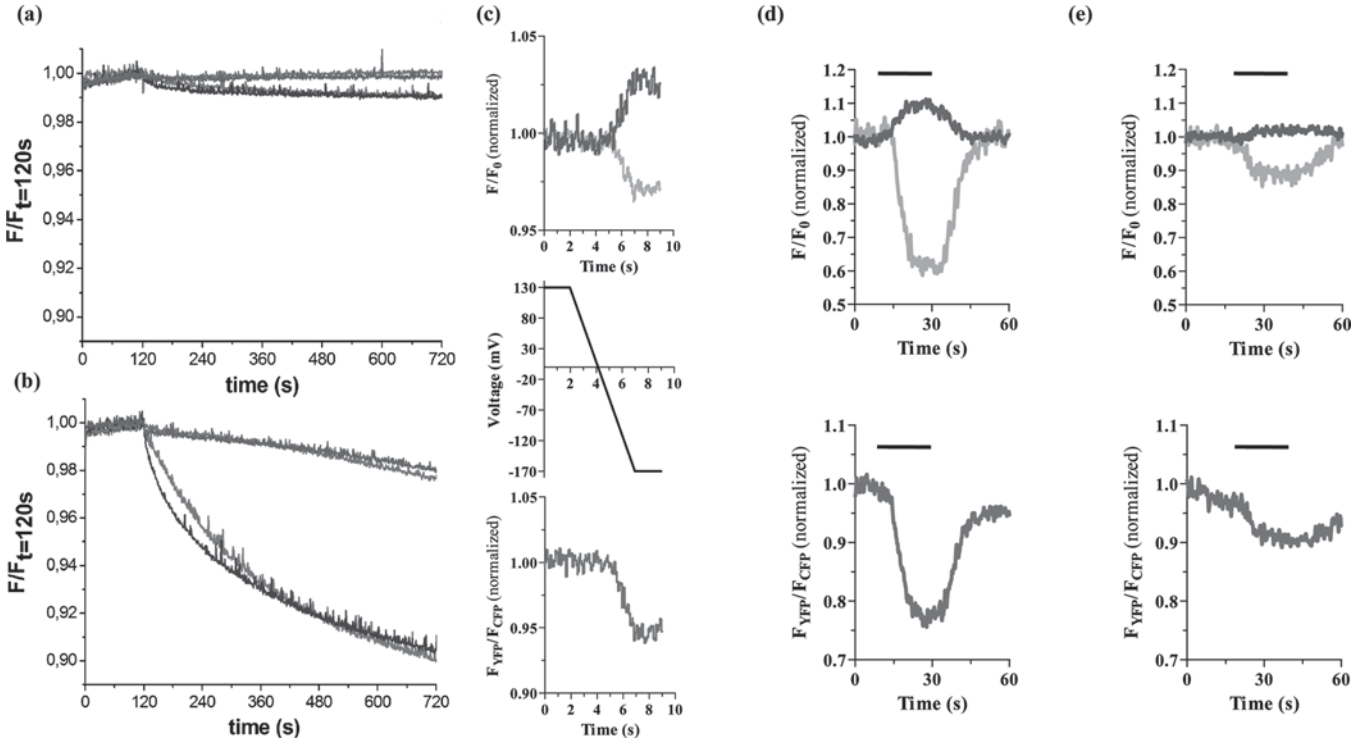

Figure 3. Transmembrane anion transporters induce changes in membrane potential. (a,b) Changes in safranin O fluorescence. The anion carrier (0.1 mol % with respect to phospholipids) was added at t = 120 s, after that the experiments were monitored over 600 s. Each trace represents the average of three trials. Compounds **1**, red trace; **2**, blue; **3**, gray; control DMSO, green. (a) Vesicles loaded with NaCl (28.8 mM NaCl, and 5 mM phosphate buffer, pH 7.2, ionic strength 40 mM) were immersed in NaCl (28.8 mM NaCl, and 5 mM phosphate buffer, pH 7.2, ionic strength 40 mM, and safranin O 0.2 μM). (b) Vesicles loaded with NaCl (28.8 mM NaCl, and 5 mM phosphate buffer, pH 7.2, ionic strength 40 mM) were immersed in Na_2SO_4 (9.6 mM Na_2SO_4, 5 mM phosphate buffer pH 7.2, ionic strength 40 mM, and safranin O 0.2 μM). (c–e) FRET changes of the VSFP2.32 voltage biosensor. (c) Voltage ramp (shown in the middle panel, from 130 to −170 mV), (d) transporter **1**, and (e) transporter **3**. Shown are the time-resolved changes in mCerulean and Citrine fluorescence emission signals in single A549 cells expressing the VSFP 2.32. The emission intensities of mCerulean (blue trace), Citrine (yellow trace), and the ratio $F_{Citrine}/F_{mCerulean}$ (red trace) were recorded simultaneously. Traces are representative of five separate experiments.

Cytotoxicity of Anion Transporters. The effects of anion transporters **1**–**3** on A549 cancer cells as well as cell lines derived from primary tumors from two nonsmall cell lung cancer patients (FIS302 and FIS303) were examined. We were interested in determine the cytotoxicity against both differentiated and cancer stem cells. Thus, cells were cultured in adherence or as spheroids and were treated 10 μM concentrations of each of the selected compounds. The results are shown in Figure 4. For all cell lines, viability after 24 h was significantly diminished in A549, FIS302, and FIS303 spheroids compared with the cells grown in monolayer by compounds **1** (p = 0.012, p < 0.0001, and p < 0.0001, respectively) and **2** (p = 0.018, p = 0.004, and p < 0.0001, respectively). On the other hand, treatment with the much less active transporter **3** did not significantly affect the viability of the treated cells. For comparative purposes doxorubicin, a classic chemotherapeutic drug, was also included in this study. These results indicate that active anion transporters selectively inhibited CSC viability. Similar results were also observed in a variety of other lung cancer cells lines (H1650, H1993, PC9) (Figure S137). For noncancerous cell lines, higher concentrations of compounds **1** and **2** are needed in order to decrease cell viability, but the differences with cancer cells were not statistically significant (data not shown). However, noncancerous cell lines are immortalized, and as such they share relevant features with cancerous cell lines. For this reason, we have performed an in vivo efficacy study in a lung cancer mouse model using these molecules and the results showed that therapeutic doses (6 mg/kg) of both anion transporters were not toxic in mice, while a decrease in tumor volume was observed (unpublished data).

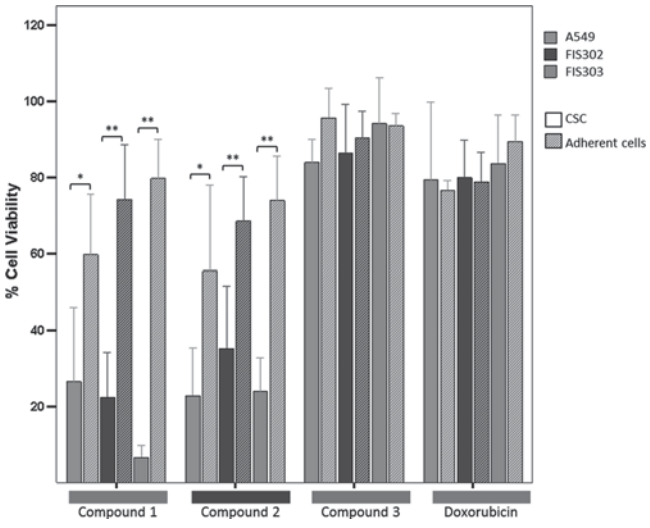

Figure 4. Cytotoxicity assays on cancer stem cells and adherent cells. A549, FIS302, and FIS303 adherent and CSCs. Cells were treated with 10 μM of each compound (**1**, **2**, or **3**). Doxorubicin (10 μM) was used as control. Mean and standard deviations of three independent experiments are shown (* p < 0.05, ** p < 0.01).

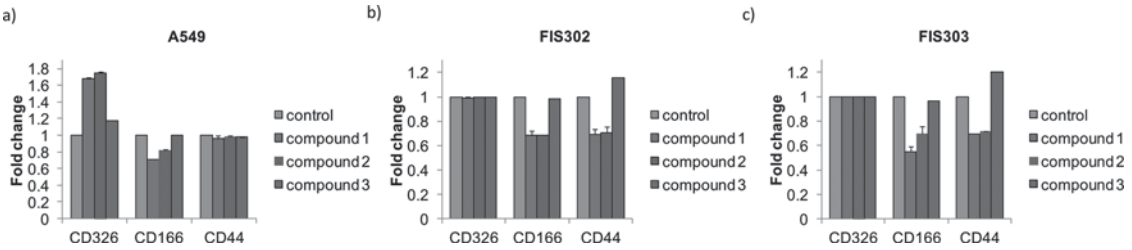

Figure 5. Compounds **1** and **2** affect expression of cancer stem cell surface markers. (a) A549, (b) FIS302, (c) FIS303 CSCs. CSCs were treated with 2.5 μM compound **1**, **2**, or **3** for 24 h, and the expression of CD326 (EpCAM), CD166, and CD44 was analyzed by flow cytometry. The expression of these markers was relativized to those in control cells. Data represent the average of three independent experiments. Bars correspond to standard deviations.

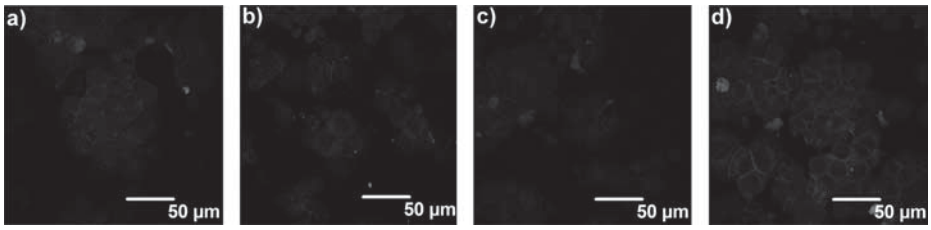

Figure 6. Compounds **1** and **2** induce tumor CSCs spheres disaggregation. E-cadherin expression in FIS302 tumor spheres growing in suspension assessed by immunofluorescence. Merged projection of both cell nuclei with pattern of DAPI-staining (blue channel) and E-cadherine staining (red channel). Scale bar is 50 μm. (a) Untreated control cells. (b) CSCs treated with compound **1**. (c) CSCs treated with compound **2**. (d) CSCs treated with compound **3**.

Anion Transporters Affect Expression of Cancer Stem Cell (CSC) Surface Markers. Stemness properties of CSCs have been associated with the expression of several cell surface markers.[30] Thus, the effect of compounds **1**−**3** on the expression of lung stem cell surface markers of A549 CSCs as well as FIS302 and FIS303, two patient-derived CSCs, was assessed by immunofluorescence and flow cytometry. Since cell viability in the presence of 10 μM concentrations of compounds **1** and **2** for 24 h is very low, cells were incubated with 2.5 μM of each compound in order to analyze potential alterations of lung stem cell surface markers before cell death. Incubation of A549 cells with 2.5 μM of **1** and **2** for 24 h led to an increase of the epithelial cell adhesion molecule CD326-(EpCAM) expression by 70% and downregulation of CD166 by 20% compared to control cells treated with DMSO. No significant changes were observed in the expression of CD44. Compound **3** induced no significant changes in the three surface markers studied here compared to control cells (Figure 5a). FIS302 patient-derived CSCs treated with compounds **1** and **2** showed a 30% decrease in CD166 and CD44 expression (Figure 5b). No significant changes were observed in the expression of EpCAM, CD44, and CD166 in the cells treated with compound **3** (Figure 5b). FIS303 patient-derived CSCs treated with compound **1** showed a 50% reduction in CD166 expression. The treatment with compound **2** led to a 30% reduction in CD166 expression. Both compounds **1** and **2** led to a 30% decrease in CD44 expression (Figure 5c). Similar to FIS302 cells, no significant changes were observed in the expression of EpCAM, CD44, and CD166 in cells treated with compound **3** (Figure 5c). Taken together, downregulation of CD166 and upregulation of CD326 (EpCAM) populations in A549 CSCs, and downregulation of CD166 and CD44 populations in FIS302 and FIS303 patient-derived CSC, suggests that the CSCs properties of A549, FIS302, and FIS303 cells are affected by compounds **1** and **2**. Further evidence came from inmunofluorescence assays (Figure 6). Thus, the size of the tumor spheres decreases when treated with compounds **1** and **2** compared to spheres treated with compound **3** or DMSO, and disaggregation was evident (Figure 6).

■ CONCLUSIONS

In summary, we have studied two highly active transmembrane anion transporters **1** and **2** capable of facilitating transmembrane transport of chloride and bicarbonate in model liposomes. These compounds induce pHi acidification and hyperpolarization of cellular membranes. We have shown that this combined effect led to loss of stemness characteristics of CSCs and selective elimination of this cell population. The fact that the structurally related yet poorly effective transporter **3** did not exert any of these effects led us to conclude that facilitated anion transport plays a crucial role in the biological action of these compounds. We conclude that small molecule anionophores could represent valuable chemotherapeutics for the manipulation of CSCs behavior.

■ ASSOCIATED CONTENT

Supporting Information

The Supporting Information is available free of charge on the ACS Publications website at DOI: 10.1021/jacs.5b09970.

Syntheses and characterization data, computational studies and descriptions of liposome-based anion transport assays and membrane potential assays. Details on cell lines and culture conditions, AO, and SNARF-1 staining, cell viability assays, microscopic FRET measurements, tumor cell preparation, cancer stem cells, flow cytometry analysis (PDF)

Crystallographic data (CIF)

Crystallographic data (CIF)

Cartesian coordinates (PDF)

AUTHOR INFORMATION

Corresponding Authors

*rperez@ub.edu

*rquesada@ubu.es

Author Contributions

●These authors contributed equally.

Notes

The authors declare no competing financial interest.

ACKNOWLEDGMENTS

This work was supported by grants from the Spanish government and the EU (FIS PI13/00089, FIS PI12/02838, FIS PI12/00956 and RD12/0036/0025), a grant from La Marató de TV3 Foundation (20132730), a grant from SEPAR (17/2014), Consejería de Educación de la Junta de Castilla y León (Project BU340U13), Ministerio de Economía y competitividad/Instituto de Salud Carlos III (SAF2014-55700-P), and ICREA Academia-2010. E.H. thanks the Junta de Castilla y León (Consejería de Educación) and the Fondo Social Europeo for a PIRTU contract. We thank Benjamín Torrejón and Esther Castaño from CCiT (Centres Científics i Tecnològics, Campus de Bellvitge, Universitat de Barcelona), Sandra Tejedor (Centro de Investigación Príncipe Felipe), Luís Korrodi-Gregório (UB), and Andrea Sancho (UBU) for their technical support.

REFERENCES

(1) Overington, J. P.; Al-Lazikani, B.; Hopkins, A. L. *Nat. Rev. Drug Discovery* **2006**, *5*, 993.

(2) (a) Gokel, G. W.; Negin, S. *Acc. Chem. Res.* **2013**, *46*, 2824. (b) Matile, S.; Fyles, T. *Acc. Chem. Res.* **2013**, *46*, 2741. (c) Otis, F.; Auger, M.; Voyer, N. *Acc. Chem. Res.* **2013**, *46*, 2934.

(3) (a) Sakai, N.; Matile, S. *Langmuir* **2013**, *29*, 9031. (b) Alfonso, I.; Quesada, R. *Chem. Sci.* **2013**, *4*, 3009.

(4) (a) Davis, A. P.; Sheppard, D. N.; Smith, B. D. *Chem. Soc. Rev.* **2007**, *36*, 348. (b) Davis, J. T.; Okunola, O.; Quesada, R. *Chem. Soc. Rev.* **2010**, *39*, 3843. (c) Busschaert, N.; Gale, P. A. *Angew. Chem., Int. Ed.* **2013**, *52*, 1374.

(5) Jentzsch, A. V.; Emery, D.; Mareda, J.; Nayak, S. K.; Metrangolo, P.; Resnati, G.; Sakai, N.; Matile, S. *Nat. Commun.* **2012**, *3*, 905.

(6) Santacroce, P. V.; Okunola, O. A.; Zavalij, P. Y.; Davis, J. T. *Chem. Commun.* **2006**, 3246.

(7) (a) Moore, S. J.; Wenzel, M.; Light, M. E.; Morley, R.; Bradberry, S. J.; Gómez-Iglesias, P.; Soto-Cerrato, V.; Pérez-Tomás, R.; Gale, P. A. *Chem. Sci.* **2012**, *3*, 2501. (b) Gale, P. A.; Tong, C. C.; Haynes, C. J. E.; Adeosun, O.; Gross, D. E.; Karnas, E.; Sedenberg, E. M.; Quesada, R.; Sessler, J. L. *J. Am. Chem. Soc.* **2010**, *132*, 3240. (c) Harrel, W. A., Jr.; Bergmeyer, M. L.; Zavalij, P. Y.; Davis, J. T. *Chem. Commun.* **2010**, *46*, 3950. (d) Martí, I.; Rubio, J.; Bolte, M.; Burguete, M. I.; Vicent, C.; Quesada, R.; Alfonso, I.; Luis, S. V. *Chem. - Eur. J.* **2012**, *18*, 16728.

(8) (a) Cooper, J. A.; Street, S. T.; Davis, A. P. *Angew. Chem., Int. Ed.* **2014**, *53*, 5609. (b) Elie, C. R.; Noujeim, N.; Pardin, C.; Schmitzer, A. R. *Chem. Commun.* **2011**, *47*, 1788.

(9) (a) Marchal, E.; Rastogi, S.; Thompson, A.; Davis, J. T. *Org. Biomol. Chem.* **2014**, *12*, 7515. (b) Busschaert, N.; Karagiannidis, L. E.; Wenzel, M.; Haynes, C. J. E.; Wells, N. J.; Young, P. G.; Makuc, D.; Plavec, J.; Jolliffe, K. A.; Gale, P. A. *Chem. Sci.* **2014**, *5*, 1118.

(10) (a) Park, E. B.; Jeong, K. S. *Chem. Commun.* **2015**, *51*, 9197. (b) Valkenier, H.; Judd, L. W.; Li, H.; Hussain, S.; Sheppard, D. N.; Davis, A. P. *J. Am. Chem. Soc.* **2014**, *136*, 12507.

(11) Sessler, J. L.; Eller, L. R.; Cho, W. S.; Nicolaou, S.; Aguilar, A.; Lee, J. T.; Lynch, V. M.; Magda, D. J. *Angew. Chem., Int. Ed.* **2005**, *44*, 5989.

(12) (a) de Greñu, B. D.; Hernandez, P. I.; Espona, M.; Quiñonero, D.; Light, M. E.; Torroba, T.; Pérez-Tomás, R.; Quesada, R. *Chem. - Eur. J.* **2011**, *17*, 14074. (b) Gale, P. A.; Perez-Tomas, R.; Quesada, R. *Acc. Chem. Res.* **2013**, *46*, 2801.

(13) Ko, S. K.; Kim, S. K.; Share, A.; Lynch, V. M.; Park, J.; Namkung, W.; Van Rossom, W.; Busschaert, N.; Gale, P. A.; Sessler, J. L.; Shin, I. *Nat. Chem.* **2014**, *6*, 885.

(14) (a) Litan, A.; Langhans, S. A. *Front. Cell. Neurosci.* **2015**, *9*, 86. (b) DiGiammarino, E. L.; Lee, A. S.; Cadwell, C.; Zhang, W.; Bothner, B.; Ribeiro, R. C.; Zambetti, G.; Kriwacki, R. W. *Nat. Struct. Biol.* **2002**, *9*, 12.

(15) (a) Webb, B. A.; Chimenti, M.; Jacobson, M. P.; Barber, D. L. *Nat. Rev. Cancer* **2011**, *11*, 671. (b) Gillies, R. J.; Raghunand, N.; Karczmar, G. S.; Bhujwalla, Z. M. *J. Magn. Reson. Imaging* **2002**, *16*, 430.

(16) (a) Damaghi, M.; Wojtkowiak, J. W.; Gillies, R. J. *Front. Physiol.* **2013**, *4*, 370. (b) Lang, F.; Stournaras, C. *Philos. Trans. R. Soc., B* **2014**, *369*, 20130108. (c) McCarty, M. F.; Whitaker. *J. Altern. Med. Rev.* **2010**, *15*, 264.

(17) (a) Sundelacruz, S.; Levin, M.; Kaplan, D. L. *Stem Cell Rev. and Rep.* **2009**, *5*, 231. (b) Wonderlin, W. F.; Woodfork, K. A.; Strobl, J. S. *J. Cell. Physiol.* **1995**, *165*, 177. (c) Sundelacruz, S.; Levin, M.; Kaplan, D. L. *PLoS One* **2008**, *3*, e3737.

(18) (a) Valent, P.; Bonnet, D.; De Maria, R.; Lapidot, T.; Copland, M.; Melo, J. V.; Chomienne, C.; Ishikawa, F.; Schuringa, J. J.; Stassi, G.; Huntly, B.; Herrmann, H.; Soulier, J.; Roesch, A.; Schuurhuis, G. J.; Wohrer, S.; Arock, M.; Zuber, J.; Cerny-Reiterer, S.; Johnsen, H. E.; Andreeff, M.; Eaves, C. *Nat. Rev. Cancer* **2012**, *12*, 767. (b) Reya, T.; Morrison, S. J.; Clarke, M. F.; Weissman, I. L. *Nature* **2001**, *414*, 105. (c) Singh, A.; Settleman, J. *Oncogene* **2010**, *29*, 4741.

(19) Yang, M.; Brackenbury, W. J. *Front. Physiol.* **2013**, *4*, 185.

(20) Vidal, S. J.; Rodriguez-Bravo, V.; Galsky, M.; Cordon-Cardo, C.; Domingo-Domenech, J. *Oncogene* **2014**, *33*, 4451.

(21) Gupta, P. B.; Onder, T. T.; Jiang, G.; Tao, K.; Kuperwasser, C.; Weinberg, R. A.; Lander, E. S. *Cell* **2009**, *138*, 645.

(22) Li, X.; Shen, B.; Yao, X. Q.; Yang, D. *J. Am. Chem. Soc.* **2009**, *131*, 13676.

(23) Carte, B.; Faulkner, D. J. *J. Org. Chem.* **1983**, *48*, 2314.

(24) (a) Saggiomo, V.; Otto, S.; Marques, I.; Felix, V.; Torroba, T.; Quesada, R. *Chem. Commun.* **2012**, *48*, 5274. (b) Valkenier, H.; Haynes, C. J. E.; Herniman, J.; Gale, P. A.; Davis, A. P. *Chem. Sci.* **2014**, *5*, 1128.

(25) Busschaert, N.; Bradberry, S. J.; Wenzel, M.; Haynes, C. J. E.; Hiscock, J. R.; Kirby, I. L.; Karagiannidis, L. E.; Moore, S. J.; Wells, N. J.; Herniman, J.; Langley, G. J.; Horton, P. N.; Light, M. E.; Marques, I.; Costa, P. J.; Félix, V.; Frey, J. G.; Gale, P. A. *Chem. Sci.* **2013**, *4*, 3036.

(26) Lagadic-Gossmann, D.; Huc, L.; Lecureur, V. *Cell Death Differ.* **2004**, *11*, 953.

(27) Sidorov, V.; Kotch, F. W.; Kuebler, J. L.; Lam, Y. F.; Davis, J. T. *J. Am. Chem. Soc.* **2003**, *125*, 2840.

(28) Akemann, W.; Mutoh, H.; Perron, A.; Rossier, J.; Knopfel, T. *Nat. Methods* **2010**, *7*, 643.

(29) Akemann, W.; Song, C.; Mutoh, H.; Knopfel, T. *Neurophotonics* **2015**, *2*, 021008.

(30) Xia, P. *Curr. Stem Cell Res. Ther.* **2014**, *9*, 102.

Molecular Cancer Therapeutics

Novel Indole-based Tambjamine-Analogues Induce Apoptotic Lung Cancer Cell Death through p38 Mitogen-Activated Protein Kinase Activation

Pilar Manuel-Manresa[1], Luís Korrodi-Gregório[1,2], Elsa Hernando[3], Alberto Villanueva[4], David Martínez-García[1], Ananda M. Rodilla[1], Ricard Ramos[5], Margarida Fardilha[2], Juan Moya[5], Roberto Quesada[3], Vanessa Soto-Cerrato[1], and Ricardo Pérez-Tomás[1]

Abstract

Lung cancer has become the leading killer cancer worldwide, due to late diagnosis and lack of efficient anticancer drugs. We have recently described novel natural-derived tambjamine analogues that are potent anion transporters capable of disrupting cellular ion balance, inducing acidification of the cytosol and hyperpolarization of cellular plasma membranes. Although these tambjamine analogues were able to compromise cell survival, their molecular mechanism of action remains largely unknown. Herein we characterize the molecular cell responses induced by highly active indole-based tambjamine analogues treatment in lung cancer cells. Expression changes produced after compounds treatment comprised genes related to apoptosis, cell cycle, growth factors and its receptors, protein kinases and topoisomerases, among others. Dysregulation of *BCL2* and *BIRC5*/survivin genes suggested the apoptotic pathway as the induced molecular cell death mechanism. In fact, activation of several proapoptotic markers (caspase-9, caspase-3, and PARP) and reversion of the cytotoxic effect upon treatment with an apoptosis inhibitor (Z-VAD-FMK) were observed. Moreover, members of the Bcl-2 protein family suffered changes after tambjamine analogues treatment, with a concomitant protein decrease towards the prosurvival members. Besides this, it was observed cellular accumulation of ROS upon compound treatment and an activation of the stress-kinase p38 MAPK route that, when inhibited, reverted the cytotoxic effect of the tambjamine analogues. Finally, a significant therapeutic effect of these compounds was observed in subcutaneous and orthotopic lung cancer mice models. Taken together, these results shed light on the mechanism of action of novel cytotoxic anionophores and demonstrate the therapeutic effects against lung cancer. *Mol Cancer Ther; 16(7); 1224–35. ©2017 AACR.*

Introduction

Lung cancer is the most common cancer that threatens human health, accounting for more than 19% of all cancer deaths in 2012 (1). Health systems have standardized clinical procedures for treating lung cancer patients being surgery, conventional platinum-based doublet chemotherapy (e.g., carboplatin/taxol or pemetrexed), and targeted therapies (e.g., erlotinib and other novel anti-EGFR-mutated receptors) the main options (2). Nevertheless, conventional chemotherapy shows low efficacy with important treatment-related toxicity. Therefore, development of novel efficient drugs is urgently needed. In this regard, the diversity of marine environment provides an extraordinary array of biologically active metabolites for the development of new anticancer therapeutics. In late 2007, trabectedin (Yondelis, PharmaMar) became the first marine anticancer drug to be approved in the European Union (3). Over the past decade, there has been an increase in the number of new anticancer lead compounds from marine life that have entered in human clinical trials (4). Nowadays, more than 592 marine compounds are included in the pipeline of modern pharmaceuticals discovery programs, showing promising antitumor and cytotoxic activities (5). The natural alkaloids tambjamines were originally isolated from marine invertebrates including bryozoans, nudibranchs, and ascidians (6). Tambjamines possess a wide spectrum of pharmacological properties and seem to be involved in the chemical defense mechanisms of the organisms from which they derive (6). Structurally, these alkaloids are characterized by a 4-methoxybipyrrole moiety shared by other families of natural products such as the prodiginines (7). It is already well known that prodiginines have proapoptotic activity against several cancer cells including lung, breast, and hematopoietic, showing the ability to overcome the multidrug resistance phenotype (8–10). Tambjamines, like prodiginines, are very efficient

[1]Cancer Cell Biology Research Group, Department of Pathology and Experimental Therapeutics, Faculty of Medicine, University of Barcelona, Barcelona, Spain. [2]Laboratory of Signal Transduction, Department of Medical Sciences, Institute for Research in Biomedicine—iBiMED, Health Sciences Program, University of Aveiro, Aveiro, Portugal. [3]Department of Chemistry, University of Burgos, Burgos, Spain. [4]Program Against Cancer Therapeutic Resistance (ProCURE), Catalan Institut of Oncology ICO, Bellvitge Biomedical Research Institute IDIBELL, L'Hospitalet, Barcelona, Spain. [5]Department of Thoracic Surgery and University of Barcelona, Hospital Universitari de Bellvitge, L'Hospitalet de Llobregat, Barcelona, Spain.

Note: Supplementary data for this article are available at Molecular Cancer Therapeutics Online (http://mct.aacrjournals.org/).

P. Manuel-Manresa and L. Korrodi-Gregório contributed equally to this article.

Corresponding Authors: Ricardo Pérez-Tomás and Vanessa Soto-Cerrato, University of Barcelona, Pavelló Central, 5a Planta, LR 5101, C./Feixa Llarga s/n L'Hospitalet de Llobregat, Barcelona 08907, Spain. Phone: 349-3402-4288; Fax: 349-3402-9082; E-mail: rperez@ub.edu; and Vanessa Soto-Cerrato, vsoto@ub.edu.

doi: 10.1158/1535-7163.MCT-16-0752

anion exchangers (anionophores) in model liposomes promoting both chloride and bicarbonate transport, which are the most abundant anions in biological environments (7, 11, 12). Their anionophoric activity has an impact on cellular ion homeostasis, intracellular pH levels, and cell survival (11, 12). Recently, we have demonstrated that synthetic tambjamine analogues induce intracellular pH acidification and cytotoxicity in lung cancer cells and human-derived cancer stem cells (CSC), and how this is related to their anion transport abilities (13). Cancer stem cells are defined as immortal cells within a tumor that have the ability to perpetuate themselves through self-renewal, to spawn differentiated progeny (non-CSCs) and contribute to acquired chemotherapy resistance in cancer (14). Moreover, their facilitated transport activity triggers hyperpolarization of plasma membrane in lung cancer cells and differentiation and cell death in CSCs, leading to an effective elimination of this tumor subpopulation (13).

Although substantial work has already been done concerning chemical characterization of tambjamines and the impact of their anionophoric properties in cell survival and differentiation, their molecular mechanism of action still remains unclear. Here, we report a detailed study of how cancer cells respond to several highly active indole-based tambjamine analogues at the transcript and protein levels. Moreover, we have elucidated the molecular cell death mechanism induced by these compounds as well as assessed their therapeutic effect *in vivo* in several lung cancer mouse models.

Materials and Methods

Synthesis of compounds

Compounds **1** to **11** were synthesized by condensation of 5-(1H-indole-2-yl)-3-methoxy-1H-pyrrole-2-carbaldehyde with the appropriate amine using acetic acid as catalyst. Detailed synthetic procedures and characterization data are provided in the Supplementary Information (S1–S36).

Cell lines and culture conditions

The human lung cancer cell lines, adenocarcinoma (A549, CCL185), squamous carcinoma (SW900, HTB59), small-cell carcinoma (DMS53, CRL2062), and large-cell carcinoma (H460, HTB177) were obtained from ATCC. All cell lines were tested and authenticated by ATCC using short tandem repeat analysis. All cell lines were cultured (passage number 10–25) following ATCC recommended media (Biological Industries) supplemented with 10% heat-inactivated FBS (Gibco, Thermo Fisher Scientific Inc.), 100 U/mL penicillin, 100 μg/mL streptomycin, and 2 mmol/L L-glutamine, all from Biological Industries. Cells were grown at 37°C in a humidified incubator (Thermo Fisher Scientific Inc.) with 5% CO_2 atmosphere. The cells were mycoplasma tested using a standard PCR technique after thawing.

Establishment of lung cancer patient–derived primary cultures

This protocol was approved by the local Ethics Committee (PR003/13) and the studies were conducted in accordance with the Declaration of Helsinki ethical guidelines, upon signed informed consent. Fresh human lung cancer tissues were obtained from 20 patients with primary lung cancer (age range 55–81 years) undergoing lobectomy or pneumonectomy at Bellvitge University Hospital from April 2013 to March 2014. Histologic diagnosis was determined based on microscopic features of carcinoma cells. Freshly obtained tumor tissue (within 1–2 hours after surgical removal) was washed in RPMI1640 medium (Biological Industries) containing 100 U/mL penicillin and 100 μg/mL streptomycin. Blood vessels and connective tissue were carefully removed and the cancerous area was then minced into small pieces less than 1 mm^3 using a scalpel. Chopped tissue was resuspended in RPMI1640 medium containing collagenase II (Sigma-Aldrich) at a concentration of 200 U/mL and digested for 2 to 4 hours at 37°C in a humidified incubator. The enzymatic digestion was stopped when most of the cells were in a single cell suspension. Following two washes in RPMI1640, cells were transferred into standard tissue culture coated flasks (TPP, Trasadingen) and cultured in the defined keratinocyte-serum free medium (DK-SFM, Gibco, Thermo Fisher Scientific Inc.) supplemented with 100 U/mL penicillin, 100 μg/mL streptomycin, 2 mmol/L L-glutamine, 20 ng/mL EGF (Sigma-Aldrich, Merck KGaA), 10 ng/mL basic-FGF (Sigma-Aldrich, Merck KGaA), 2% B27 (Gibco, Thermo Fisher Scientific Inc.), and 0.25 mg/mL amphotericin B (Sigma-Aldrich, Merck KGaA). All lung cancer patient derived cultures were maintained at 37°C in a humidified incubator (Thermo Fisher Scientific Inc.) with 5% CO_2. Culture medium was changed every 2–3 days. Cells were passaged after detachment with TrypLE Express (Invitrogen, Thermo Fisher Scientific Inc.), when the cells reached 80%–90% confluence. We were able to establish two lung cancer primary cultures (PC), one derived from an adenocarcinoma tumor (PC#8) and the other derived from a squamous cell carcinoma (PC#13), which were used for subsequent viability assays. Lung cancer patient–derived PCs were characterized by immunofluorescence, according to their epithelial or mesenchymal biomarker expression, using cytokeratin-8 (catalog no. IF13, Oncogene, Merck KGaA) for the epithelial phenotype and vimentin (catalog no. 3932, Cell Signaling Technology Inc.) for the mesenchymal phenotype.

Cell viability assays

Cell viability was evaluated using the methylthiazoletetrazolium (MTT, Sigma-Aldrich, Merck KGaA) colorimetric assay. Cells were harvested (10^4 cells/well) in 96-well plates in a final volume of 100 μL and allowed to grow overnight. At the following day, vehicle solution (DMSO, Sigma-Aldrich, Merck KGaA) or experimental compounds were added at a single point (10 μmol/L) or at different ranging concentrations (0.8–100 μmol/L for compounds **1** and **2**, 1.6–200 μmol/L for cisplatin) to the assay plate. Cells were incubated for 24 hours and after the treatment period, 10 μL of MTT (5 mg/mL) were added and the plates were incubated for 4 hours at 37°C. Crystals were dissolved in 100 μL of DMSO, after which the reading was taken spectrophotometrically at 570 nm using a multiwell plate reader (Multiskan FC, Thermo Fisher Scientific Inc.). Cell viability and inhibitory concentration (IC) values were obtained using GraphPad Prism V5.0 for Windows (GraphPad Software). All data are shown as the mean value ± SD of three independent experiments. Statistical analysis (one-way ANOVA) was carried out with the Statgraphics plus 5.1. Statistical package (Manugistics). Cisplatin was bought from Alfa Aesar (Thermo Fisher Scientific Inc.).

Gene expression analysis

The A549 cell line was seeded at a density of 2×10^5 cells in 60-mm plates and allowed to grow for 24 hours. Subsequently, cells were exposed to the IC_{50} of the tambjamine analogues **1** or **2** for 6 or 16 hours. Total RNA was extracted and purified using the column-based RNeasy Mini Kit (Qiagen), according to the

manufacturer's protocol. Total RNA concentration and purity was checked in a nano spectrophotometer (Implen GmbH) and integrity was analyzed using an Agilent 2100 Bioanalyzer (Agilent Technologies). For the reverse transcription, 1 μg of total RNA was used for cDNA synthesis using a mixture of random hexamers and oligo-dT primers and following the RT^2 First Strand Kit protocol (Qiagen). The Human RT^2 RNA Quality Control PCR Array (PAHS-999ZA format A, Qiagen) was used to assess the cDNA quality and to check for genomic DNA contamination in an ABI PRISM 7700 Sequence Detection System (Applied Biosystems, Thermo Fisher Scientific Inc.). For gene expression analysis, cDNAs of control and treated cells were mixed with RT^2 SYBR ROX mastermix (Qiagen) and dispensed in the RT^2 Profiler PCR Array of Human Cancer Drug Targets (PAHS-507A format E, Qiagen). After 2-minute centrifugation at 300 × *g*, the array was placed in an ABI PRISM 7900HT real-time PCR system (Applied Biosystems, Thermo Fisher Scientific Inc.) and the analysis was carried out according to manufacturer's instructions. Dissociation curves (melting curves) were carefully analyzed using SDS software v2.3 and RQ Manager v1.2 (both from Applied Biosystems, Thermo Fisher Scientific Inc.) to choose only the highly specific reaction products in the downstream analysis. The threshold cycle (C_T) values obtained were analyzed in Qiagen Data Analysis Center (Qiagen) to retrieve the fold-regulation values for each gene. The network of most altered genes upon compounds treatment was produced in Cytoscape open-source software (Cytoscape Consortium; ref. 15) with data extracted from Gene Network Central (GNC-Pro, Qiagen).

Western blot analysis

A549 cells were seeded in 100-mm culture plates (10^6 cells) and allowed to grow for 24 hours. Afterward, they were exposed to compounds **1, 2** (IC_{25}, IC_{50}, and IC_{75} values), or **3** (10 μmol/L) for 24 hours. Total protein extracts were obtained from cells by the addition of lysis buffer containing 0.1% SDS, 1% NP-40, 0.5% sodium deoxycholate, 50 mmol/L sodium fluoride, 40 mmol/L β-glycerophosphate, 200 μmol/L sodium orthovanadate, 1 mmol/L phenylmethylsulfonyl fluoride, and protease inhibitor cocktail (Roche Diagnostics) in 1× PBS. Protein concentration was determined by BCA protein assay (Pierce, Thermo Fisher Scientific Inc.) using BSA (Pierce, Thermo Fisher Scientific Inc.) as a standard. For Western blot analysis, 30 μg of protein extracts were first separated by SDS-PAGE and transferred to Immobilon-P polyvinylidene difluoride (PVDF) membranes (EMD Millipore, Merck KGaG). Membranes were blocked in either 5% dry milk or BSA, both diluted in TBS–Tween (50 mmol/L Tris–HCl pH 7.5, 150 mmol/L NaCl, 0.1% Tween-20) for 1 hour and then incubated overnight with primary antibodies, according to the manufacturer's instructions. Antibodies were obtained from the following sources: anti-caspase-3 (catalog no. 9662), anti-cleaved-caspase-3 (catalog no. 9661), anti-caspase-9 (catalog no. 9502), anti-PARP1 (catalog no. 9542), anti-Bak (catalog no. 6947), anti-Bax (catalog no. 2772), anti-Bcl-2 (catalog no. 4223), anti-Mcl-1 (catalog no. 4572), anti-phospho-p38 MAPK (Thr180/Tyr182, catalog no. 4511), anti-p38 MAPK (catalog no. 9212), and anti-Survivin (catalog no. 2808) were all obtained from Cell Signaling Technology Inc.; anti-Actin (I-19, catalog no. sc-1616) from Santa Cruz Biotechnology Inc and anti-Vinculin (catalog no. V-4505) from Sigma-Aldrich, Merck KGaA. Antibody binding was detected with goat anti-mouse IgG-HRP (catalog no. sc-2005), goat anti-rabbit IgG-HRP (catalog no. sc-2004), or donkey anti-goat IgG-HRP (catalog no. sc-2020), all from Santa Cruz Biotechnology Inc. and the ECL Detection Kit (Amersham, GE Healthcare). Actin or vinculin were used as gel loading controls. The results shown are representative of Western blot analysis data obtained from at least three independent experiments. Images were captured on an Image Quant LAS 500 (GE Healthcare) and band densitometries were retrieved using the Image Studio Lite software (v5.0, LI-COR Biosciences).

Inhibitor assays

Determination of viable cells (A549 cell line) after different inhibitors treatment was performed using the dual DNA intercalating Fluorescent Dyes Kit MUSE Cell Count & Viability Assay (EMD Millipore, Merck KGaG). In brief, 2×10^5 cells/well in DMEM medium were seeded in a six-well plate. After 24 hours, tambjamine analogues **1** and **2** at higher IC_{75} value were added, and incubated for 6 hours in a 5% CO_2 cell culture incubator (Thermo Fisher Scientific Inc.). A pan-caspases inhibitor (Z-VAD-FMK; BD Bioscience) or a p38 MAPK inhibitor (SB202190; Cell Signaling Technology Inc.) was added at 20 and 30 μmol/L respectively, 2 hours before compound **1** or **2** exposure. Afterward, cells were collected and were incubated with the Cell Count & Viability reagent for 5 minutes. Viability of treated cells was analyzed using the flow cytometry based MUSE Cell Analyzer (EMD Millipore, Merck KGaA) according to the manufacturer's protocol. Viability was calculated as a percentage related to control cells and results shown were obtained from at least three independent experiments. Statistical analysis (one-way ANOVA) was carried out with the Statgraphics plus 5.1. Statistical package (Manugistics).

Evaluation of reactive oxygen species formation

Quantitative measurements of reactive oxygen species (ROS) in A549 cells were performed using the MUSE Oxidative Stress Kit (EMD Millipore, Merck KGaG), based on dihydroethidium (DHE), a well-characterized reagent that has extensively been used to detect reactive oxidative species in cellular populations. In brief, 2×10^5 cells/well in DMEM medium were seeded in a six-well plate. Twenty-four hours after seeding, tambjamine analogues **1** and **2** at higher IC_{75} value were added, and incubated for 6 hours in a 5% CO_2 cell culture incubator (Thermo Fisher Scientific Inc.). A positive control, named tert-butyl hydroperoxide (TBHP, Sigma-Aldrich, Merck KGaA) was used at 2.5 mmol/L for 2 hours, and the nontransporter tambjamine analogue (compound **3**) was used as a negative control at 10 μmol/L for 6 hours. Afterward, cells were harvested and processed with the Oxidative Stress Kit according to the manufacturer's protocol. The percentage of ROS-positive and -negative cells was calculated and results shown were obtained from at least three independent experiments. Statistical analysis (one-way ANOVA) was carried out with the Statgraphics plus 5.1. Statistical package (Manugistics).

***In vivo* evaluation of indole-based tambjamine analogues therapeutic effect**

For the purpose of this article, two murine models have been designed: the subcutaneous and the orthotopic model systems. Five-week-old female Crl:NU-Foxn1nu mice strain (Envigo) were used in this study. All animal studies were approved by the Autonomic Ethic Committee (Generalitat de Catalunya) under the protocol 9111. To generate the subcutaneous xenograft model, mice were subcutaneously implanted with 4.5×10^6 DMS53

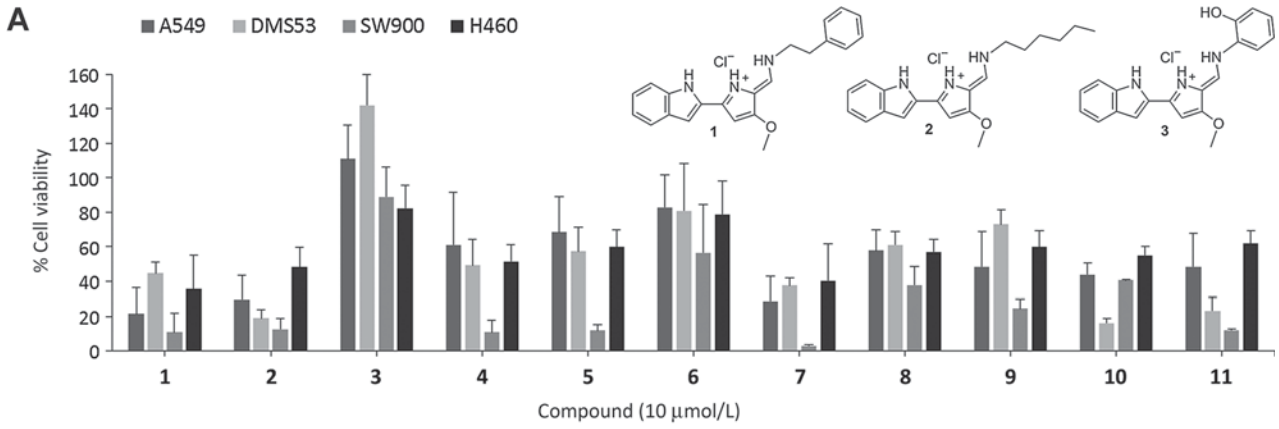

B

	A549	DMS53	SW900	H460	PC#8	PC#13
1	10.66 ± 0.68	8.04 ± 0.45	8.67 ± 0.06	8.37 ± 0.24	4.04 ± 1.29	4.34 ± 0.25
2	7.61 ± 0.23	6.46 ± 0.52	7.55 ± 0.89	7.29 ± 0.29	3.34 ± 0.86	4.03 ± 0.19
CDDP	IC > 200	107.9 ± 31.16	49.4 ± 10.56	74.2 ± 6.72	49.28 ± 9.88	79.57 ± 9.37

Figure 1.
Effect of indole-based tambjamine analogues on cell survival. **A,** Single point screening of synthetic tambjamine analogues **1** to **11** (10 μmol/L) on a panel of lung cancer cell lines (A549, DMS53, SW900, and H460). **B,** IC_{50} values of selected compounds (**1** and **2**) on lung cancer cell lines and lung cancer patient-derived primary cultures (PC#8 and PC#13). For comparison purposes, cisplatin (CDDP) was used as the standard clinical chemotherapeutic agent. Viability was measured using the MTT assay after 24 hours of treatment. Results were obtained from at least three independent experiments, and bar represents the mean ± SD.

cells suspended in a 1:1 solution of RPMI1460:Matrigel (BD Bioscience). For the orthotopic model, subcutaneous xenografts of DMS53 in exponential growth from three different animals were aseptically isolated and placed at room temperature in DMEM supplemented with 10% FBS plus 50 U/mL penicillin and 50 mg/mL streptomycin and the surgical resection tumors were implanted in Crl:NU-Foxn1nu mice following previously reported procedures (16, 17). Briefly, mice were anesthetized with a continuous flow of 1% to 3% isoflurane/oxygen mixture (2 L/minutes) and subjected to right thoracotomy. Mice were situated in left lateral decubitus position and a small transverse skin incision (around 5–8 mm) was made in the right chest wall. Chest muscles were separated by a sharp dissection and costal and intercostal muscles were exposed. An intercostal incision of 2–4 mm on the third or fourth rib on the chest wall was made and a small tumor piece of 2 to 4 mm^3 was introduced into the chest cavity. The tumor specimen was deposited between the second and the third lung lobule. Next, the chest wall incision was closed with surgery staples, and finally chest muscles and skin were closed. Mice were inspected twice a week, and monitored for the presence of breathing problems.

Mice bearing homogeneous subcutaneous tumors (approximately 150–200 mm^3) were randomly allocated to three treatment groups ($n = 7$/treatment). For DMS53 orthotopic-derived model, mice were randomly allocated ($n = 6$/treatment) and the treatment started 30 days after tumor implantation. Compounds **1** and **2** were diluted in 7.5% DMSO/0.8% Tween-80. All treatments were intraperitoneally administrated at a dose of 6 mg/kg in alternating days during 20 days. Tumor growth was recorded two to three times per week starting from the first day of treatment (day 0) and tumor volume (in mm^3), estimated according to the formula $V \times 0.25(ab^2)/2$, where a is the length or biggest diameter and b is the width or smallest diameter). After the final dose of the treatment, animals were sacrificed and tumors were dissected out and weighed.

Liver and kidney samples were fixed in 4% paraformaldehyde overnight, embedded in paraffin, and cut into sections (5 μm). Paraffin-embedded sections were deparaffinized in xylene and gradually rehydrated for hematoxylin and eosin staining. Stained liver and kidney sections were gradually dehydrated and mounted for hepatotoxicity and nephrotoxicity examination, respectively.

Results

Indole-based tambjamine analogues are cytotoxic against lung cancer cells

To measure the inhibitory effect of novel tambjamine analogues (**1–11**; Supplementary Fig. S1) on tumor cell proliferation, we have first performed a single-point MTT assay at 10 μmol/L in four commonly used lung cancer cell lines (A549, DMS53, SW900, and H460). After 24 hours of treatment, most of the compounds showed significant cell viability decrease, being compounds **1** and **2** the most promising anticancer agents (Fig. 1A). Then, IC_{50} values of the selected compounds were calculated in the same cell lines as well as in both adenocarcinoma and squamous patient-derived PCs (Fig. 1B and Supplementary Figs. S37 and S38). The two selected compounds had similar potency against all the cell lines in the study, showing IC_{50} values below 10 μmol/L. When compared with *cis*-diamminedichloroplatinum (II) (CDDP), commonly known as cisplatin, the standard chemotherapeutic agent used for lung cancer treatment in the clinic, the IC_{50} values of this compound were all much higher than the ones of compounds **1** and **2**. Interestingly, lung cancer patient–derived PCs were more sensitive to our compounds, showing IC_{50} values below 5 μmol/L whereas for cisplatin they were higher than 45 μmol/L (Fig. 1B). This IC_{50} value for cisplatin is in accordance

with published data (18, 19). Therefore, the selected tambjamine analogues displayed better cytotoxic activity against a panel of lung cancer cell lines and PCs than the current clinical standard treatment.

Indole-based tambjamine analogues alter the expression of several cellular key genes

To identify gene expression changes at the cellular level, we have used a profiler array consisting of 84 genes that are known cancer drug targets. The selected compounds **1** and **2** were tested in the adenocarcinoma cell line A549 at their respective IC_{50} values during two incubation periods (6 and 16 hours, for raw data please check Supplementary File S1). Both compounds have produced changes in several genes from diverse functional groups (Table 1). In general, the observed alterations (higher than 1.5-fold regulation in at least two conditions) were more evident at 16 hours with a clear tendency to genes downregulation. In total, 26 genes were modulated, in which 20 were downregulated by compounds **1** or **2** exposure. Downregulated genes included those related to: apoptosis, cell cycle, growth factors and receptors, protein kinases, topoisomerases, to name a few. Especially relevant for cell viability were genes related to cell death like the antiapoptotic B-cell lymphoma 2 (*BLC2*) and the inhibitor of apoptosis (IAP) family member *BIRC5*/Survivin, as well as those related to cell cycle (e.g., *CDK1* and *CDK2*). The remaining six genes were upregulated and related to drug metabolism, protein kinases, transcription factors, cathepsins, and heat shock proteins (Table 1). Concerning genes that are altered more than three-fold regulation in at least two conditions, we have obtained *CDC25A*, *FIGF*/VEGFD, *IGF1*, *NFKB1*, and *PTGS2*/Cox-2. Six randomly selected genes were reconfirmed by another methodology (Supplementary Table S1; Supplementary Fig. S39). Similar results were obtained using another lung cancer cell line from squamous carcinoma SW900 (77% gene match; Supplementary Table S2; raw data are present in Supplementary File S1), suggesting that they may be implicated in tambjamine mechanism of action. Interestingly, three genes that were previously altered more than three-fold in A549 cell line (*FIGF*, *IGF*, and *NFKB1*) were not altered, *IGF* and *NFKB1* or inversely regulated, *FIGF*, in the SW900 cell line. We further analyzed the altered genes using protein–protein interaction data and functional data extracted from Gene Network Central (GNC-Pro, Qiagen). The results showed that compound-modulated genes formed a highly connected network (Fig. 2), suggesting that these genes work as a functional module at the molecular level. The network also showed that *NFKB1* and *TP53* are hubs (densely connected nodes), which integrate signals from the other nodes. Although these genes are hubs in our system, we did not observe any consistent transcriptional change in both cell line models.

Indole-based tambjamine analogues induce apoptosis in lung cancer cells

Because we have obtained alterations in genes related to apoptosis and cell cycle and these processes are deeply involved in cell viability, we checked if these mechanisms are activated in our cellular model. We were unable to detect any cell-cycle arrest for either compounds tested, whereas cisplatin produced the well-documented G_2–M phase arrest (Supplementary Fig. S40; ref. 20). To elucidate if apoptosis is the molecular mechanism of cell death induced by these compounds, the expression levels of

Table 1. Genes modulated after indole-based tambjamine analogues treatment

		1		2		
Gene name	**Protein name**	**6 h**	**16 h**	**6 h**	**16 h**	**Functional gene grouping**
Downregulated						
ABCC1	ATP-binding cassette, sub-family C, member 1	−1.11	−1.61	−1.48	−2.32	Drug metabolism
AURKA	Aurora kinase A	−2.53	−2.37	−2.69	−4.13	Protein kinases
AURKB	Aurora kinase B	−1.96	−2.43	−2.16	−5.03	Protein kinases
BCL2	B-cell CLL/lymphoma 2	−2.17	1.10	−1.83	−1.90	Apoptosis
BIRC5	Baculoviral IAP repeat containing 5, Survivin	−2.08	−2.37	−2.53	−4.72	Apoptosis
CDC25A	Cell division cycle 25 homolog A	−2.30	−1.75	−3.72	−4.11	Cell cycle
CDK1	Cyclin-dependent kinase 1	−1.97	−2.71	−2.41	−3.94	Cell cycle
CDK2	Cyclin-dependent kinase 2	−1.81	−1.73	−1.24	−3.21	Cell cycle
ERBB3	Receptor tyrosine-protein kinase erbB-3, HER3	−2.42	−1.35	−2.81	−2.18	Growth factors and receptors
ESR2	Estrogen receptor 2	−1.65	−1.20	−2.87	−1.78	Hormone receptors
FIGF	C-fos induced growth factor, VEGFD	−2.25	−1.65	−3.57	−3.74	Growth factors and receptors
HDAC8	Histone deacetylase 8	−1.87	1.11	−1.52	−2.01	Histone deacetylases
HSP90AA1	Heat shock protein 90 kDa alpha, member 1	−1.84	−1.62	−1.43	−2.47	Heat shock proteins
IGF1	Insulin-like growth factor 1, Somatomedin C	−4.89	−17.47	−3.48	−42.18	Growth factors and receptors
NTN3	Netrin 3	−1.81	−2.11	−2.85	−1.17	Structural protein
PARP2	Poly (ADP-ribose) polymerase 2	−1.29	−1.63	−1.63	−2.20	Poly ADP-ribose polymerases
PDGFRA	Platelet-derived growth factor receptor alpha	−3.55	−1.59	1.10	−2.48	Growth factors and receptors
PLK1	Polo-like kinase 1	−2.24	−2.46	−2.36	−4.13	Protein kinases
PLK4	Polo-like kinase 4	−1.36	−2.51	−1.20	−2.02	Protein kinases
TOP2A	Topoisomerase (DNA) II alpha 170 kDa	−2.06	−2.78	−2.09	−4.30	Topoisomerases, type II
Upregulated						
CTSL1	Cathepsin L1	1.30	1.92	2.03	2.07	Cathepsins
CTSS	Cathepsin S	1.24	2.69	1.71	2.08	Cathepsins
HSP90B1	Heat shock protein 90 kDa beta, member 1	2.00	1.95	1.63	1.97	Heat shock proteins
NFKB1	Nuclear factor NF-kappa-B p105 subunit	3.88	1.23	3.14	−1.01	Transcription factors
PRKCE	Protein kinase C, epsilon	1.52	−1.04	2.53	1.95	Protein kinases
PTGS2	Prostaglandin-endoperoxide synthase 2, COX-2	6.46	−1.23	19.29	2.90	Drug metabolism

NOTE: The A549 lung adenocarcinoma cell line was treated with the IC_{50} values of compounds **1** or **2** and the expression of 84 genes related to cancer drug targets was analyzed by qRT-PCR (Qiagen RT2 Profiler Array). Fold regulation values of the most altered genes are presented.

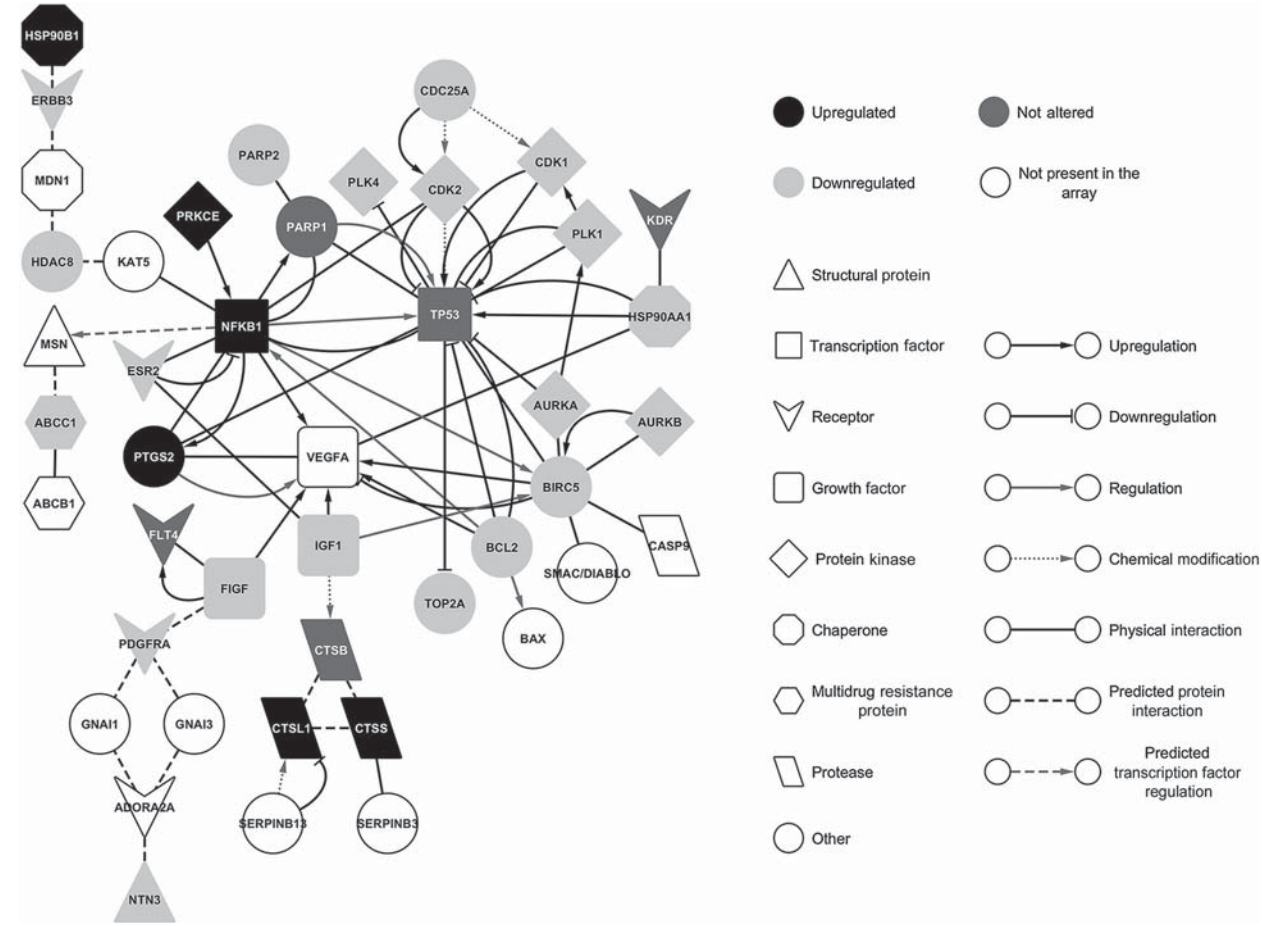

Figure 2.
Indole-based tambjamine analogues effect on cellular signaling pathways. A directed-network of differentially expressed genes after compounds **1** or **2** treatment in A549 cells was constructed from the RT-PCR array results and data extracted from Gene Network Central (GNC-Pro).

apoptosis-related proteins were analyzed by Western blot analysis because a decrease in the anti-apoptotic proteins Bcl-2 and survivin was detected in the gene expression array. The adenocarcinoma cell line A549 was treated with compounds **1** or **2** at the IC_{25}, IC_{50}, and IC_{75} concentrations for 24 hours. The results showed that, at higher concentrations, compounds activated the proteolysis of both initiator pro-caspase-9 (*CASP9* gene) and executioner pro-caspase-3 (*CASP3* gene; Fig. 3A). Moreover, activation of the final apoptotic executioner PARP was also induced. Similar results were also obtained in the small cell carcinoma cell line DMS53 (Supplementary Fig. S41). In addition, we checked the levels of the apoptotic complexes Bak/Mcl-1 (*BAK*/*MCL1* genes) and Bax/Bcl-2 (*BAX*/*BCL2* genes). The pro-apoptotic effectors of the mitochondrial pathway (Bak and Bax) showed an increase in their protein levels after 24 hours treatment. On the contrary, Mcl-1 and Bcl-2 that are prosurvival members of the Bcl-2 family of proteins presented a decrease on their protein levels after treatment (Fig. 3A–C). The results for Bcl-2 protein expression corroborated the gene expression decrease previously observed in the profiler array (Table 1). Also in accordance with those results, downregulation of the key oncogene BIRC5/Survivin was observed at the protein level by Western blot analysis. A549 cells treated with compounds **1** or **2** (IC_{25}, IC_{50}, and IC_{75}) during 24 hours showed a dose-dependent decrease of survivin, indicating that this protein might play an important role on the cell death fate after compounds exposure (Fig. 3A).

To further investigate the involvement of caspases activation on compounds-mediated apoptosis, A549 cells were treated 2 hours with a broad-spectrum caspase inhibitor, Z-VAD-FMK, and then with compounds **1** or **2** for 6 hours. Cell viability was then assessed by flow cytometry and results showed that the decrease in cell viability induced by compounds treatment was significantly reversed by the pan-caspase inhibitor Z-VAD-FMK (Fig. 3D), corroborating that apoptosis is involved in compounds-induced cell death.

Cytotoxic effect of compounds is triggered via a ROS-activated stress kinase pathway

The unbalance of ionic homeostasis produced by tambjamine analogues (13) could be initiating ROS production. Therefore, we tested whether compounds **1** and **2** could promote ROS accumulation in cells. Interestingly, after 6 hours treatment with compounds **1** or **2** (at higher IC_{75} value), there is a significant ROS formation compared with the nontreated condition or when

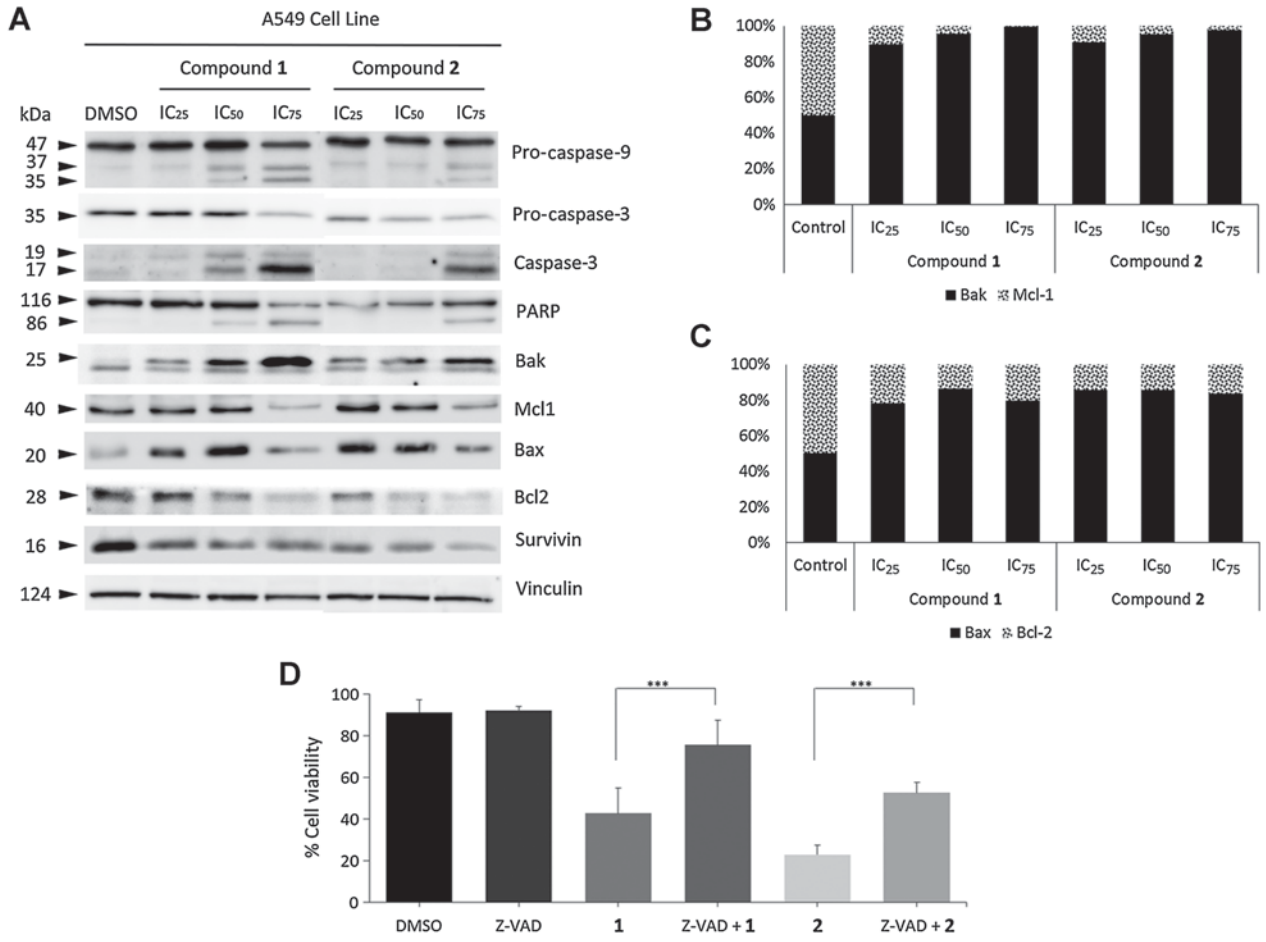

Figure 3.

Analysis of the apoptotic pathway after indole-based tambjamine analogues exposure. **A,** After 24 hours of treatment with the IC_{25}, IC_{50}, and IC_{75} values of compounds **1** or **2**, the expression of several apoptotic markers was analyzed by Western blot analysis in A549 cell line. **B** and **C,** Bcl-2 family protein complexes (Bak/Mcl-1 and Bax/Bcl-2, respectively) ratios are represented in bar graphs. **D,** A549 cells were treated with 20 μmol/L of Z-VAD-FMK for 2 hours followed by compounds **1** or **2** for 6 hours. Cell viability was measured using the flow cytometry–based MUSE Cell Analyzer Kit. Results were obtained from at least three independent experiments. Bars represent the mean ± SD. Statistically significant results are indicated as *, $P < 0.05$; **, $P < 0.01$ and ***, $P < 0.001$.

the nontransporter tambjamine analogue (compound **3**) is used (Fig. 4A). The effect of compounds is similar to the commonly used ROS stressor TBHP. The p38 MAPK signaling is one of the stress sensor pathways downstream of ROS formation that plays an essential role in inflammation, cell differentiation, growth, and death. Thus, we have investigated by Western blot analysis, the phosphorylation of p38 MAP kinase after treatment with indole-based tambjamine analogues **1**, **2,** or **3** in A549 cells. After 24 hours treatment with compounds **1** or **2** (IC_{25}, IC_{50}, and IC_{75}), p38 MAPK (*MAPK14* gene) phosphorylation increased in a dose–response manner without any alteration in the total protein expression levels (Fig. 4B). Conversely, compound **3** (nontransporter) had no effect on the p38 MAPK activation. The ROS inducer TBHP was shown before to also activate the p38 MAPK pathway (21). To further investigate whether activation of p38 MAPK was related to cell death, A549 cells were pretreated with the p38 MAPK inhibitor SB202190 (30 μmol/L) for 2 hours before compounds treatment. A significant reversion of cell death induced by compounds **1** and **2** was observed upon inhibitor pretreatment, which indicates that compounds-mediated cell death is upstream regulated by the p38 MAPK signaling pathway (Fig. 4C).

Therapeutic effect on *in vivo* mice models

To corroborate the anticancer activity of the indole-based tambjamine analogues seen in several lung cancer cell lines and patient-derived PCs, we evaluated the therapeutic effect of compounds **1** and **2** in established DMS53 human small cell lung carcinoma growing subcutaneous and orthotopically in nude mice models. The DMS53 cell line was selected for their ability to grow well in the flank (for subcutaneous model) and in the lung (for orthotopic model) after cell inoculation. Mice bearing DMS53 xenografts were treated with compounds **1** or **2** (6 mg/kg in saline with 7.5% of DMSO/0.8% Tween-80) or vehicle control (7.5% of DMSO/0.8% Tween-80) in alternating days during 20 days. As shown in Fig. 5A and B, compound **2** produced a significant decrease in tumor growth in subcutaneous models. Furthermore, treatment with compound **2**

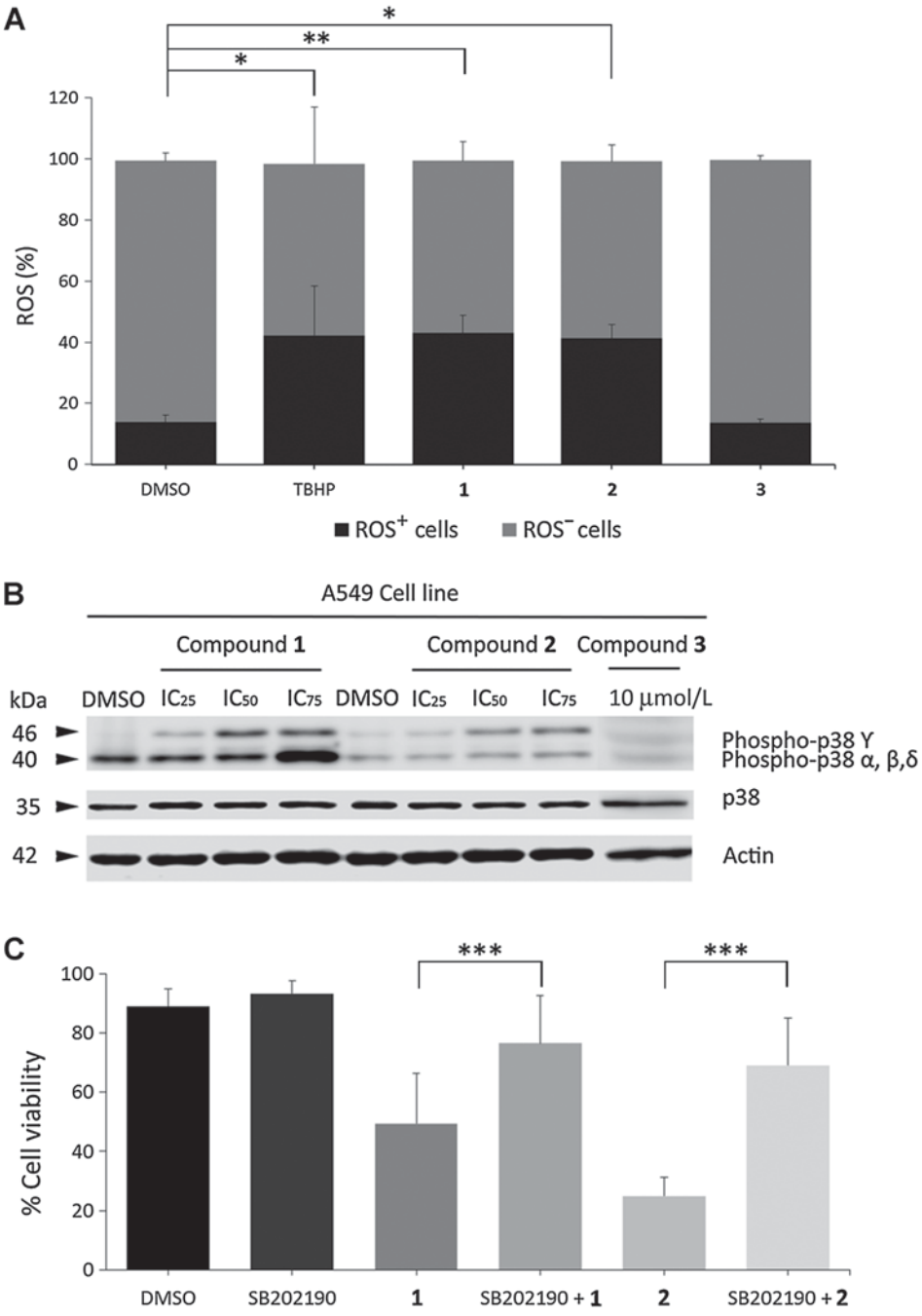

Figure 4.

Indole-based tambjamine analogues induce ROS, causing cellular stress by p38 MAPK activation. **A,** A549 cells were treated with compounds **1**, **2**, or **3** (negative control) for 6 hours or with TBHP (positive control) for 2 hours. ROS formation was measured using the flow cytometry–based MUSE Oxidative Stress Kit. **B,** Phosphorylation levels of the stress kinase p38 MAPK were assessed by Western blot analysis in A549 cells exposed to the IC_{25}, IC_{50}, and IC_{75} values of compounds **1, 2**, or **3** for 24 hours. **C,** A549 cells were treated with 30 µmol/L of SB20219 for 2 hours followed by compounds **1** or **2** for 6 hours. Cell viability was measured using the flow cytometry–based MUSE Cell Analyzer Kit. Results were obtained from at least three independent experiments. Bars represent the mean ± SD. Statistically significant results are indicated as *, $P < 0.05$; **, $P < 0.01$, and ***, $P < 0.001$.

significantly ($P < 0.05$) reduced lung cancer tumor progression in the orthotopic lung model (Fig. 5C). Importantly, as a single agent the treatment with compounds **1** or **2** did not produce any obvious toxicity (hepatotoxicity and nephrotoxicity; Fig. 5D), diarrhea, or significant body weight loss (Supplementary Fig. S42).

Discussion

Chemotherapeutic agents based on natural compounds are a potent source of anticancer drugs. Tambjamine analogues of natural compounds tambjamines have already demonstrated a good pharmacological activity and to have remarkable anticancer effects (6, 7, 11–13). In this study, we analyzed the cytotoxic effect and consequent induced cell death and elucidated the molecular mechanism of action of novel synthesized indole-based tambjamine analogues in lung cancer cells. We have observed a significant cytotoxic effect (less than 10 µmol/L at 24 hours) of the selected compounds in several lung cancer cell lines. Moreover, the selected compounds showed IC_{50} values remarkably lower than cisplatin, the main chemotherapeutic agent used in the treatment of lung cancer patients.

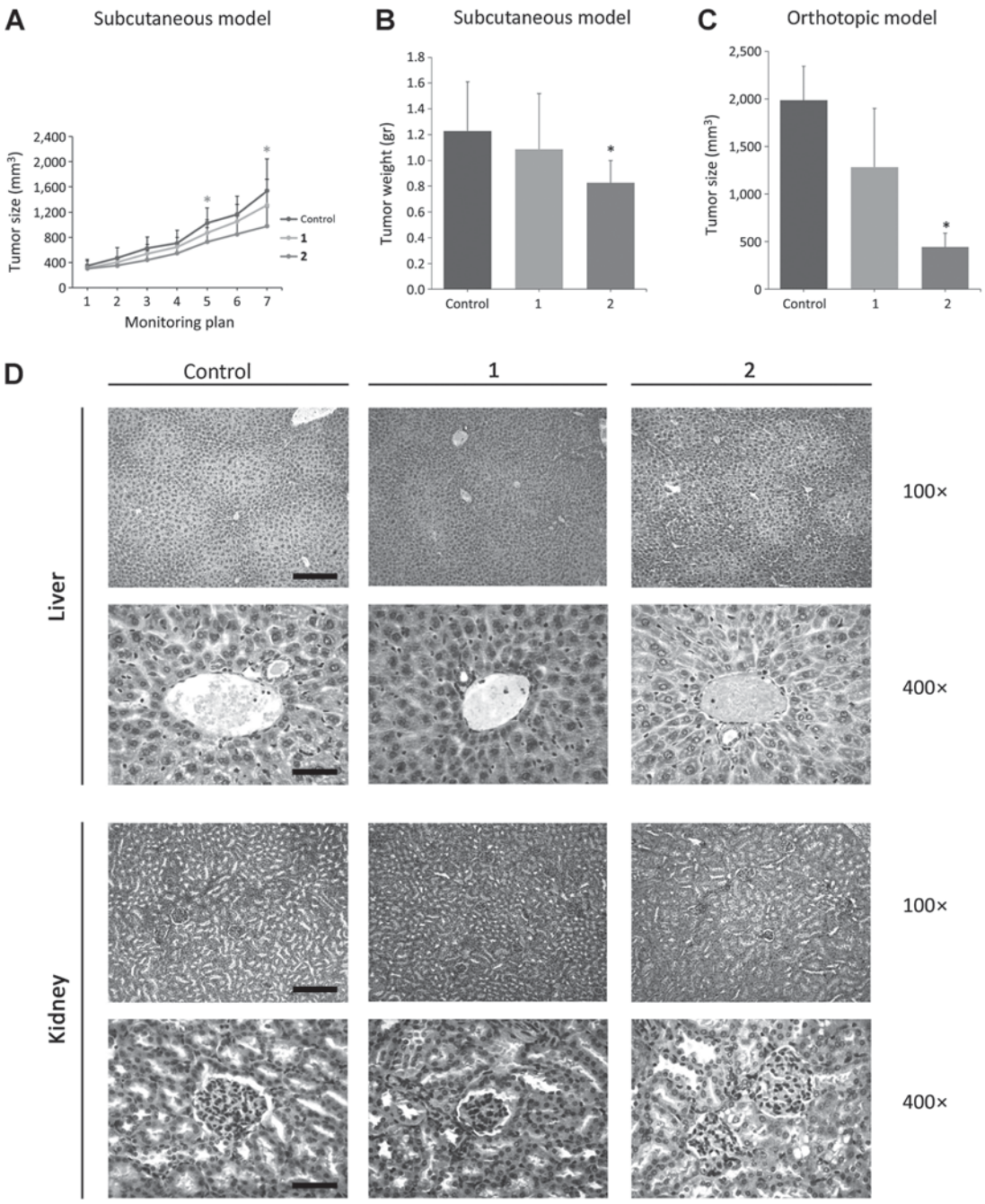

Figure 5.

Therapeutic effect of indole-based tambjamine-analogues in lung cancer *in vivo* mouse models. **A,** Growth curve of subcutaneous tumor volumes after compound treatment show significantly differences between compound **2** versus control. **B,** The weight of subcutaneous tumors compared with control animals is significantly lower after compound **2** treatment. **C,** Compound **2** treatment reduce significantly the tumor weight in orthotopic DMS53 mouse xenograft model. Statistical analysis was performed using the nonparametric tests. *, $P < 0.05$. **D,** Representative illustrations of liver and kidney histology using hematoxylin–eosin staining, at 100× and 400× magnifications (scale bars correspond to 200 and 50 μm, respectively). Histopathologic examination of mice liver and kidney detected no obvious pathologic changes after compound **1** or **2** treatment.

We have recently demonstrated how tambjamine analogues are able to alter the plasma membrane potential and decrease the intracellular pH in the A549 lung adenocarcinoma cell line (13). Changes in the ion homeostasis of the plasma membrane potential have already been associated with apoptosis-induced cell death in several cell types (S49, Jurkat, HL60, and thymocytes; refs. 22, 23). These observations, in addition to our transcriptomic results and the failure to arrest cell cycle, led us to further

investigate the molecular events related to the apoptotic process after cell treatment with these compounds.

The mitochondrial apoptotic pathway is closely regulated by the dynamic equilibrium of a group of proteins belonging to the Bcl-2 family with pro-apoptotic (e.g., Bax and Bak) and anti-apoptotic (e.g., Bcl-2 and Mcl-1) functions (24–26). The disruption of this equilibrium leads to the mitochondrial outer membrane permeabilization (MOMP) with the consequent release of cytochrome-c from the mitochondria and activation of initiator caspase-9. The initiator caspase-9 then activates the effector caspase-3 that cleaves regulatory and structural molecules (e.g., PARP), culminating in the death of the cell (24, 26). In this study, the activation of the intrinsic mitochondrial pathway and the cleavage of pro-caspase-9 and pro-caspase-3, as well as their substrate PARP were observed in lung cancer cells. In addition, the unbalance of the apoptotic pairs (Bcl-2/Bax and Mcl-1/Bak) towards the pro-apoptotic proteins unveils the final fate of these cells (27). In our system, the expression levels of prosurvival members of the Bcl-2 family (Bcl-2 and Mcl-1) decreased in a dose-dependent manner and the pro-apoptotic proteins (Bax and Bak) increased after the treatment. In terms of Bcl-2, this decrease further corroborates our transcriptomic results and shows that this alteration is occurring at the gene level. The IAP proteins (IAPs, e. g., XIAP and survivin) are proteins that maintain the small leakages of cytochrome-*c* or small activations of death receptors controlled by inhibiting the initiator and effector caspases. Survivin is a member of the IAP family that prevents mitochondrial-dependent apoptosis through the inhibition of caspase-9 and caspase-3 by direct or indirect binding (24, 28). Interestingly, after compounds treatment we have seen a downregulation of survivin, at both the transcript and protein levels, which also contributes to the triggering of the apoptotic cell death. Furthermore, using a pan-caspase inhibitor, we were able to significantly reverse the cytotoxic effect of our compounds. These results clearly indicate that compounds induce cell death through apoptosis by activating apoptosis-related proteins (caspase-9 and caspase-3) and decreasing the levels of anti-apoptotic proteins (Bcl-2, Mcl-1, and survivin).

The ionophoric activity of tambjamine analogues has an impact on cellular ion homeostasis and intracellular pH levels (13), thus, it is feasible that their actions will produce a cellular stress. Several recent works have shown that unbalanced ionic homeostasis is deeply involved in ROS generation (29–31). In our hands, treatment with the selected compounds induced a clear ROS production and this could be mediated by the anion transport because our previous work has shown that these compounds also induce cellular acidification (13). Conversely, the nontransporter compound neither produced pH changes nor generated ROS.

The MAPKs are crucial signaling players in the integration of stress signals and their conversion to cellular responses (32). One major MAPK signaling pathway that is important for detecting cellular stress, including intracellular acidosis and ROS, is the p38 MAPK cascade (32–34). The p38 MAPK-mediated apoptosis leads to caspase activation (35, 36), and several chemotherapeutic drugs have been shown to promote this cascade in order to produce apoptotic cancer cell death (36–42). Moreover, reversion of the apoptotic-mediated cell death produced by chemotherapeutic drugs that de-polymerize (nocodazole, vincristine, and vinblastine) or stabilize (taxol) microtubules was achieved by using p38 MAPK-specific inhibitors (e.g., SB203580 and SB202190). Likewise, genotoxic agents (cisplatin and oxaliplatin) and topoisomerase II inhibitors (doxorubicin) were also able to activate p38 MAPK route (43, 44). Nowadays, a dual-role of this route is known with the action as tumor suppressor or tumor promoter largely depending on the type of cancer and tumor stage (45). Interestingly, our results have shown a robust p38 MAPK activation and using the specific p38 MAPK inhibitor, SB202190, we were able to significantly restore cell viability. Reversion of cell death using the pan-caspase inhibitor or the stress kinase inhibitor is very similar, which foresight that our compounds mediate cell death by apoptosis mainly through the p38 MAPK route.

Moreover, several transcription factors have been implicated in the regulation of both anti-apoptotic proteins, survivin, and Bcl-2: Sp1, p53, NF-κB, and STAT3 (38, 46–48). Although Sp1, NF-κB, and STAT3 are generally implicated in transactivation of Bcl-2 and survivin genes, p53 was shown to be responsible for transcriptional repression of these genes. In addition, these transcription factors are all substrates of the p38 MAPK signaling pathway (49). In fact, several articles connect p38 MAPK activation with a downregulation of survivin and Bcl-2 expressions (39, 40, 50–53). Nevertheless, caution should be taken because other pathways are also involved in the activation/repression of these transcription factors and so, crosstalk with other routes is possible. Further experiments are underway to understand the regulation of these genes, which have a profound impact in the fate of the cells by apoptosis. Our study has also shown the therapeutic effect of our compounds in a preclinical setting using subcutaneous and orthotopic mouse models for lung cancer, which indicates a good potential for pharmaceutical development.

In conclusion, we have shown the cytotoxic effect of novel indole-based tambjamine analogues towards lung cancer cells *in vitro* and *in vivo*. We have also identified several gene-expression profile alterations produced by our compounds in lung cancer cells and have shown that the main molecular route of induced cell death is apoptosis, which might be activated by the p38 MAPK through ROS cellular stress induction. Ultimately, by understanding the mechanism of action through which these natural-based small molecules mediate their effect in cancer cells will provide a way to improve future studies of drug efficacy and pharmacodynamics, as well as establish drug–response biomarkers and synergistic drug combinations.

Disclosure of Potential Conflicts of Interest

No potential conflicts of interest were disclosed.

Authors' Contributions

Conception and design: L. Korrodi-Gregório, R. Quesada, V. Soto-Cerrato, R. Pérez-Tomás

Development of methodology: P. Manuel-Manresa, L. Korrodi-Gregório, E. Hernando, A. Villanueva, A.M. Rodilla, R. Ramos, V. Soto-Cerrato

Acquisition of data (provided animals, acquired and managed patients, provided facilities, etc.): P. Manuel-Manresa, L. Korrodi-Gregório, E. Hernando, A. Villanueva, D. Martínez-García, A.M. Rodilla, R. Ramos, J. Moya

Analysis and interpretation of data (e.g., statistical analysis, biostatistics, computational analysis): P. Manuel-Manresa, L. Korrodi-Gregório, D. Martínez-García, A.M. Rodilla, R. Ramos, R. Quesada, V. Soto-Cerrato, R. Pérez-Tomás

Writing, review, and/or revision of the manuscript: P. Manuel-Manresa, L. Korrodi-Gregório, D. Martínez-García, R. Ramos, M. Fardilha, R. Quesada, V. Soto-Cerrato, R. Pérez-Tomás

Administrative, technical, or material support (i.e., reporting or organizing data, constructing databases): L. Korrodi-Gregório, R. Quesada, R. Pérez-Tomás

Study supervision: L. Korrodi-Gregório, M. Fardilha, R. Quesada, V. Soto-Cerrato, R. Pérez-Tomás

Acknowledgments

We thank Beatriz Barroso from CCiTUB (Centres Científics i Tecnològics Universitat de Barcelona, Barcelona, Spain) for technical assistance.

Grant Support

This work was supported by grants from the Spanish Government and EU funds through the Fondo de Investigaciones Sanitarias (FIS, project PI13/00089) and from La Marató de TV3 Foundation (project 20132730) to R. Pérez-Tomás. R. Ramos was supported by the Sociedad Española de Neumología y Cirugía Torácica (SEPAR, Project 017/2013), R. Quesada by the Consejería de Educación de la Junta de Castilla y León (project BU340U13) and by the La Marató de TV3 Foundation (project 20132732) and A. Villanueva by the FIS (project PI13/01339). This work was also supported by an individual grant from FCT ((Fundação para a Ciência e a Tecnologia; SFRH/BPD/91766/2012) to L. Korrodi-Gregório) and a predoctoral fellowship awarded from the Government of Catalonia through L'Agència de Gestió d'Ajuts Universitaris i de Recerca (AGAUR; FI-DGR 2016) to D. Martínez-García.

The costs of publication of this article were defrayed in part by the payment of page charges. This article must therefore be hereby marked *advertisement* in accordance with 18 U.S.C. Section 1734 solely to indicate this fact.

Received November 10, 2016; revised December 16, 2016; accepted March 22, 2017; published OnlineFirst April 10, 2017.

References

1. Ferlay J, Soerjomataram I, Ervik M, Dikshit R, Eser S, Mathers C, et al. GLOBOCAN 2012 v1.0, Cancer Incidence and Mortality Worldwide: IARC CancerBase No. 11 [Internet]. Lyon, France: International Agency for Research on Cancer; 2013 [cited 2016 Jul 20]. Available from: http://globocan.iarc.fr.
2. Carrera PM, Ormond M. Current practice in and considerations for personalized medicine in lung cancer: from the patient's molecular biology to patient values and preferences. Maturitas 2015;82:94–9.
3. Molinski TF, Dalisay DS, Lievens SL, Saludes JP. Drug development from marine natural products. Nat Rev Drug Discov 2009;8:69–85.
4. Simmons TL, Andrianasolo E, McPhail K, Flatt P, Gerwick WH. Marine natural products as anticancer drugs. Mol Cancer Ther 2005;4:333–42.
5. Mayer AM, Glaser KB, Cuevas C, Jacobs RS, Kem W, Little RD, et al. The odyssey of marine pharmaceuticals: a current pipeline perspective. Trends Pharmacol Sci 2010;31:255–65.
6. Carbone M, Irace C, Costagliola F, Castelluccio F, Villani G, Calado G, et al. A new cytotoxic tambjamine alkaloid from the Azorean nudibranch Tambja ceutae. Bioorg Med Chem Lett 2010;20:2668–70.
7. Gale PA, Perez-Tomas R, Quesada R. Anion transporters and biological systems. Acc Chem Res 2013;46:2801–13.
8. Llagostera E, Soto-Cerrato V, Montaner B, Perez-Tomas R. Prodigiosin induces apoptosis by acting on mitochondria in human lung cancer cells. Ann N Y Acad Sci 2003;1010:178–81.
9. Perez-Tomas R, Montaner B, Llagostera E, Soto-Cerrato V. The prodigiosins, proapoptotic drugs with anticancer properties. Biochem Pharmacol 2003;66:1447–52.
10. Soto-Cerrato V, Llagostera E, Montaner B, Scheffer GL, Perez-Tomas R. Mitochondria-mediated apoptosis operating irrespective of multidrug resistance in breast cancer cells by the anticancer agent prodigiosin. Biochem Pharmacol 2004;68:1345–52.
11. Iglesias Hernandez P, Moreno D, Javier AA, Torroba T, Perez-Tomas R, Quesada R. Tambjamine alkaloids and related synthetic analogs: efficient transmembrane anion transporters. Chem Commun 2012;48:1556–8.
12. Hernando E, Soto-Cerrato V, Cortes-Arroyo S, Perez-Tomas R, Quesada R. Transmembrane anion transport and cytotoxicity of synthetic tambjamine analogs. Org Biomol Chem 2014;12:1771–8.
13. Soto-Cerrato V, Manuel-Manresa P, Hernando E, Calabuig-Farinas S, Martinez-Romero A, Fernandez-Duenas V, et al. Facilitated anion transport induces hyperpolarization of the cell membrane that triggers differentiation and cell death in cancer stem cells. J Am Chem Soc 2015;137:15892–8.
14. Gupta PB, Chaffer CL, Weinberg RA. Cancer stem cells: mirage or reality? Nat Med 2009;15:1010–2.
15. Shannon P, Markiel A, Ozier O, Baliga NS, Wang JT, Ramage D, et al. Cytoscape: a software environment for integrated models of biomolecular interaction networks. Genome Res 2003;13:2498–504.
16. Ambrogio C, Carmona FJ, Vidal A, Falcone M, Nieto P, Romero OA, et al. Modeling lung cancer evolution and preclinical response by orthotopic mouse allografts. Cancer Res 2014;74:5978–88.
17. Ambrogio C, Gomez-Lopez G, Falcone M, Vidal A, Nadal E, Crosetto N, et al. Combined inhibition of DDR1 and Notch signaling is a therapeutic strategy for KRAS-driven lung adenocarcinoma. Nat Med 2016;22:270–7.
18. Yan R, Yang Y, Zeng Y, Zou G. Cytotoxicity and antibacterial activity of Lindera strychnifolia essential oils and extracts. J Ethnopharmacol 2009;121:451–5.
19. Zhan M, Qu Q, Wang G, Zhou H. Let-7c sensitizes acquired cisplatin-resistant A549 cells by targeting ABCC2 and Bcl-XL. Pharmazie 2013;68:955–61.
20. Mueller S, Schittenhelm M, Honecker F, Malenke E, Lauber K, Wesselborg S, et al. Cell-cycle progression and response of germ cell tumors to cisplatin *in vitro*. Int J Oncol 2006;29:471–9.
21. Yang Y, Liu X, Huang J, Zhong Y, Mao Z, Xiao H, et al. Inhibition of p38 mitogen-activated protein kinase phosphorylation decrease tert-butyl hydroperoxide-induced apoptosis in human trabecular meshwork cells. Mol Vis 2012;18:2127–36.
22. Dallaporta B, Marchetti P, de Pablo MA, Maisse C, Duc H-T, Métivier D, et al. Plasma membrane potential in thymocyte apoptosis. J Immunol 1999;162:6534–42.
23. Bortner CD, Gómez-Angelats M, Cidlowski JA. Plasma membrane depolarization without repolarization is an early molecular event in anti-Fas-induced apoptosis. J Biol Chem 2001;276:4304–14.
24. Ghobrial IM, Witzig TE, Adjei AA. Targeting apoptosis pathways in cancer therapy. CA Cancer J Clin 2005;55:178–94.
25. Wong RS. Apoptosis in cancer: from pathogenesis to treatment. J Exp Clin Cancer Res 2011;30:87.
26. Bai L, Wang S. Targeting apoptosis pathways for new cancer therapeutics. Annu Rev Med 2014;65:139–55.
27. Czabotar PE, Lessene G, Strasser A, Adams JM. Control of apoptosis by the BCL-2 protein family: implications for physiology and therapy. Nat Rev Mol Cell Biol 2014;15:49–63.
28. Pavlyukov MS, Antipova NV, Balashova MV, Vinogradova TV, Kopantzev EP, Shakhparonov MI. Survivin monomer plays an essential role in apoptosis regulation. J Biol Chem 2011;286:23296–307.
29. Ko SK, Kim SK, Share A, Lynch VM, Park J, Namkung W, et al. Synthetic ion transporters can induce apoptosis by facilitating chloride anion transport into cells. Nat Chem 2014;6:885–92.
30. Saha T, Hossain MS, Saha D, Lahiri M, Talukdar P. Chloride-mediated apoptosis-inducing activity of Bis(sulfonamide) anionophores. J Am Chem Soc 2016;138:7558–67.
31. Zhao W, Lu M, Zhang Q. Chloride intracellular channel 1 regulates migration and invasion in gastric cancer by triggering the ROS-mediated p38 MAPK signaling pathway. Mol Med Rep 2015;12:8041–7.
32. Wagner EF, Nebreda AR. Signal integration by JNK and p38 MAPK pathways in cancer development. Nat Rev Cancer 2009;9:537–49.
33. Zarubin T, Han J. Activation and signaling of the p38 MAP kinase pathway. Cell Res 2005;15:11–8.
34. Son Y, Kim S, Chung HT, Pae HO. Reactive oxygen species in the activation of MAP kinases. Methods Enzymol 2013;528:27–48.
35. Tsuchiya T, Tsuno NH, Asakage M, Yamada J, Yoneyama S, Okaji Y, et al. Apoptosis induction by p38 MAPK inhibitor in human colon cancer cells. Hepatogastroenterology 2008;55:930–5.
36. Li QC, Liang Y, Tian Y, Hu GR. Arctigenin induces apoptosis in colon cancer cells through ROS/p38MAPK pathway. J BUON 2016;21:87–94.
37. Olson JM, Hallahan AR. p38 MAP kinase: a convergence point in cancer therapy. Trends Mol Med 2004;10:125–9.

38. Bodur C, Kutuk O, Karsli-Uzunbas G, Isimjan TT, Harrison P, Basaga H. Pramanicin analog induces apoptosis in human colon cancer cells: critical roles for Bcl-2, Bim, and p38 MAPK signaling. PLoS One 2013; 8:e56369.
39. Hsiao PW, Chang CC, Liu HF, Tsai CM, Chiu TH, Chao JI. Activation of p38 mitogen-activated protein kinase by celecoxib oppositely regulates survivin and gamma-H2AX in human colorectal cancer cells. Toxicol Appl Pharmacol 2007;222:97–104.
40. Liu HF, Hu HC, Chao JI. Oxaliplatin down-regulates survivin by p38 MAP kinase and proteasome in human colon cancer cells. Chem Biol Interact 2010;188:535–45.
41. Ahn J, Won M, Choi JH, Kim YS, Jung CR, Im DS, et al. Reactive oxygen species-mediated activation of the Akt/ASK1/p38 signaling cascade and p21(Cip1) downregulation are required for shikonin-induced apoptosis. Apoptosis 2013;18:870–81.
42. Pan J, Chang Q, Wang X, Son Y, Zhang Z, Chen G, et al. Reactive oxygen species-activated Akt/ASK1/p38 signaling pathway in nickel compound-induced apoptosis in BEAS 2B cells. Chem Res Toxicol 2010;23:568–77.
43. Hernandez Losa J, Parada Cobo C, Guinea Viniegra J, Sanchez-Arevalo Lobo VJ, Ramon y Cajal S, Sanchez-Prieto R. Role of the p38 MAPK pathway in cisplatin-based therapy. Oncogene 2003;22:3998–4006.
44. Fujie Y, Yamamoto H, Ngan CY, Takagi A, Hayashi T, Suzuki R, et al. Oxaliplatin, a potent inhibitor of survivin, enhances paclitaxel-induced apoptosis and mitotic catastrophe in colon cancer cells. Jpn J Clin Oncol 2005;35:453–63.
45. Garcia-Cano J, Roche O, Cimas FJ, Pascual-Serra R, Ortega-Muelas M, Fernandez-Aroca DM, et al. p38MAPK and chemotherapy: we always need to hear both sides of the story. Front Cell Dev Biol 2016;4:69.
46. Chen X, Duan N, Zhang C, Zhang W. Survivin and tumorigenesis: molecular mechanisms and therapeutic strategies. J Cancer 2016;7:314–23.
47. Li F, Altieri DC. Transcriptional analysis of human survivin gene expression. Biochem J 1999;344:305–11.
48. Carpenter RL, Lo HW. STAT3 target genes relevant to human cancers. Cancers 2014;6:897–925.
49. Cuadrado A, Nebreda AR. Mechanisms and functions of p38 MAPK signalling. Biochem J 2010;429:403–17.
50. Cao W, Xie YH, Li XQ, Zhang XK, Chen YT, Kang R, et al. Burn-induced apoptosis of cardiomyocytes is survivin dependent and regulated by PI3K/Akt, p38 MAPK and ERK pathways. Basic Res Cardiol 2011;106:1207–20.
51. Changchien JJ, Chen YJ, Huang CH, Cheng TL, Lin SR, Chang LS. Quinacrine induces apoptosis in human leukemia K562 cells via p38 MAPK-elicited BCL2 down-regulation and suppression of ERK/c-Jun-mediated BCL2L1 expression. Toxicol Appl Pharmacol 2015;284:33–41.
52. Chen YJ, Liu WH, Kao PH, Wang JJ, Chang LS. Involvement of p38 MAPK- and JNK-modulated expression of Bcl-2 and Bax in Naja nigricollis CMS-9-induced apoptosis of human leukemia K562 cells. Toxicon 2010;55:1306–16.
53. Hui K, Yang Y, Shi K, Luo H, Duan J, An J, et al. The p38 MAPK-regulated PKD1/CREB/Bcl-2 pathway contributes to selenite-induced colorectal cancer cell apoptosis in vitro and in vivo. Cancer Lett 2014;354:189–99.

Published OnlineFirst April 10, 2017; DOI: 10.1158/1535-7163.MCT-16-0752

AACR American Association for Cancer Research

Molecular Cancer Therapeutics

Novel Indole-based Tambjamine-Analogues Induce Apoptotic Lung Cancer Cell Death through p38 Mitogen-Activated Protein Kinase Activation

Pilar Manuel-Manresa, Luís Korrodi-Gregório, Elsa Hernando, et al.

Mol Cancer Ther 2017;16:1224-1235. Published OnlineFirst April 10, 2017.

BIBLIOGRAPHY

Acunzo, M. *et al.* (2012) "MiR-130a targets MET and induces TRAIL-sensitivity in NSCLC by downregulating miR-221 and 222," *Oncogene*. NIH Public Access, 31(5), pp. 634–642. doi: 10.1038/onc.2011.260.

Adachi, M. *et al.* (2000) "Significance of integrin alpha5 gene expression as a prognostic factor in node-negative non-small cell lung cancer.," *Clinical cancer research : an official journal of the American Association for Cancer Research*, 6(1), pp. 96–101.

Adams, J. M. and Cory, S. (2007) "The Bcl-2 apoptotic switch in cancer development and therapy," *Oncogene*, pp. 1324–1337. doi: 10.1038/sj.onc.1210220.

Ajani, J. A. *et al.* (2015) "Cancer stem cells: The promise and the potential," *Seminars in Oncology*, 42(S1), pp. S3–S17. doi: 10.1053/j.seminoncol.2015.01.001.

Aldrich, L. N. *et al.* (2010) "Total synthesis and biological evaluation of tambjamine K and a library of unnatural analogs," *Bioorganic and Medicinal Chemistry Letters*, 20(17), pp. 5207–5211. doi: 10.1016/j.bmcl.2010.06.154.

Alfarouk, K. O. *et al.* (2014) "Glycolysis, tumor metabolism, cancer growth and dissemination. A new pH-based etiopathogenic perspective and therapeutic approach to an old cancer question," *Oncoscience*. Impact Journals, LLC, 1(12), p. 777. doi: 10.18632/oncoscience.109.

Allison, A. C. and Young, M. R. (1969) "Vital staining and fluorescence microscopy of lysosomes," *Lysosomes in biology and pathology*, 2, pp. 600–628.

De Almagro, M. C. *et al.* (2017) "Coordinated ubiquitination and phosphorylation of RIP1 regulates necroptotic cell death," *Cell Death and Differentiation*. Nature Publishing Group, 24(1), pp. 26–37. doi: 10.1038/cdd.2016.78.

Amable, L. (2016) "Cisplatin resistance and opportunities for precision medicine," *Pharmacological Research*, pp. 27–36. doi: 10.1016/j.phrs.2016.01.001.

Ambrogio, C. *et al.* (2014) "Modeling lung cancer evolution and preclinical response by orthotopic mouse allografts," *Cancer Research*, 74(21), pp. 5978–5988. doi: 10.1158/0008-5472.CAN-14-1606.

Ambrogio, C. *et al.* (2016) "Combined inhibition of DDR1 and Notch signaling is a therapeutic strategy for KRAS-driven lung adenocarcinoma," *Nature Medicine*, 22(3), pp. 270–277. doi: 10.1038/nm.4041.

American Cancer Society (2016a) *Tests for Non-Small Cell Lung Cancer*. Available at: https://www.cancer.org/cancer/non-small-cell-lung-cancer/detection-diagnosis-staging/how-diagnosed.html (Accessed: February 5, 2018).

American Cancer Society (2016b) *Treating Non-Small Cell Lung Cancer*. Available at: https://www.cancer.org/cancer/non-small-cell-lung-cancer/treating.html (Accessed: February 5, 2018).

American Cancer Society (2017a) *How Are Oral Cavity and Oropharyngeal Cancers Diagnosed?* Available at: https://www.cancer.org/cancer/oral-cavity-and-oropharyngeal-cancer/detection-diagnosis-staging/how-diagnosed.html (Accessed: February 5, 2018).

American Cancer Society (2017b) *Targeted Therapy Drugs for Non-Small Cell Lung Cancer*. Available at: https://www.cancer.org/cancer/non-small-cell-lung-cancer/treating/targeted-therapies.html (Accessed: February 5, 2018).

American Cancer Society (2017c) *Treating Oral Cavity and Oropharyngeal Cancer*. Available at: https://www.cancer.org/cancer/oral-cavity-and-oropharyngeal-cancer/treating.html (Accessed: July 5, 2017).

Arafat, K. *et al.* (2013) "Inhibitory Effects of Salinomycin on Cell Survival, Colony Growth, Migration, and Invasion of Human Non-Small Cell Lung Cancer A549 and LNM35: Involvement of NAG-1," *PLoS ONE*. Edited by R. A. de Mello, 8(6). doi: 10.1371/journal.pone.0066931.

Ashcroft, F. (2000) *Ion channels and disease: channelopathies*, *Nature Cell Biology*. Academic Press.

Ávalos, Y. *et al.* (2014) "Tumor Suppression and Promotion by Autophagy," *BioMed Research International*. Hindawi, p. 603980. doi: 10.1155/2014/603980.

Bai, L. and Wang, S. (2014) "Targeting Apoptosis Pathways for New Cancer Therapeutics," *Annual Review of Medicine*, 65(1), pp. 139–155. doi: 10.1146/annurev-med-010713-141310.

Balkwill, F. R., Capasso, M. and Hagemann, T. (2012) "The tumor microenvironment at a glance," *Journal of Cell Science*, 125(23), pp. 5591–5596. doi: 10.1242/jcs.116392.

Bao, R. and Chan (2011) "Novel compounds in the treatment of lung cancer: current and developing therapeutic agents," *Journal of Experimental Pharmacology*, 3, pp. 21–34. doi: 10.2147/JEP.S7804.

Basit, F., Cristofanon, S. and Fulda, S. (2013) "Obatoclax (GX15-070) triggers necroptosis by promoting the assembly of the necrosome on autophagosomal membranes," *Cell Death and Differentiation*, 20(9), pp. 1161–1173. doi: 10.1038/cdd.2013.45.

Basso, A. D. *et al.* (2002) "Akt forms an intracellular complex with heat shock protein 90 (Hsp90) and Cdc37 and is destabilized by inhibitors of Hsp90 function," *Journal of Biological Chemistry*. American Society for Biochemistry and Molecular Biology, 277(42), pp. 39858–39866. doi: 10.1074/jbc.M206322200.

Batandier, C., Leverve, X. and Fontaine, E. (2004) "Opening of the mitochondrial permeability transition pore induces reactive oxygen species production at the level of the respiratory chain complex I.," *The Journal of biological chemistry*. American Society for Biochemistry and Molecular Biology, 279(17), pp. 17197–204. doi: 10.1074/jbc.M310329200.

Begum, S. *et al.* (2015) "An integrated genome-wide approach to discover deregulated microRNAs in non-small cell lung cancer: Clinical significance of MIR-23b-3p deregulation," *Scientific Reports*. Nature Publishing Group, 5. doi: 10.1038/srep13236.

Bender, E. (2014) “Epidemiology: The dominant malignancy.,” *Nature*. Nature Publishing Group, 513(7517), pp. 2011–2012. doi: 10.1038/513S2a.

Berezhnov, A. V. *et al.* (2016) “Intracellular pH modulates autophagy and mitophagy,” *Journal of Biological Chemistry*, 291(16), pp. 8701–8708. doi: 10.1074/jbc.M115.691774.

Berg, G. (2000) “Diversity of antifungal and plant-associated Serratia plymuthica strains,” *Journal of Applied Microbiology*, 88(6), pp. 952–960. doi: 10.1046/j.1365-2672.2000.01064.x.

Berghe, T. Vanden *et al.* (2010) “Necroptosis, necrosis and secondary necrosis converge on similar cellular disintegration features,” *Cell Death and Differentiation*, 17(6), pp. 922–930. doi: 10.1038/cdd.2009.184.

Berghe, T. Vanden *et al.* (2014) “Regulated necrosis: The expanding network of non-apoptotic cell death pathways,” *Nature Reviews Molecular Cell Biology*, pp. 135–147. doi: 10.1038/nrm3737.

Bjørkøy, G. *et al.* (2009) “Monitoring Autophagic Degradation of p62/SQSTM1,” in *Methods in enzymology*, pp. 181–197. doi: 10.1016/S0076-6879(08)03612-4.

Borrelli, K. W. *et al.* (2005) “PELE: Protein energy landscape exploration. A novel Monte Carlo based technique,” *Journal of Chemical Theory and Computation*. American Chemical Society, 1(6), pp. 1304–1311. doi: 10.1021/ct0501811.

Borrelli, K. W., Benjamin, C. and Guallar, V. (2010) “Exploring hierarchical refinement techniques for induced fit docking with protein and ligand flexibility,” *Journal of Computational Chemistry*. Wiley Subscription Services, Inc., A Wiley Company, 31(6), pp. 1224–1235. doi: 10.1002/jcc.21409.

Bosetti, F. *et al.* (2004) “Increased state 4 mitochondrial respiration and swelling in early post-ischemic reperfusion of rat heart,” *FEBS Letters*, 563(1–3), pp. 161–164. doi: 10.1016/S0014-5793(04)00294-7.

Boulares, A. H. *et al.* (1999) “Role of poly(ADP-ribose) polymerase (PARP) cleavage in apoptosis. Caspase 3-resistant PARP mutant increases rates of apoptosis in transfected cells.,” *The Journal of biological chemistry*. American Society for Biochemistry and Molecular Biology, 274(33), pp. 22932–40. doi: 10.1074/JBC.274.33.22932.

Boya, P. (2012) “Lysosomal Function and Dysfunction: Mechanism and Disease,” *Antioxidants & Redox Signaling*, 17(5), pp. 766–774. doi: 10.1089/ars.2011.4405.

Boya, P. and Kroemer, G. (2008) “Lysosomal membrane permeabilization in cell death,” *Oncogene*, 27(50), pp. 6434–6451.

Bunn, P. A. *et al.* (2016) “Small cell lung cancer: Can recent advances in biology and molecular biology be translated into improved outcomes?,” *Journal of Thoracic Oncology*. NIH Public Access, 11(4), pp. 453–474. doi: 10.1016/j.jtho.2016.01.012.

Busschaert, N. *et al.* (2010) “Tripodal transmembrane transporters for bicarbonate,” *Chem. Commun.* The Royal Society of Chemistry, 46(34), pp. 6252–6254. doi: 10.1039/C0CC01684E.

Busschaert, N. *et al.* (2012) “Squaramides as potent transmembrane anion transporters,” *Angewandte Chemie - International Edition*. WILEY-VCH Verlag, 51(18), pp. 4426–4430. doi: 10.1002/anie.201200729.

Busschaert, N. *et al.* (2014) “Thiosquaramides: pH switchable anion transporters,” *Chem. Sci.*, 5(9), pp. 3617–3626. doi: 10.1039/C4SC01629G.

Busschaert, N. *et al.* (2017) “A synthetic ion transporter that disrupts autophagy and induces apoptosis by perturbing cellular chloride concentrations,” *Nature Chemistry*. Nature Publishing Group, 9(7), pp. 667–675. doi: 10.1038/nchem.2706.

Busschaert, N. and Gale, P. A. (2013) “Small-Molecule Lipid-Bilayer Anion Transporters for Biological Applications,” *Angewandte Chemie International Edition*, 52(5), pp. 1374–1382.

Cairns, R. A., Harris, I. S. and Mak, T. W. (2011) “Regulation of cancer cell metabolism,” *Nature Reviews Cancer*. Nature Publishing Group, pp. 85–95. doi: 10.1038/nrc2981.

Calderwood, S. K. and Gong, J. (2016) “Heat Shock Proteins Promote Cancer: It’s a Protection Racket,” *Trends in Biochemical Sciences*, pp. 311–323. doi: 10.1016/j.tibs.2016.01.003.

Cancer Research UK (2017) *Chemotherapy treatment - Lung cancer - Cancer Research UK*. Available at: http://www.cancerresearchuk.org/about-cancer/lung-cancer/treatment/chemotherapy/chemotherapy-treatment (Accessed: July 5, 2017).

Carbone, M. *et al.* (2010) “A new cytotoxic tambjamine alkaloid from the Azorean nudibranch Tambja ceutae,” *Bioorganic & medicinal chemistry letters*, 20(8), pp. 2668–2670.

Carte, B. and Faulkner, D. J. (1983) “Defensive Metabolites from Three Nembrothid Nudibranchs,” *Journal of Organic Chemistry*. American Chemical Society, 48(14), pp. 2314–2318. doi: 10.1021/jo00162a003.

Casey, J. R., Grinstein, S. and Orlowski, J. (2009) “Sensors and regulators of intracellular pH,” *Nature Reviews Molecular Cell Biology*, 11. doi: 10.1038/nrm2820.

Castillo-Avila, W. *et al.* (2005) “Non-apoptotic concentrations of prodigiosin (H+/Cl- symporter) inhibit the acidification of lysosomes and induce cell cycle blockage in colon cancer cells,” *Life Sci*, 78(2), pp. 121–127. doi: 10.1016/j.lfs.2005.04.059.

Castro, A. J. (1967) “Antimalarial Activity of Prodigiosin,” *Nature*. Nature Publishing Group, 213(5079), pp. 903–904. doi: doi:10.1038/213903a0.

Cavalcanti, B. C. *et al.* (2008) “Cytotoxic and genotoxic effects of tambjamine D, an alkaloid isolated from the nudibranch Tambja eliora, on Chinese hamster lung fibroblasts,” *Chemico-Biological Interactions*. Elsevier, 174(3), pp. 155–162. doi: 10.1016/j.cbi.2008.05.029.

Chakraborty, K., Leung, K. and Krishnan, Y. (2017) “High lumenal chloride in the lysosome is critical for lysosome function,” *eLife*. eLife Sciences Publications Limited, 6, p. e28862. doi: 10.7554/eLife.28862.

Champa, D. *et al.* (2016) “Obatoclax kills anaplastic thyroid cancer cells by inducing lysosome neutralization and necrosis.,” *Oncotarget*, 7(23), pp. 18–23. doi: 10.18632/oncotarget.9121.

Chang, J. C. (2016) “Cancer stem cells: Role in tumor growth, recurrence, metastasis, and treatment resistance.,” *Medicine*, 95(1 Suppl 1), pp. S20-5. doi: 10.1097/MD.0000000000004766.

Chen, G. *et al.* (2013) “miR-146a Inhibits Cell Growth, Cell Migration and Induces Apoptosis in Non-Small Cell Lung Cancer Cells,” *PLoS ONE*. Edited by S. P. Chellappan, 8(3), p. e60317. doi: 10.1371/journal.pone.0060317.

Chen, Z. *et al.* (2014) “Non-small-cell lung cancers: a heterogeneous set of diseases,” *Nature Reviews Cancer*, 14(8), pp. 535–546. doi: 10.1038/nrc3775.

Cheng, G. *et al.* (2003) “Decrease of intracellular ATP content downregulated UCP2 expression in mouse hepatocytes.,” *Biochemical and biophysical research communications*, 308(3), pp. 573–80.

Chi, A. C., Day, T. A. and Neville, B. W. (2015) “Oral cavity and oropharyngeal squamous cell carcinoma-an update,” *CA: A Cancer Journal for Clinicians*, 65(5), pp. 401–421. doi: 10.3322/caac.21293.

Chiappori, A. *et al.* (2014) “Obatoclax Mesylate, a Pan–Bcl-2 Inhibitor, in Combination with Docetaxel in a Phase 1/2 Trial in Relapsed Non–Small-Cell Lung Cancer,” *Journal of Thoracic Oncology*, 9(1), pp. 121–125. doi: 10.1097/JTO.0000000000000027.

Choi, K. S. (2012) “Autophagy and cancer,” *Experimental and Molecular Medicine*, 44(2), pp. 109–120. doi: 10.3858/emm.2012.44.2.033.

Cirman, T. *et al.* (2004) “Selective Disruption of Lysosomes in HeLa Cells Triggers Apoptosis Mediated by Cleavage of Bid by Multiple Papain-like Lysosomal Cathepsins,” *Journal of Biological Chemistry*. in Press, 279(5), pp. 3578–3587. doi: 10.1074/jbc.M308347200.

Cossins, B. P., Hosseini, A. and Guallar, V. (2012) “Exploration of protein conformational change with PELE and meta-dynamics,” *Journal of Chemical Theory and Computation*. American Chemical Society, 8(3), pp. 959–965. doi: 10.1021/ct200675g.

Coulthard, L. R. *et al.* (2009) “p38MAPK: stress responses from molecular mechanisms to therapeutics,” *Trends in Molecular Medicine*, pp. 369–379. doi: 10.1016/j.molmed.2009.06.005.

Couraud, S. *et al.* (2012) “Lung cancer in never smokers - A review,” *European Journal of Cancer*, 48(9), pp. 1299–1311. doi: 10.1016/j.ejca.2012.03.007.

Coussens, L. M. and Werb, Z. (2002) “Inflammation and cancer,” *Nature*, 420(6917), pp. 860–867. doi: 10.1038/nature01322.

Cui, R. *et al.* (2015) “MicroRNA-224 promotes tumor progression in nonsmall cell lung cancer,” *Proceedings of the National Academy of Sciences*, 112(31), pp. E4288–E4297. doi: 10.1073/pnas.1502068112.

Cummings, B. S., Schnellmann, R. G. and Schnellmann, R. G. (2004) “Measurement of cell death in mammalian cells.,” *Current protocols in pharmacology*. NIH Public Access, Chapter 12, p. Unit 12.8. doi: 10.1002/0471141755.ph1208s25.

da Cunha Santos, G., Shepherd, F. A. and Tsao, M. S. (2011) "EGFR Mutations and Lung Cancer," *Annual Review of Pathology: Mechanisms of Disease*, 6(1), pp. 49–69. doi: 10.1146/annurev-pathol-011110-130206.

Czabotar, P. E. *et al.* (2014) "Control of apoptosis by the BCL-2 protein family: Implications for physiology and therapy," *Nature Reviews Molecular Cell Biology*, pp. 49–63. doi: 10.1038/nrm3722.

Dacic, S. *et al.* (2010) "miRNA expression profiling of lung adenocarcinomas: correlation with mutational status," *Modern pathology*, 23(12), pp. 1577–1582.

Damaghi, M., Wojtkowiak, J. W. and Gillies, R. J. (2013) "pH sensing and regulation in cancer," *Front Physiol*. Frontiers Media SA, 4, p. 370. doi: 10.3389/fphys.2013.00370.

Darshan, N. and Manonmani, H. K. (2015) "Prodigiosin and its potential applications," *Journal of Food Science and Technology*, 52(9), pp. 5393–5407. doi: 10.1007/s13197-015-1740-4.

Daugaard, I. and Hansen, T. B. (2017) "Biogenesis and Function of Ago-Associated RNAs," *Trends in Genetics*, pp. 208–219. doi: 10.1016/j.tig.2017.01.003.

Davies, M. A. (2011) "Regulation, role, and targeting of Akt in cancer," *Journal of Clinical Oncology*, 29(35), pp. 4715–4717. doi: 10.1200/JCO.2011.37.4751.

Davis, J. T., Okunola, O. and Quesada, R. (2010) "Recent advances in the transmembrane transport of anions," *Chemical Society Reviews*. The Royal Society of Chemistry, 39(10), p. 3843. doi: 10.1039/b926164h.

Delbridge, A. R. D. *et al.* (2016) "Thirty years of BCL-2: translating cell death discoveries into novel cancer therapies," *Nature Reviews Cancer*, 16(2), pp. 99–109. doi: 10.1038/nrc.2015.17.

Denduluri, S. K. *et al.* (2015) "Insulin-like growth factor (IGF) signaling in tumorigenesis and the development of cancer drug resistance.," *Genes & Diseases*, 2(1), pp. 14–20. doi: 10.1016/j.gendis.2014.10.004.

Denton, D., Nicolson, S. and Kumar, S. (2012) "Cell death by autophagy: Facts and apparent artefacts," *Cell Death and Differentiation*, pp. 87–95. doi: 10.1038/cdd.2011.146.

DiCiccio, J. E. and Steinberg, B. E. (2011) "Lysosomal pH and analysis of the counter ion pathways that support acidification.," *The Journal of general physiology*. Rockefeller University Press, 137(4), pp. 385–90. doi: 10.1085/jgp.201110596.

Dolado, I. and Nebreda, A. R. (2007) "Regulation of Tumorigenesis by p38α MAP Kinase," in *Stress-Activated Protein Kinases*. Berlin, Heidelberg: Springer Berlin Heidelberg, pp. 99–128. doi: 10.1007/4735_2007_0245.

Dragu, D. L. *et al.* (2015) "Therapies targeting cancer stem cells: Current trends and future challenges.," *World journal of stem cells*. Baishideng Publishing Group Inc, 7(9), pp. 1185–201. doi: 10.4252/wjsc.v7.i9.1185.

Ehrlich, P. (1909) "Ueber Den Jetzigen Stand Der Karzinomforschung," *Nederlandsch Tijdschrift voor Geneeskunde*, (5), pp. 273–290. doi: 10.1002/cber.19090420105.

Elmore, S. (2007) “Apoptosis: a review of programmed cell death.,” *Toxicologic pathology*. NIH Public Access, 35(4), pp. 495–516. doi: 10.1080/01926230701320337.

Eramo, A. *et al.* (2008) “Identification and expansion of the tumorigenic lung cancer stem cell population,” *Cell Death and Differentiation*, 15(3), pp. 504–514. doi: 10.1038/sj.cdd.4402283.

Espona-Fiedler, M. *et al.* (2012) “Identification of dual mTORC1 and mTORC2 inhibitors in melanoma cells: prodigiosin vs. obatoclax,” *Biochem Pharmacol*, 83(4), pp. 489–496. doi: 10.1016/j.bcp.2011.11.027.

Facchinetti, F. *et al.* (2017) “Mechanisms of Resistance to Target Therapies in Non-small Cell Lung Cancer,” in *Handbook of experimental pharmacology*. Springer, Berlin, Heidelberg, pp. 1–27. doi: 10.1007/164_2017_16.

Feng, I.-C. *et al.* (2017) “Cantharidic acid induces apoptosis through the p38 MAPK signaling pathway in human hepatocellular carcinoma,” *Environmental Toxicology*. doi: 10.1002/tox.22513.

Ferlay, J. *et al.* (2015) “Cancer incidence and mortality worldwide: Sources, methods and major patterns in GLOBOCAN 2012,” *International Journal of Cancer*, 136(5), pp. E359–E386. doi: 10.1002/ijc.29210.

Fulda, S. and Vucic, D. (2012) “Targeting IAP proteins for therapeutic intervention in cancer,” *Nature Reviews Drug Discovery*. Nature Publishing Group, p. 331. doi: 10.1038/nrd3698.

Fumarola, C. *et al.* (2014) “Targeting PI3K/AKT/mTOR pathway in non small cell lung cancer,” *Biochemical Pharmacology*. Elsevier, pp. 197–207. doi: 10.1016/j.bcp.2014.05.011.

Gale, P. A., Pérez-Tomás, R. and Quesada, R. (2013) “Anion transporters and biological systems,” *Accounts of Chemical Research*, 46(12), pp. 2801–2813. doi: 10.1021/ar400019p.

Galluzzi, L. *et al.* (2015) “Autophagy in malignant transformation and cancer progression,” *The EMBO Journal*, 34(7), pp. 856–880. doi: 10.15252/embj.201490784.

Galluzzi, L. *et al.* (2015) “Essential versus accessory aspects of cell death: Recommendations of the NCCD 2015,” *Cell Death and Differentiation*, pp. 58–73. doi: 10.1038/cdd.2014.137.

Galluzzi, L., Blomgren, K. and Kroemer, G. (2009) “Mitochondrial membrane permeabilization in neuronal injury,” *Nature Reviews Neuroscience*, 10(7), pp. 481–494. doi: 10.1038/nrn2665.

Galluzzi, L., Bravo-San Pedro, J. M. and Kroemer, G. (2014) “Organelle-specific initiation of cell death,” *Nature Cell Biology*. Nature Publishing Group, pp. 728–736. doi: 10.1038/ncb3005.

Galluzzi, L., Kepp, O. and Kroemer, G. (2016) “Mitochondrial regulation of cell death: a phylogenetically conserved control,” *Microbial Cell*, 3(3), pp. 101–108. doi: 10.15698/mic2016.03.483.

García-Valverde, M. *et al.* (2012) “Conformational analysis of a model synthetic prodiginine,” *Journal of Organic Chemistry*, 77(15), pp. 6538–6544. doi: 10.1021/jo301008c.

Geng, L. *et al.* (2014) “MicroRNA-103 promotes colorectal cancer by targeting tumor suppressor DICER and PTEN,” *International Journal of Molecular Sciences*, 15(5), pp. 8458–8472. doi: 10.3390/ijms15058458.

Glick, D., Barth, S. and Macleod, K. F. (2010) “Autophagy: cellular and molecular mechanisms,” *The Journal of Pathology*, 221(1), pp. 3–12. doi: 10.1002/path.2697.

Goard, C. A. and Schimmer, A. D. (2013) “An evidence-based review of obatoclax mesylate in the treatment of hematological malignancies,” *Core Evidence*. Dove Press, pp. 15–26. doi: 10.2147/CE.S42568.

Goldstraw, P. *et al.* (2016) “The IASLC lung cancer staging project: Proposals for revision of the TNM stage groupings in the forthcoming (eighth) edition of the TNM Classification for lung cancer,” *Journal of Thoracic Oncology*. Elsevier, pp. 39–51. doi: 10.1016/j.jtho.2015.09.009.

Golstein, P. and Kroemer, G. (2007) “Cell death by necrosis: towards a molecular definition,” *Trends in Biochemical Sciences*, 32(1), pp. 37–43. doi: 10.1016/j.tibs.2006.11.001.

Gomes, A., Fernandes, E. and Lima, J. L. F. C. (2005) “Fluorescence probes used for detection of reactive oxygen species,” *Journal of Biochemical and Biophysical Methods*, pp. 45–80. doi: 10.1016/j.jbbm.2005.10.003.

Granato, A. C. *et al.* (2005) “Produtos naturais da ascídia Botrylloides giganteum, das esponjas Verongula gigantea, Ircinia felix, Cliona delitrix e do nudibrânquio Tambja eliora, da costa do Brasil,” *Quimica Nova*. SBQ, 28(2), pp. 192–198. doi: 10.1590/S0100-40422005000200005.

Le Grand, M. *et al.* (2017) “Akt targeting as a strategy to boost chemotherapy efficacy in non-small cell lung cancer through metabolism suppression,” *Scientific Reports*. Nature Publishing Group, 7, p. 45136. doi: 10.1038/srep45136.

Grebner, C. *et al.* (2016) “Binding Mode and Induced Fit Predictions for Prospective Computational Drug Design,” *Journal of Chemical Information and Modeling*. American Chemical Society, 56(4), pp. 774–787. doi: 10.1021/acs.jcim.5b00744.

Green, D. R., Galluzzi, L. and Kroemer, G. (2014) “Metabolic control of cell death,” *Science*. doi: 10.1126/science.1250256.

Green, D. R. and Levine, B. (2014) “To Be or Not to Be? How Selective Autophagy and Cell Death Govern Cell Fate,” *Cell*, 157(1), pp. 65–75. doi: 10.1016/j.cell.2014.02.049.

Green, D. R. and Llambi, F. (2015) “Cell death signaling,” *Cold Spring Harbor Perspectives in Biology*. Cold Spring Harbor Laboratory Press, 7(12), p. a006080. doi: 10.1101/cshperspect.a006080.

Grivennikov, S. I., Greten, F. R. and Karin, M. (2010) “Immunity, inflammation, and cancer.,” *Cell*. NIH Public Access, 140(6), pp. 883–99. doi: 10.1016/j.cell.2010.01.025.

Gupta, N. *et al.* (2017) “Changing Trends in oral cancer – a global scenario,” *Nepal Journal of Epidemiology*. International Nepal Epidemiological Association, 6(4), p. 613. doi: 10.3126/nje.v6i4.17255.

Gupta, P. B. *et al.* (2009) “Identification of Selective Inhibitors of Cancer Stem Cells by High-Throughput Screening,” *Cell*, 138(4), pp. 645–659. doi: 10.1016/j.cell.2009.06.034.

Ha, M. and Kim, V. N. (2014) “Regulation of microRNA biogenesis,” *Nature Reviews Molecular Cell Biology*, pp. 509–524. doi: 10.1038/nrm3838.

Habela, C. W. *et al.* (2009) “Chloride Accumulation Drives Volume Dynamics Underlying Cell Proliferation and Migration,” *Journal of Neurophysiology*. American Physiological Society, 101(2), pp. 750–757. doi: 10.1152/jn.90840.2008.

Hale, A. N. *et al.* (2013) “Autophagy: Regulation and role in development,” *Autophagy*. Taylor & Francis, pp. 951–972. doi: 10.4161/auto.24273.

Halestrap, A. P. (1994) “Regulation of mitochondrial metabolism through changes in matrix volume,” *Biochemical Society Transactions*, 22(2), pp. 522–529. doi: 10.1042/bst0220522.

Halestrap, A. P. (2009) “What is the mitochondrial permeability transition pore?,” *Journal of Molecular and Cellular Cardiology*. Academic Press, 46(6), pp. 821–831. doi: 10.1016/J.YJMCC.2009.02.021.

Han, H. *et al.* (2013) “A c-Myc-MicroRNA functional feedback loop affects hepatocarcinogenesis,” *Hepatology*, 57(6), pp. 2378–2389.

Han, S. B. *et al.* (2001) “Prodigiosin blocks T cell activation by inhibiting interleukin-2Ralpha expression and delays progression of autoimmune diabetes and collagen-induced arthritis.,” *The Journal of pharmacology and experimental therapeutics*, 299(2), pp. 415–425.

Hanahan, D. and Weinberg, R. A. (2011) “Hallmarks of cancer: The next generation,” *Cell*, pp. 646–674. doi: 10.1016/j.cell.2011.02.013.

Hayes, J., Peruzzi, P. P. and Lawler, S. (2014) “MicroRNAs in cancer: Biomarkers, functions and therapy,” *Trends in Molecular Medicine*, pp. 460–469. doi: 10.1016/j.molmed.2014.06.005.

Hayflick, L. (1965) “The limited in vitro lifetime of human diploid cell strains,” *Experimental Cell Research*. Academic Press, 37(3), pp. 614–636. doi: 10.1016/0014-4827(65)90211-9.

He, M. and Xue, Y. (2017) “MicroRNA-148a suppresses proliferation and invasion potential of non-small cell lung carcinomas via regulation of STAT3.,” *OncoTargets and therapy*. Dove Press, 10, pp. 1353–1361. doi: 10.2147/OTT.S123518.

Hecht, S. S. (2012) “Lung carcinogenesis by tobacco smoke,” *International Journal of Cancer*. Wiley Subscription Services, Inc., A Wiley Company, 131(12), pp. 2724–2732. doi: 10.1002/ijc.27816.

Heidari, N., Hicks, M. A. and Harada, H. (2010) “GX15-070 (obatoclax) overcomes glucocorticoid resistance in acute lymphoblastic leukemia through induction of apoptosis and autophagy.,” *Cell death & disease*. Nature Publishing Group, 1(9), p. e76. doi: 10.1038/cddis.2010.53.

Hernandez, C., Huebener, P. and Schwabe, R. F. (2016) “Damage-associated molecular patterns in cancer: A double-edged sword,” *Oncogene*. NIH Public Access, pp. 5931–5941. doi: 10.1038/onc.2016.104.

Hernández, P. I. *et al.* (2012) “Tambjamine alkaloids and related synthetic analogs: efficient transmembrane anion transporters,” *Chemical Communications*, 48(10), pp. 1556–1558.

Hernando, E. *et al.* (2014) “Transmembrane anion transport and cytotoxicity of synthetic tambjamine analogs.,” *Organic & biomolecular chemistry*, 12(11), pp. 1771–8. doi: 10.1039/c3ob42341g.

Herranz, H. and Cohen, S. M. (2010) *MicroRNAs and gene regulatory networks: Managing the impact of noise in biological systems*, *Genes and Development*. doi: 10.1101/gad.1937010.

Hers, I., Vincent, E. E. and Tavaré, J. M. (2011) "Akt signalling in health and disease," *Cellular Signalling*, pp. 1515–1527. doi: 10.1016/j.cellsig.2011.05.004.

Hirai, H. *et al.* (2010) "MK-2206, an Allosteric Akt Inhibitor, Enhances Antitumor Efficacy by Standard Chemotherapeutic Agents or Molecular Targeted Drugs In vitro and In vivo," *Molecular Cancer Therapeutics*. American Association for Cancer Research, 9(7), pp. 1956–1967. doi: 10.1158/1535-7163.MCT-09-1012.

Hirsch, F. R. *et al.* (2017) "Lung cancer: current therapies and new targeted treatments," *The Lancet*, pp. 299–311. doi: 10.1016/S0140-6736(16)30958-8.

Hu, X. *et al.* (2014) "Efficacy and potential microRNA mechanism for computed tomography-guided percutaneous radiofrequency ablation of primary lung cancer and lung metastasis from liver cancer," *Cellular Physiology and Biochemistry*, 33(5), pp. 1261–1271. doi: 10.1159/000358694.

Hübner, C. A. and Jentsch, T. J. (2002) "Ion channel diseases," *Human molecular genetics*, 11(20), pp. 2435–2445.

Huczynski, A. (2012) "Salinomycin - A New Cancer Drug Candidate," *Chemical Biology & Drug Design*, 79(3), pp. 235–238. doi: 10.1111/j.1747-0285.2011.01287.x.

Ian Storer, R., Aciro, C. and Jones, L. H. (2011) "Squaramides: physical properties, synthesis and applications," *Chemical Society Reviews*. The Royal Society of Chemistry, 40(5), p. 2330. doi: 10.1039/c0cs00200c.

IARC (2005) "Tumours of the Oral Cavity and Oropharynx," *Pathology and Genetics of Head and Neck Tumours*, pp. 163–181.

Ibrahim, D. *et al.* (2014) "Prodigiosin - an antibacterial red pigment produced by Serratia marcescens IBRL USM 84 associated with a marine sponge Xestospongia testudinaria," *Journal of Applied Pharmaceutical Science*, 4(10), pp. 1–6. doi: 10.7324/JAPS.2014.40101.

Ichim, G. and Tait, S. W. G. (2016) "A fate worse than death: apoptosis as an oncogenic process," *Nature Reviews Cancer*, 16(8), pp. 539–548. doi: 10.1038/nrc.2016.58.

Ikeda, R. *et al.* (2011) "Isolation and characterization of gemcitabine-resistant human non-small cell lung cancer A549 cells," *International Journal of Oncology*, 38(2), pp. 513–519. doi: 10.3892/ijo.2010.866.

Inamura, K. and Ishikawa, Y. (2016) "MicroRNA In Lung Cancer: Novel Biomarkers and Potential Tools for Treatment," *Journal of Clinical Medicine*. Multidisciplinary Digital Publishing Institute (MDPI), 5(3), p. 36. doi: 10.3390/jcm5030036.

Incoronato, M. *et al.* (2010) "MiR-212 increases tumor necrosis factor–related apoptosis-inducing ligand sensitivity in non–small cell lung cancer by targeting the antiapoptotic protein PED," *Cancer research*, 70(9), pp. 3638–3646.

Incoronato, M. *et al.* (2011) “Epigenetic regulation of miR-212 expression in lung cancer,” *PLoS ONE*, 6(11), p. e27722.

Jacobsen, K. *et al.* (2017) “Convergent Akt activation drives acquired EGFR inhibitor resistance in lung cancer,” *Nature Communications*. Nature Publishing Group, 8(1), p. 410. doi: 10.1038/s41467-017-00450-6.

Jangamreddy, J. R. *et al.* (2013) “Salinomycin induces activation of autophagy, mitophagy and affects mitochondrial polarity: differences between primary and cancer cells,” *Biochimica et Biophysica Acta (BBA)-Molecular Cell Research*, 1833(9), pp. 2057–2069.

Javadov, S., Chapa-Dubocq, X. and Makarov, V. (2017) “Different approaches to modeling analysis of mitochondrial swelling.” doi: 10.1016/j.mito.2017.08.004.

Jiang, M. *et al.* (2013) “Relative expressions of miR-205-5p, miR-205-3p, and miR-21 in tissues and serum of non-small cell lung cancer patients,” *Molecular and Cellular Biochemistry*. Springer US, 383(1–2), pp. 67–75. doi: 10.1007/s11010-013-1755-y.

Jin, Z. and El-Deiry, W. S. (2005) “Overview of cell death signaling pathways,” *Cancer Biology and Therapy*, pp. 139–163. doi: 10.4161/cbt.4.2.1508.

Kaasik, A. *et al.* (2007) “Regulation of mitochondrial matrix volume,” *Am J Physiol Cell Physiol*, 292, pp. 157–163. doi: 10.1152/ajpcell.00272.2006.

Kågedal, K. *et al.* (2001) “Sphingosine-induced apoptosis is dependent on lysosomal proteases,” *Biochemical Journal*. Portland Press Limited, 359(2), pp. 335–343. doi: 10.1042/bj3590335.

Kalbáčová, M. *et al.* (2003) “Comparison of the effect of mitochondrial inhibitors on mitochondrial membrane potential in two different cell lines using flow cytometry and spectrofluorometry,” *Cytometry Part A*. Wiley Subscription Services, Inc., A Wiley Company, 52A(2), pp. 110–116. doi: 10.1002/cyto.a.10031.

Kalbe, C., Marten, P. and Berg, G. (1996) “Strains of the genus Serratia as beneficial rhizobacteria of oilseed rape with antifungal properties,” *Microbiological Research*. Urban & Fischer, 151(4), pp. 433–439. doi: 10.1016/S0944-5013(96)80014-0.

Kang, R. *et al.* (2011) “The Beclin 1 network regulates autophagy and apoptosis,” *Cell Death & Differentiation*, 18(4), pp. 571–580. doi: 10.1038/cdd.2010.191.

Kantari, C. and Walczak, H. (2011) “Caspase-8 and Bid: Caught in the act between death receptors and mitochondria,” *Biochimica et Biophysica Acta - Molecular Cell Research*, pp. 558–563. doi: 10.1016/j.bbamcr.2011.01.026.

Kellar, A., Egan, C. and Morris, D. (2015) “Preclinical Murine Models for Lung Cancer: Clinical Trial Applications.,” *BioMed research international*. Hindawi, 2015, p. 621324. doi: 10.1155/2015/621324.

Kim, I., Rodriguez-Enriquez, S. and Lemasters, J. J. (2007) “Selective degradation of mitochondria by mitophagy,” *Archives of Biochemistry and Biophysics*. Academic Press, 462(2), pp. 245–253. doi: 10.1016/j.abb.2007.03.034.

Kim, K.-Y. *et al.* (2011) “Salinomycin-induced apoptosis of human prostate cancer cells due to accumulated reactive oxygen species and mitochondrial membrane depolarization,” *Biochemical and Biophysical Research Communications*. Academic Press, 413(1), pp. 80–86. doi: 10.1016/J.BBRC.2011.08.054.

Kim, K.-Y. *et al.* (2017) “Salinomycin Induces Reactive Oxygen Species and Apoptosis in Aggressive Breast Cancer Cells as Mediated with Regulation of Autophagy.,” *Anticancer research*. International Institute of Anticancer Research, 37(4), pp. 1747–1758. doi: 10.21873/anticanres.11507.

Kim, K. H. and Lee, M.-S. (2014) “Autophagy—a key player in cellular and body metabolism,” *Nature Reviews Endocrinology*, 10(6), pp. 322–337. doi: 10.1038/nrendo.2014.35.

Klymkowsky, M. W. and Savagner, P. (2009) “Epithelial-mesenchymal transition: a cancer researcher’s conceptual friend and foe.,” *The American journal of pathology*. American Society for Investigative Pathology, 174(5), pp. 1588–93. doi: 10.2353/ajpath.2009.080545.

Knight, N. J. *et al.* (2016) “QSAR analysis of substituent effects on tambjamine anion transporters,” *Chem. Sci.*, 7(2), pp. 1600–1608. doi: 10.1039/C5SC03932K.

Ko, S.-K. *et al.* (2014) “Synthetic ion transporters can induce apoptosis by facilitating chloride anion transport into cells,” *Nature chemistry*, 6(10), pp. 885–892.

Komatsu, M. and Ichimura, Y. (2010) “Physiological significance of selective degradation of p62 by autophagy,” *FEBS letters*, 584(7), pp. 1374–1378. doi: 10.1016/j.febslet.2010.02.017.

Kotev, M. *et al.* (2017) “Inhibition of Human Enhancer of Zeste Homolog 2 with Tambjamine Analogs,” *Journal of Chemical Information and Modeling*. American Chemical Society, 57(8), pp. 2089–2098. doi: 10.1021/acs.jcim.7b00178.

Kotev, M., Soliva, R. and Orozco, M. (2016) “Challenges of docking in large, flexible and promiscuous binding sites,” *Bioorganic and Medicinal Chemistry*. Elsevier, 24(20), pp. 4961–4969. doi: 10.1016/j.bmc.2016.08.010.

Koul, H. K., Pal, M. and Koul, S. (2013) “Role of p38 MAP Kinase Signal Transduction in Solid Tumors,” *Genes & Cancer*, 4(9–10), pp. 342–359. doi: 10.1177/1947601913507951.

Kroemer, G. *et al.* (2007) “Mitochondrial membrane permeabilization in cell death,” *Physiological Reviews*, 87(1), pp. 99–163. doi: 10.1152/physrev.00013.2006.

Kroemer, G. *et al.* (2009) “Classification of Cell Death 2009,” *Cell death and differentiation*. NIH Public Access, 16(1), pp. 3–11. doi: 10.1038/cdd.2008.150.Classification.

Kroemer, G., Galluzzi, L. and Brenner, C. (2007) “Mitochondrial membrane permeabilization in cell death,” *Physiological Reviews*, 87(1), pp. 99–163.

Kroemer, G. and Jäättelä, M. (2005) “Lysosomes and autophagy in cell death control,” *Nature Reviews Cancer*, pp. 886–897. doi: 10.1038/nrc1738.

Kroemer, G. and Levine, B. (2008) “Autophagic cell death: The story of a misnomer,” *Nature Reviews Molecular Cell Biology*. Nature Publishing Group, pp. 1004–1010. doi: 10.1038/nrm2529.

Kubli, D. A. and Gustafsson, Å. B. (2012) “Mitochondria and mitophagy: The yin and yang of cell death control,” *Circulation Research*, 111(9), pp. 1208–1221. doi: 10.1161/CIRCRESAHA.112.265819.

Kwon, K.-Y. Y., Viollet, B. and Yoo, O. J. (2011) “CCCP induces autophagy in an AMPK-independent manner,” *Biochemical and Biophysical Research Communications*. Academic Press, 416(3–4), pp. 343–348. doi: 10.1016/j.bbrc.2011.11.038.

Lagadic-Gossmann, D., Huc, L. and Lecureur, V. (2004) “Alterations of intracellular pH homeostasis in apoptosis: origins and roles,” 11(9), pp. 953–961. doi: 10.1038/sj.cdd.4401466.

Landi, M. T. *et al.* (2010) “MicroRNA expression differentiates histology and predicts survival of lung cancer,” *Clinical Cancer Research*. American Association for Cancer Research, 16(2), pp. 430–441. doi: 10.1158/1078-0432.CCR-09-1736.

Langer, C. J. *et al.* (2014) “Randomized phase II study of carboplatin and etoposide with or without obatoclax mesylate in extensive-stage small cell lung cancer,” *Lung Cancer*, 85(3), pp. 420–428. doi: 10.1016/j.lungcan.2014.05.003.

Lara, P. N. *et al.* (2015) “Phase II study of the AKT inhibitor MK-2206 plus erlotinib in patients with advanced non-small cell lung cancer who previously progressed on erlotinib,” *Clinical Cancer Research*, 21(19), pp. 4321–4326. doi: 10.1158/1078-0432.CCR-14-3281.

Lawen, A. (2003) “Apoptosis - An introduction,” *BioEssays*, pp. 888–896. doi: 10.1002/bies.10329.

Lazaro, J. E. H. *et al.* (2002) “Heptyl prodigiosin, a bacterial metabolite, is antimalarial in vivo and non-mutagenic in vitro.,” *Journal of natural toxins*, 11(4), pp. 367–77.

Leist, M. *et al.* (1997) “Intracellular Adenosine Triphosphate (ATP) Concentration: A Switch in the Decision Between Apoptosis and Necrosis,” *The Journal of Experimental Medicine*. Rockefeller University Press, 185(8), pp. 1481–1486. doi: 10.1084/jem.185.8.1481.

Li, H. *et al.* (2017) “Bypassing CFTR dysfunction in cystic fibrosis with alternative pathways for anion transport,” *Current Opinion in Pharmacology*, pp. 91–97. doi: 10.1016/j.coph.2017.10.002.

Li, J. *et al.* (2015) “MicroRNA-148a suppresses invasion and metastasis of human non-small-cell lung cancer,” *Cellular Physiology and Biochemistry*, 37(5), pp. 1847–1856. doi: 10.1159/000438546.

Li, J. *et al.* (2016) “Synergistic effects of sorafenib in combination with gemcitabine or pemetrexed in lung cancer cell lines with K-ras mutations.,” *Contemporary oncology (Poznan, Poland)*, 20(1), pp. 33–8. doi: 10.5114/wo.2016.58499.

Li, L. *et al.* (2007) “Honokiol induces a necrotic cell death through the mitochondrial permeability transition pore,” *Cancer Research*, 67(10), pp. 4894–4903. doi: 10.1158/0008-5472.CAN-06-3818.

Li, M. *et al.* (2013) “miR-205 targets PTEN and PHLPP2 to augment AKT signaling and drive malignant phenotypes in non-small cell lung cancer,” *Cancer Research*, 73(17), pp. 5402–5415. doi: 10.1158/0008-5472.CAN-13-0297.

Li, Q. *et al.* (2015) “Arctigenin induces apoptosis in colon cancer cells through ROS / p38MAPK pathway,” 21(1), pp. 87–94.

Li, Y. *et al.* (2010) “miR-146a suppresses invasion of pancreatic cancer cells,” *Cancer Research*, 70(4), pp. 1486–1495. doi: 10.1158/0008-5472.CAN-09-2792.

Liao, Y. and Hung, M. C. (2010) “Physiological regulation of Akt activity and stability,” *American Journal of Translational Research*, pp. 19–42. doi: 20182580.

Liberti, M. V. and Locasale, J. W. (2016) “The Warburg Effect: How Does it Benefit Cancer Cells?,” *Trends in Biochemical Sciences*, pp. 211–218. doi: 10.1016/j.tibs.2015.12.001.

Linkermann, A. *et al.* (2014) “Regulated cell death and inflammation: An auto-amplification loop causes organ failure,” *Nature Reviews Immunology*, pp. 759–767. doi: 10.1038/nri3743.

Litan, A. and Langhans, S. A. (2015) “Cancer as a channelopathy: ion channels and pumps in tumor development and progression.,” *Frontiers in cellular neuroscience*. Frontiers Media SA, 9, p. 86. doi: 10.3389/fncel.2015.00086.

Llagostera, E. *et al.* (2003) “Prodigiosin induces apoptosis by acting on mitochondria in human lung cancer cells,” *Annals of the New York Academy of Sciences*, 1010, pp. 178–181.

Lodish, H. and A. Berk, S. L. Zipursky, P. Matsudaira, D. B. and J. D. (2000) “Intracellular Ion Environment and Membrane Electric Potential,” in *Molecular Cell Biology*. 4th ed. New York: W. H. Freeman.

Lomonosova, E. and Chinnadurai, G. (2008) “BH3-only proteins in apoptosis and beyond: an overview,” *Oncogene*, 27(S1), pp. S2–S19. doi: 10.1038/onc.2009.39.

Lu, Y. *et al.* (2013) “Two Pore Channel 2 (TPC2) Inhibits Autophagosomal-Lysosomal Fusion by Alkalinizing Lysosomal pH,” *Journal of Biological Chemistry*. American Society for Biochemistry and Molecular Biology, 288(33), pp. 24247–24263. doi: 10.1074/jbc.M113.484253.

Lu, Y. *et al.* (2014) “Vacuolin-1 potently and reversibly inhibits autophagosome-lysosome fusion by activating RAB5A,” *Autophagy*. Taylor & Francis, 10(11), pp. 1895–1905. doi: 10.4161/auto.32200.

Lu, Z.-M. *et al.* (2014) “Micro-ribonucleic acid expression profiling and bioinformatic target gene analyses in laryngeal carcinoma,” *OncoTargets and therapy*, 7, p. 525.

MacDonagh, L. *et al.* (2016) “Lung cancer stem cells: The root of resistance,” *Cancer Letters*. Elsevier, pp. 147–156. doi: 10.1016/j.canlet.2016.01.012.

Madeira, A. *et al.* (2009) “Coupling surface plasmon resonance to mass spectrometry to discover novel protein-protein interactions.,” *Nature protocols*. Nature Publishing Group, 4(7), pp. 1023–1037. doi: 10.1038/nprot.2009.84.

Magee, P., Shi, L. and Garofalo, M. (2015) “Role of microRNAs in chemoresistance,” *Annals of translational medicine*. AME Publications, 3(21), p. 332. doi: 10.3978/j.issn.2305-5839.2015.11.32.

Maltese, W. A. and Overmeyer, J. H. (2014) “Methuosis: nonapoptotic cell death associated with vacuolization of macropinosome and endosome compartments,” *American Journal of Pathology*, 184(6), pp. 1630–1642. doi: 10.1016/j.ajpath.2014.02.028.

Manderville, R. A. (2001) “Synthesis, proton-affinity and anti-cancer properties of the prodigiosin-group natural products.,” *Current medicinal chemistry. Anti-cancer agents*, 1(2), pp. 195–218.

Manning, B. D. and Toker, A. (2017) “AKT/PKB Signaling: Navigating the Network,” *Cell*. Elsevier, pp. 381–405. doi: 10.1016/j.cell.2017.04.001.

Mantovani, A. *et al.* (2008) “Cancer-related inflammation,” *Nature*, pp. 436–444. doi: 10.1038/nature07205.

Manuel-Manresa, P. *et al.* (2017) “Novel indole-based tambjamine-analogues induce apoptotic lung cancer cell death through p38 mitogen-activated protein kinase activation,” *Molecular Cancer Therapeutics*, 16(7). doi: 10.1158/1535-7163.MCT-16-0752.

Martín-Hernán, F. *et al.* (2013) “Oral cancer, HPV infection and evidence of sexual transmission.,” *Medicina oral, patología oral y cirugía bucal*, 18(3), pp. e439-44. doi: 10.4317/medoral.18419.

Martin, B. *et al.* (2015) “Early Process Development of a Squaramide-Based CXCR2 Receptor Antagonist,” *Organic Process Research and Development*. American Chemical Society, 19(8), pp. 1038–1043. doi: 10.1021/acs.oprd.5b00072.

Mathew, R. *et al.* (2009) “Autophagy Suppresses Tumorigenesis through Elimination of p62,” *Cell*. Cell Press, 137(6), pp. 1062–1075. doi: 10.1016/j.cell.2009.03.048.

Mbah, N. E., Overmeyer, J. H. and Maltese, W. A. (2017) “Disruption of endolysosomal trafficking pathways in glioma cells by methuosis-inducing indole-based chalcones,” *Cell Biology and Toxicology*, 33(3), pp. 263–282. doi: 10.1007/s10565-016-9369-2.

McCoy, F. *et al.* (2010) “Obatoclax induces Atg7-dependent autophagy independent of beclin-1 and BAX/BAK,” *Cell Death and Disease*. Nature Publishing Group, 1(12), p. e108. doi: 10.1038/cddis.2010.86.

McCubrey, J. A., LaHair, M. M. and Franklin, R. A. (2006) “Reactive Oxygen Species-Induced Activation of the MAP Kinase Signaling Pathways,” *Antioxidants & Redox Signaling*, 8(9–10), pp. 1775–1789. doi: 10.1089/ars.2006.8.1775.

McIlwain, D. R., Berger, T. and Mak, T. W. (2013) “Caspase functions in cell death and disease,” *Cold Spring Harbor Perspectives in Biology*, 5(4), pp. 1–28. doi: 10.1101/cshperspect.a008656.

Miko, E. *et al.* (2009) “Differentially expressed microRNAs in small cell lung cancer,” *Experimental lung research*, 35(8), pp. 646–664.

De Milito, A. *et al.* (2007) “Proton Pump Inhibitors Induce Apoptosis of Human B-Cell Tumors through a Caspase-Independent Mechanism Involving Reactive Oxygen Species,” *Cancer Research*, 67(11), pp. 5408–5417. doi: 10.1158/0008-5472.CAN-06-4095.

Miller, K. D. *et al.* (2016) “Cancer treatment and survivorship statistics, 2016,” *CA: A Cancer Journal for Clinicians*, 66(4), pp. 271–289. doi: 10.3322/caac.21349.

Mindell, J. A. (2012) “Lysosomal Acidification Mechanisms,” *Annual Review of Physiology*, 74(1), pp. 69–86. doi: 10.1146/annurev-physiol-012110-142317.

Mittal, D. *et al.* (2014) “New insights into cancer immunoediting and its three component phases-elimination, equilibrium and escape,” *Current Opinion in Immunology*, pp. 16–25. doi: 10.1016/j.coi.2014.01.004.

Mittal, V. *et al.* (2016) “The Microenvironment of Lung Cancer and Therapeutic Implications,” in *Advances in experimental medicine and biology*, pp. 75–110. doi: 10.1007/978-3-319-24932-2_5.

Montaner, B. and Perez-Tomas, R. (2001) “Prodigiosin-induced apoptosis in human colon cancer cells,” *Life Sci*, 68(17), pp. 2025–2036. doi: 10.1016/s0024-3205(01)01002-5.

Montaner, B. and Perez-Tomas, R. (2003) “The prodigiosins: a new family of anticancer drugs,” *Curr Cancer Drug Targets*, 3(1), pp. 57–65. doi: 10.2174/1568009033333772.

Montani, F. *et al.* (2015) “MiR-test: A blood test for lung cancer early detection,” *Journal of the National Cancer Institute*. Oxford University Press, 107(6). doi: 10.1093/jnci/djv063.

Moreno-Gonzalez, G., Vandenabeele, P. and Krysko, D. V. (2016) “Necroptosis: A Novel Cell Death Modality and Its Potential Relevance for Critical Care Medicine,” *American Journal of Respiratory and Critical Care Medicine*, 194(4), pp. 415–428. doi: 10.1164/rccm.201510-2106CI.

Morrison, D. K. (2012) “MAP kinase pathways,” *Cold Spring Harbor Perspectives in Biology*, 4(11), pp. a011254–a011254. doi: 10.1101/cshperspect.a011254.

Mueller, S. *et al.* (2006) “Cell-cycle progression and response of germ cell tumors to cisplatin in vitro.,” *International journal of oncology*, 29(2), pp. 471–9.

Muenst, S. *et al.* (2016) “The immune system and cancer evasion strategies: therapeutic concepts,” *Journal of Internal Medicine*, 279(6), pp. 541–562. doi: 10.1111/joim.12470.

Münster, P. N. *et al.* (2001) “Inhibition of heat shock protein 90 function by ansamycins causes the morphological and functional differentiation of breast cancer cells,” *Cancer Research*. American Association for Cancer Research, 61(7), pp. 2945–2952.

Murrow, L. and Debnath, J. (2013) “Autophagy as a stress response and quality control mechanism—implications for cell injury and human disease,” *Annual review of pathology*, 8, p. 105.

National Collaborating Centre for Cancer (2011) *The Diagnosis and Treatment of Lung Cancer (Update)*, *The Diagnosis and Treatment of Lung Cancer (Update)*. National Collaborating Centre for Cancer (UK).

Naujokat, C. and Steinhart, R. (2012) “Salinomycin as a drug for targeting human cancer stem cells.,” *Journal of biomedicine & biotechnology*. Hindawi, 2012, p. 950658. doi: 10.1155/2012/950658.

Neel, D. S. and Bivona, T. G. (2017) “Resistance is futile: overcoming resistance to targeted therapies in lung adenocarcinoma,” *npj Precision Oncology*, 1(1), p. 3. doi: 10.1038/s41698-017-0007-0.

Neri, D. and Supuran, C. T. (2011) *Interfering with pH regulation in tumours as a therapeutic strategy*, *Nature Reviews Drug Discovery*. doi: 10.1038/nrd3554.

Nguyen, H. H. *et al.* (2015) “Surface plasmon resonance: A versatile technique for biosensor applications,” *Sensors (Switzerland)*. Multidisciplinary Digital Publishing Institute, pp. 10481–10510. doi: 10.3390/s150510481.

Nguyen, M. *et al.* (2007) “Small molecule obatoclax (GX15-070) antagonizes MCL-1 and overcomes MCL-1-mediated resistance to apoptosis,” *Proceedings of the National Academy of Sciences*, 104(49), pp. 19512–19517. doi: 10.1073/pnas.0709443104.

Olenych, S. G. *et al.* (2007) “The fluorescent protein color palette,” *Curr Protoc Cell Biol*, Chapter 21, p. Unit 21 5. doi: 10.1002/0471143030.cb2105s36.

Oliveto, S. *et al.* (2017) “Role of microRNAs in translation regulation and cancer World Journal of Biological Chemistry,” *World J Biol Chem February World J Biol Chem*, 26(81), pp. 45–56. doi: 10.4331/wjbc.v8.i1.45.

Olmo, F. *et al.* (2014) “Synthesis and biological evaluation of N, N ’-squaramides with high in vivo efficacy and low toxicity: Toward a low-cost drug against Chagas disease,” *Journal of Medicinal Chemistry*. American Chemical Society, 57(3), pp. 987–999. doi: 10.1021/jm4017015.

Ouyang, L. *et al.* (2012) “Programmed cell death pathways in cancer: A review of apoptosis, autophagy and programmed necrosis,” *Cell Proliferation*, 45(6), pp. 487–498. doi: 10.1111/j.1365-2184.2012.00845.x.

Overmeyer, J. H. *et al.* (2008) “Active Ras Triggers Death in Glioblastoma Cells through Hyperstimulation of Macropinocytosis,” *Molecular Cancer Research*, 6(6), pp. 965–977. doi: 10.1158/1541-7786.MCR-07-2036.

Overmeyer, J. H. *et al.* (2011) “A chalcone-related small molecule that induces methuosis, a novel form of non-apoptotic cell death, in glioblastoma cells,” *Molecular Cancer*. BioMed Central, 10(1), p. 69. doi: 10.1186/1476-4598-10-69.

Panayotopoulou, E. G. *et al.* (2017) “Targeting of apoptotic pathways by SMAC or BH3 mimetics distinctly sensitizes paclitaxel-resistant triple negative breast cancer cells,” *Oncotarget*, 8(28), pp. 45088–45104. doi: 10.18632/oncotarget.15125.

Pardoll, D. M. (2012) “The blockade of immune checkpoints in cancer immunotherapy,” *Nature Reviews Cancer*, pp. 252–264. doi: 10.1038/nrc3239.

Parks, S. K. *et al.* (2013) “Disrupting proton dynamics and energy metabolism for cancer therapy,” *Nature Reviews Cancer*, 13(9), pp. 611–623. doi: 10.1038/nrc3579.

Parzych, K. R. and Klionsky, D. J. (2014) “An Overview of Autophagy: Morphology, Mechanism, and Regulation,” *Antioxidants & Redox Signaling*. Mary Ann Liebert, Inc., 20(3), pp. 460–473. doi: 10.1089/ars.2013.5371.

Pasparakis, M. and Vandenabeele, P. (2015) “Necroptosis and its role in inflammation,” *Nature*, pp. 311–320. doi: 10.1038/nature14191.

Pattabiraman, D. R. and Weinberg, R. A. (2014) “Tackling the cancer stem cells-what challenges do they pose?,” *Nature Reviews Drug Discovery*. Nature Publishing Group, pp. 497–512. doi: 10.1038/nrd4253.

Pavlova, N. N. and Thompson, C. B. (2016) “The Emerging Hallmarks of Cancer Metabolism,” *Cell Metabolism*, pp. 27–47. doi: 10.1016/j.cmet.2015.12.006.

Pedersen, S. F. and Stock, C. (2013) “Ion channels and transporters in cancer: Pathophysiology, regulation, and clinical potential,” in *Cancer Research*, pp. 1658–1661. doi: 10.1158/0008-5472.CAN-12-4188.

Peng, Y. and Croce, C. M. (2016) “The role of MicroRNAs in human cancer,” *Signal Transduction and Targeted Therapy*, 1, p. 15004.

Perez-Tomas, R. *et al.* (2003) “The prodigiosins, proapoptotic drugs with anticancer properties,” *Biochem Pharmacol*, 66(8), pp. 1447–1452. doi: 10.1016/s0006-2952(03)00496-9.

Perez-Tomas, R. and Montaner, B. (2003) “Effects of the proapoptotic drug prodigiosin on cell cycle-related proteins in Jurkat T cells,” *Histol Histopathol*, 18(2), pp. 379–385.

Perez-Tomas, R. and Vinas, M. (2010) “New insights on the antitumoral properties of prodiginines,” *Curr Med Chem*. Bentham Science Publishers B.V., 17(21), pp. 2222–2231. doi: 10.2174/092986710791331103.

Petrie, E. J., Hildebrand, J. M. and Murphy, J. M. (2017) “Insane in the membrane: a structural perspective of MLKL function in necroptosis,” *Immunology and Cell Biology*, 95(2), pp. 152–159. doi: 10.1038/icb.2016.125.

Pinkerton, D. M. *et al.* (2010) “Antimicrobial and cytotoxic activities of synthetically derived tambjamines C and E - J, BE-18591, and a related alkaloid from the marine bacterium Pseudoalteromonas tunicata,” *Chem Biodivers*, 7(5), pp. 1311–1324. doi: 10.1002/cbdv.201000030.

Polyak, K. and Hahn, W. C. (2006) “Roots and stems: Stem cells in cancer,” *Nature Medicine*. Nature Publishing Group, pp. 296–300. doi: 10.1038/nm1379.

Polyak, K. and Weinberg, R. A. (2009) “Transitions between epithelial and mesenchymal states: acquisition of malignant and stem cell traits,” *Nature Reviews Cancer*, 9(4), pp. 265–273. doi: 10.1038/nrc2620.

Prevarskaya, N., Skryma, R. and Shuba, Y. (2010) “Ion channels and the hallmarks of cancer,” *Trends in Molecular Medicine*, 16(3), pp. 107–121. doi: 10.1016/j.molmed.2010.01.005.

Rabinowits, G. *et al.* (2009) “Exosomal microRNA: a diagnostic marker for lung cancer,” *Clinical lung cancer*, 10(1), pp. 42–46.

Ram, H. *et al.* (2011) “Oral Cancer: Risk Factors and Molecular Pathogenesis,” *Journal of Maxillofacial and Oral Surgery*. Springer, 10(2), pp. 132–137. doi: 10.1007/s12663-011-0195-z.

Repnik, U., Hafner Česen, M. and Turk, B. (2014) “Lysosomal membrane permeabilization in cell death: Concepts and challenges,” *Mitochondrion*, 19, pp. 49–57. doi: 10.1016/j.mito.2014.06.006.

Robertson, C. A., Evans, D. H. and Abrahamse, H. (2009) “Photodynamic therapy (PDT): A short review on cellular mechanisms and cancer research applications for PDT,” *Journal of Photochemistry and Photobiology B: Biology*. Elsevier, pp. 1–8. doi: 10.1016/j.jphotobiol.2009.04.001.

Robinson, M. W. *et al.* (2012) “Synthesis and Evaluation of Indole-Based Chalcones as Inducers of Methuosis, a Novel Type of Nonapoptotic Cell Death,” *Journal of Medicinal Chemistry*, 55(5), pp. 1940–1956. doi: 10.1021/jm201006x.

Rodilla, A. M. *et al.* (2017) “Synthetic tambjamine analogues induce mitochondrial swelling and lysosomal dysfunction leading to autophagy blockade and necrotic cell death in lung cancer,” *Biochemical Pharmacology*. Elsevier, 126, pp. 23–33. doi: 10.1016/j.bcp.2016.11.022.

Rouslin, W., Broge, C. W. and Grupp, I. L. (1990) “ATP depletion and mitochondrial functional loss during ischemia in slow and fast heart-rate hearts.,” *The American journal of physiology*, 259(6 Pt 2), pp. H1759–H1766. doi: 10.1152/ajpheart.1990.259.6.H1759.

Rusten, T. E. and Stenmark, H. (2010) “p62, an autophagy hero or culprit?,” *Nature Cell Biology*. Nature Publishing Group, 12(3), pp. 207–209. doi: 10.1038/ncb0310-207.

Saha, T. *et al.* (2016) “Chloride-Mediated Apoptosis-Inducing Activity of Bis(sulfonamide) Anionophores,” *Journal of the American Chemical Society*. American Chemical Society, 138(24), pp. 7558–7567. doi: 10.1021/jacs.6b01723.

Sanfiorenzo, C. *et al.* (2013) “Two panels of plasma microRNAs as non-invasive biomarkers for prediction of recurrence in resectable NSCLC,” *PLoS ONE*, 8(1), p. e54596.

Sato, S., Fujita, N. and Tsuruo, T. (2000) “Modulation of Akt kinase activity by binding to Hsp90,” *Proc Natl Acad Sci U S A*. National Academy of Sciences, 97(20), pp. 10832–10837. doi: 10.1073/pnas.170276797.

Sato, T. *et al.* (1998) “Prodigiosins as a new group of H+/Cl- symporters that uncouple proton translocators,” *Journal of Biological Chemistry*, 273(34), pp. 21455–21462. doi: 10.1074/jbc.273.34.21455.

Schieber, M. and Chandel, N. S. (2014) “ROS function in redox signaling and oxidative stress.,” *Current biology : CB*. NIH Public Access, 24(10), pp. R453-62. doi: 10.1016/j.cub.2014.03.034.

Schimmer, A. D. *et al.* (2014) “A Multicenter Phase I/II Study of Obatoclax Mesylate Administered as a 3- or 24-Hour Infusion in Older Patients with Previously Untreated Acute Myeloid Leukemia,” *PLoS ONE*. Edited by M. R. Baer, 9(10), p. e108694. doi: 10.1371/journal.pone.0108694.

Schneider, J. L. and Cuervo, A. M. (2014) “Autophagy and human disease: emerging themes,” *Current Opinion in Genetics & Development*, 26, pp. 16–23. doi: 10.1016/j.gde.2014.04.003.

Schulze, A. and Harris, A. L. (2012) “How cancer metabolism is tuned for proliferation and vulnerable to disruption,” *Nature*, 491(7424), pp. 364–373. doi: 10.1038/nature11706.

Scrima, M. *et al.* (2012) “Signaling networks associated with AKT activation in non-small cell lung cancer (NSCLC): New insights on the role of phosphatydil-inositol-3 kinase,” *PLoS ONE*. Edited by A. Fusco. Public Library of Science, 7(2), p. e30427. doi: 10.1371/journal.pone.0030427.

Sena, L. A. and Chandel, N. S. (2012) “Physiological Roles of Mitochondrial Reactive Oxygen Species,” *Molecular Cell*. Cell Press, 48(2), pp. 158–167. doi: 10.1016/J.MOLCEL.2012.09.025.

SEOM (2016) “Las Cifras del Cáncer en España 2016,” *Sociedad Española de Oncología Médica*, pp. 1–20.

Serrano-Puebla, A. and Boya, P. (2016) “Lysosomal membrane permeabilization in cell death: new evidence and implications for health and disease,” *Annals of the New York Academy of Sciences*, 1371(1), pp. 30–44. doi: 10.1111/nyas.12966.

Sessler, J. L. *et al.* (2005) “Synthesis, anion-binding properties, and in vitro anticancer activity of prodigiosin analogues,” *Angewandte Chemie - International Edition*. WILEY-VCH Verlag, 44(37), pp. 5989–5992. doi: 10.1002/anie.200501740.

Sessler, J. L. *et al.* (2005) “Synthesis, Anion-Binding Properties, and In Vitro Anticancer Activity of Prodigiosin Analogues,” *Angewandte Chemie International Edition*, 44(37), pp. 5989–5992.

Shaw, A. T. and Engelman, J. A. (2013) “ALK in lung cancer: Past, present, and future,” *Journal of Clinical Oncology*. American Society of Clinical Oncology, pp. 1105–1111. doi: 10.1200/JCO.2012.44.5353.

Shen, H.-M. and Mizushima, N. (2014) “At the end of the autophagic road: an emerging understanding of lysosomal functions in autophagy,” *Trends in Biochemical Sciences*. Elsevier Current Trends, 39(2), pp. 61–71.

Shen, Z. (2011) “Genomic instability and cancer: An introduction,” *Journal of Molecular Cell Biology*. Oxford University Press, pp. 1–3. doi: 10.1093/jmcb/mjq057.

Sherman, C. D. (2005) “Multistage Carcinogenesis Models.” BC Decker, 3, pp. 275–285. doi: 10.1002/0470011815.b2a07037.

Shirmanova, M. V. *et al.* (2017) “Chemotherapy with cisplatin: Insights into intracellular pH and metabolic landscape of cancer cells in vitro and in vivo,” *Scientific Reports*. Nature Publishing Group, 7(1), p. 8911. doi: 10.1038/s41598-017-09426-4.

Slee, E. A., Adrain, C. and Martin, S. J. (2001) “Executioner Caspase-3, -6, and -7 Perform Distinct, Non-redundant Roles during the Demolition Phase of Apoptosis,” *Journal of Biological Chemistry*. American Society for Biochemistry and Molecular Biology, 276(10), pp. 7320–7326. doi: 10.1074/jbc.M008363200.

Soliev, A. B., Hosokawa, K. and Enomoto, K. (2011) “Bioactive pigments from marine bacteria: applications and physiological roles.,” *Evidence-based complementary and alternative medicine : eCAM*. Hindawi, 2011, p. 670349. doi: 10.1155/2011/670349.

Son, Y. *et al.* (2011) “Mitogen-Activated Protein Kinases and Reactive Oxygen Species: How Can ROS Activate MAPK Pathways?” Hindawi, 2011. doi: 10.1155/2011/792639.

Soriano, J. *et al.* (2014) “Regulated necrosis in HeLa cells induced by ZnPc photodynamic treatment: a new nuclear morphology.,” *International journal of molecular sciences*. Multidisciplinary Digital Publishing Institute (MDPI), 15(12), pp. 22772–85. doi: 10.3390/ijms151222772.

Soto-Cerrato, V. *et al.* (2004) “Mitochondria-mediated apoptosis operating irrespective of multidrug resistance in breast cancer cells by the anticancer agent prodigiosin,” *Biochemical Pharmacology*, 68(7), pp. 1345–1352.

Soto-Cerrato, V. *et al.* (2015) “Facilitated Anion Transport Induces Hyperpolarization of the Cell Membrane That Triggers Differentiation and Cell Death in Cancer Stem Cells,” *Journal of the American Chemical Society*, 137(50), pp. 15892–15898. doi: 10.1021/jacs.5b09970.

Stamelos, V. A. *et al.* (2016) “The BH3 Mimetic Obatoclax Accumulates in Lysosomes and Causes Their Alkalinization,” *PLoS ONE*. Edited by A. Villunger. Public Library of Science, 11(3), p. e0150696. doi: 10.1371/journal.pone.0150696.

Stock, C. and Schwab, A. (2009) “Protons make tumor cells move like clockwork,” *Pflügers Archiv - European Journal of Physiology*, 458(5), pp. 981–992. doi: 10.1007/s00424-009-0677-8.

Subramanian, J. and Govindan, R. (2007) “Lung Cancer in Never Smokers : A Review,” *J Clin Onccol*, 25(5), pp. 561–70. doi: 10.1200/JCO.2006.06.8015.

Sun, S., Schiller, J. H. and Gazdar, A. F. (2007) “Lung cancer in never smokers - A different disease,” *Nature Reviews Cancer*. Nature Publishing Group, pp. 778–790. doi: 10.1038/nrc2190.

Sun, Y. *et al.* (2013) “Expression of miR-150 and miR-3940-5p is reduced in non-small cell lung carcinoma and correlates with clinicopathological features,” *Oncology reports*, 29(2), pp. 704–712.

Talmadge, J. E. and Fidler, I. J. (2010) “AACR centennial series: The biology of cancer metastasis: Historical perspective,” *Cancer Research*, pp. 5649–5669. doi: 10.1158/0008-5472.CAN-10-1040.

Tanigaki, K. *et al.* (2002) “BE-18591 as a new H+/Cl− symport ionophore that inhibits immunoproliferation and gastritis,” *FEBS Letters*. No longer published by Elsevier, 524(1–3), pp. 37–42. doi: 10.1016/S0014-5793(02)02996-4.

Taylor, R. C., Cullen, S. P. and Martin, S. J. (2008) “Apoptosis: Controlled demolition at the cellular level,” *Nature Reviews Molecular Cell Biology*. Nature Publishing Group, pp. 231–241. doi: 10.1038/nrm2312.

Teicher, B. A. (2014) “Targets in small cell lung cancer,” *Biochemical Pharmacology*. Elsevier, pp. 211–219. doi: 10.1016/j.bcp.2013.09.014.

The American Cancer Society (2014) “The History of Cancer,” *ACS-American Cancer Society*, pp. 1–16. doi: 10.1038/nrc1279.

Toker, A. and Marmiroli, S. (2014) “Signaling specificity in the Akt pathway in biology and disease,” *Advances in Biological Regulation*, pp. 28–38. doi: 10.1016/j.jbior.2014.04.001.

Tomasetti, C., Li, L. and Vogelstein, B. (2017) “Stem cell divisions, somatic mutations, cancer etiology, and cancer prevention,” *Science*, 355(6331), pp. 1330–1334. doi: 10.1126/science.aaf9011.

Torre, L. A. *et al.* (2015) “Global cancer statistics, 2012,” *CA: A Cancer Journal for Clinicians*, 65(2), pp. 87–108. doi: 10.3322/caac.21262.

Travis, W. D. *et al.* (2010) “Pathologic diagnosis of advanced lung cancer based on small biopsies and cytology: A paradigm shift,” *Journal of Thoracic Oncology*, 1 April, pp. 411–414. doi: 10.1097/JTO.0b013e3181d57f6e.

Travis, W. D. *et al.* (2011) “International association for the study of lung cancer/American Thoracic Society/ European Respiratory Society international multidisciplinary classification of lung adenocarcinoma,” *Journal of Thoracic Oncology*. Elsevier, pp. 244–285. doi: 10.1097/JTO.0b013e318206a221.

Travis, W. D. (2011) “Pathology of Lung cancer,” *Clinics in Chest Medicine*, 32(4), pp. 669–692. doi: 10.1016/j.ccm.2011.08.005.

Tseng, C.-W. *et al.* (2011) “Integrative network analysis reveals active microRNAs and their functions in gastric cancer,” *BMC systems biology*, 5(1), p. 99.

Tummers, B. and Green, D. R. (2017) “Caspase-8: regulating life and death,” *Immunological Reviews*, pp. 76–89. doi: 10.1111/imr.12541.

U.S. National Library of Medicine (2010) “How Tobacco Smoke Causes Disease The Biology and Behavioral Basis for Smoking-Attributable Disease A Report of the Surgeon General How Tobacco Smoke Causes Disease : The Biology and Behavioral Basis for Smoking-Attributable Disease A Report of the Surgeon.”

Valent, P. *et al.* (2012) “Cancer stem cell definitions and terminology: the devil is in the details,” *Nature Reviews Cancer*, 12(11), pp. 767–775. doi: 10.1038/nrc3368.

Vandenabeele, P. *et al.* (2010) “Molecular mechanisms of necroptosis: an ordered cellular explosion,” *Nature Reviews Molecular Cell Biology*. Nature Publishing Group, 11(10), pp. 700–714. doi: 10.1038/nrm2970.

Del Vescovo, V. *et al.* (2014) “MicroRNAs as lung cancer biomarkers,” *World journal of clinical oncology*, 5(4), p. 604.

Vidal, S. J. *et al.* (2014) “Targeting cancer stem cells to suppress acquired chemotherapy resistance,” *Oncogene*, 33(36), pp. 4451–4463. doi: 10.1038/onc.2013.411.

Wagner, E. F. and Nebreda, Á. R. (2009) “Signal integration by JNK and p38 MAPK pathways in cancer development,” *Nature Reviews Cancer*. Nature Publishing Group, 9(8), pp. 537–549. doi: 10.1038/nrc2694.

Walker, D. M., Boey, G. and McDonald, L. A. (2003) “The pathology of oral cancer,” *Pathology*. Elsevier, pp. 376–383. doi: 10.1080/00313029310001602558.

Wang, C.-H. *et al.* (2013) "Oxidative stress response elicited by mitochondrial dysfunction: Implication in the pathophysiology of aging," *Experimental Biology and Medicine*, 238, pp. 450–460. doi: 10.1177/1535370213493069.

Wang, J. *et al.* (2015) "Characterization of microRNA transcriptome in tumor, adjacent, and normal tissues of lung squamous cell carcinoma," *The Journal of thoracic and cardiovascular surgery*, 149(5), p. 1404–1414. e4.

Wang, Y. (2011) "Effects of salinomycin on cancer stem cell in human lung adenocarcinoma A549 cells.," *Medicinal chemistry (Shāriqah (United Arab Emirates))*, 7(2), pp. 106–11.

Wang, Y. *et al.* (2013) "Identification of predictive biomarkers for early diagnosis of larynx carcinoma based on microRNA expression data," *Cancer Genetics*. Elsevier, 206(9–10), pp. 340–346. doi: 10.1016/j.cancergen.2013.09.005.

Warburg, O. (1956) "On the Origin of Cancer Cells," *Source: Science, New Series*, 123(123), pp. 309–314. doi: 10.1126/science.123.3191.309.

Webb, B. A. *et al.* (2011) "Dysregulated pH: a perfect storm for cancer progression," *Nature Reviews Cancer*, 11(9), pp. 671–677. doi: 10.1038/nrc3110.

Weinberg, R. A. (1996) "How cancer arises.," *Scientific American*, pp. 62–70. doi: 10.1038/scientificamerican0996-62.

Whitacre, C. M. *et al.* (2002) "Photodynamic therapy of human breast cancer xenografts lacking caspase-3," *Cancer Letters*, 179(1), pp. 43–49. doi: 10.1016/S0304-3835(01)00853-9.

White, E. (2015) "The role for autophagy in cancer," *Journal of Clinical Investigation*, pp. 42–46. doi: 10.1172/JCI73941.

White, K. A., Grillo-Hill, B. K. and Barber, D. L. (2017) "Cancer cell behaviors mediated by dysregulated pH dynamics at a glance.," *Journal of cell science*. The Company of Biologists Ltd, 130(4), pp. 663–669. doi: 10.1242/jcs.195297.

Wicha, M. S., Liu, S. and Dontu, G. (2006) "Cancer stem cells: An old idea - A paradigm shift," *Cancer Research*, pp. 1883–1890. doi: 10.1158/0008-5472.CAN-05-3153.

Wirawan, E. *et al.* (2012) "Autophagy: For better or for worse," *Cell Research*, pp. 43–61. doi: 10.1038/cr.2011.152.

Wong, R. S. (2011) "Apoptosis in cancer: from pathogenesis to treatment," *Journal of Experimental & Clinical Cancer Research*. BioMed Central, 30(1), p. 87. doi: 10.1186/1756-9966-30-87.

Xiang, J. and Wu, J. (2010) "Feud or Friend? The Role of the miR-17-92 Cluster in Tumorigenesis," *Current Genomics*. Bentham Science Publishers, 11(2), pp. 129–135. doi: 10.2174/138920210790886853.

Xu, H. and Ren, D. (2015) "Lysosomal Physiology," *Annual Review of Physiology*, 77(1), pp. 57–80. doi: 10.1146/annurev-physiol-021014-071649.

Xu, L. *et al.* (2011) “Down-regulation of miR-212 expression by DNA hypermethylation in human gastric cancer cells.,” *Medical oncology (Northwood, London, England)*, 28 Suppl 1, pp. S189-96. doi: 10.1007/s12032-010-9691-0.

Xu, Q. *et al.* (2012) “A regulatory circuit of miR-148a/152 and DNMT1 in modulating cell transformation and tumor angiogenesis through IGF-IR and IRS1,” *Journal of Molecular Cell Biology*, 5(1), pp. 3–13.

Xu, X. *et al.* (2017) “miR-30a-5p enhances paclitaxel sensitivity in non-small cell lung cancer through targeting BCL-2 expression,” *Journal of Molecular Medicine*, 95(8), pp. 861–871. doi: 10.1007/s00109-017-1539-z.

Xuan, Y. and Hu, X. (2009) “Naturally-occurring shikonin analogues - A class of necroptotic inducers that circumvent cancer drug resistance,” *Cancer Letters*, 274(2), pp. 233–242. doi: 10.1016/j.canlet.2008.09.029.

Yan, R. *et al.* (2009) “Cytotoxicity and antibacterial activity of Lindera strychnifolia essential oils and extracts,” *Journal of Ethnopharmacology*, 121(3), pp. 451–455. doi: 10.1016/j.jep.2008.06.010.

Yanaihara, N. *et al.* (2006) “Unique microRNA molecular profiles in lung cancer diagnosis and prognosis,” *Cancer Cell*, 9(3), pp. 189–198. doi: 10.1016/j.ccr.2006.01.025.

Yang, J. *et al.* (2015) “Serum miR-152, miR-148a, miR-148b, and miR-21 as novel biomarkers in non-small cell lung cancer screening,” *Tumor Biology*, 36(4), pp. 3035–3042.

Youle, R. J. and Strasser, A. (2008) “The BCL-2 protein family: Opposing activities that mediate cell death,” *Nature Reviews Molecular Cell Biology*, pp. 47–59. doi: 10.1038/nrm2308.

Yu, S. P., Canzoniero, L. M. . and Choi, D. W. (2001) “Ion homeostasis and apoptosis,” *Current Opinion in Cell Biology*. Elsevier Current Trends, pp. 405–411. doi: 10.1016/S0955-0674(00)00228-3.

Zappa, C. and Mousa, S. A. (2016) “Non-small cell lung cancer: current treatment and future advances,” *Translational Lung Cancer Research*, 5(3), pp. 288–300. doi: 10.21037/tlcr.2016.06.07.

Zhan, C. *et al.* (2014) “Identification of reference miRNAs in human tumors by TCGA miRNA-seq data,” *Biochemical and Biophysical Research Communications*, 453(3), pp. 375–378.

Zhang, H. *et al.* (2011) “MiR-148a promotes apoptosis by targeting Bcl-2 in colorectal cancer,” *Cell Death & Differentiation*, 18(11), pp. 1702–1710.

Zhang, J. P. *et al.* (2014) “MicroRNA-148a suppresses the epithelial–mesenchymal transition and metastasis of hepatoma cells by targeting Met/Snail signaling,” *Oncogene*, 33(31), pp. 4069–4076.

Zhang, S. and Yu, D. (2010) “PI(3)king apart PTEN’s role in cancer,” *Clinical Cancer Research*, pp. 4325–4330. doi: 10.1158/1078-0432.CCR-09-2990.

Zhang, W. and Dolan, M. E. (2010) “The emerging role of microRNAs in drug responses.,” *Current opinion in molecular therapeutics*. NIH Public Access, 12(6), pp. 695–702.

Zhang, Y. *et al.* (2015) “Waltonitone induces apoptosis through mir-663-induced Bcl-2 downregulation in non-small cell lung cancer,” *Tumor Biology*, 36(2), pp. 871–876.

Zhao, J. *et al.* (2015) “MicroRNA-7: a promising new target in cancer therapy,” *Cancer Cell Int*. BioMed Central, 15(1), p. 103. doi: 10.1186/s12935-015-0259-0.

Zhao, L. *et al.* (2015) “Staurosporine induces platelet apoptosis through p38 mitogen-activated protein kinase signaling pathway,” *Clinical Laboratory*, 61(7), pp. 717–726. doi: 10.7754/Clin.Lab.2014.141103.

Zhu, J. *et al.* (2017) “CD73/NT5E is a target of miR-30a-5p and plays an important role in the pathogenesis of non-small cell lung cancer,” *Molecular Cancer*. BioMed Central, 16(1), p. 34. doi: 10.1186/s12943-017-0591-1.

Zong, W. X. and Thompson, C. B. (2006) “Necrotic death as a cell fate,” *Genes and Development*. Cold Spring Harbor Laboratory Press, pp. 1–15. doi: 10.1101/gad.1376506.

Zorov, D. B., Juhaszova, M. and Sollott, S. J. (2014) “Mitochondrial reactive oxygen species (ROS) and ROS-induced ROS release.,” *Physiological reviews*. American Physiological Society, 94(3), pp. 909–50. doi: 10.1152/physrev.00026.2013.

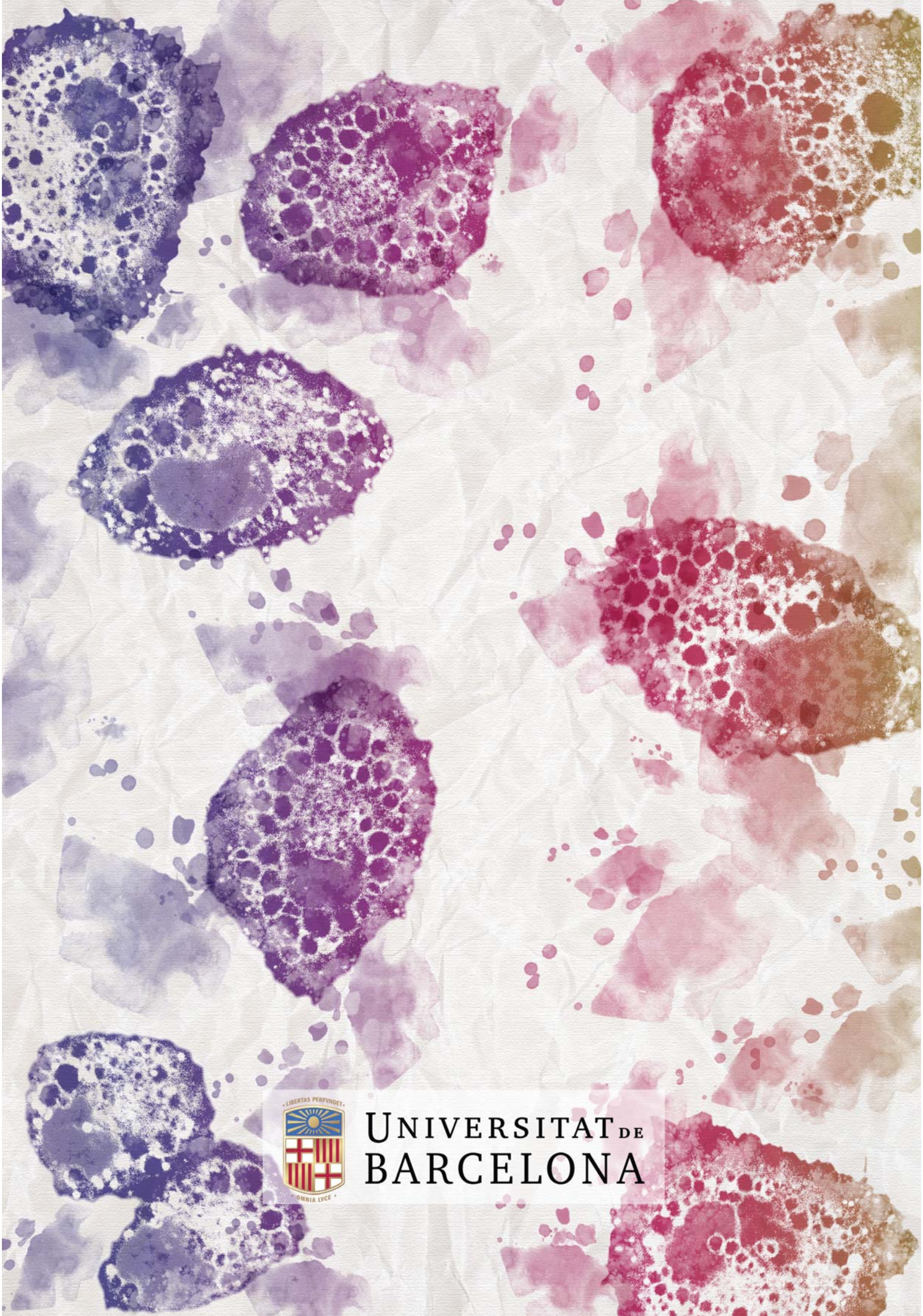
LIBERTAS PERFVNDET
OMNIA LVCE
UNIVERSITAT DE
BARCELONA